Synchrotron studies of “self-compression” in urea inclusion compounds

by

BO WANG

B.S., Southeast University, 2010

AN ABSTRACT OF A DISSERTATION

submitted in partial fulfillment of the requirements for the degree

DOCTOR OF PHILOSOPHY

Department of Chemistry
College of Arts and Sciences

KANSAS STATE UNIVERSITY
Manhattan, Kansas

2017

Abstract

Urea inclusion compounds (UICs) are classic examples of nanoporous, host:guest materials in which the linear channels of the honeycomb structure of the urea host can include various types of long-chain compounds (the guests). By using synchrotron X-ray radiation sources, a deeper understanding of these materials is made possible through detailed structural studies. In particular, this dissertation describes a series of structural phase transitions that occur upon cooling two related UICs containing alkanedione guest molecules.

UICs may be classified as either commensurate or incommensurate structures, depending on whether the repeat lengths of the host (c_h) and guest (c_g) along the channel axis are related by a small whole number ratio. Crystals of 2,8-nonanedione/urea and 2,11-dodecanedione/urea, which are incommensurate structures at room temperature, undergo “lock-in” phase transitions below room temperature to generate commensurate structures in which the guest repeat lengths are elongated. Upon nucleation and growth of these elongated, commensurate phases, other molecules in the same channels are compressed to give successively shorter guest repeat lengths. Further lock-in phase transitions give a multitude of commensurate and incommensurate phases during cooling. The crystal structures of two of these commensurate phases have been determined using synchrotron sources. The “self-compression” observed in these 1-D crystals serves as a paradigm for understanding solid-state reactions in three-dimensional crystals.

Synchrotron studies of “self-compression” in urea inclusion compounds

by

BO WANG

B.S., Southeast University, 2010

A DISSERTATION

submitted in partial fulfillment of the requirements for the degree

DOCTOR OF PHILOSOPHY

Department of Chemistry
College of Arts and Sciences

KANSAS STATE UNIVERSITY
Manhattan, Kansas

2017

Approved by:

Major Professor
Mark D. Hollingsworth

Abstract

Urea inclusion compounds (UICs) are classic examples of nanoporous, host:guest materials in which the linear channels of the honeycomb structure of the urea host can include various types of long-chain compounds (the guests). By using synchrotron X-ray radiation sources, a deeper understanding of these materials is made possible through detailed structural studies. In particular, this dissertation describes a series of structural phase transitions that occur upon cooling two related UICs containing alkanedione guest molecules.

UICs may be classified as either commensurate or incommensurate structures, depending on whether the repeat lengths of the host (c_h) and guest (c_g) along the channel axis are related by a small whole number ratio. Crystals of 2,8-nonanedione/urea and 2,11-dodecanedione/urea, which are incommensurate structures at room temperature, undergo “lock-in” phase transitions below room temperature to generate commensurate structures in which the guest repeat lengths are elongated. Upon nucleation and growth of these elongated, commensurate phases, other molecules in the same channels are compressed to give successively shorter guest repeat lengths. Further lock-in phase transitions give a multitude of commensurate and incommensurate phases during cooling. The crystal structures of two of these commensurate phases have been determined using synchrotron sources. The “self-compression” observed in these 1-D crystals serves as a paradigm for understanding solid-state reactions in three-dimensional crystals.

Table of Contents

List of Figures

List of Tables

Acknowledgements

I would like to acknowledge Dr. Mark Hollingsworth for all of his help and support throughout years. He is truly a scientist who dedicates all his life to solid-state chemistry. From him, I learned not only various techniques, but also how to do research with critical thinking. Years of immersing myself in this group has greatly altered my philosophy, and I will benefit from this throughout all my life no matter what my career will be. I would also like to acknowledge the members of the Hollingsworth group that I had the privilege of working with: Dr. Ilya Frantsuzov, Shane Nichols, Angela Adams, Keith Alquist, Adam Lechner. They are role models for me, especially Dr. Ilya Frantsuzov, who has spent much time and effort to improve this dissertation. The work described here could not have been accomplished without his help. Also, I want to thank my committee members, Dr. Stefan Bossmann, Dr. Daniel Higgins, and Dr. James Edgar for their time and feedback. I would especially like to thank Dr. Bossmann, who has supported me and my family in so many ways. I would like to thank many of the students and faculty in the Kansas State Chemistry Department for their help and guidance. Lastly, I would like to thank the beamline scientists and colleagues who helped me obtain high-quality data, especially Dr. Yu-Sheng Chen (APS), Dr. Simon Teat (ALS), and Dr. Bart Kahr (NYU).

Dedication

This work has been dedicated to my daughter, Mia, as she gives me endless happiness and courage to face everyday challenges. I wish my little angel a wonderful life. I want to especially thank my loving wife, Jing Yu, for everything she has done for me. She is truly an inspiration to me, and I am extremely proud of her for everything that she has accomplished. I also want to thank my parents and grandparents for everything they have taught me and have given me. They named me “Bo” when I was born, meaning knowledgeable in Chinese, as they hope me to be a doctor when I grow up. I feel very lucky that I can finally fulfill our family’s dream.

Chapter 1. General Introduction

1.1. Crystallography and synchrotron radiation.

This dissertation relies heavily on synchrotron X-ray crystallography. X-rays were first discovered by Wilhelm Röntgen in 1895.[1] In 1913, father-and-son William Henry Bragg and William Lawrence Bragg laid the foundation of crystallography by proposing Bragg's law and determining the crystal structures of simple minerals. They revolutionized all areas of science by introducing X-ray diffraction as a powerful method of determining the atomic structures of crystals and received the Noble Prize for this work in 1915.[2] From 1913 until the present, milestone crystal structures were treated as breakthroughs in science: these include the crystal structures of diamond,[3] hexamethylbenzene,[4] penicillin,[5] sodium rubidium (+)-tartrate tetrahydrate,[6] deoxyribonucleic acid, [7, 8, 9, 10] myoglobin,[11] lysozyme,[12, 13] AlMn alloy,[14] potassium channel, [15] ribosome,[16, 17, 18] and RNA polymerase.[19]

X-rays are electromagnetic waves with wavelengths (λ) between 0.1 and 100 Å (*i.e.*, between the wavelength regions of ultraviolet radiation (UV) and γ-rays). Electromagnetic waves are so-called transverse waves. Here, two components, an electric component ($\vec{E}$) and a magnetic component ($\vec{B} = \mu_0 \cdot \vec{H}$), are oscillating perpendicular to the direction of the wave propagation. In the X-ray region, there are three main categories of interaction: photoelectric absorption, elastic Thomson scattering, and inelastic Compton scattering. For X-ray diffraction analysis, the elastic Thomson scattering is the primary interaction. For scattering from atoms, atomic scattering factors are used to describe the relationship between scattering strength and scattering angle at a given wavelength. Atomic scattering factors $f(\sin\theta/\lambda)$ for each atom can be found in the International Tables for Crystallography.[20]

Crystals play a central role in this dissertation. The crystal structure of the rapidly quenched alloy of Al and Mn is especially relevant to this dissertation because this discovery opened up a large area of physical and materials research on quasicrystals.[14, 21] This discovery

led to the new definition of "crystal" by the International Union of Crystallography (IUCr):

> "A material is a crystal if it has **essentially** a sharp diffraction pattern. The word **essentially** means that most of the intensity of the diffraction is concentrated in relatively sharp Bragg peaks, besides the always present diffuse scattering. In all cases, the positions of the diffraction peaks can be expressed by
>
> $$\mathbf{H} = \sum_{i-1}^{n} h_i \boldsymbol{a}_i^* \ (n \geq 3)$$
>
> Here $\boldsymbol{a}_i^*$ and h_i are the basis vectors of the reciprocal lattice and integer coefficients respectively, and the number *n* is the minimum for which the positions of the peaks can be described with integer coefficient h_i. The conventional crystals are a special class, though very large, for which n = 3."[22]

This IUCr definition emphasizes that a "crystal" has a sharp diffraction pattern. For a material to have a sharp diffraction pattern, it must contain a regular arrangement of atoms or molecules. A perfect 3-D crystal has perfect periodicity. A crystal of this kind contains a basic unit cell or lattice, which is described by three basis vectors: ***a***, ***b***, and ***c***, with α as the angle between ***b*** and ***c***, β as the angle between ***a*** and ***c***, and γ as the angle between ***a*** and ***b.*** Bragg's law describes diffraction conditions for such a crystal. Miller planes (*hkl*) are used to define lattice planes, which intersect the basic vectors ***a*** at ***a***/*h*, ***b*** at ***b***/*k*, and ***c*** at ***c***/*l.* For diffracted X-rays to have constructive interference, the path length difference of incoming and outgoing X-rays scattered from adjacent Miller planes must be integral multiples of the X-ray wavelength $n\lambda$. The relationship governing the formation of scattered waves that constructively interfere is called Bragg's law: $n\lambda = 2d\sin\theta_{hkl.}$

The reciprocal lattice is used to help construct and understand X-ray diffraction. A direct

lattice has three basic vectors ***a***, ***b***, and ***c***. A reciprocal lattice can be also defined with three basic vectors ***a****, ***b****, and ***c****. The relationship of direct and reciprocal lattices' vectors can be expressed:

$$\begin{pmatrix} \boldsymbol{a} \\ \boldsymbol{b} \\ \boldsymbol{c} \end{pmatrix} (\boldsymbol{a}^* \quad \boldsymbol{b}^* \quad \boldsymbol{c}^*) = \mathbf{I}$$

It can be shown that ***a**** = (***b*** × ***c***)/V, ***b**** = (***a*** × ***c***)/V, and ***c**** = (***a*** × ***b***)/V, where V is the unit cell volume. Thus, ***a**** is perpendicular the ***bc*** plane, ***b**** is perpendicular the ***ac*** plane, and ***c**** is perpendicular the ***ab*** plane. Any reciprocal lattice point (*hkl*) represents a set of planes. And through Bragg's law, the distance of between a reciprocal lattice point (*hkl*) and the origin (000) gives the d-spacing between (*hkl*) planes in the direct lattice.

In this dissertation, synchrotron oscillation images are relied on heavily to extract information about our supramolecular systems. In acquiring an oscillation image, a crystal is mounted so that it can be rotated about a direct crystal axis. Take a hexagonal channel system for example: by applying a beam of X-rays perpendicular to the channel ***c*** axis whilerotating the crystal about the ***c*** axis, the ***a*b**** plane is perpendicular to the axis of rotation. If the ***a*b**** plane contains the reciprocal lattice origin (000), Bragg's law is fulfilled and diffraction occurs whenever the (*hk*0) points reach the circumference of the sphere with radius 1/λ. Thus diffraction results in a line of spots containing *l* = 0 reciprocal lattice points in the (*hk*0) plane. Moving along the ***c*** axis, reciprocal planes with *l* = 1, -1, 2, -2, and so forth would result in more lines of diffraction. This configuration used for channel axis of oscillation images is shown in Figure 1.1.

Synchrotron radiation is an electromagnetic radiation that is emitted when charged particles (*e.g.*, electrons) are moving at relativistic velocities along a curved trajectory with a large radius of curvature.[23] A typical electron accelerator emits synchrotron radiation in a wide range of wavelengths from microwaves to hard X-rays. This research utilizes both second and third generation synchrotron radiation sources at the Advanced Photon Source (APS) and the

Advanced Light Source (ALS).

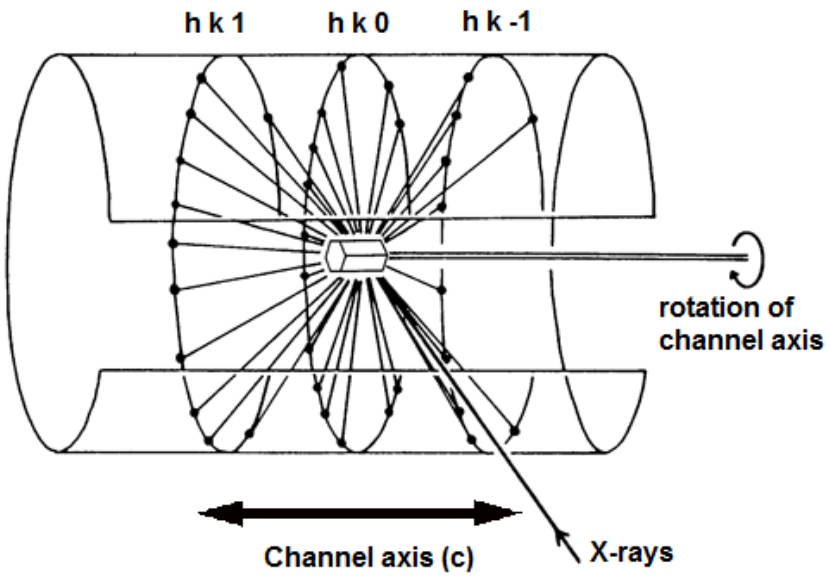

Figure 1.1. A schematic depiction of the X-ray oscillation image method. A crystal is aligned perpendicular to the beam and is rotated about its channel axis. Adapted by Mark Hollingsworth from "Crystal Structure Analysis: A Primer", by Glusker and Trueblood.[24]

1.2. Urea inclusion compounds (UICs)

Supramolecular chemistry is chemistry beyond the molecule. This field focuses on nonbonded interactions such as charge-charge interactions (100-350 kJ mol^{-1}), charge-dipole interactions (50-200 kJ mol^{-1}), dipole-dipole interactions (5-50 kJ mol^{-1}), hydrogen bonding (4-60 kJ mol^{-1}), charge-π interaction, π-π interaction, dispersion forces, and hydrophobic effects.[25] Modern supramolecular chemistry encompasses a diversity of fields, including host-guest systems, molecular machines, molecular recognition, self-assembly processes, and supramolecular photochemistry. Crown ethers,[26, 27, 28] cyclodextrins,[29, 30] and calixarenes[31] are examples of supramolecular materials. The discovery of the ability of crown ethers to complex with spherical alkali metal cations by Pedersen in 1967 signaled the beginning of host-guest

chemistry.[32] In a host-gust system, one species (the 'guest') is spatially confined within another species (the 'host'). Hosts can be large organic molecules that recognize certain smaller guests that are included within the host's cavity or supramolecular architecture.[25] Clathrates form between host clathrands and guests through the inclusion of guest molecules in the clathrand's extramolecular cavities. The term is sometimes used interchangeably with "solid-state inclusion compound". Examples of solid-state inclusion compounds are urea and thiourea inclusion compounds,[33] inclusion compounds of perhydrotriphenylene,[34] and zeolites.[35]

Historically, urea is a very important compound. The synthesis of urea from ammonium cyanate by Friedrich Wöhler in 1828 laid the foundation of organic chemistry.[36] His synthesis showed that chemicals found in living things can be produced with "inorganic materials". A high-resolution neutron structure of urea was reported in 1984 by Swaminathan and co-workers.[37] Its tetragonal structure has space group $P\bar{4}21m$, with ***a*** = ***b*** = 5.565(1) Å, and ***c*** = 4.684(1) Å.[37] As shown in Figure 1.2, urea molecules form a tight hydrogen bonding network, with each carbonyl group making four N-H---O hydrogen bonds.

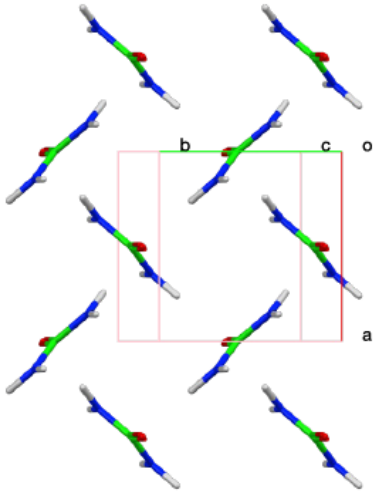

Figure 1.2. Crystal structure of urea, drawn from the 12 K neutron diffraction structure determined by Swaminathan and co-workers. The CSD refcode is UREAXX12.[37]

When urea is crystalized with long-chain molecules, such as n-alkanes, α,ω-dihaloalkanes, alkanones, or diacyl peroxides, urea inclusion compounds (UICs) are formed.[38,39] There are at least three forms of UICs whose structures have been determined. Depending on the geometry of the host urea's structure, the three forms are: a typical helical form, a stacked-loop form,[40] and a zigzag form.[41] In the helical form, hydrogen bonding networks tether urea molecules into helical ribbons. The space group of the hexagonal host structure is $P6_122$ (or the enantiomorphic $P6_522$), with $\boldsymbol{a} = \boldsymbol{b} \approx 8.22$ Å at room temperature. Two helical ribbons of urea molecules run in opposite directions and are related by a twofold axis perpendicular to the channel axis. One turn of the helix contains six urea molecules. On average, the host repeat length, c_g, is approximately11.02 Å,[42] and the hexagonal tunnel 'diameter' is between 5.5 and 5.8 Å.[43] This hexagonal form is frequently observed with alkane and alkanone guests.

A second form has a stacked-loop structure.[40] In this form, the urea host molecules are also tethered via hydrogen bonding, but here the space group is $P2_1/c$ or $P2_1/n$. Examples of guests that give this form are compounds of the formula $X(CH_2)_6Y$, where X and/or Y = Br, Cl, CN, or NC.[40, 44, 45]

The third "zigzag" form has only been observed in sebaconitrile/urea and 1,7-diaminoheptane/urea/methanol.[41, 46] In this form, the urea channels offset at the junction between the termini of guest molecules. In sebaconitrile/urea, the host channel repeat length (c_g) is 13.26 Å.

The helical form of UICs have been studied extensively studied since their discovery.[42] As introduced in the paragraph above, the helical channel has a fairly reliable host repeat length (c_h) of approximately 11.02 Å. The guest repeat length (c_g) is dependent on the molecular structure of the guest. UICs can be classified into commensurate or incommensurate systems, depending on the different periodicities of the host (c_h) and guest (c_g) along the channel axis (as shown in Figure 1.3). In incommensurate UICs, there are no sufficiently small integers m and n

for which m × c_h = n × c_g. In commensurate UICs, there are sufficiently small integers m and n for which m × c_h' = n × c_g'. (The prime is used with commensurate UICs to differentiate the host repeat from the actual length of the *c* axis for the unit cell of the commensurate structure (*i.e.*, *c* = m × c_h'.)

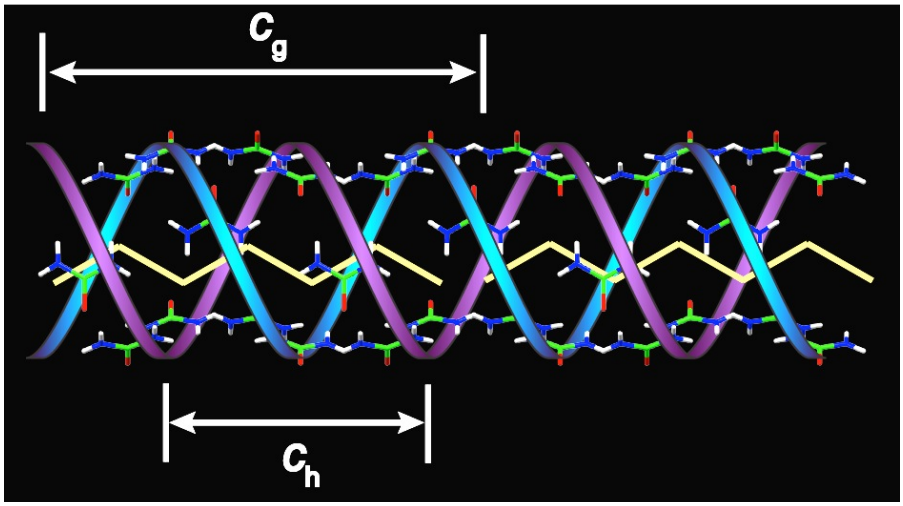

Figure 1.3. A schematic representation of the host structure of a UIC, showing the following terms: c_h (host repeat), c_g (guest repeat).

Most *n*-alkane UICs and alkanone UICs are incommensurate, which makes them aperiodic composites by construction. Along with quasicrystals and incommensurately modulated crystals, aperiodic composites constitute the three classes of aperiodic crystals.[47] Their diffraction patterns cannot be indexed with three indices *h*, *k*, and *l*. Instead, higher dimensional indices are required to describe their diffraction patterns. In a crystal with a single incommensurate direction ***c***, the positions of the Bragg peaks may be described by the following equation:

$$\mathbf{Q}_{hklm} = h\boldsymbol{a}^* + k\boldsymbol{b}^* + l\boldsymbol{c}_h^* + m\boldsymbol{c}_g^*$$

Where $\boldsymbol{a}^*$, $\boldsymbol{b}^*$, $\boldsymbol{c}_h^*$, and $\boldsymbol{c}_g^*$ are the reciprocal unit cell vectors, and $\boldsymbol{c}_h^*$ and $\boldsymbol{c}_g^*$ refer to the host and the guest parameters. The usage of the indices is described in earlier work by Guérin,

et al.: "a convenient but simplistic labeling is that (*h k* 0 0), (*h k* l 0), (*h k* 0 *m*) and (*h k l m*) with *l* and *m* different from zero are the common, host, guest, and satellite Bragg peaks, respectively."[48] A misfit parameter, defined by the ratio $\gamma = c_h/c_g$, is widely used in studying UICs .

In some cases, a long-range modulation appears in the system. Here a fifth direction, $\boldsymbol{c}_m$, is also needed to describe the position of Bragg peaks.[48, 49, 50] In five-dimensions the reciprocal image is given by:

$\mathbf{Q}_{hklmn} = h\cdot\boldsymbol{a}^* + k\cdot\boldsymbol{b}^* + l\cdot\boldsymbol{c}_h^* + m\cdot\boldsymbol{c}_g^* + n\cdot\boldsymbol{c}_m^*$.

The supplementary misfit parameter (δ) is defined as $\delta = c_h/c_m = \boldsymbol{c}_m^*/\boldsymbol{c}_h^*$.

1.3. Phase transition in UICs

Since early in 1952, structural studies on alkane/ureas have been conducted. Several series of substituted alkanes in urea have been explored. In the room temperature X-ray diffraction pattern of short chain UICs of *n*-alkanes, guests diffract as diffuse layer lines, whereas with longer chain lengths (thirteen carbons and higher) weak discrete scattering appears within these layer lines.[51] These observations indicate that in UICs containing short chain n-alkanes, the guests are ordered only along the channel direction (1-D ordering), and that positional correlations between channels (3-D ordering) become more prominent with longer chain lengths. In short chain alkanes/urea, diffuse planes from the guests show quadratic broadening. This indicates liquid-like or paracrystalline one-dimensional ordering.[52] The guest repeat (c_g) in alkane/urea inclusion compounds can be measured from the spacing between thediffuse planes exhibited by the guests. It has a linear relationship with the number of the carbons in the chain(n):

$c_g(n) = [(n-1)\times 1.277+3.48]$ Å.[53]

Much attention has been paid on the phase transitions of alkanes/urea. The most

common and important type is the ferroelastic type of phase transitions of alkanes/urea: typically, the helical host structures with hexagonal space group $P6_122$ at high temperature are distorted at low temperature to form orthorhombic host structures in space group $P2_12_12_1$. The phase transition temperature (T_c) depends on the alkane chain length. The longer the chain length, the higher the value of T_c. This ferroelastic phase transition is characterized by a shearing of the structure in the basal plane and a herringbone-like arrangement of the guests. [54] Experimentally, the characteristics of this phase transition in various alkane/urea inclusion compounds (decane, hexadecane, eicosane, and hexatriacontane) were measured in 1977 by Yozo Chatani and coworkers.[55] Alkane/urea inclusion compounds have many types of phase transitions in high dimensions (discussed below). Each alkane/urea shows different behavior. Recently, synchrotron radiation has helps us understand the phase transitions of UICs in unprecedented detail.

The UIC of *n*-heptane shows two phase transitions.[56] The misfit parameter γ is measured to be 0.981 (close to unity, but it is incommensurate), throughout three phases. The high temperature phase (*e.g.,* at room temperature) has space group $P6_122$. Only the host lattice generates Bragg reflections, whereas the guest lattice only shows diffuse sheets perpendicular to $\boldsymbol{c}^*$ in reciprocal space. This suggests there is no long-range lateral ordering for the guest. At T_{c1} = 145 K, a ferroelastic phase transition occurs, the symmetry of the host lattice is reduced to $P2_111$, with a 2-fold screw axis along ***a***. The guest still shows only 1-D ordering, as no Bragg reflections were observed from the guest lattice. At T_{c2} = 130 K, a "phase ordering" phase transition occurs. The composite system is described in superspace group $P2_111(0\beta\gamma)$, with γ = 0.981. The intermodulation of the host-guest can be indicated here by the emergence of satellites peaks. Furthermore, the diffraction patterns showed hexagons on each (*hk*0*m*) planes. This is due to a three-dimensional lateral ordering of the guest in the adjacent channel ($\Delta_g \neq 0$), and a sixfold twinning. The vector of guest in adjacent channels is given by

$\boldsymbol{c}_{g+}^* = \beta\boldsymbol{b}^* + \gamma\boldsymbol{c}_h^*$; this relationship gives $\Delta_g = \beta \times c_g/2$. The β is measured to be temperature dependent, and it evolves continuously from 0.5 to 0467 upon cooling.

n-Dodecane/urea shows a similar sequence of phase transitions as *n*-heptane/urea.[57] In the high temperature phase, the guest exhibits only quasi-one dimensional liquidlike ordering. Here, the host structure is found in space group $P6_122$, as manifested in the helical form of UICs. When cooled below T_c = 248 K, additional ordering of the guests gives rise to a phase transition. The system is described by the four-dimensional superspace group $P6_122(00\gamma)$, where γ = 0.632(5). When cooled below T_{c1} = 123 K, a ferroelastic phase transition occurs, and the symmetry of the host lattice is reduced to monoclinic $P2_1$. The guests in adjacent channels are shifted along the ***a*** direction by $\Delta_g = \alpha \times c_g/2$, with α = 0.160 and c_g = 17.40 Å. Thus the composite system is described in superspace group $P12_11(\alpha 0\gamma)$.

n-Hexadecane/urea has been studied extensively. In 1952, Smith published the crystal structure of *n*-hexadecane/urea. Although he treated the system as commensurate with $1c_g' = 2c_h'$, which is incorrect, the helical host structure was first determined at that time.[58] Later on, from 1987 to 1990, Forst and coworkers determined that this system is incommensurate and reported the existence of four phase transitions.[59] A ferroelastic phase transition was observed at 148 K, and a long modulation was observed along ***c*** direction at 120 K. They also attempted to solve the disordered crystal structure, but soon realized the great difficulty in dealing with the ferroelastic phase transitions, which, at a low temperature, result in six orientations of twin domains.[60]

n-Heptadecane/urea's modulated structure was published in 1997 by T. Weber and coworkers. The system is described in $P6_122(00\gamma)$, with γ = 0.4646(5). The value of c_g was measured to be 23.713(1) Å at 293K. The crystal structure involved the inclusion of transverse and longitudinal modulation functions.[61]

n-Octadecane/urea shows rich phase transition behavior.[49] The misfit parameter γ is

measured to be 0.43776(2) throughout all of the observed phases. The high temperature phase is described in the four-dimensional spacegroup $P6_122(00\gamma)$. This indicates that the intermodulation of the host and guest is already pronounced at room temperature. When cooled below T_{c1} = 160 K, the system undergoes a ferroelastic phase transition into superspace group $P2_12_12_1(00\gamma)$. In this orthorhombic basis, distortion is not observed. (Only the Laue symmetry has changed.) When cooled below T_{c2} = 152.8(4) K, the system shows a long-range modulation in superspace group $C222_1(00\gamma)(10\delta)$, with δ = 0.0576(6). In this phase, there is a ferroelastic distortion in the ***ab*** plane. When further cooled below T_{c3}=109(4) K, the system is once again primitive, as in Phase II, but with an additional long-range modulation that gives rise to a five-dimernsional superspace group $P2_12_12_1(00\gamma)(00\delta)$.

n-Nonadecane/urea was studied extensively due to its rich behavior of phase transitions. In 1996, Lefort and coworkers measured the misfit parameters γ to be 0.418. In this material, a ferroelastic phase transition occurs around 160 K. Lefort and co-workers also assigned the space group as $P2_12_12_1$ for the low-temperature ferroelastic phase. Satellite reflections were observed for the first time to show that there is an incommensurate modulation in a composite system.[62] Later in 2004, Bourgeois and coworkers found out that by applying 6 kbar of hydrostatic pressure, no ferroelastic distortion can be found at lowered temperature. They concluded that medium hydrostatic pressure affects the collective properties and interactions in this composite inclusion system.[63] In 2011, a temperature-pressure phase diagram of *n*-nonadecane/urea was published by Toudic and coworkers.[64] In 2008, Toudic and coworkers noticed the rich phase transition behavior of this system by analyzing the neutron diffraction patterns from *n*-nonadecane-d_{40}/urea-d_4. There are two phase transitions. Below T_{c1} = 149 K, a hexagonal-to-orthorhombic transition occurs. However, the superstructure layer lines (with $h + k$ = odd) contained only satellite reflections. This indicated that the doubling of the unit cell results from the alternation of intermodulation between host and guest in adjacent channels, but not

from either herringbone ordering of the guest or shearing of the host. When cooled below T_{c2} = 129 K, the common, host, and guest Bragg peaks appear. This indicates that the mean structure of host and guest adopt a twofold screw along the orthorhombic axis.[65] Later on, in 2013, Mariette and coworkers concluded that the superspace group of *n*-nonadecane/urea in Phase II (below T_{c1} = 158.5K) is $C222_1(00\gamma)(10\delta)$, with γ = 0.418, and δ = 0.090.[66] This modulation wavelength is estimated to be larger than 500 Å.[66]

n-Tetracosane/urea has two phase transitions, which are very similar to those observed in *n*-octadecane/urea.[48] At high temperatures, the system is in superspace group $P6_122(00\gamma)$, with γ = 0.3369. Below, T_{c1} = 179(1) K, a ferroelastic phase transition occurs. The lower symmetry Phase II has superspace group of $C222_1(00\gamma)(10\delta)$, with δ = 0.025(1). This corresponds to a long-range modulation wavelength of 440(16) Å. Below T_{c2} = 163.0(5) K, Phase III has superspace group $P2_12_12_1(00\gamma)(00\delta)$.

One question is when and whether a guest would lock into a commensurate structure with the host. Many alkane/urea inclusion compounds exist in five-dimensional superspace groups in their low temperate phases. With high-resolution synchrotron measurements, incommensurate-to-commensurate lock-in phase transitions were observed in octane/urea, undecane/urea, and a commensurate structure was found in eicosane/urea.[67] Although an early theoretical study has been done on this system, no accurate prediction can be made as to whether the system is commensurate, incommensurate or has a lock-in phase transition at low temperatures.[38]

Although the host structure has been determined for several UICs,[56] guest structures are very difficult to determine. Even today, no accurate crystal structures of alkane/urea inclusion compounds have been published. There are several reasons for this difficulty. First, most alkanes/urea are incommensurate and therefore need superspace groups to describe their symmetries. Second, due to dynamics nature of the system, guests are not static, but are

constantly translating or rotating about the channel axis, and this creates longitudinal and lateral disorder. Third, various types of phase transitions further complicate the system. In particular, ferroelastic phase transitions, which give rise to six non-merohedral twins, make structure determination very difficult. Fourth, due to their structural flexibility, long-chain guests in UICs might have different conformations (although extended zigzag conformation of guests was assumed in earlier publications).[58]

Commensurate UICs offered great opportunities to determine the complete crystal structure of the composite system, and therefore to probe the molecular structure of both host and guest unambiguously. Of the three forms mentioned above, the zig-zag and stacked-loop forms are both commensurate with $1c_g' = 1c_h'$.[44, 68] As for the helical form, however, only a handful of guests are known to form commensurate structures with urea. Notable among these are UICs containing bis(methyl ketone)s. The Hollingsworth group found that due to strong hydrogen bonding between the carbonyl groups of the guest molecules and urea, $\alpha+1,\omega-1$-bis(methyl ketone)s can form commensurate structures with urea. Those commensurate UICs containing diketones exhibit strong 3-D ordering of guests. In almost all cases, the offsets of the guests in adjacent channels (Δ_g) are zero. Their diffraction patterns can be indexed with three indices, *h*, *k*, and *l*. Crystal structures of 2,7-octanedione/urea,[69] 2,9-decanedione/urea,[70] 2,10-undecanedione/urea,[71] and 2,12-tridecanedione[72] have been published, and the structure of 2,15-hexadecanedione/urea has been solved.[73] Helical wheel diagrams are useful to predict the conformations of the diketone guests in these commensurate inclusion compounds.[69, 72]

2,7-octanedione/urea has a commensurate structure with $6c_g' = 7c_h'$ and has space group $P6_122$. The unit cell is ***a*** = ***b*** = 8.211(4) Å, ***c*** = 76.91(5) Å at 291 K. The adjacent guest molecules in a channel are related by a sixfold screw along the channel axis.[69]

2,9-decanedione/urea has a commensurate structure with $3c_g' = 4c_h'$ and has space group $P3_112$. The unit cell is ***a*** = ***b*** = 8.229(2) Å, ***c*** = 44.16(2) Å. The guest coils by 0.4 Å to

lock into this commensurate structure. The adjacent guest molecules in a channel are related by a threefold screw along the channel axis.[70]

2,10-undecanedione/urea has a commensurate structure with $2c_g' = 3c_h'$ and has space group $C222_1$. The unit cell is ***a*** = 8.345(1), ***b*** = 13.939(3) Å, ***c*** = 32.982(6). The adjacent guest molecules in a channel are related by a twofold screw along the channel axis. This crystal grown at room temperature shows 12 twins that are epitaxially matched across two types of twin boundaries. Due to the lowered symmetry, this material is shown to be ferroelastic; that is, the domains can be reoriented by application of an external force.[71, 74]

2,12-tridecanedione/urea has a commensurate structure with $3c_g' = 5c_h'$ and has space group $P3_112$. The unit cell is ***a*** = ***b*** = 8.1660(10) Å, ***c*** = 55.2445(13) Å at 198 K. The adjacent guest molecules in a channel are related by a threefold screw along the channel axis. This trigonal crystal shows chiral twinning and rotational twinning at the same time.[72]

1.4. Stress in solid phase

Solid-state chemistry has attracted scientists' attention for many years.[75] By studying chemical reactions in the solid state, researchers can gain much insight into reaction mechanisms and explore novel reactions, such as grinding reactions[76] and single-crystal-to-single-crystal (SCSC) reactions.[77, 78, 79] Moreover, future functional materials, *e.g.*, actuators,[80, 81] and storage materials,[82] can be designed with a better understanding of solid-state chemistry. However, when one carries out reactions in crystalline materials, one problem is that crystals are often cracked or shattered during the course of the reactions. This can be understood by considering that since molecules are well-packed in the solid-state, alteration of molecular shapes or formation of new product molecules during reactions generates stress. The stress is due to the repulsive nature of van der Waals interactions when atoms are too close to each other. Mechanical stress in organic crystals has been observed decades ago. Upon photolysis

of a diundecanoyl peroxide crystal, a pair of CO_2 molecules and a pair of free radicals were formed. The formation of the products was shown to create huge stresses in the crystal, which was estimated to be at least 20 kbar.[83, 84, 85, 86] A modified linear elasticity theory was used to estimate the range of the stress in those complicated systems. The range of the stress transmission was found to be at least 6 to 10 molecules.[87] Because the transmission of anisotropic stress is so complicated in a 3-D crystal, simple systems such as isotropic or 1-D channel structures are needed to probe mechanical stresses in the solid-state if one is to gain a better understanding of how mechanical stress influences structures. Urea inclusion compounds (UICs), which usually have a channel structure, offer a simplified way to study stress in crystals.[88]

Stress also plays an important role in solid-phase transitions. Pressure-induced phase transitions are widely studied in various crystalline materials.[89] With developments in equipment, e.g., diamond anvil cells, much attention has been given to high-pressure studies of solids.[90] In UIC systems, phase transitions of nonadecane/urea were studied in a helium atmosphere pressurized up to 5.5 kbar.[64] In that study, Toudic and co-workers found that this UIC has a hexagonal incommensurate structure at high temperature. It undergoes different types of phase transitions to incommensurate orthorhombic structures below and above 3.5 kbar. Encouragingly, a lock-in phase transition of hexadecane/urea was observed with a helium pressure of 4 kbar at room temperature.[91] In a study of $X(CH_2)_6Y$/urea crystals, with X or Y = Br or Cl,[92] crystals of $X(CH_2)_6Y$/urea have commensurate structures with $1c_g' = 1c_h'$. During growth, the guests shorten themselves to be commensurate with the host. For example, $Br(CH_2)_6Br$ is expected to have a c_g of 12.8 Å, which is 1.8 Å longer than the required guest repeat for the structure with $1c_g' = 1c_h'$. In order to shorten, the guests in these UICs coil into gauche conformations, and they tilt away from the channel axis. Because of the predominance of one of two gauche conformations in which the zig-zag chain of the methylene is oriented differently,

the guests generate lattice strain so that the unit cell is distorted by 10% from a hexagonal structure at 100 K. In addition to the lateral strain generated by the orientation of the guests, the coiling of the guests generates longitudinal stress along the channel axes. Although 1,6-dibromohexane/urea, the guest with the longest natural (*i.e.*, extended) length in this series, shows the most gradual shift toward hexagonal metric symmetry upon heating, this UIC has the lowest temperature for a first-order phase transition to an undistorted structure in which the guest elongates by 1.8 Å along the channel axis. This can be explained by a guest-induced stress. Because 1,6-dibromohexane is coiled the most to accommodate the commensurate structure, this guest exerts the highest longitudinal stress in the series of UIC crystals. This makes 1,6-dibromohexane/urea the least stable and leads to the lowest phase transition temperature in this series of $X(CH_2)_6Y$/urea crystals.

1.5. The proposals

In this thesis, there are two main chapters regarding 2,8-nonanedione/urea and 2,11-dodecanedione/urea. Phase transitions of the two UICs are thoroughly studied with synchrotron X-ray diffraction methods. To rationalize the phase transition behavior of the two UICs, a unique "self-compression" mechanism is proposed. This thesis work is aimed to answer some important questions, such as how pressure can affect phase transition behavior, and what factors control an incommensurate-to-commensurate lock-in phase transition in aperiodic composite systems.

1.6. References

1. Maddox, J., The sensational discovery of X-rays. *Nature* **1995,** *375*, 183.
2. Perutz, M. F., How W. L. Bragg invented X-ray analysis. *Acta Crystallogr. Sect. A* **1990,** *46*, 633-643.
3. Bragg, W. H., Bragg, W. L., The structure of the diamond. *Proc. R. Soc. A* **1913,** *89*, 277-291.
4. Lonsdale, K., The structure of the benzene ring in $C_6(CH_3)_6$. *Proc. R. Soc. A* **1929,** *123*,

494-515.
5. http://www.nobelprize.org/nobel_prizes/chemistry/laureates/1964/perspectives.html.
6. Bijvoet, J. M.; Peerdeman, A. F.; van Bommel, A. J., Determination of the absolute configuration of optically active compounds by means of X-rays. *Nature* **1951,** *168*, 271-272.
7. Franklin, R. E.; Gosling, R. G., Molecular configuration in sodium thymonucleate. *Nature* **1953,** *171*, 740-741.
8. Watson, J. D.; Crick, F. H. C., Molecular structure of nucleic acids - a structure for deoxyribose nucleic acid. *Nature* **1953,** *171*, 737-738.
9. Wilkins, M. H. F.; Stokes, A. R.; Wilson, H. R., Molecular structure of deoxypentose nucleic acids. *Nature* **1953,** *171*, 738-740.
10. Franklin, R. E.; Gosling, R. G., Evidence for 2-chain helix in crystalline structure of sodium deoxyribonucleate. *Nature* **1953,** *172*, 156-157.
11. Kendrew, J. C.; Bodo, G.; Dintzis, H. M.; Parrish, R. G.; Wyckoff, H.; Phillips, D. C., 3-Dimensional model of the myoglobin molecule obtained by X-ray analysis. *Nature* **1958,** *181*, 662-666.
12. Blake, C. C. F.; Koenig, D. F.; Mair, G. A.; North, A. C. T.; Phillips, D. C.; Sarma, V. R., Structure of hen egg-white lysozyme - a 3-dimensional Fourier synthesis at 2 Å resolution. *Nature* **1965,** *206*, 757-761.
13. Kim, S. H.; Quigley, G.; Suddath, F. L.; A, M.; Sneden, D.; Kim, J. J.; J., W.; P., B.; Rich, A., The three-dimensional structure of yeast phenylalanine transfer RNA: shape of molecule at 5.5 Å resolution. *Proc. Natl. Acad. Sci. U.S.A.* **1972,** *69*, 3746-3750.
14. Shechtman, D.; Blech, I.; Gratias, D.; Cahn, J. W., Metallic phase with long-range orientational order and no translational symmetry. *Phys. Rev. Lett.* **1984,** *53*, 1951-1953.
15. Doyle, D. A.; Cabral, J. M.; Pfuetzner, R. A.; Kuo, A. L.; Gulbis, J. M.; Cohen, S. L.; Chait, B. T.; MacKinnon, R., The structure of the potassium channel: Molecular basis of K^+ conduction and selectivity. *Science* **1998,** *280*, 69-77.
16. Ban, N.; Nissen, P.; Hansen, J.; Moore, P. B.; Steitz, T. A., The complete atomic structure of the large ribosomal subunit at 2.4 Å resolution. *Science* **2000,** *289*, 905-920.
17. Schluenzen, F.; Tocilj, A.; Zarivach, R.; Harms, J.; Gluehmann, M.; Janell, D.; Bashan, A.; Bartels, H.; Agmon, I.; Franceschi, F.; Yonath, A., Structure of functionally activated small ribosomal subunit at 3.3 Å resolution. *Cell* **2000,** *102*, 615-623.
18. Yusupov, M. M.; Yusupova, G. Z.; Baucom, A.; Lieberman, K.; Earnest, T. N.; Cate, J. H. D.; Noller, H. F., Crystal structure of the ribosome at 5.5 Å resolution. *Science* **2001,** *292*, 883-896.
19. Cramer, P.; Bushnell, D. A.; Kornberg, R. D., Structural basis of transcription: RNA polymerase II at 2.8 Å resolution. *Science* **2001,** *292*, 1863-1876.
20. Cromer, D. T.; Waber, J. T., *International Tables for Crystallography*, Vol. C; Table 4.2.4.2. The Kynoch Press: Birmingham, U.K., 1991.
21. Janssen, T.; Chapuis, G.; de Boissieu, M., *Aperiodic Crystals: From Modulated Phases to Quasicrystals*. Oxford University Press: Oxford, 2007.
22. http://reference.iucr.org/dictionary/Crystal.
23. Margaritondo, G., *Introduction to Synchrotron Radiation*. Oxford Universiy Press: New York, 1988.
24. Glusker, J. P.; Trueblood, K. N., *Crystal Structure Analysis: A Primer*. Oxford University Press: New York, 1985; p 48.
25. Steed, J. W.; Atwood, J. L., *Supramolecular Chemistry*, Second edition. Wiley: Chichester, UK, 2009 p393-398.
26. Tachibana, Y.; Kawasaki, H.; Kihara, N.; Takata, T., Sequential O- and N-acylation protocol for high-yield preparation and modification of rotaxanes: Synthesis, functionalization, structure, and intercomponent interaction of rotaxanes. *J. Org. Chem.* **2006,** *71*, 5093-5104.

27. Badjic, J. D.; Ronconi, C. M.; Stoddart, J. F.; Balzani, V.; Silvi, S.; Credi, A., Operating molecular elevators. *J. Am. Chem. Soc.* **2006,** *128*, 1489-1499.
28. Chiu, C. W.; Lai, C. C.; Chiu, S. H., "Threading-followed-by-swelling": A new protocol for rotaxane synthesis. *J. Am. Chem. Soc.* **2007,** *129*, 3500-3501.
29. Del Valle, E. M. M., Cyclodextrins and their uses: a review. *Process Biochem* **2004,** *39* (9), 1033-1046.
30. Yu, G. C.; Jie, K. C.; Huang, F. H., Supramolecular amphiphiles based on host-guest molecular recognition motifs. *Chem. Rev.* **2015,** *115*, 7240-7303.
31. Gutsche, C. D., Calixarenes. *Acc. Chem. Res.* **1983,** *16*, 161-170.
32. Pedersen, C. J., Cyclic polyethers and their complexes with metal salts. *J. Am. Chem. Soc.* **1967,** *89*, 2495-&.
33. Harris, K. D. M., Meldola lecture: understanding the properties of urea and thiourea inclusion compounds. *Chem. Soc. Rev.* **1997,** *26* (4), 279-289.
34. Hoss, R.; Konig, O.; Kramer-Hoss, V.; Berger, U.; Rogin, P.; Hulliger, J., Crystallization of supramolecular materials: perhydrotriphenylene (PHTP) inclusion compounds with nonlinear optical properties. *Angew. Chem. Int. Ed.* **1996,** *35*, 1664-1666.
35. Davis, M. E.; Lobo, R. F., Zeolite and molecular-sieve synthesis. *Chem. Mater.* **1992,** *4*, 756-768.
36. Cohen, P. S.; Cohen, S. M., Wohler's synthesis of urea: How do the textbooks report it? *J. Chem. Educ.* **1996,** *73*, 883-886.
37. Swaminathan, S.; Craven, B. M.; Mcmullan, R. K., The crystal-structure and molecular thermal motion of urea at 12-K, 60-K and 123-K from neutron-diffraction. *Acta Crystallogr. Sect. B* **1984,** *40*, 300-306.
38. Harris, K. D. M., Meldola lecture: understanding the properties of urea and thiourea inclusion compounds. *Chem. Soc. Rev.* **1997,** *26*, 279-289.
39. Redlich, O.; Gable, C. M.; Dunlop, A. K.; Millar, R. W., Addition compounds of urea and organic substances. *J. Am. Chem. Soc.* **1950,** *72*, 4153-4160.
40. Hollingsworth, M. D.; Peterson, M. L.; Pate, K. L.; Dinkelmeyer, B. D.; Brown, M. E., Unanticipated guest motion during a phase transition in a ferroelastic inclusion compound. *J. Am. Chem. Soc.* **2002,** *124*, 2094-2095.
41. Hollingsworth, M. D.; Santarsiero, B. D.; Harris, K. D. M., Zigzag Channels In the Structure Of Sebaconitrile/Urea. *Angew. Chem. Int. Ed.* **1994,** *33*, 649-652.
42. Hollingsworth, M. D.; Harris, K. D. M., Urea, thiourea and selenourea. 1996; *Comprehensive Supramolecular Chemistry*, Vol. 6, Oxford, Elsevier Science Ltd., p 177-237.
43. George, A. R.; Harris, K. D. M., Representing and understanding geometric features of one-dimensional tunnel structures in solidi inclusion compounds. *J. Mol. Graph.* **1995,** *13*, 138-141.
44. Hollingsworth, M. D.; Werner-Zwanziger, U.; Brown, M. E.; Chaney, J. D.; Huffman, J. C.; Harris, K. D. M.; Smart, S. P., Spring-loading at the molecular level: relaxation of guest-induced strain in channel inclusion compounds. *J. Am. Chem. Soc.* **1999,** *121*, 9732-9733.
45. Hollingsworth, M. D.; Peterson, M. L.; Dinkelmeyer, B. D., Space group assignment and evaluation of end-for-end guest disorder in urea inclusion compounds. *Trans. Am. Cryst. Assn.* **2012,** *43*, 113-127.
46. Lee, S. O.; Kariuki, B. M.; Richardson, A. L.; Harris, K. D. M., A new type of layered structure for urea inclusion compounds containing local segments of tunnels. *J. Am. Chem. Soc.* **2001,** *123*, 12684-12685.
47. Janssen, T.; Chapuis, G.; de Boissieu, M. *Aperiodic Crystals*. Oxford University Press: New York, 2007.
48. Guérin, L.; Mariette, C.; Rabiller, P.; Huard, M.; Ravy, S.; Fertey, P.; Nichols, S. M.; Wang, B.; Mannsfeld, S. C. B.; Weber, T.; Hollingsworth, M. D.; Toudic, B., Long-range

modulation of a composite crystal in a five-dimensional superspace. *Phys. Rev. B* **2015,** *91*, 184101.
49. Mariette, C.; Frantsuzov, I.; Wang, B.; Guérin, L.; Rabiller, P.; Hollingsworth, M. D.; Toudic, B., Frustrated pretransitional phenomena in aperiodic composites. *Phys. Rev. B* **2016,** *94*, 184105.
50. Huard, M.; Toudic, B.; Rabiller, P.; Ecolivet, C.; Guérin, L.; Bourges, P.; Breczewski, T.; Hollingsworth, M. D., Confined linear molecules inside an aperiodic supramolecular crystal: The sequence of superspace phases in *n*-hexadecane/urea. *J. Chem. Phys.* **2011,** *135*, 204505.
51. Weber, T.; Boysen, H.; Honal, M.; Frey, F.; Neder, R. B., Diffuse and satellite scattering in urea inclusion compounds with various alkane molecules. *Z. Krystallog.* **1996,** *211*, 238-246.
52. Weber, T.; Boysen, H.; Frey, F., Longitudinal positional ordering of n-alkane molecules in urea inclusion compounds. *Acta Crystallogr. B* **2000,** *56*, 132-141.
53. Lenné, H. U.; Mez, H. C.; Schlenk, W., Jr., Lengths of molecules in inclusion channels of urea and thiourea. *Justus Liebigs Ann. Chem.* **1970,** ***732***, 70-96.
54. Lynden-Bell, R. M., The orientational order/disorder phase transition of urea paraffin inclusion compounds. *Mol. Phys.* **1993,** *79*, 313-321.
55. Chatani, Y.; Taki, Y.; Tadokoro, H., Low-temperature form of urea adducts with *n*-paraffins. *Acta Crystallogr. B* **1977,** *33*, 309-311.
56. Mariette, C.; Huard, M.; Rabiller, P.; Nichols, S. M.; Ecolivet, C.; Janssen, T.; Alquist, K. E.; Hollingsworth, M. D.; Toudic, B., A molecular "phase ordering" phase transition leading to a modulated aperiodic composite in n-heptane/urea. *J. Chem. Phys.* **2012,** *136*, 104507.
57. Mariette, C.; Guérin, L.; Rabiller, P.; Chen, Y. S.; Bosak, A.; Popov, A.; Hollingsworth, M. D.; Toudic, B., The creation of modulated monoclinic aperiodic composites in *n*-alkane/urea compounds. *Z. Kristallogr.* **2015,** *230*, 5-11.
58. Smith, A. E., The crystal structure of the urea-hydrocarbon complexes. *Acta Crystallogr.* **1952,** *5*, 224-235.
59. Forst, R.; Jagodzinski, H.; Boysen, H.; Frey, F., Diffuse-scattering and disorder in urea inclusion compounds $OC(NH_2)_2$+C_nH_{2n+2}. *Acta Crystallogr. B* **1987,** *43*, 187-197.
60. Forst, R.; Jagodzinski, H.; Boysen, H.; Frey, F., The disordered crystal structure of urea inclusion compounds $OC(NH_2)_2$ + C_nH_{2n+2}. *Acta Crystallogr. B* **1990,** ***46*** (1), 70-78.
61. Weber, T.; Boysen, H.; Frey, F.; Neder, R. B., Modulated structure of the composite crystal urea n-heptadecane. *Acta Crystallogr.* **1997,** *53*, 544-552.
62. Lefort, R.; Etrillard, J.; Toudic, B.; Guillaume, F.; Breczewski, T.; Bourges, P., Incommensurate intermodulation of an organic intergrowth compound observed by neutron scattering. *Phys. Rev. Lett.* **1996,** *77*, 4027-4030.
63. Bourgeois, L.; Toudic, B.; Ecolivet, C.; Ameline, J. C.; Bourges, P.; Guillaume, F.; Breczewski, T., Interactions in self-organized nanoporous organic crystals. *Phys. Rev. Lett.* **2004,** *93*, 026101.
64. Toudic, B.; Rabiller, P.; Bourgeois, L.; Huard, M.; Ecolivet, C.; McIntyre, G. J.; Bourges, P.; Breczewski, T.; Janssen, T., Temperature-pressure phase diagram of an aperiodic host guest compound. *EPL* **2011,** *93*, 16003.
65. Toudic, B.; Garcia, P.; Odin, C.; Rabiller, P.; Ecolivet, C.; Collet, E.; Bourges, P.; McIntyre, G. J.; Hollingsworth, M. D.; Breczewski, T., Hidden degrees of freedom in aperiodic materials. *Science* **2008,** *319*, 69-71.
66. Mariette, C.; Guérin, L.; Rabiller, P.; Ecolivet, C.; Garcia-Orduna, P.; Bourges, P.; Bosak, A.; de Sanctis, D.; Hollingsworth, M. D.; Janssen, T.; Toudic, B., Critical phenomena in higher dimensional spaces: The hexagonal-to-orthorhombic phase transition in aperiodic *n*-nonadecane/urea. *Phys. Rev. B* **2013,** *87*, 104101.
67. Commensurate alkane/ureas, unpublished work by Mark D. Hollingsworth, Bo Wang, Shane M. Nichols, and Ilya Frantsuzov.

68. Hollingsworth, M. D.; Santarsiero, B. D.; Harris, K. D. M., Zigzag channels in the structure of sebaconitrile/urea. *Angew. Chem. Int. Ed.* **1994,** *33*, 649-652.
69. Brown, M. E.; Chaney, J. D.; Santarsiero, B. D.; Hollingsworth, M. D., Superstructure topologies and host-guest interactions in commensurate inclusion compounds of urea with bis(methyl ketone)s. *Chem. Mater.* **1996,** *8*, 1588-1591.
70. Hollingsworth, M. D.; Brown, M. E.; Hillier, A. C.; Santarsiero, B. D.; Chaney, J. D., Superstructure control in the crystal growth and ordering of urea inclusion compounds. *Science* **1996,** *273*, 1355-1359.
71. Brown, M. E.; Hollingsworth, M. D., Stress-induced domain reorientation in urea inclusion-compounds. *Nature* **1995,** *376*, 323-327.
72. Hollingsworth, M. D.; Brown, M. E.; Dudley, M.; Chung, H.; Peterson, M. L.; Hillier, A. C., Template effects, asymmetry, and twinning in helical inclusion compounds. *Angew. Chem. Int. Ed.* **2002,** *41*, 965–969.
73. Crystal structure of 2,15-hexadecanedione/urea, unpublished work by Bo Wang, Michael E. Borwn, and Mark D. Hollingsworth.
74. Hollingsworth, M. D.; Peterson, M. L.; Rush, J. R.; Brown, M. E.; Abel, M. J.; Black, A. A.; Dudley, M.; Raghothamachar, B.; Werner-Zwanziger, U.; Still, E. J.; Vanecko, J. A., Memory and perfection in ferroelastic inclusion compounds. *Cryst. Growth. Des.* **2005,** *5*, 2100-2116.
75. Paul, I. C.; Curtin, D. Y., Thermally induced organic reactions in the solid state. *Acc. Chem. Res.* **1973,** *6*, 217-225.
76. Rothenberg, G.; Downie, A. P.; Raston, C. L.; Scott, J. L., Understanding solid/solid organic reactions. *J. Am. Chem. Soc.* **2001,** *123*, 8701-8708.
77. Halasz, I., Single-crystal-to-single-crystal reactivity: gray, rather than black or white. *Cryst. Growth. Des.* **2010,** *10*, 2817-2823.
78. Kaupp, G., Solid-state reactions, dynamics in molecular crystals. *Curr. Opin. Solid State Mater. Sci.* **2002,** *6*, 131-138.
79. Harada, J.; Nakajima, R.; Ogawa, K., X-ray diffraction analysis of photochromic reaction of fulgides: crystalline state reaction induced by two-photon excitation. *J. Am. Chem. Soc.* **2008,** *130*, 7085-7091.
80. Skoko, Z.; Zamir, S.; Naumov, P.; Bernstein, J., The thermosalient phenomenon. "Jumping crystals" and crystal chemistry of the anticholinergic agent oxitropium bromide. *J. Am. Chem. Soc.* **2010,** *132*, 14191-14202.
81. Sahoo, S. C.; Panda, M. K.; Nath, N. K.; Naumov, P., Biomimetic crystalline actuators: structure-kinematic aspects of the self-actuation and motility of thermosalient crystals. *J. Am. Chem. Soc.* **2013,** *135*, 12241-12251.
82. Maji, T. K.; Mostafa, G.; Matsuda, R.; Kitagawa, S., Guest-induced asymmetry in a metal-organic porous solid with reversible single-crystal-to-single-crystal structural transformation. *J. Am. Chem. Soc.* **2005,** *127*, 17152-17153.
83. Hollingsworth, M. D.; Swift, J. A.; Kahr, B., J. Michael McBride at 65 - an appreciation. *Cryst. Growth. Des.* **2005,** *5*, 2022-2035.
84. McBride, J. M.; Segmuller, B. E.; Hollingsworth, M. D.; Mills, D. E.; Weber, B. A., Mechanical stress and reactivity in organic solids. *Science* **1986,** *234*, 830-835.
85. Hollingsworth, M. D.; McBride, J. M., Photochemical mechanism in single crystal: FTIR studies of diacyl peroxides. *Advances in Photochemistry*, Vol. 15, Volman, D. H., Hammond, G. S., and Gollnick, K. eds., Wiley & Sons: New York, 1990; pp. 279-379.
86. McBride, J. M., The role of local stress in solid-state radical reactions. *Acc. Chem. Res.* **1983,** *16*, 304-312.
87. Hollingsworth, M. D.; McBride, J. M., Infrared studies of long-range stress in solid-state peroxide photoreactions. *Mol. Cryst. Liq. Cryst.* **1988,** *161*, 25-41.
88. Hollingsworth, M. D.; Harris, K. D. M.; Jones, W.; Thomas, J. M., ESR and X-ray

diffraction studies of diacyl peroxides in urea and aluminosilicate hosts. *J. Incl. Phenom.* **1987,** *5*, 273-277.
89. Bhardwaj, P.; Singh, S., Pressure induced structural phase transitions-a review. *Cent. Eur. J. Chem.* **2012,** *10*, 1391-1422.
90. Shekar, N. V. C.; Rajan, K. G., Kinetics of pressure induced structural phase transitions - a review. *Bull. Mater. Sci.* **2001,** *24*, 1-21.
91. Toudic, B.; Aubert, F.; Ecolivet, C.; Bourges, P.; Breczewski, T., Pressure-induced lock-in in an aperiodic nanoporous crystal. *Phys. Rev. Lett* **2006,** *96*, 145503.
92. Hollingsworth, M. D.; Werner-Zwanziger, U.; Brown, M. E.; Chaney, J. D.; Huffman, J. C.; Harris, K. D. M.; Smart, S. P., Spring-loading at the molecular level: relaxation of guest-induced strain in channel inclusion compounds. *J. Am. Chem. Soc.* **1999,** *121*, 9732-9733.

Chapter 2. "Self-compression" in phase transitions of 2,8-nonanedione/urea

2.1. Earlier work on 2,8-nonanedione/urea

Crystals of 2,8-nonanedione/urea have been studied previously using X-ray film techniques.[1, 2] In 1996, Hollingsworth and coworkers measured the guest repeat length (c_g) of 2,8-nonanedione/urea to be 13.57(5) Å from X-ray measurements.[1] They proposed that this UIC has a commensurate phase with $4c_g' = 5c_h'$, but they stated that they could not exclude a structure with $9c_g' = 11c_h'$. AFM images of this UIC showed that the {001} face of the crystal was very rough.[1] In the same year, Brown and coworkers published infrared absorption (IR) spectra of this UIC. In the IR spectra, there is a broad peak at 1723 cm^{-1} (FWHM = 15 cm^{-1}), which indicates different environments for the carbonyl groups of the guest.[2]

Synchrotron work on this UIC was first conducted at APS beamline 14-BM-C in 2012. From the X-ray oscillation images, a sequence of intriguing phase transitions was observed. In order to rationalize the phase transition behavior, a "self-compression" mechanism was proposed. This 1-D channel system serves as a perfect model to study the effect of stress in solid-state transformations.

To substantiate the "self-compression" mechanism, synchrotron X-ray studies on 2,8-nonanedione/urea, 2,8-nonanedione/urea-d_4, mixed crystals of 2,8-nonanedione:2-nonanone/urea, and 4,4'-oxybis(2-butanone)/urea were conducted. Data analyses of these synchrotron studies are described in this chapter. In addition, experiments involving the low-temperature growth and preparation of crystals of 2,8-nonanedione/urea, and the procedures for solving its crystal structure are presented here.

2.2.1. Synchrotron studies of 2,8-nonanedione/urea grown above 265 K

The DSC trace of crystals of 2,8-nonanedione/urea shows broad exothermic phase transitions at 260.6 K (ΔH = -0.8 J/g) and 214.6 K (ΔH = -0.3 J/g) on the cooling curve, as shown in Figure 2.2.1.1.[3] The corresponding endotherms occurred at peak positions of 268.5 K (ΔH = 4.4 J/g) and 222.8 K (ΔH = 0.2 J/g) in the heating curve. In synchrotron studies conducted at the Advanced Photon Source (APS) at Argonne National Laboratory on crystals of 2,8-nonanedione/urea grown above 265 K, an intriguing series of phase transitions was observed. There are at least four phases, with three phase transitions being inferred from the X-ray data.

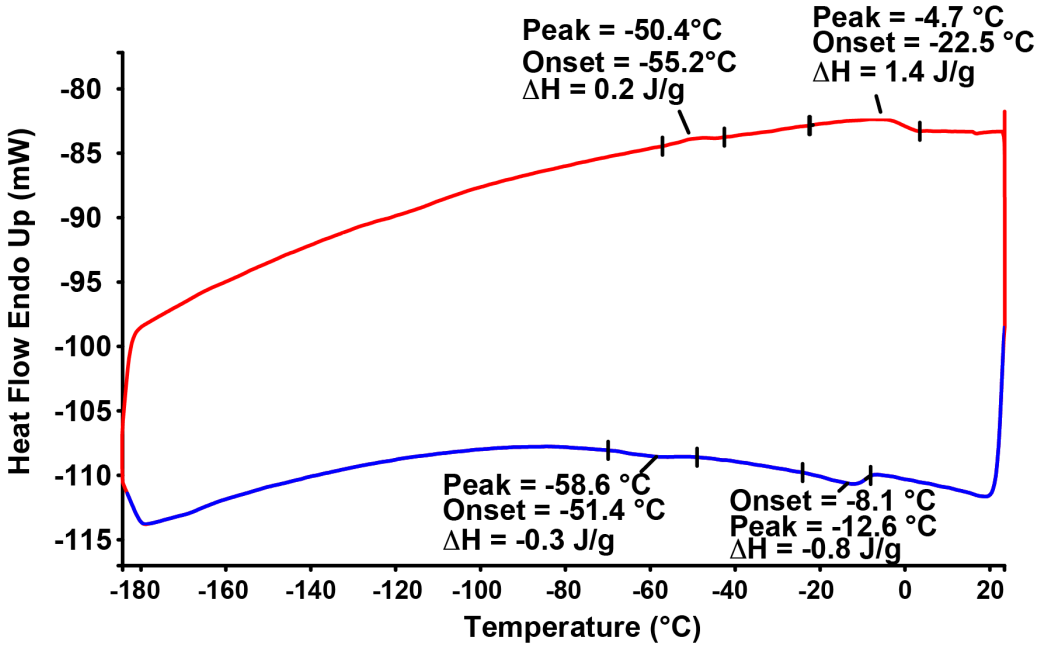

Figure 2.2.1.1. DSC trace of 2,8-nonanedione/urea. The blue line is for the cooling scan, and the red line is for the heating scan. The scan rate is 20 K/min, and the scan ranges were from 298 K to 88 K and 88 K to 298 K. Exothermic phase transitions were observed at peak position of 260.6 K and 214.6 K on the cooling curve. The corresponding endotherms occurred at peak positions of 268.5 K and 222.8 K on the heating curve.[3]

In order to establish the unit cell parameters of this UIC, 1619 host reflections from a synchrotron X-ray dataset of 2,8-nonanedione/urea were used. The data was collected using an ADSC Quantum 315R CCD detector with a 360º phi rotation (1º frames, detector distance = 200.0 mm, λ = 0.97870 Å).[4] The hexagonal unit cell parameters were determined to be ***a*** = ***b*** = 8.232(2) Å, ***c*** = 11.022(2) Å at 290.8 K (290.0 K reading calibrated).[5] Based on the systematic absences of $l \neq 6n$ for the (0 0 *l*) layer line, and a successful structure solution of the host structure (Figure 2.2.1.2), the space group of the host was uniquely identified as $P6_122$. The host structure was solved isotropically (discussed in Appendix 5.1.1). The hexagonal channel can be treated in either a hexagonal setting or an orthorhombic setting. In this hexagonal phase: $\boldsymbol{a}_h = \boldsymbol{b}_h$, (the subscript "h" indicates a hexagonal setting), and $\boldsymbol{a}_o = \boldsymbol{b}_o/\sqrt{3}$ (the subscript "o" indicates an orthorhombic setting). When a ferrodistortive ferroelastic phase transition occurs, $\boldsymbol{a}_o \neq \boldsymbol{b}_o/\sqrt{3}$.

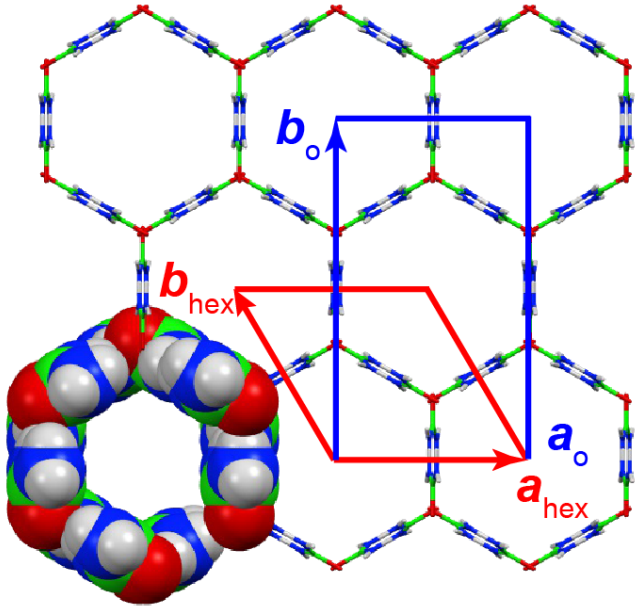

Figure 2.2.1.2. Channel axis view (along ***c***) of the host structure of 2,8-nonanedione/urea at 290.8 K.[4] The red arrows show the hexagonal axes, and the blue arrows show the orthorhombic axes.

A 60° X-ray oscillation image at 289.6(3) K is shown in Figure 2.2.1.3 (see discussion of channel axis oscillation images in Section 1.1). After unwarping, the profile of the (-1 0 *l m*)$_h$ layer line (using a hexagonal basis) was fit with the FibonacciBuild script for Matlab R2014.[6] In the unwarping process using WxDiff,[7] data obtained from a flat detector was transformed so that it matches that of a cylindrical detector (as in an oscillation image on a Weissenberg camera).

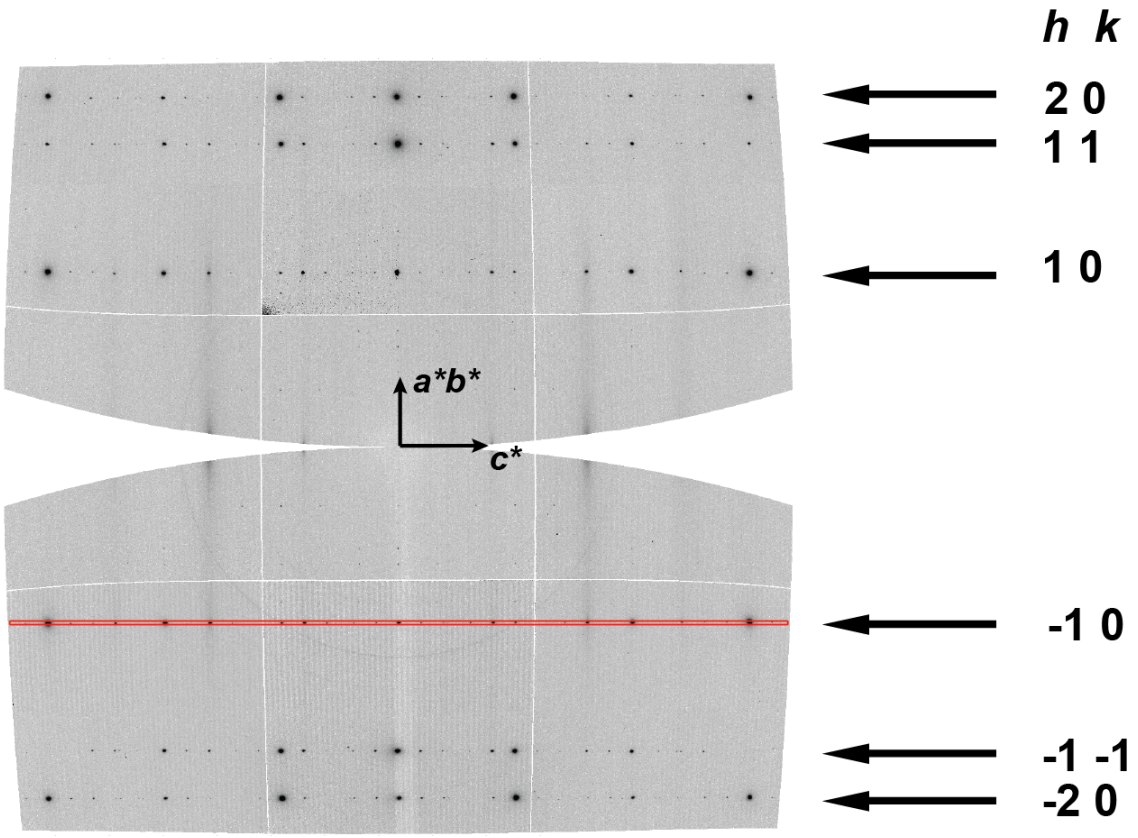

Figure 2.2.1.3. Unwarped synchrotron oscillation image of 2,8-nonanedione/urea at 289.3(3) K. The measurement was taken on APS beamline 14-BM-C with d = 500.0 mm, φ = 0-60°, exposure = 10 s, and λ = 0.97870 Å. Because there is no distortion observed in the ***a*b**** plane, this frame shows that the crystal has hexagonal metric symmetry, which is supported by the crystal structure of the host. The analysis discussed in the text was based on the (-1 0 *l m*)$_h$ layer line, as shown by the red rectangle.[8]

As shown in Figure 2.2.1.4, using the host peaks at $(-1\ 0\ -3\ 0)_h$ and $(-1\ 0\ 3\ 0)_h$ as reference points, a least squares (l.s.) refinement of the misfit parameter (γ) using the peak positions indexed in the profile yielded a convergent value of 0.80768(7). Because the original data underwent a 10-fold interpolation prior to fitting, the standard error of the mean reported by the program was multiplied by the square root of 10 to account for this artificial increase in the number of data points. This treatment of standard error of the mean will be applied to all profile fits in the text below. Unfortunately, as a consequence of imperfect peak shape modeling (hence, heteroscedasticity due to the presence of non-noise residuals) there was an additional factor that inflated these errors by one or two orders of magnitude. This factor varies between individual fits and cannot easily be corrected.

These (inflated) misfit parameter errors of the mean represent the precision of the fit for that layer line. In addition, some variation in the misfit parameter is usually observed between layer lines, likely due to slight detector and crystal misalignment. These are on the order of ±0.0001 as seen in Figure 3.2.10.3, and are generally larger than the quoted precision for a specific layer line. However, when comparing relative peak positions on the same layer line, as is done for the majority of the analyses here, the precision of the fit is a better metric of the error, bearing in mind it is inflated. Throughout this dissertaton, unless otherwise stated, errors are reported as standard errors of the mean. The term e.s.d. refers to the standard deviation of the sample. Using the separations of the (-1 0 -3 0) and (-1 0 3 0) peaks during a temperature scan from 114.8 K to 291.5 K,[9] the thermal expansion along the channel axis can be described with

$$\boldsymbol{c} = 10.977(2) + 1.555(9) \times 10^{-4}\, T \text{ Å}.$$[10]

Using c_h = 11.022(2) Å (290.0 K) and $\gamma = c_h/c_g$ = 0.80768(7), c_g = 13.646(3) Å.

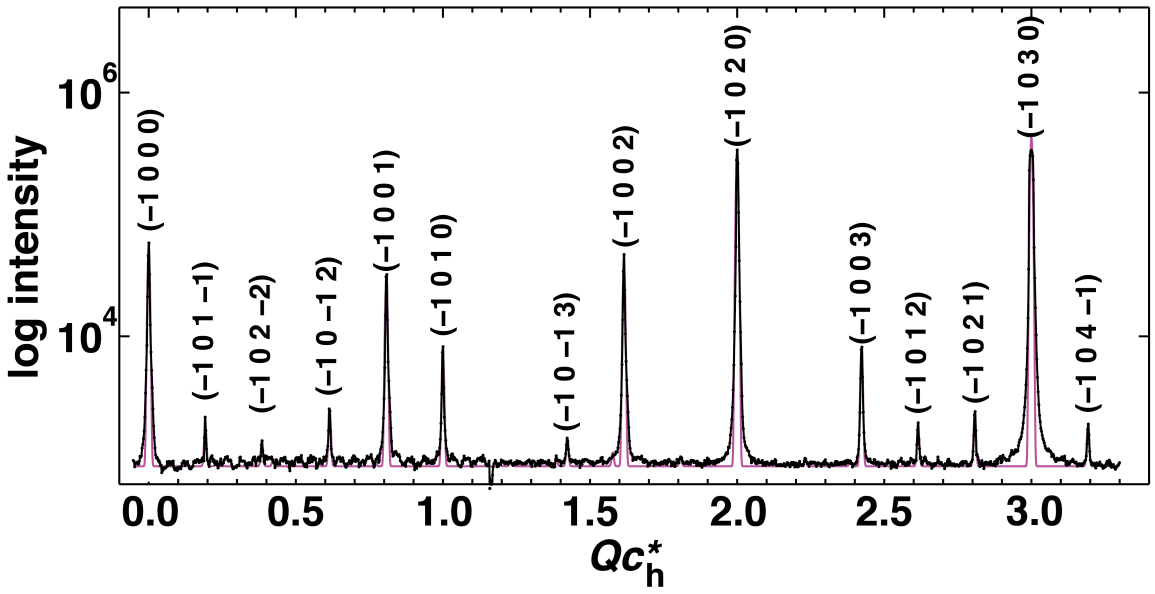

Figure 2.2.1.4. Profile of the (-1 0 *l* *m*)$_h$ layer line of the unwarped channel axis oscillation image of 2,8-nonanedione/urea at 289.3(3) K. The profile was fit as an incommensurate phase with γ = 0.80768(7). The measurement was made on APS beamline 14-BM-C with d = 500.0 mm, φ = 0-60°, exposure = 10 s, and λ = 0.97870 Å.[8]

Upon cooling from 290.0 K to 266.6(7) K, the X-ray patterns were essentially identical. The superspace group of incommensurate UICs is conventionally described by using the mean structure of the host urea subsystem. Thus, above 266.6(7) K, 2,8-nonanedione/urea is described by a four-dimensional superspace group $P6_122(00\gamma)$ (in this case γ = 0.80768(7)), which is the same as reported for many alkane/urea systems.[11, 12, 13] There are also weak diffuse layer lines perpendicular to ***c****, indicating displacive disorder of the guest along the ***c*** axis, as expected in an incommensurate structure.[1, 14] However, the appearance of guest Bragg peaks and satellites shows that the guests are ordered in local regions, and that there is intermodulation between host and the guest.[15] Since the guest reflections share the same lattice lines with the host

reflections along ***c****, this indicates that the offset (Δ_g) between guests in adjacent channels is 0 Å.[16] From above discussions, it is clear that, unlike most of the diketone UICs studied thus far, [1, 2, 17, 18] 2,8-nonanedione/urea is incommensurate above 266.6(7) K.

When the crystal was cooled below 266.6(7) K, a phase transition was observed in 2,8-nonanedione/urea. The X-ray oscillation image of the crystal at 246.6 (6) K is shown in Figure 2.2.1.5.[19] This oscillation image clearly shows that new layer lines have emerged, as the peaks are split in the ***a*b**** plane, which indicates that the urea channel is distorted away from hexagonal metric symmetry in the ***ab*** plane below the phase transition. During the phase transition, the Laue symmetry is lowered from hexagonal to orthorhombic. This distortion in the ***ab*** plane is a ferrodistortive ferroelastic phase transition, as the ordering of the guest has lowered the symmetry of the whole system. Ferroelastic phase transitions have been reported in a variety of alkane UICs,[20, 21, 22] and in one alkanedione UIC.[23] By measuring the distance between the $(2\ 0\ 1)_o$ and $(-2\ 0\ 1)_o$ peaks and between the $(0\ 4\ 1)_o$ and $(0\ -4\ 1)_o$ peaks, the evolution of the unit-cell parameters is obtained.[24] As shown in Figure 2.2.1.6, ***a*** increases and ***b*** decreases below the phase transition.

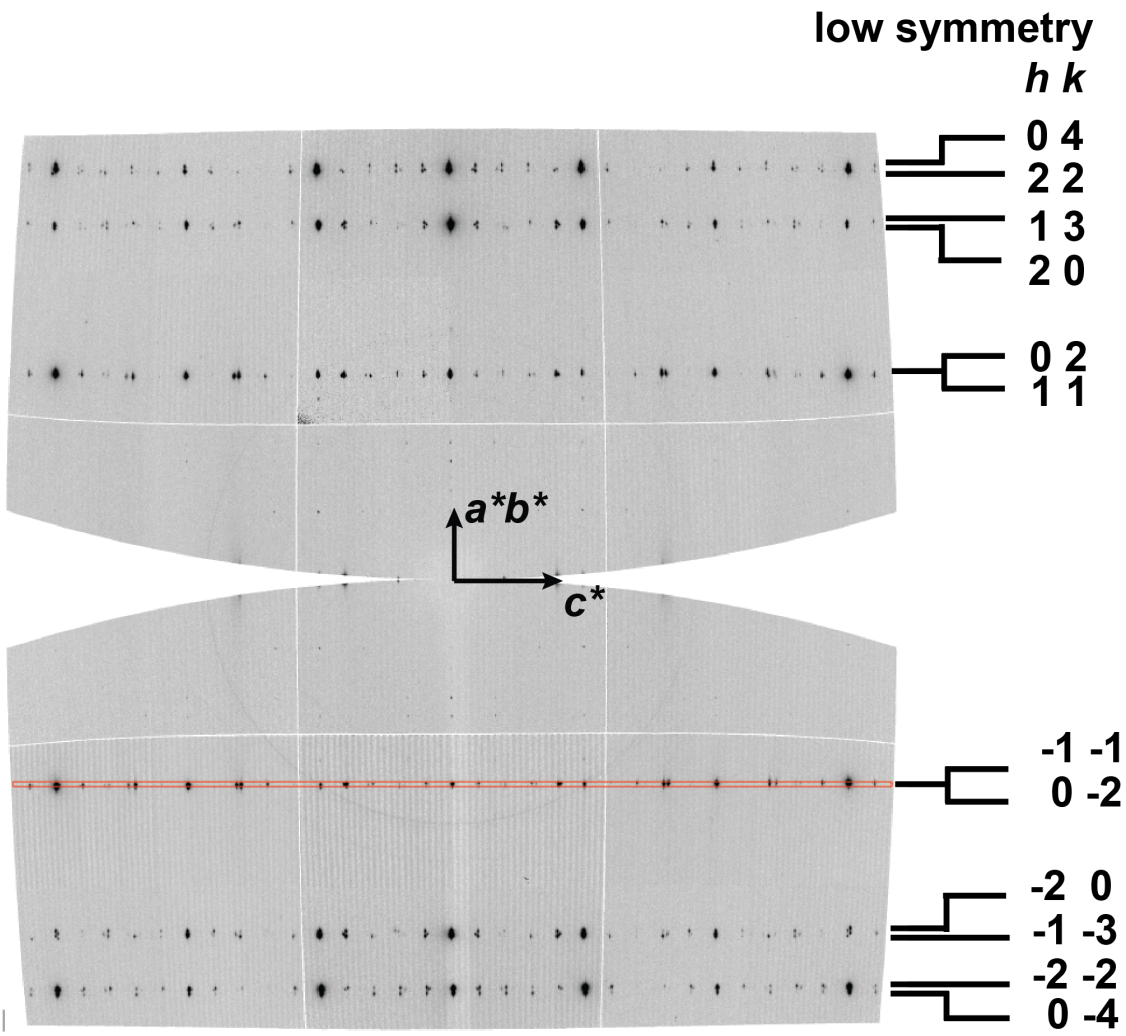

Figure 2.2.1.5. Unwarped synchrotron oscillation image of 2,8-nonanedione/urea taken on APS beamline 14-BM-C at 246.6(6) K with d = 500.0 mm, ϕ = 0-60°, exposure = 10 s, and λ = 0.97870 Å. The analysis discussed in the text was based on the (0 -2 *l m*)$_o$ and (-1 -1 *l m*)$_o$ layer lines, as shown by the red rectangle.[19]

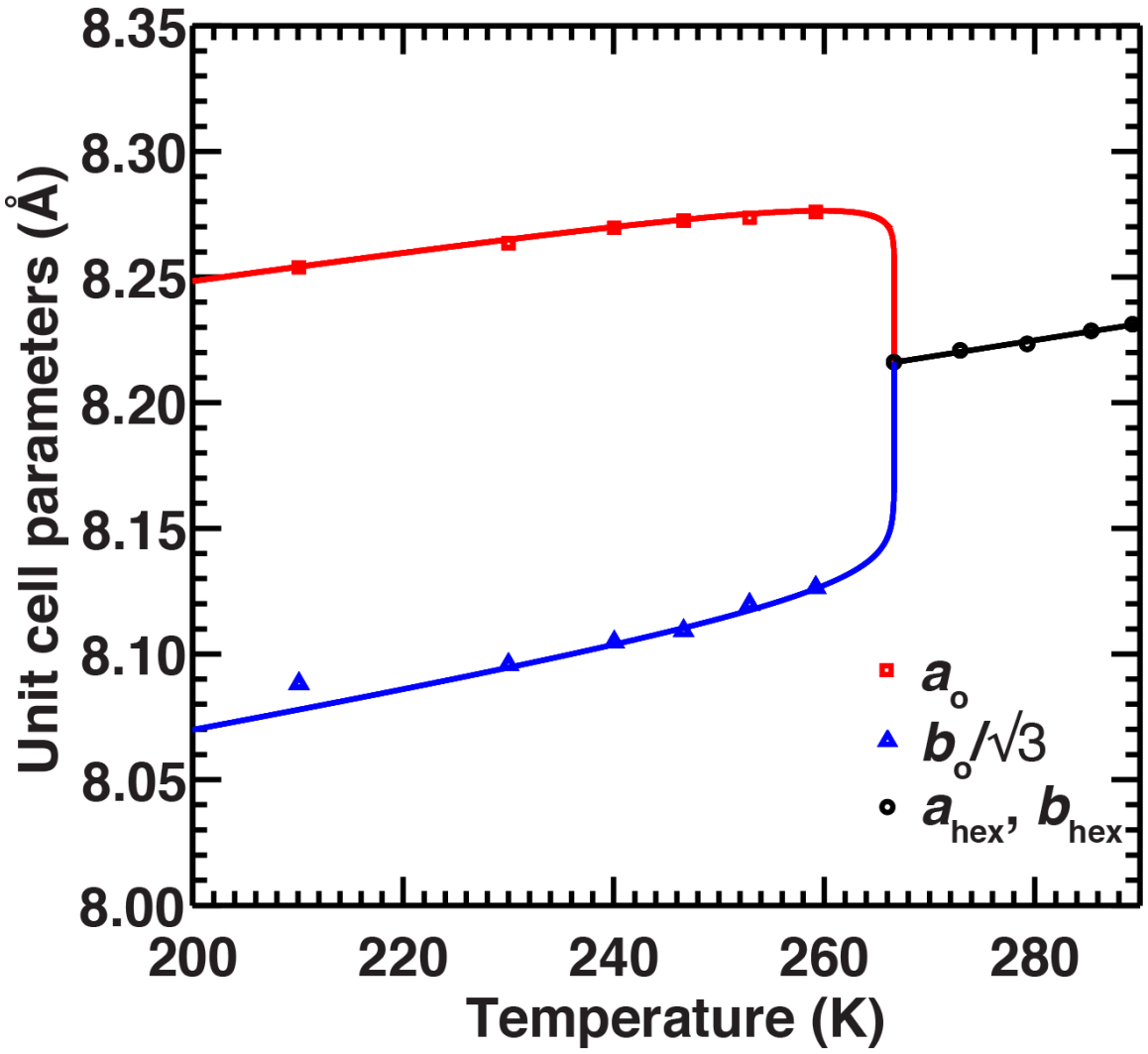

Figure 2.2.1.6. Temperature evolution of the unit-cell parameters of 2,8-nonanedione/urea. For the hexagonal phase (black circles), the cell parameters were measured from the $(\pm 1\ 0\ 0\ 0)_h$ peaks and fit to $\boldsymbol{a} = \boldsymbol{b} = 0.000658 \times T + 8.04$ Å. For the orthorhombic phase, the cell parameters $\boldsymbol{a}_o$ (red squares) and $\boldsymbol{b}_o$ (blue triangles) were measured from the positions of the $(\pm 2\ 0\ 1)_o$ and $(0\ \pm 4\ 1)_o$ peaks.[24] This measurement shows that the unit cell is distorted by 2.0% away from hexagonal metric symmetry in the ***ab*** plane at 210 K. The cell parameters below T_c were fit to $\pm A(T_c - T) + (0.000658 \times T + 8.04)$. The curvature of the fit around the phase transition (determined by β) is not certain due to a lack of data in the vicinity of the phase transition.

Doubling of the unit cell in the ***ab*** plane sometimes leads to "superstructure" layer lines with $h + k$ = odd. However, in this case, such superstructure layer lines were not observed. Only the layer lines with $h + k$ = even were observed. This indicates that in the phase transition, the symmetry has been lowered from a hexagonal lattice to a C-centered orthorhombic Bravais lattice, instead of a primitive orthorhombic lattice. The space group of the distorted phase ($C222_1$) is discussed together with the crystal structure in Section 2.3. From the $(0\ -2\ l\ m)_o$ and $(-1\ -1\ l\ m)_o$ layer line profile analysis (shown in Figure 2.2.1.7), we can see that the crystal is composed of two structures with different guest repeat lengths at 246.6(6) K. One of the components is a commensurate structure with $4c_g' = 5c_h'$ in which c_g' = 11.015(2)/0.8 = 13.769(2) Å. Here, c_h is calculated from $\boldsymbol{c}$ = 10.977(2) +1.555(9) × 10^{-4} T Å, as discussed earlier in this section. The other component is an incommensurate structure with γ = 0.8178, having c_g = 11.015(2)/0.81784(4) = 13.468(7) Å.

Since this UIC is incommensurate at room temperature and forms a commensurate structure below 266.6(7) K, it is clear that this is an incommensurate-to-commensurate type phase transition. During the phase transition, c_g elongates by 11.019(2) × (5/4 - 1/0.80768) = 0.131(2), using c_h at 266.6(7) K. Although a lock-in phase transition of *n*-hexadecane/urea was previously observed under 4 kbar of hydrostatic helium pressure at room temperature,[25] there are no reports in the literature of thermal lock-in phase transitions in UIC systems. As shown by the DSC data, the lowering in enthalpy (ΔH) is the driving force for the phase transition, most likely due to the formation of hydrogen bonds between host and guest molecules. Host-guest hydrogen bonding networks are exhibited by many UICs containing diketones.[1, 2, 17, 18] For example, in the case of 2,9-decanedione/urea, the guest actually coils and shortens by 0.4 Å to form hydrogen bonds between its carbonyls and the urea host.[1] The

presence of host-guest hydrogen bonds in this commensurate component with $4c_g' = 5c_h'$ is proven by the crystal structure of this phase (Section 2.3).

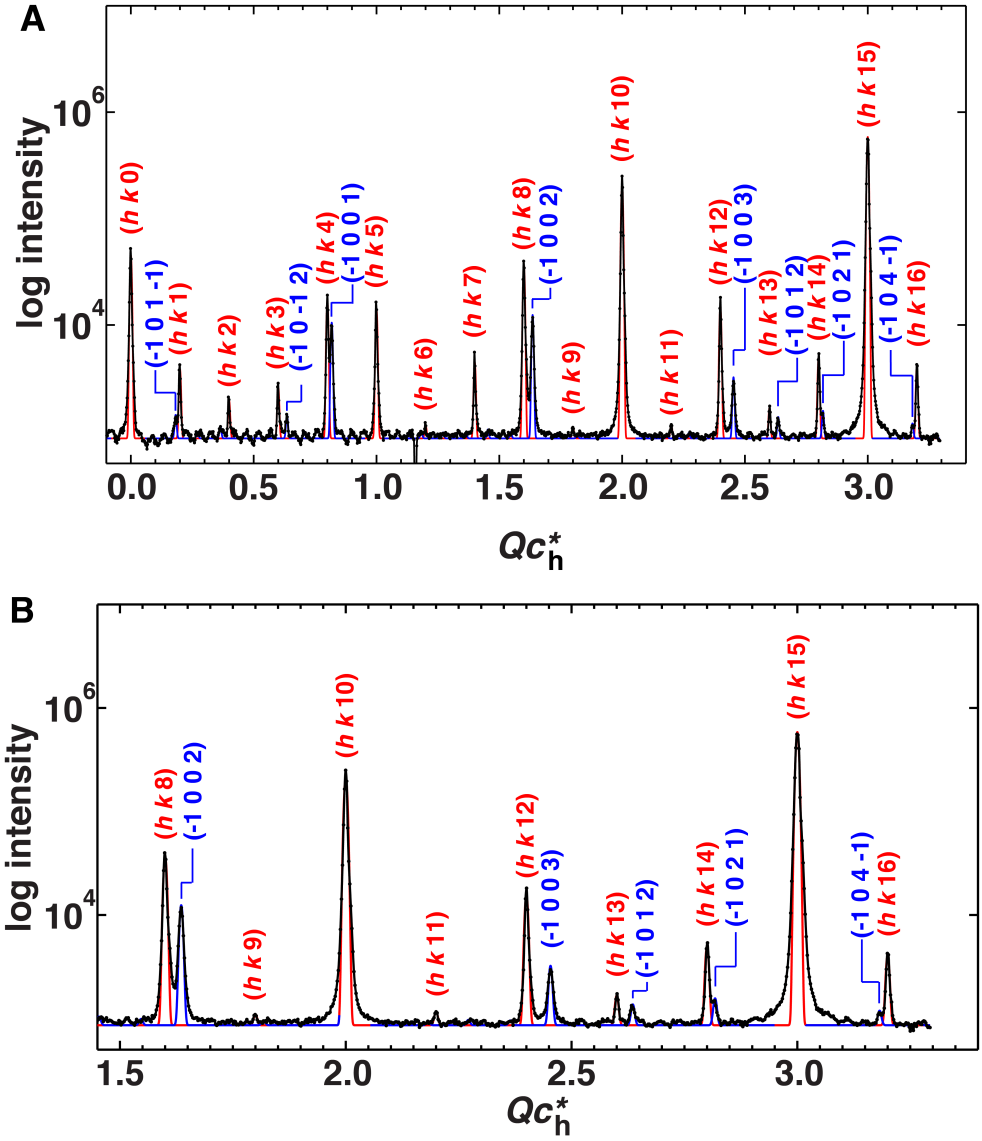

Figure 2.2.1.7. (A) Profile analysis of the (0 -2 *l m*)$_o$ and (-1 -1 *l m*)$_o$ layer lines in the unwarped synchrotron oscillation image of 2,8-nonanedione/urea at 246.6(6) K. The profile was modeled with a commensurate phase with $4c_g' = 5c_h'$ (red), and fit to an incommensurate phase (blue) with $\gamma = 0.81784(4)$. (B) An enlargement of the range $\boldsymbol{Qc}_h^*$ from 1.45 to 3.3. The measurement was made using a 60° ϕ rotation about the ***c*** axis at a detector distance of 500.0 mm on APS beamline 14-BM-C with $\lambda = 0.97870$ Å.[19]

Besides this incommensurate-to-commensurate phase transition, the system is further complicated with a second component, as shown by the profile analysis in Figure 2.2.1.7. In addition to the ferroelastically distorted commensurate structure analyzed above, an undistorted component coexists, as shown in Figure 2.2.1.8. The profile analysis in Figure 2.2.1.7 shows the undistorted component is incommensurate with a misfit parameter γ = 0.81784(4), c_g = 11.015(2)/0.81784(4) = 13.468(7) Å. This is 11.015(2) × (1/0.8077 - 1/0.8178) = 0.168(2) Å shorter than c_g using the room-temperature value of γ.

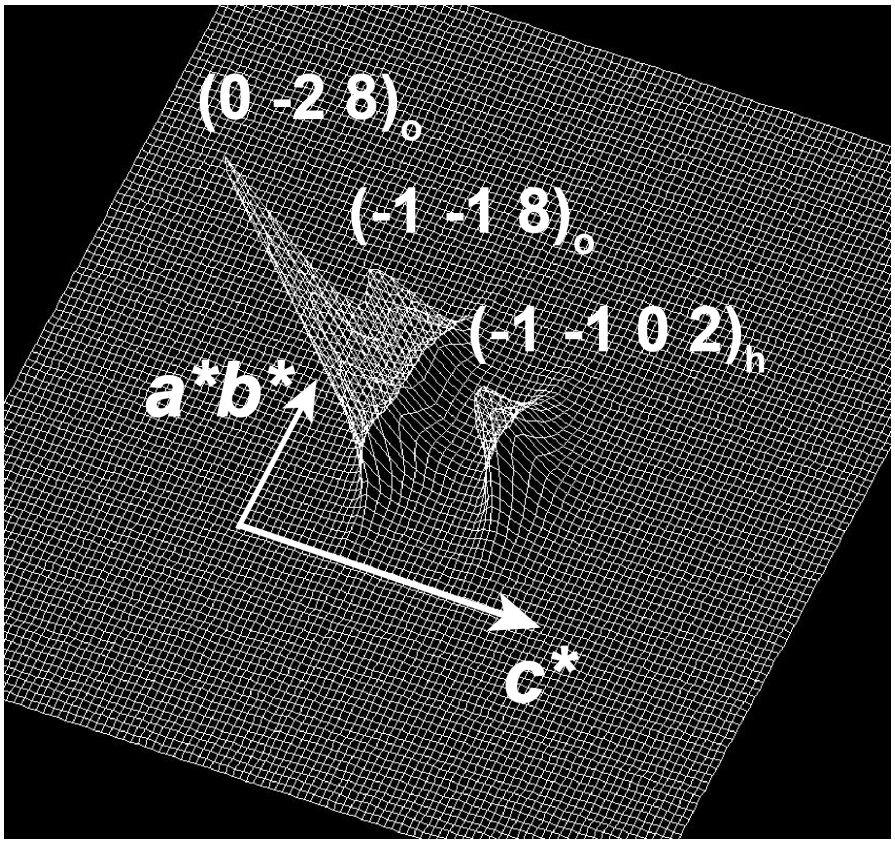

Figure 2.2.1.8. A 3-D view of a region of the oscillation image of 2,8-nonanedione/urea at 246.6(6) K.[19] The $(0\ -2\ 8)_o$ and $(-1\ -1\ 8)_o$ peaks show that the commensurate phase with $4c_g' = 5c_h'$ is ferroelastically distorted in the ***ab*** plane, whereas the $(-1\ -1\ 0\ 2)_h$ peak shows that the incommensurate phase is not distorted. The figure was generated with Adxv.[26]

To rationalize this shortened incommensurate phase, we have to consider that during the incommensurate-to-commensurate phase transition, the commensurate guest repeat elongates, while the host repeat remains essentially fixed. If the guest molecules in the emerging commensurate phase occupy more space along the channel axis, other guests in the same channel can either protrude from the ends of the crystal or be compressed. As shown in Figure 2.2.1.9 (A), if the guest molecules belonging to the incommensurate component start protruding from the ends of the channel below the phase transition, γ shoud not change from its room-temperature value. On the other hand, as shown in Figure 2.2.1.9 (B), if the incommensurate guest molecules are pinned by the commensurate phase with $4c_g' = 5c_h'$, regions that remain between commensurate areas will be compressed by the growth of the commensurate phase. As a result, those incommensurate regions will have larger γ than at room temperature, corresponding to smaller values of c_g. Moreover, as the elongated commensurate phase grows, the shortened regions would be further compressed. This is the proposed “self-compression” mechanism by which locked-in portions of the crystal compress those inbetween.

The synchrotron data strongly supports the self-compression mechanism. Profile analyses of the $(0\ -2\ l\ m)_o$ and $(-1\ -1\ l\ m)_o$ layer lines of oscillation images of 2,8-nonanedione/urea show that the undistorted incommensurate structure is continuously shortened between 266.6(7) K and 219.5(5) K (Table 2.2.1.1). The experimentally determined value of c_g of the undistorted component decreases linearly according to the relationship

$c_g = 11.26(4) + 0.009(2) \times T$ Å. (Figure 2.2.1.10 (A)).[27]

The linear regression has an R-value of 0.99857. Based on this measurement, the undistorted component is shortened by 13.646(4) - 13.225(14) = 0.421(15) Å at 219.5 K.

Accounting for the shrinking of the host repeat, the incommensurate component is compressed by 11.012(2) × (1/0.8077 - 1/0.8326) = 0.408(2) Å between 266.6(7) and 219.5(5) K via self-compression.

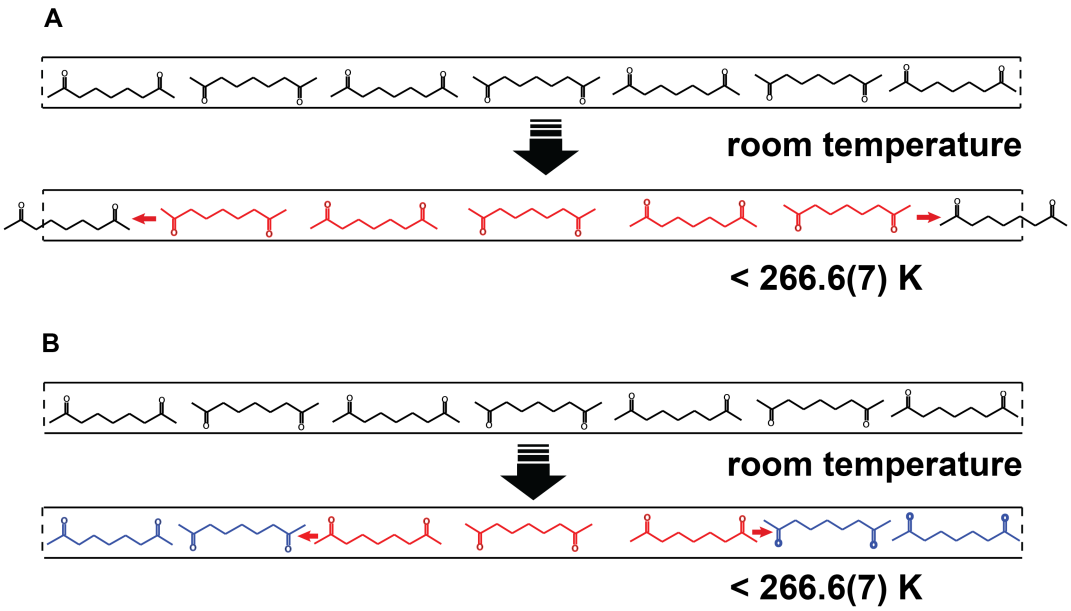

Figure 2.2.1.9. A schematic drawing of two possible mechanisms during cooling through the lock-in phase transition. (A) As the temperature is lowered and the commensurate phase grows, guests in the same channel could protrude from the ends of the host channel. Red molecules are those that have elongated to fit $4c_g' = 5c_h'$. (B) During cooling, regions between elongated commensurate guests (red) are compressed, as indicated by blue molecules.

It is noteworthy that as c_g of the incommensurate phase shrinks from 13.646 to 13.255 Å upon cooling, there are no other lock-in transitions to commensurate structures that would fit in that range. In particular, the graph of c_g versus temperature (Figure 2.2.1.10 (A)) contains no plateau for a commensurate phase with $9c_g' = 11c_h'$ (γ = 0.81818, c_g' = 13.46 Å at 246.6 K) even though this phase should have a good structural relationship between the host and the guest, where nine guest molecules fit in one unit cell spanning

the length of eleven turns of the urea helix. A threefold screw axis would be possible in this structure, with the asymmetric unit containing three guest molecules, or half that number, if there were a twofold axis perpendicular to the channel axis. See Section 2.2.9 below for a successful isolation of this phase using an analog of 2,8-nonanedione as guest. The evolution of peak positions and intensities through the lock-in phase transition is demonstrated in Figure 2.2.1.10 (B) for the $(0\ -2\ l\ m)_o$ and $(-1\ -1\ l\ m)_o$ layer lines, created using the stacked_plot script for MATLAB R2014.[28]

Temperature (K)	c_h (Å), SEM = 0.002	γ of the undistorted phase	c_g (Å)
289.3	11.022	0.8077(2)	13.646(4)
285.3	11.021	0.8075(2)	13.649(4)
279.3	11.020	0.80750(14)	13.647(3)
272.9	11.019	0.8076(2)	13.645(4)
266.6	11.018	0.8077(2)	13.642(4)
259.2	11.017	0.8106(2)	13.591(4)
253.5	11.016	0.8141(2)	13.532(4)
246.6	11.015	0.8178(3)	13.469(6)
240.0	11.014	0.8212(4)	13.412(7)
235.0	11.013	0.8241(5)	13.364(9)
230.0	11.013	0.8271(6)	13.315(10)
225.3	11.012	0.8297(7)	13.272(12)
*219.5	11.011	0.8326(8)	13.225(14)
*215.0	11.011	0.8356(16)	13.18(3)
*210.1	11.010	0.8391(24)	13.12(4)
*205.4	11.009	0.8419(24)	13.08(4)
*201.4	11.008	0.8445(43)	13.04(7)
*197.6	11.008	0.8475(46)	12.99(7)
*193.8	11.007	0.8490(50)	12.96(7)
*189.3	11.006	0.8519(50)	12.92(7)
*185.8	11.006	0.8555(50)	12.86(7)
*181.5	11.005	0.8555(50)	12.86(7)
*178.2	11.005	0.8555(50)	12.86(7)
*169.1	11.003	0.8555(50)	12.86(7)
*155.3	11.001	0.8555(50)	12.86(7)
*139.2	10.999	0.8555(50)	12.86(7)
*124.5	10.996	0.8555(50)	12.85(7)
*110.7	10.994	0.8555(50)	12.85(7)

Table 2.2.1.1. Misfit parameter γ and c_g of the undistorted incommensurate phase of 2,8-nonanedione/urea as a function of temperature. The sequence was analyzed with profiles of the $(0\ -2\ l\ m)_o$ and $(-1\ -1\ l\ m)_o$ layer lines. *Data below 219.5 K shows complications from extra phases.[29] The values of γ obtained below 197.6 K were obtained by modeling the profile instead of fitting with a least squares routine. In each case, the errors were assigned to be 0.0005.

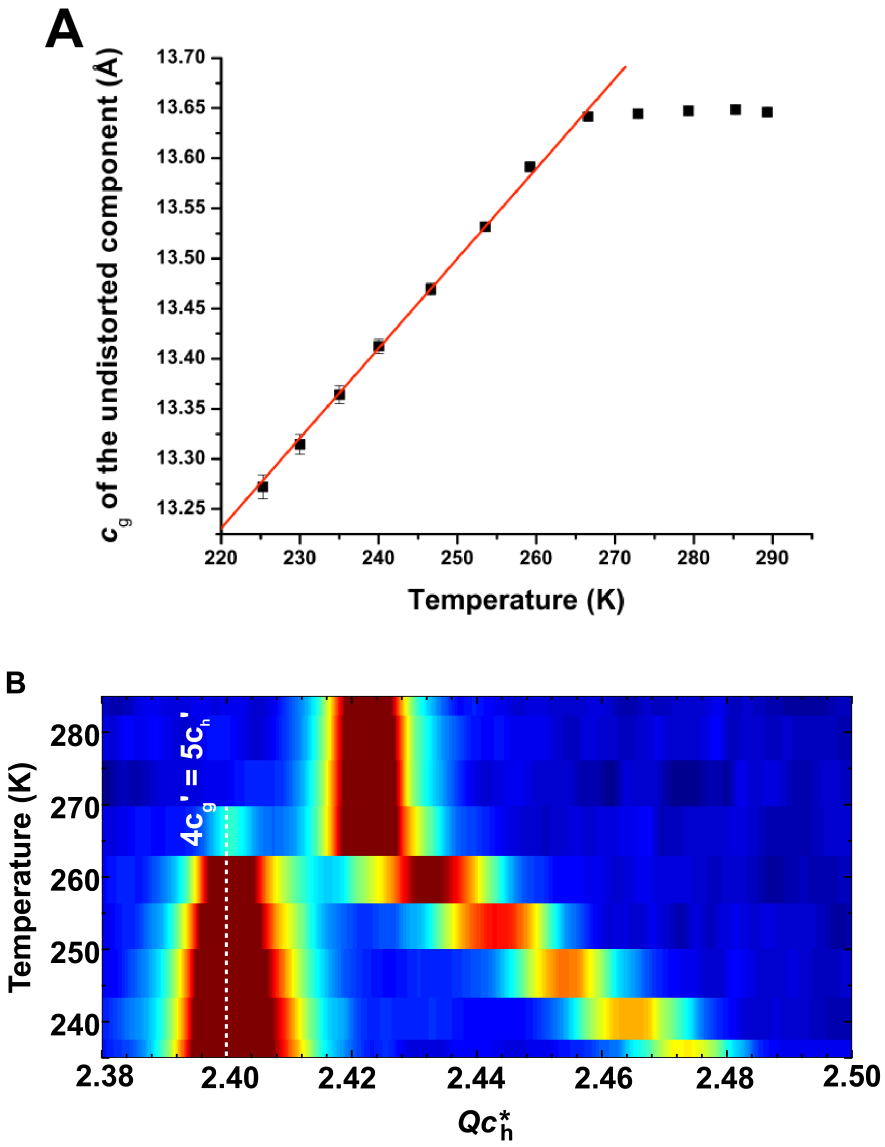

Figure 2.2.1.10. (A) Temperature evolution of the value of c_g of the undistorted incommensurate component (data from Table 2.2.1.1). This was determined from least squares fits of all the corresponding peaks in the (0 -2 *l m*)$_o$ and (-1 -1 *l m*)$_o$ layer lines. Measurements were made using 60° ϕ rotations about the ***c*** axis at a distance of 500.0 mm on APS beamline 14-BM-C with λ = 0.97870 Å.[29] (B) Temperature evolution of the overlapping (0 -2 *l m*)$_o$ and (-1 -1 *l m*)$_o$ layer lines of 2,8-nonanedione/urea upon cooling from 289.3 K to 235.0 K.[29] Intensities are on a logarithmic color scale, with red being most intense. The commensurate phase is labeled with $4c_g' = 5c_h'$.

In order to obtain an accurate phase transition temperature and to measure the evolution of peak intensities in the oscillation images of 2,8-nonanedione/urea, temperature scans (both heating and cooling) were repeated at beamline 14-BM-C. By comparing the temperatures from the Oxford Cryostream (Oxford Cryosystems Ltd.) at 100.0 K and 290.0 K with those from a calibrated thermocouple at the sample position, a temperature calibration with T_{actual} = 0.984861 × T_{cryo} + 5.24 was obtained.[5] These experiments are also useful for studies of deuterium isotope effects, which will be discussed in Section 2.2.2. As shown in Figure 2.2.1.11, normalized intensities from the sum of $(0\ -2\ 12)_o$ and $(-1\ -1\ 12)_o$ peaks from the $4c_g' = 5c_h'$ phase were fit to $A(T_c - T)^{\beta}$.[11, 13, 22] The phase transition temperatures were measured to be 265.4(5) K for cooling and 271.9(3) K for heating. The critical exponents, β, were measured to be 0.53(2) for cooling and 0.61(6) for heating. From this analysis, it can be shown that the phase transition exhibits hysteresis, with T_{c1} being 6.5(6) K higher during heating than it is while cooling.

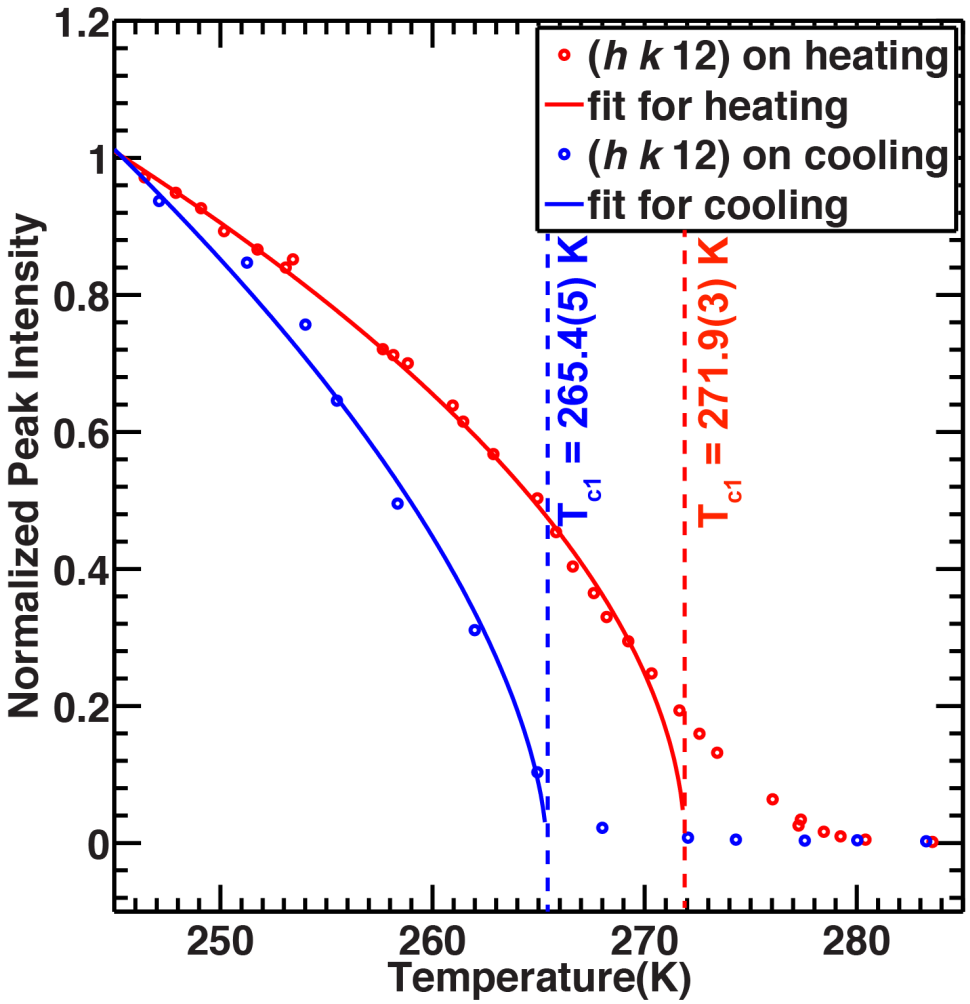

Figure 2.2.1.11. Normalized peak intensities as a function of temperature. The measurements were made from the sum intensities of the $(0\ -2\ 12)_o$ and $(-1\ -1\ 12)_o$ reflections from the phase with $4c_g' = 5c_h'$. Solid lines are fits to $A(T_c - T)^{\beta}$. Measurements were made using 60° ϕ rotations about the crystal ***c*** axis at a detector distance of 500.0 mm on APS beamline 14-BM-C with λ = 0.97870 Å.[9]

The self-compression mechanism that has been proposed to rationalize the phase transition of 2,8-nonanedione/urea during cooling from room temperature to 219.5(5) K is an astonishing example of how stress generated in a crystal can affect its

structure. An important question, however, is whether this is a general phenomenon. Upon further cooling, 2,8-nonanedione/urea shows that the self-compression associated with the lock-in transition to the phase with $4c_g' = 5c_h'$ is not an isolated incident.

A second phase transition was observed upon cooling the crystal further. In the first dataset described above (from the APS_A_098 series) this occurred below 219.5(5) K, as demonstrated by the emergence of new Bragg peaks in the oscillation images (Figure 2.2.1.12). As shown in Figure 2.2.1.12, at least four phases coexist in 2,8-nonanedione/urea at 215.0(5) K. There are two additional commensurate phases besides the one with $4c_g' = 5c_h'$, a phase with $9c_g' = 11c_h'$, and another phase with $14c_g' = 17c_h'$. As these two commensurate phases emerge, the compressed incommensurate phase is shortened even further, having $\gamma = 0.83561(15)$ at 215.0(5) K, equating to $c_g = 13.177(3)$ Å (using $c_h = 11.011(2)$ Å).

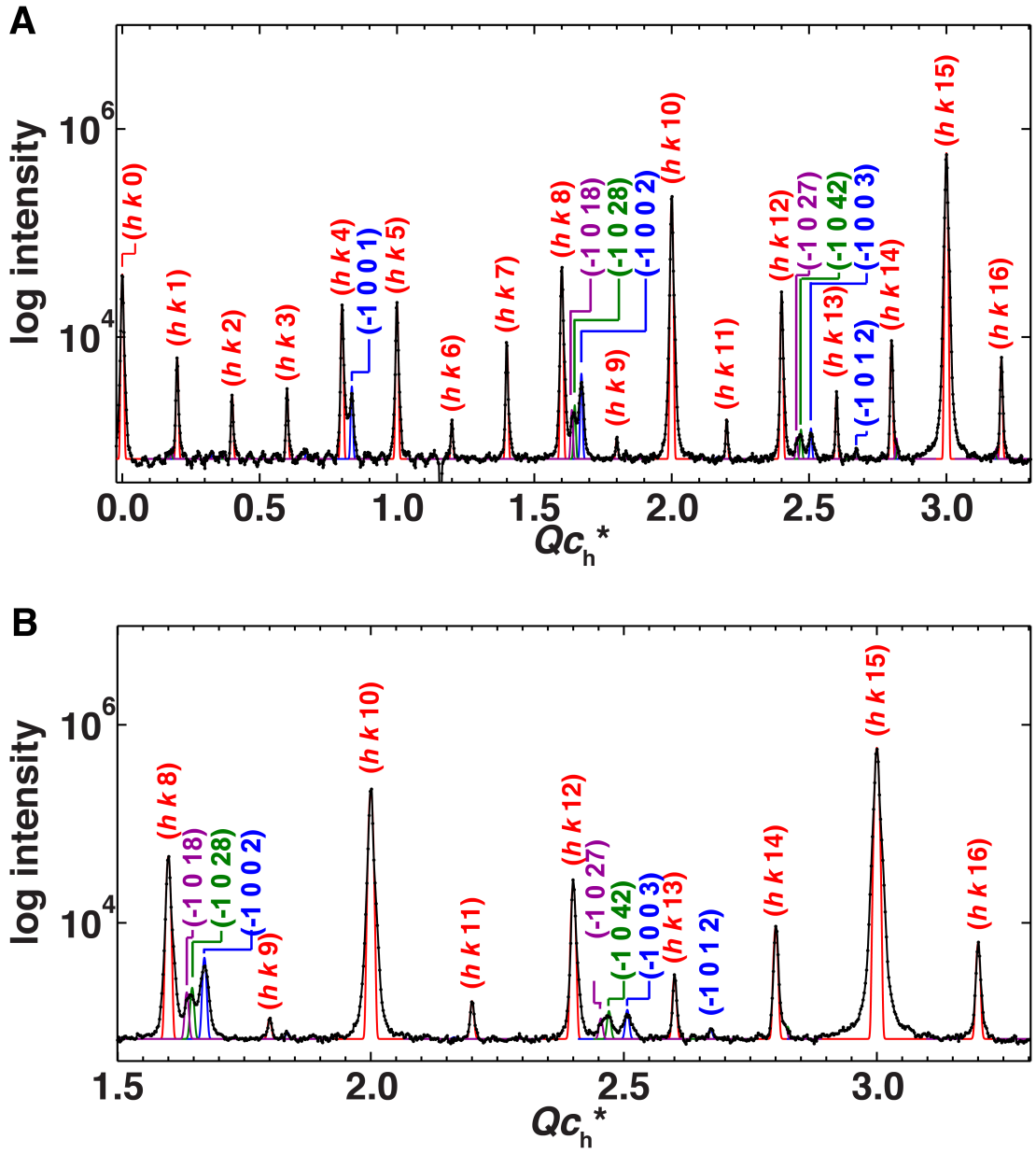

Figure 2.2.1.12. (A) Profile analysis of the (0 -2 *l m*)$_o$ and (-1 -1 *l m*)$_o$ layer lines of the unwarped synchrotron oscillation image of 2,8-nonanedione/urea at 215.0(5) K. The profile was modeled with three commensurate phases: $4c_g' = 5c_h'$ (red), $9c_g' = 11c_h'$ (purple), and $14c_g' = 17c_h'$ (green), and an incommensurate phase fit with γ = 0.83561(15) (blue). (B) An enlargement of the profile. The measurement was made using a 60° ϕ rotation about the crystal ***c*** axis at a detector distance of 500.0 mm on APS beamline 14-BM-C with λ = 0.97870 Å.[30]

The integrated intensities of the peaks in the $(0\ -2\ l\ m)_o$ and $(-1\ -1\ l\ m)_o$ layer lines from the emerging commensurate phases and the shortened phase are shown as a function of temperature in Figure 2.2.1.13 (A). The integrated intensity from $\boldsymbol{Qc_h^*}$ = 1.63 to 1.66 covers the $(h\ k\ 18)_o$ peak of the phase with $9c_g' = 11c_h'$ and the $(h\ k\ 28)_o$ peak of the phase with $14c_g' = 17c_h'$. The peak intensities for the phase with $4c_g' = 5c_h'$ and the compressed phase are estimated by peak fitting, instead of integration.[31]

Figure 2.2.1.13 (A) shows that the integrated intensities from the commensurate phases with $14c_g' = 17c_h'$ and $9c_g' = 11c_h'$ grew rapidly during cooling from 219.5 K to 190 K, whereas the intensity from the shortened structure diminished quickly.

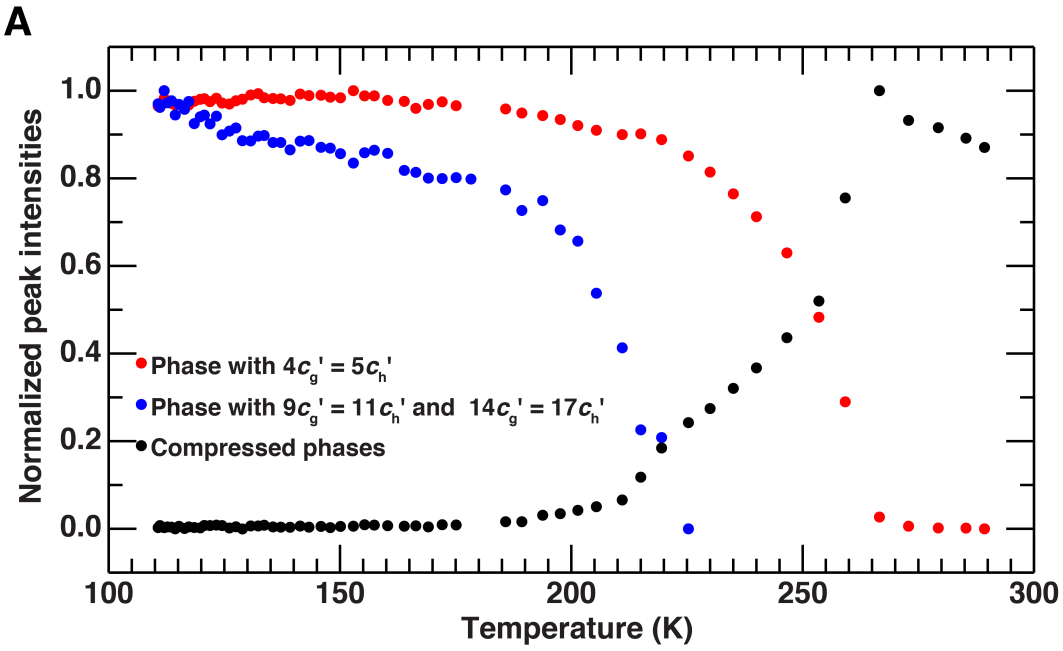

Figure 2.2.1.13. (A) Integrated peak intensities of the commensurate and incommensurate components of the $(0\ -2\ l\ m)_o$ and $(-1\ -1\ l\ m)_o$ layer lines of 2,8-nonanedione/urea between 289.3 K and 110.7 K. Measurements were made using 60° ϕ rotations about the crystal ***c*** axis at a detector distance of 500.0 mm on APS beamline 14-BM-C with λ = 0.97870 Å.[32]

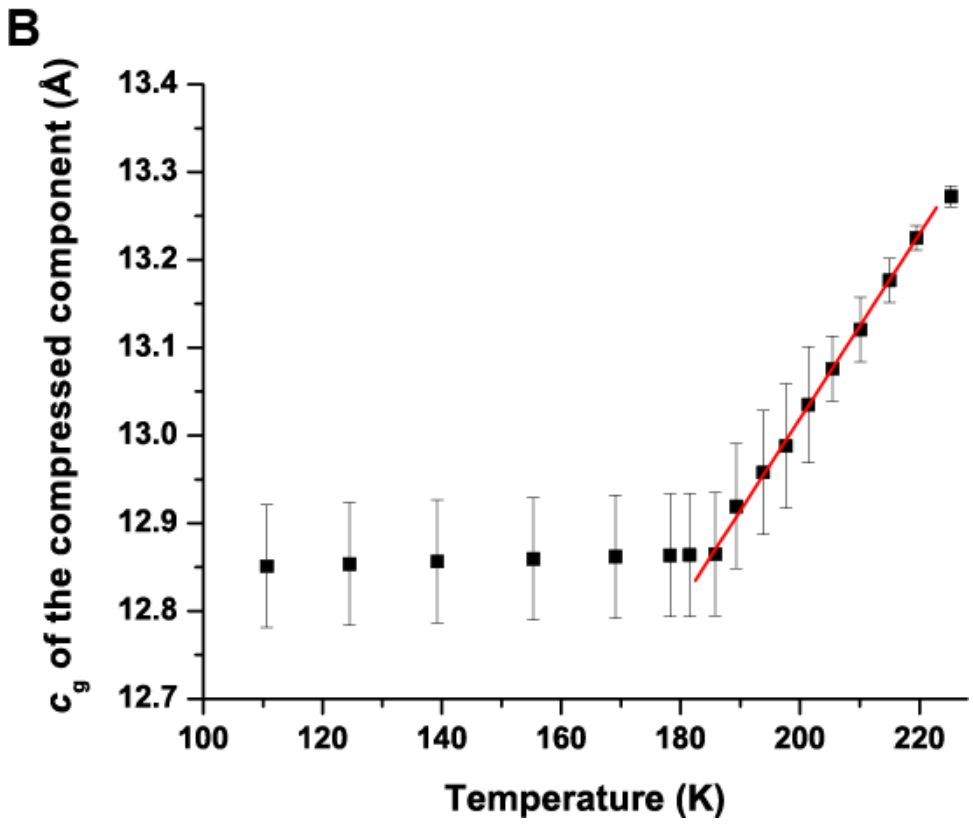

Figure 2.2.1.13. (B) Temperature evolution of c_g of the shortened component (data from Table 2.2.1.1). The value of c_g was determined from least squares fits of all the corresponding peaks in the (0 -2 *l m*)$_o$ and (-1 -1 *l m*)$_o$ layer lines. From 219.5 to 185.8 K, the linear least squares line for the plot of c_g versus temperature was c_g = 10.9(3) + 0.0105(12) × *T* Å.

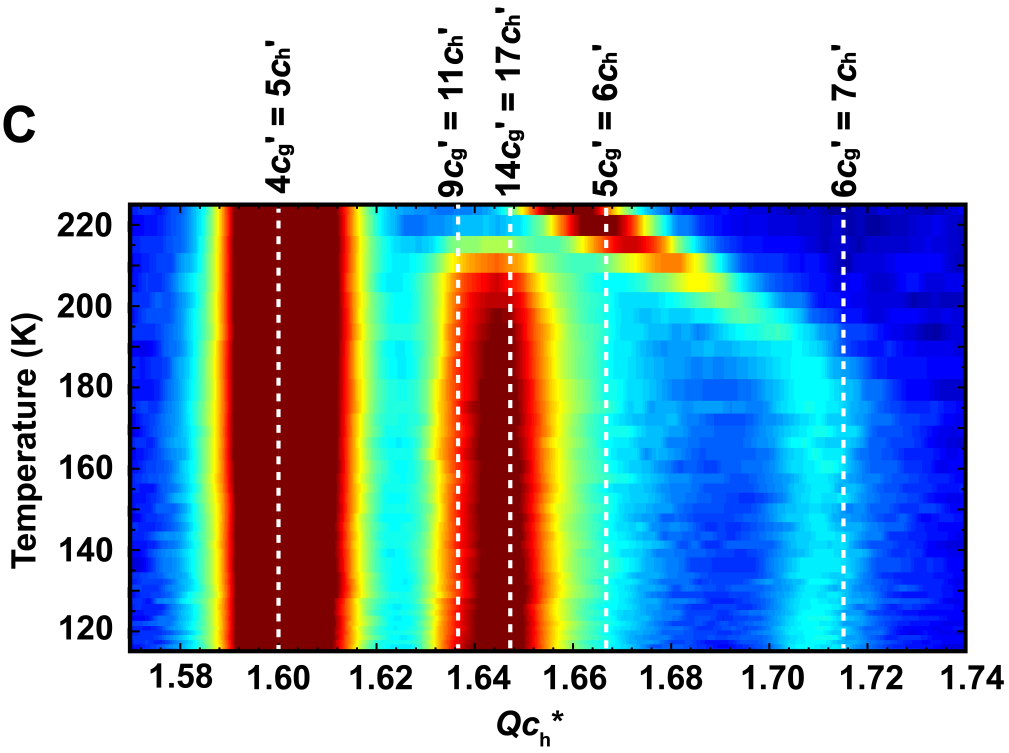

Figure 2.2.1.13. (C) Temperature evolution of the profile of the overlapping (0 -2 *l* *m*)$_o$ and (-1 -1 *l* *m*)$_o$ layer lines of 2,8-nonanedione/urea upon cooling from 220 K to 110 K.[29] Layer line profiles are shown on a logarithmic color scale, with red being most intense. Five commensurate phases are labeled with mc_g' = nc_h'.

By the formation of commensurate phases with 9c_g' = 11c_h' and 14c_g' = 17c_h', the shortened incommensurate phase was further compressed below these phase transitions. As shown in Figure 2.2.1.13 (B), c_g of the compressed phase can be fit to a linear relationship with c_g = 10.9(3) + 0.0105(12) × *T* Å (R = 0.99956) in the range 219.5 to 185.8 K. This slope is similar to that determined between 225 and 266.6 K (c_g = 11.26(4) + 0.009(2) × *T* Å, see Figure 2.2.1.10 (A)). Determining whether the two lock-in events produce different amounts of compression, as would be indicated by these two slopes being different, will require further investigation.

As shown in Figure 2.2.1.13 (B), the compressed phase stops contracting around

185.8(5) K. According to the profiles of the $(0\ -2\ l\ m)_o$ and $(-1\ -1\ l\ m)_o$ layer lines, the misfit parameter for this compressed component remains constant at $\gamma = 0.8555$ between 185.8 K and 110.7 K. Because of the small shrinkage of the host along the channel axis over this temperature range, this corresponds to a guest repeat that ranges from 12.865 Å at 185.8 K to 12.851 Å at 110.7 K.

The intensities of the phases with $9c_g' = 11c_h'$ and $14c_g' = 17c_h'$ increase by 29.4% from 185.8 K to 110.7 K (Figure 2.2.1.13 (A)). This raises the question of why the compressed phase stops shrinking below 185.8 K if the elongated commensurate phases keep growing when the crystal is cooled. One possibility for the plateau in the misfit parameter is that the compressed phase is actually a commensurate structure with $6c_g' = 7c_h'$. Such a phase would have a misfit parameter of $\gamma = 0.8571$ and a guest repeat that is only 0.025 Å shorter than the value of 12.865 Å at 185.8 K. Although this difference is well beyond the error limits that are expected with such high-resolution data, the relatively dense host-guest hydrogen bonding expected for a structure with $6c_g' = 7c_h'$ makes the prospect of a commensurate phase very appealing. In the structure of 2,7-octanedione/urea determined by Brown, et al.,[2] for example, each guest forms two hydrogen bonds with the host. The helical wheel diagram from that publication for a structure with $6c_g' = 7c_h'$ shows that odd-chain guests can most readily adopt either of two equivalent structures, as shown in Figure 2.2.1.14 (A) and (D), each of which has a relatively small torsion angle between the carbonyl groups. Since there is no apparent reason for the guest to stop shrinking just before it reaches such an ideal, commensurate structure, the measurement of the most compressed guest repeat at 185.8 K and below deserves carefuly scrutiny.

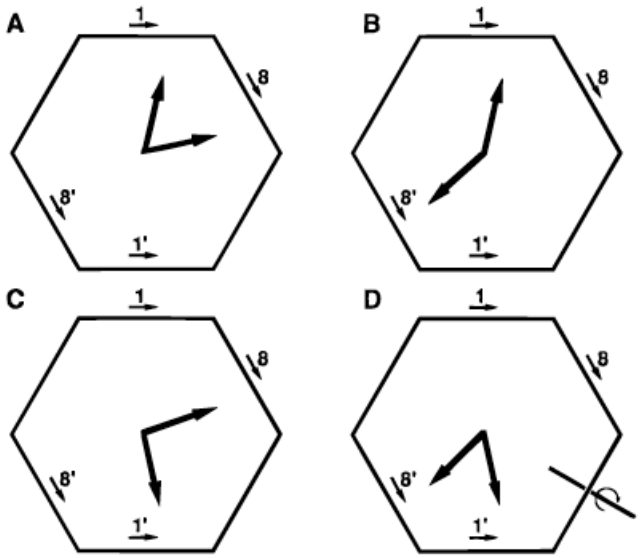

Figure 2.2.1.14. Helical wheel diagram of 2,7-octanedione/urea, which has a commensurate structure with $6c_g' = 7c_h'$.[2] Because it is an even-chain guest, 2,7-octanedione/urea adopts structure B, which has the largest torsion angle between C=O groups in the guest. Odd-chain guests such as the compressed 2,8-nonanedione should adopt smaller torsion angles. Note that diagrams A and C are related by a twofold axis perpendicular to the channel axis.

The intensities of the peaks from the most compressed state are weak below 190K, as shown in Figure 2.2.1.13 (A). In addition, there is a possibility that the (*h k* 0 2) peaks of the compressed phase might overlap with the (*h k* 29) peaks of the commensurate phase with $14c_g' = 17c_h'$. However, as shown in Figure 2.2.1.15, the temperature evolution of the peak intensities in the $(0\ -2\ l\ m)_o$ and $(-1\ -1\ l\ m)_o$ layer lines shows that the (0 -2 29) and (-1 -1 29) peaks for the phase with $14c_g' = 17c_h'$ are weak in the region of interest near $\mathbf{Q}c_h^* = 1.711$ below 219.5 K. This is best seen at 211.0 K, the dashed red profile has high intensities for the (0 -2 28) and (-1 -1 28) peaks of the phase with $14c_g' = 17c_h'$, but barely any intensities for the (0 -2 29) and (-1 -1 29) peaks of that phase.

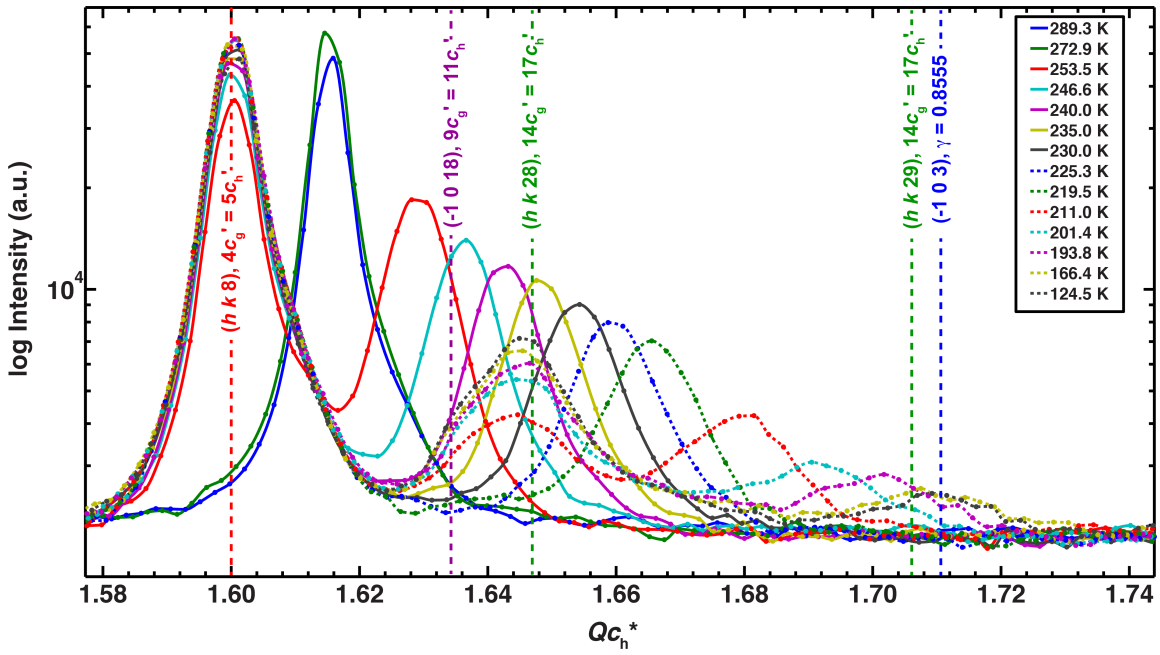

Figure 2.2.1.15. Temperature evolution of the peak intensities in the (0 -2 *l m*)$_o$ and (-1 -1 *l m*)$_o$ layer lines. Measurements were made using a 60° ϕ rotations about the crystal ***c*** axis at a detector distance of 500.0 mm on APS beamline 14-BM-C with λ = 0.97870 Å.[29]

The profile analysis of the (0 -2 *l m*)$_o$ and (-1 -1 *l m*)$_o$ layer lines of the unwarped synchrotron oscillation image of 2,8-nonanedione/urea at 185.8(5) K is shown in Figure 2.2.1.16. Besides the above-mentioned commensurate phases with $14c_g' = 17c_h'$ and $9c_g' = 11c_h'$, another commensurate phase with $5c_g' = 6c_h'$ was modeled to fit a weak shoulder at $\mathbf{Q}c_h^*$ = 1.667. Further evidence for this phase is given in Section 2.2.2 below. The most compressed phase was modeled with a misfit parameter of γ = 0.8555.

As mentioned above, the modeled misfit parameter for this most compressed phase is very close to a commensurate phase with $6c_g' = 7c_h'$ (γ = 0.8571), but analysis of structure layer lines have shown that it is best described with γ = 0.8555, which presents a conflict between the measurement and the above reasoning. The question of whether the most compressed state is commensurate with $6c_g' = 7c_h'$ can be resolved by

considering the possibility that the host repeat length (c_h) is slightly different in this most compressed phase, as discussed below.

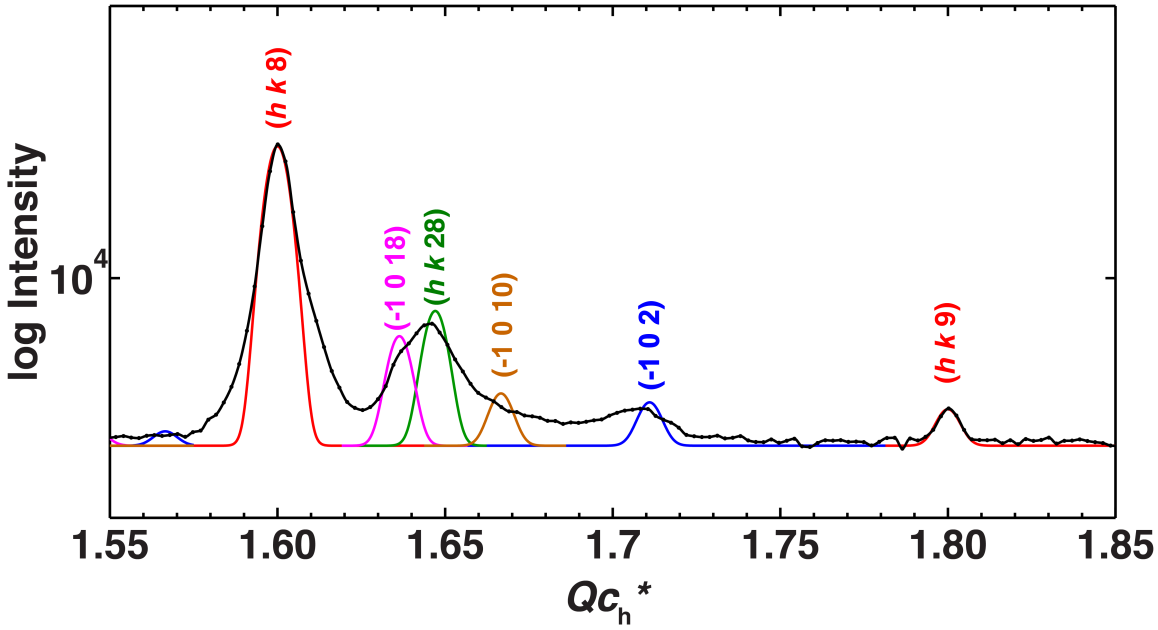

Figure 2.2.1.16. Profile analysis of the (0 -2 *l* *m*)$_o$ and (-1 -1 *l* *m*)$_o$ layer lines of the unwarped synchrotron oscillation image of 2,8-nonanedione/urea at 185.8(5) K. The profile was modeled with four commensurate phases: $4c_g' = 5c_h'$ (red), $9c_g' = 11c_h'$ (magenta), $14c_g' = 17c_h'$ (green), $5c_g' = 6c_h'$ (brown) and an incommensurate phase with $\gamma = 0.8555$ (blue). The measurement was made using a 60° ϕ rotation about the crystal ***c*** axis at a detector distance of 500.0 mm on APS beamline 14-BM-C with $\lambda = 0.97870$ Å.[33]

Over-exposed frames show that superstructure layer lines (*h* + *k* = odd, using the orthorhombic setting) are present only for the most compressed phase, as seen in Figure 2.2.1.17. Since superstructure layer lines for all of the phases except the most compressed phase are absent, this shows that apart from the most compressed phase, all of the structures are C-centered. The most compressed phase is the only primitive

phase. The c_g of the most compressed state can therefore be measured without overlap from the other phases by using profiles of the superstructure layer lines. Figure 2.2.1.17 (B) shows the profile of the (0 -1 *l m*)$_o$ layer line modeled as a commensurate phase with $6c_g' = 7c_h'$. The essentially perfect overlap of observed and calculated peak positions throughout the profile demonstrates that the compression stops at a plateau with a commensurate relationship $6c_g' = 7c_h'$. This enables the guest molecules to be related by a sixfold screw axis along the channel. However, this requires the host repeat to be 0.021 Å longer than that measured in other phases. Because no superstructure host peaks have been observed for this phase in the unlabeled material, this conclusion relies in part on the shrinkage of the host observed in 2,8-nonanedione/urea-d_4 (Section 2.2.2). Elongation of the host repeat by the guest has been observed in other UICs containing bis(methyl ketone)s. For example, both 2,15-hexadecanedione/urea and 1,10-diacetoxydecane/urea have commensurate structures with $1c_g' = 2c_h'$. In the former the guest shortens by 0.6 Å and c_h' = 11.0687 Å, while in the latter the guest only shortens by 0.08 Å and consequently c_h' = 10.9985 Å.[34]

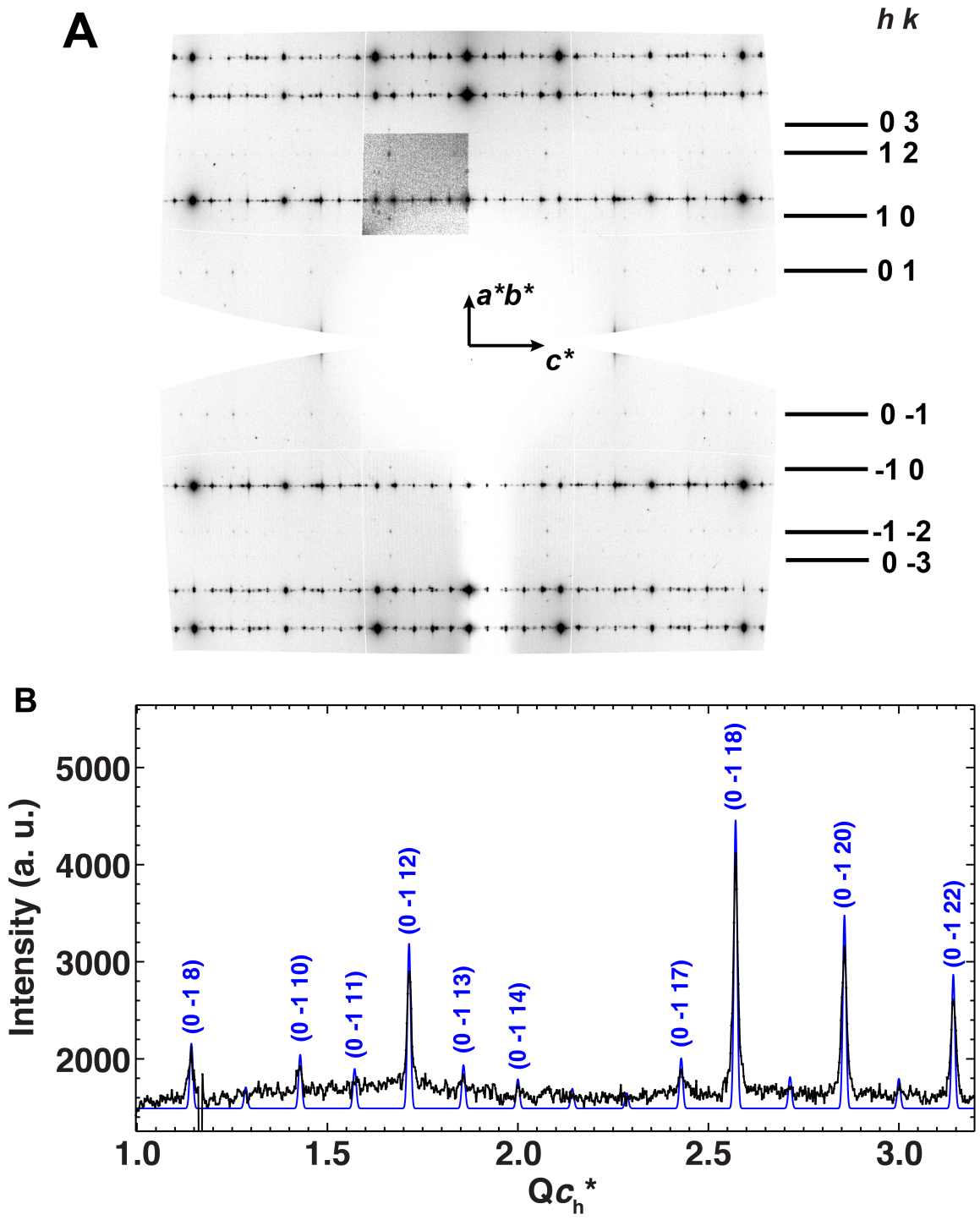

Figure 2.2.1.17. (A) Unwarped synchrotron oscillation image of 2,8-nonanedione/urea taken on APS beamline 14-BM-C at 108.0(1) K with d = 500.0 mm, ϕ = 0-60°, exposure = 10.0 s, and λ = 0.97870 Å, without attenuation.[35] (B) Profile of the (0 -1 *l m*)$_o$ layer line of this image modeled as a commensurate phase with $6c_g' = 7c_h'$.

To obtain accurate phase transition temperatures for the commensurate phases with $9c_g' = 11c_h'$ and $14c_g' = 17c_h'$, normalized peak intensities around $\mathbf{Q}c_h^* = 2.45$ were measured. For the phase with $9c_g' = 11c_h'$, intensities of the $(0\ -1\ 27)_h$ peaks were fit to $A(T_c - T)^{\beta}$, as shown in Figure 2.2.1.18 (A). The phase transition temperatures were measured to be 222.5(9) for cooling and 230.2(4) K for heating. The critical exponents, β, were measured to be 0.363(10) for cooling and 0.38(4) for heating. From this analysis, it can be shown that there is a hysteresis effect on the phase transition temperatures, as the T_c on heating is 7.7(10) K higher than it is on cooling. For the phase with $14c_g' = 17c_h'$, intensities of the $(0\ -2\ 42)_o$ and $(-1\ -1\ 42)_o$ peaks were also fit to $A(T_c - T)^{\beta}$, as shown in Figure 2.2.1.18 (B). The phase transition temperatures were measured to be 222.3(4) for cooling and 230.2(5) K for heating. The critical exponents, β, were measured to be 0.46(5) for cooling and 0.50(5) for heating. This phase also shows hysteresis as the T_c on heating is 7.9(6) K higher than it is on cooling. Comparison of these analyses shows that the commensurate phases with $9c_g' = 11c_h'$ and $14c_g' = 17c_h'$ have same phase transition temperatures. Notice that these two commensurate phases are not formed when the guest repeat first reaches the requisite length at around 240 K (see Table 2.2.1.1). It is proposed that the lock-ins are favored enthalpically, but not entropically.

The two lock-in phase transitions occurring at around 222 K on cooling produce further self-compression in the crystal. At 219.5(5) K, the compressed incommensurate phase has c_g = 13.225(14) Å and c_h = 11.011(2) Å. At that temperature the two commensurate phases would have c_g' = 13.371(2) Å for $14c_g' = 17c_h'$, and c_g' = 13.458(2) Å for $9c_g' = 11c_h'$. During lock-in, the guest repeat length extends by 0.146(2) Å to the phase with $14c_g' = 17c_h'$, and by 0.233(2) Å to the phase with $9c_g' = 11c_h'$. Then, as the two commensurate phases grow on cooling, the compressed phase is shortened

further until it reaches a commensurate plateau with $6c_g' = 7c_h'$ at 185.8(5) K. At that temperature the most compressed state has c_g' = 11.006(2)/0.8555 = 12.865(2) Å compared with c_g = 11.018(2)/0.8077 = 13.641(2) Å at 266.6(7) K. Therefore, between 266.6(7) and 185.8(5) K, c_g in the most compressed phase is reduced by 0.776(3) Å, of which 11.006(2) × (1/0.8077 - 1/0.8555) = 0.761(2) Å is via self-compression and (11.018(2) - 11.006(2))/0.8077 = 0.015(3) Å is due to thermal shrinking of the host.

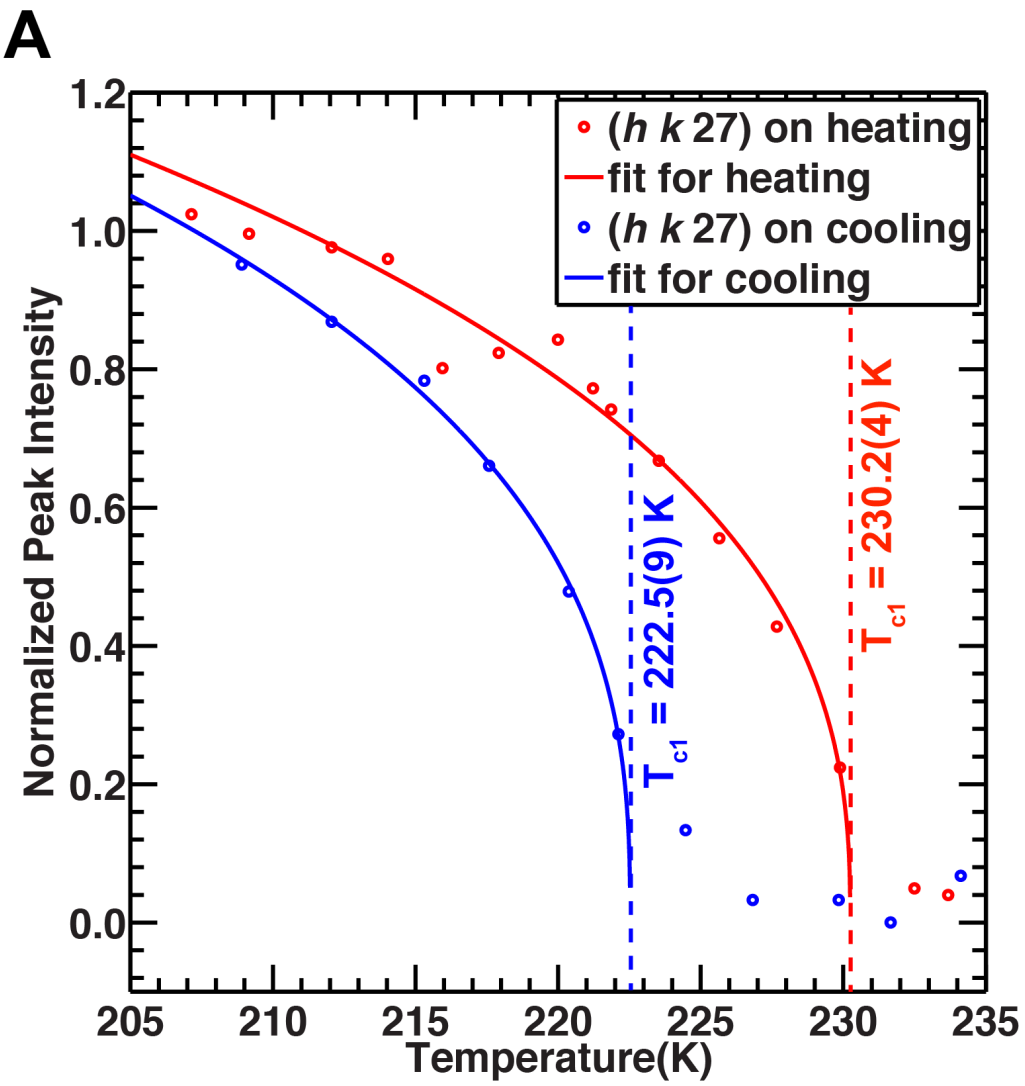

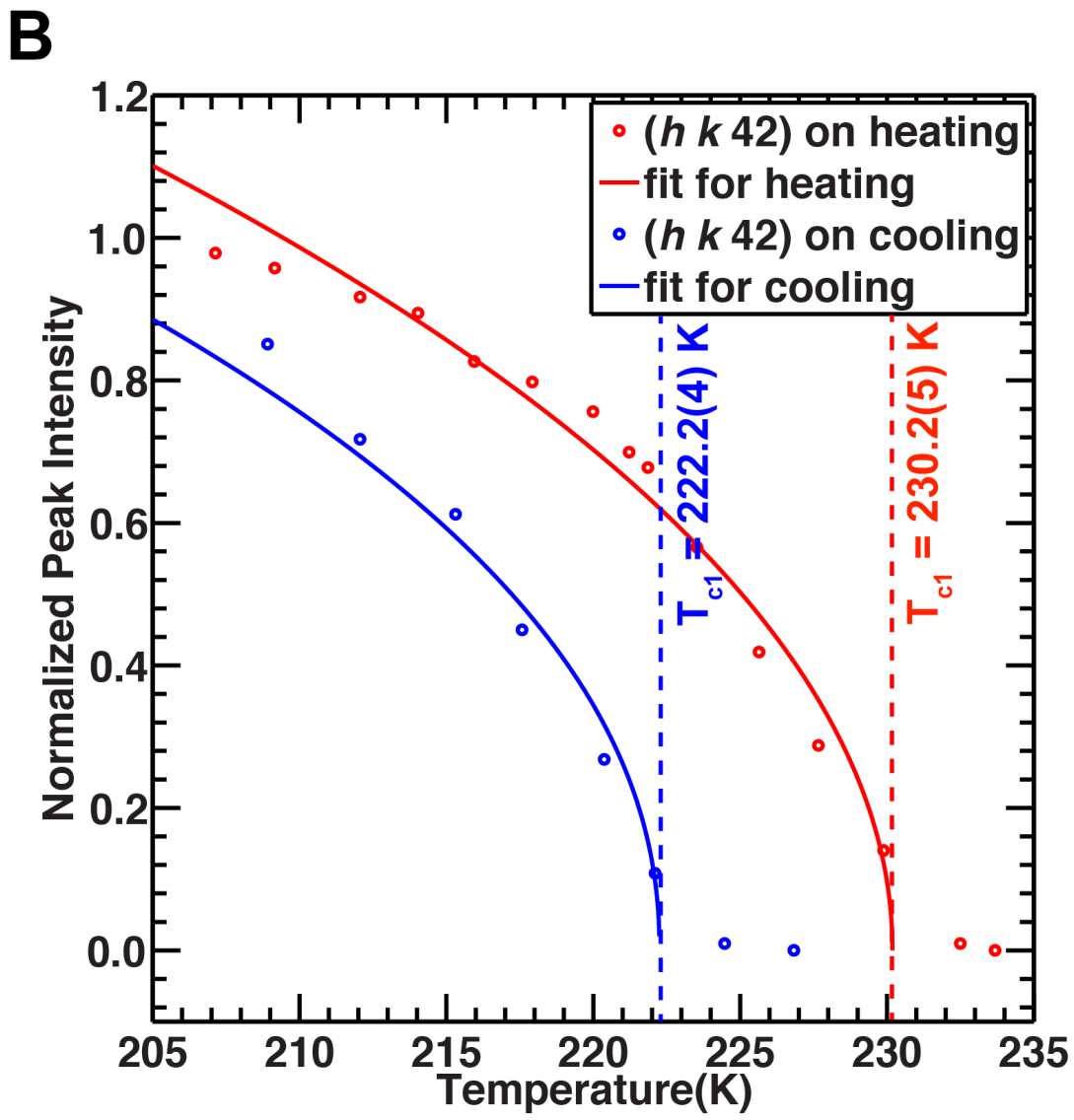

Figure 2.2.1.18. Normalized peak intensities as a function of temperature. (A) The measurements were made from the peak intensities of $(-1\ 0\ 27)_h$ of the $9c_g' = 11c_h'$ phase. (B) The measurements were made from the sum intensities of $(0\ -2\ 42)_o$ and $(-1\ -1\ 42)_o$ peaks of the $14c_g' = 17c_h'$ phase. Solid lines are fits to $A(T_c - T)^{\beta}$. Measurements were made using 60° ϕ rotations about the crystal ***c*** axis at a detector distance of 500.0 mm on APS beamline 14-BM-C at the APS with λ = 0.97870 Å.[36]

In 2,8-nonanedione/urea, we have established that there are at least four lock-in phase transitions, as shown in Table 2.2.1.2. The first phase transition at 265.4(5) K on cooling is due to an incommensurate to commensurate lock-in to a structure with $4c_g' = 5c_h'$. Earlier work using infrared spectroscopy showed that at room temperature, 2,8-nonanedione/urea has a low host-guest hydrogen bonding density,[2] which is now attributed to the incommensurate structure of this material. Once the temperature is lowered, a commensurate structure with $4c_g' = 5c_h'$ is favored enthalpically, since this structure is expected to have a higher host-guest hydrogen bonding density than the incommensurate structure. The second and third phase transitions at 222.5(9) K and 222.2(4) K on cooling are due to incommensurate to commensurate lock-in to structures with $9c_g' = 11c_h'$ and $14c_g' = 17c_h'$, respectively. These two commensurate phases are also favored enthalpically, since the DSC trace exhibits a broad exothermic peak at 214 K on cooling, as shown in Figure 2.2.1.1. Although an extra commensurate pahse with $5c_g' = 6c_h'$ was included in Figure 2.2.1.15, the peak intensenties from this phase are weak. At 185.8(5) K, a fourth incommensurate to commensurate phase transition occurs, as the most compressed state locks-in to a phase with $6c_g' = 7c_h'$.

Incommensurately modulated phases of inorganic insulators such as $NaNO_2$ and K_2SeO_4 are stable as a function of temperature when the force constants between first- and second- neighbor layers fulfill a certain criteria. When anharmonic effects are taken into account to solve the phase of atoms for the most stable phase, a so-called Sine-Gordon equation is obtained. This equation describes soliton walls, which separate commensurately modulated phases. At the incommensurate-to-commensurate lock-in phase transition, the number of solitons may become zero.[37] Using a classical one-dimensional model (FVdM), incommensurate, commensurate and chaotic phases were explored.[38] In the model, an array of atoms (with lattice constant a_0) are connected with harmonic springs and interact with a periodic potential (with period b). When the

potential is strong, the lattice favors a commensurate arrangement, in which $m \times a_0 = n \times b$, for sufficiently-small integers m and n.[38] There are a number of descriptors used for different types of structures. When commensurate relationships fill up the whole range of possible a_0 and b, the system is termed a complete devil's staircase. When incommensurate phases exist between the commensurate phases, it is an incomplete devil's staircase. This latter term fits the behavior of 2,8-nonanedione/urea, since besides commensurate phases, compressed incommensurate phases are present.

Commensurate phase lock-in temperatures	Phase transition temperatures on heating (K)	Phase transition temperatures on cooling (K)
$4c_g' = 5c_h'$	271.9(3)	265.4(5)
$9c_g' = 11c_h'$	230.2(4)	222.5(9)
$14c_g' = 17c_h'$	230.2(5)	222.2(4)
$6c_g' = 7c_h'$	*203.8(3)	*185.8(5)

Table 2.2.1.2. Compiled phase transition temperatures based the X-ray analysis. *The transition temperatures for the phase with $6c_g' = 7c_h'$ were from APS_A_098 (no temperature calibration) while the rest were from APS_B_204 (temperature calibration included), thus not directly comparable.

To find the best commensurate ratios of UIC systems, a program was written to generate a devil's staircase-like diagram (Figure 2.2.1.19). For a range of initial c_g values the program picks the lowest integers (m and n) that satisfy the condition $m \times c_g' = n \times c_h' \pm 0.15$ Å (using m, n <100, c_h = 11.022 Å, and an increment of c_g of 0.001 Å).

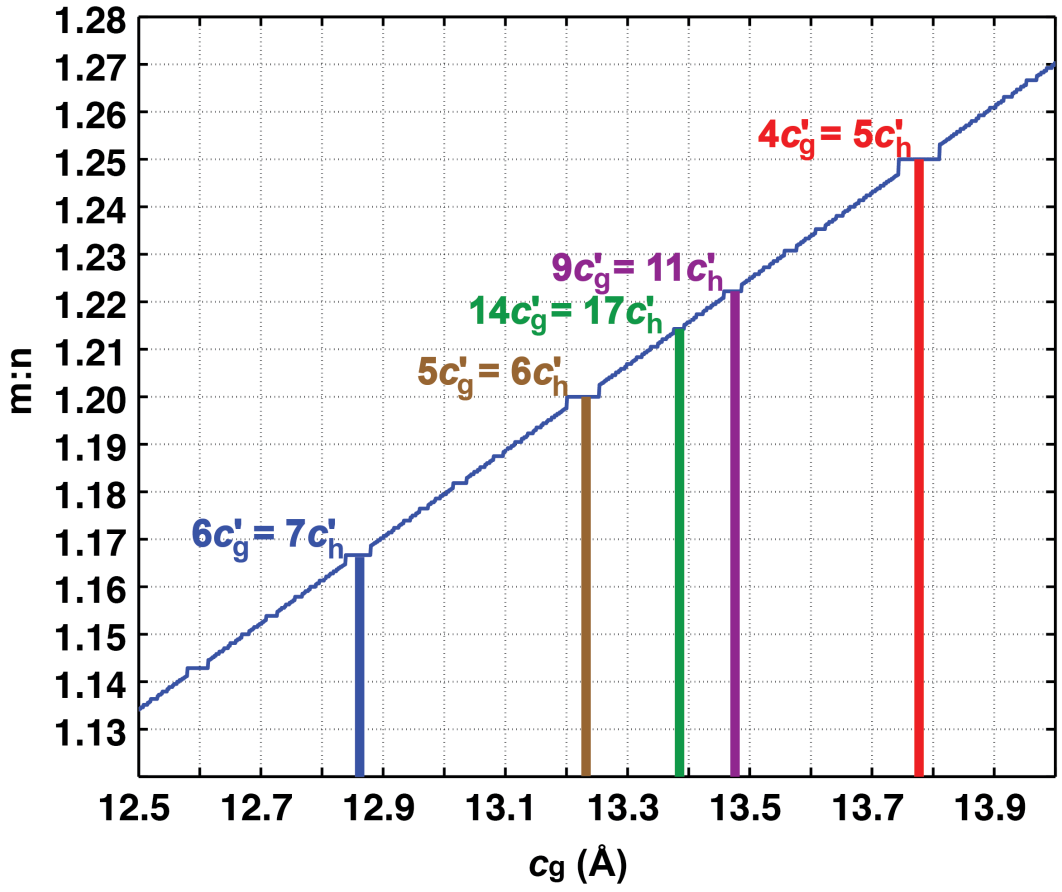

Figure 2.2.1.19. "Devil's staircase" for UICs using c_h = 11.022 Å, showing the region in the vicinity of c_g for 2,8-nonanedione/urea (13.646(2) Å at 289.3(3) K). The five commensurate phases discussed previously are shown. Note that c_h shrinks by 0.028 Å between room temperature and 110 K. Thus, at low temperatures, the commensurate phases will have correspondingly smaller values of c_g than shown here.

In summary, to rationalize the observation of the series of phase transitions of 2,8-nonanedione/urea, we propose the stress-induced self-compression mechanism

(shown in Figure 2.2.1.20). If the crystal is grown above 265 K, the number of urea and guest molecules are fixed by the incommensurate relationship of c_h:c_g = 0.80768(7). The incommensurate-to-commensurate lock-in at 265.4(5) K results in an elongation of c_g by 11.019(2) × (5/4 - 1/0.8077) = 0.131(2) Å. As the $4c_g' = 5c_h'$ structures grow from their nucleation sites within the crystal, regions left over have less space along the channel to accommodate the guest molecules. As the stress accumulates during the growth of the commensurate phase with $4c_g' = 5c_h'$, nearby guest molecules along the channel are compressed and shortened, as shown by progressively smaller values of c_g for the compressed phase from 265 K to 215 K (Figure 2.2.1.21). When cooled below ca. 222 K, the compressed incommensurate component locks-in to two commensurate phases with $9c_g' = 11c_h'$ and $14c_g' = 17c_h'$. This also entails an enlongation of c_g by 0.233 (2) Å and 0.146(2) Å for the two commensurate phases, respectively. More stress accumulates on cooling, and the c_g of the compressed component keeps decreasing. Finally, the compressed state reaches a commensurate plateau with $6c_g' = 7c_h'$. The extreme compression of guest molecules in this final phase causes its host repeat to elongate by 0.021 Å relative to the rest of the crystal.

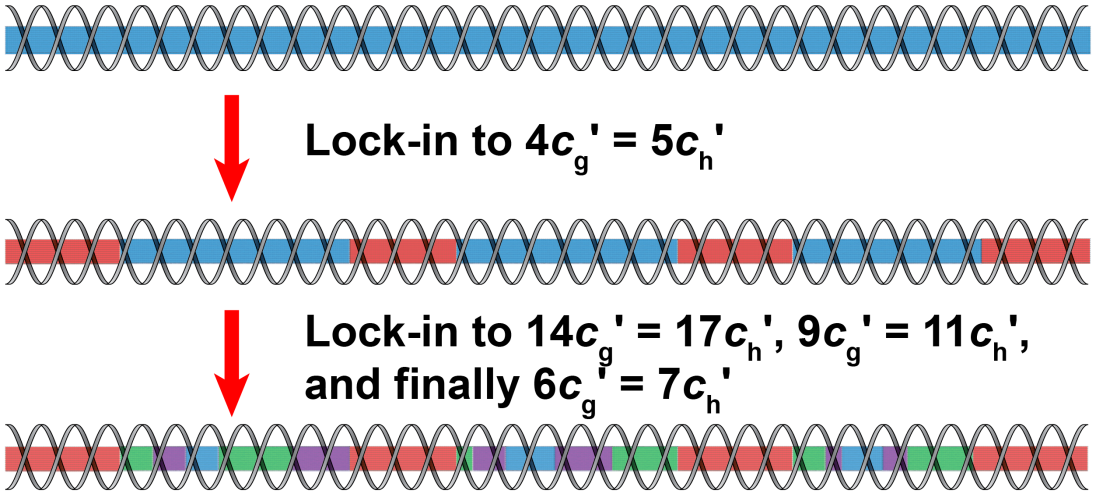

Figure 2.2.1.20. A simple schematic representation of the proposed mechanisms of the phase transitions in 2,8-nonanedione/urea. The grey helices represent the host, whereas the colored rectangles represent different guest phases. When the UIC is cooled below the first phase transition, the regions with $4c_g' = 5c_h'$ (red blocks) emerge and exert stress on the remaining incommensurate regions (blue). When the UIC is cooled below the second set of phase transitions, the shortened structures (blue) are partially transformed to structures with $9c_g' = 11c_h'$ (purple) and $14c_g' = 17c_h'$ (green), with the remaining regions (blue) being further compressed until they become the phase with $6c_g' = 7c_h'$.

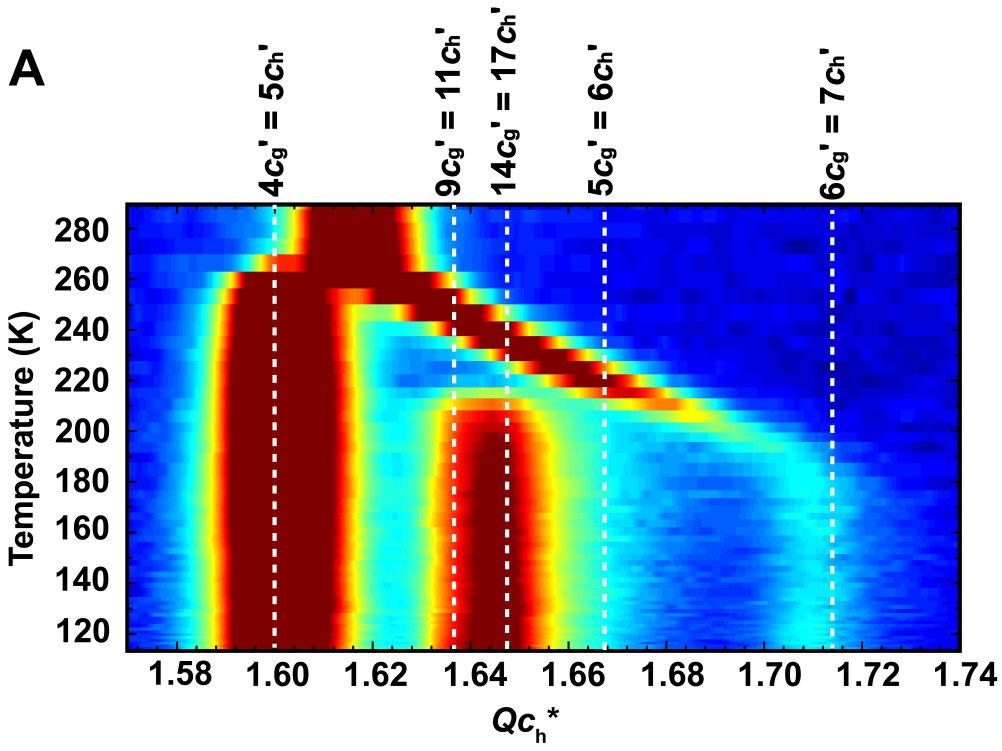
A
4c_g' = 5c_h'
9c_g' = 11c_h'
14c_g' = 17c_h'
5c_g' = 6c_h'
6c_g' = 7c_h'
Temperature (K)
280
260
240
220
200
180
160
140
120
1.58
1.60
1.62
1.64
1.66
1.68
1.70
1.72
1.74
Qc_h*

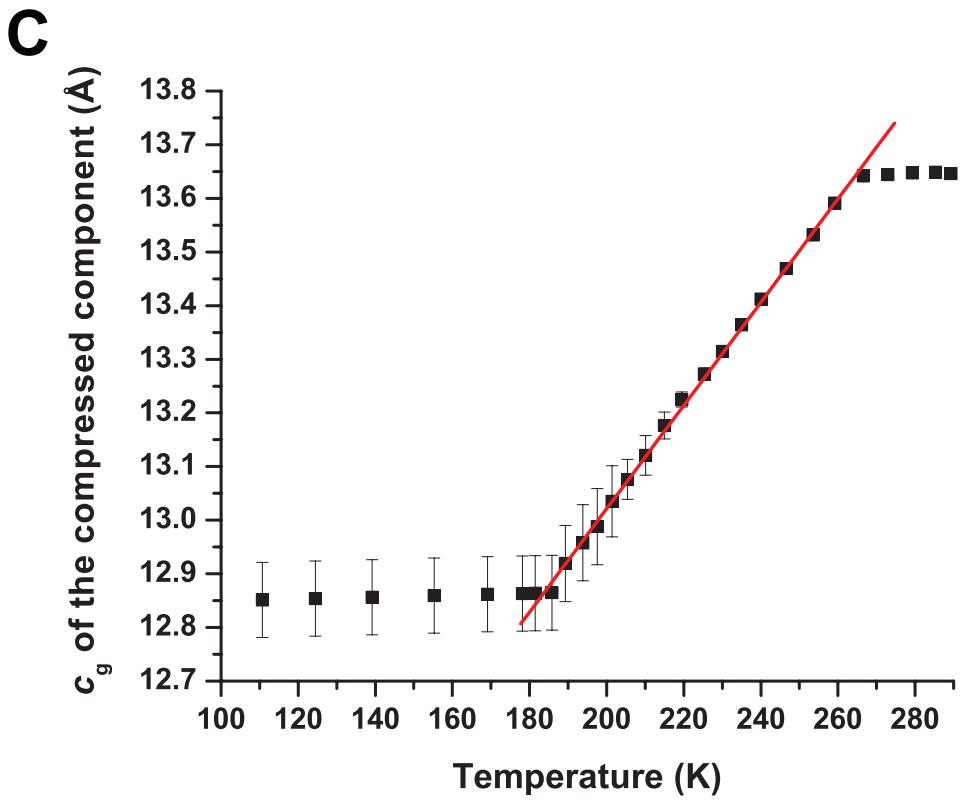

Figure 2.2.1.21. (A) Temperature evolution of the (-1 0 *l* *m*)$_h$ and overlapping (0 -2 *l* *m*)$_o$ and (-1 -1 *l* *m*)$_o$ layer lines of 2,8-nonanedione/urea upon cooling from 290 to 110 K. Five commensurate phases are labeled with mc_g' = nc_h'. Layer line profiles are shown on a logarithmic color scale, with red being most intense. Measurements were made using 60° ϕ rotations about the crystal ***c*** axis at a detector distance of 500.0 mm on APS beamline 14-BM-C with λ = 0.97870 Å.[39] (B) Stacked profiles of synchrotron oscillation images from **Qc_h*** = 1.47 to 1.77 of the (0 -2 *l* *m*)$_o$ and (-1 -1 *l* *m*)$_o$ layer lines. (C) Temperature evolution of c_g of the shortened component (data is shown in Table 2.2.1.1). This was determined from least squares fits of all the corresponding peaks in the (0 -2 *l* *m*)$_o$ and (-1 -1 *l* *m*)$_o$ layer lines. The red line is fit to a linear relationship with c_g = 11.10(2) + 0.00963(10) × *T* Å (R = 0.99921).

2.2.2. Sequence with 2,8-nonanedione/urea-d_4 grown at 293.2 K

As shown in Section 2.2.1, 2,8-nonanedione/urea locks into various commensurate phases upon cooling, causing self-compression. It is intriguing to investigate if any perturbations of the system can yield a different result. In this study, deuterium labeled host, urea-d_4, was used to probe any differences between it and its unlabeled analog.

During initial studies, synchrotron oscillation images were obtained at ALS beamline 8.2.2.[40] A temperature scan from 290 K to 100 K was conducted to study the phase transitions. For the oscillation images, a distance of 650.0 mm and 60° ϕ rotation were used with an exposure of 5 s for the 12400 keV (0.999868 Å) synchrotron beam. The (-1 0 *l m*)$_h$ layer line has stronger intensity and better alignment than the (1 0 *l m*)$_h$ layer line, so this layer line was analysed. The temperature scan showed a sequence of events similar to that observed with the protiated host (Section 2.2.1), also exhibiting four to five lock-in phase transitions.

To establish the room temperature unit cell parameters of the urea host structure, 1531 host reflections were obtained from a synchrotron X-ray dataset of 2,8-nonanedione/urea-d_4 on APS beamline 14-BM-C. Here, a 293º phi rotation with 1º frames, a detector distance of 200.0 mm, and a wavelength of 0.97870 Å were used.[41] The hexagonal host unit cell dimensions were determined to be ***a*** = ***b*** = 8.2236(13) Å, ***c*** = 11.0075(16) Å at 290.8 K (290.0 K reading calibrated).[5] Although lengths of the ***a*** and ***b*** axes for the urea-d_4 isotopomer are not significantly different from the value obtained for 2,8-nonanedione/urea under the same conditions (8.232(2) Å – see Section 2.2.1), the length of the ***c*** axis is measurably shorter for 2,8-nonanedione/urea-d_4 than it is for 2,8-nonanedione/urea (11.022(2) Å).

By measuring the separations of the (1 0 -3 0)$_h$ and (1 0 3 0)$_h$ peaks (or their low-

symmetry counterparts) during a temperature scan from 290.6(8) to 155.6 K,[42] a thermal expansion of the channel axis is observed, which can be described with $\boldsymbol{c}$ = 10.962(2) + 1.56(4) × 10^{-4} T Å.[43] The phases of this UIC at different temperatures were evaluated by fitting the peaks in the diffraction patterns with four indices (*h k l m*); the misfit parameters were analysed using FibonacciBuild Version 5.11.[6]

As shown in Figure 2.2.2.1, at 287 K, 2,8-nonanedione/urea-d_4 has an incommensurate phase with γ = 0.80734(5), c_g = 13.634(3) Å (using c_h = 11.007(2) Å). As shown in Figure 2.2.2.2 (A), at 230 K, the UIC has two components, a commensurate phase with $4c_g' = 5c_h'$ and an incommensurate phase with γ = 0.8298(5), c_g = 13.210(8) Å (using c_h = 10.962(2) Å). In order to obtain accurate phase transition temperatures and to measure the peak intensity evolution in 2,8-nonanedione/urea-d_4, temperature scans (both heating and cooling) were repeated on beamline 14-BM-C.[44] As shown in Figure 2.2.2.2 (B), normalized intensities from the $(0\ 2\ 12)_o$ and $(1\ 1\ 12)_o$ peaks from the phase with $4c_g' = 5c_h'$ were fit to $A(T_c - T)^{\beta}$. The phase transition temperatures were measured to be 267.43(14) for cooling and 273.9(4) K for heating, with critical exponents, β, of 0.538(14) for cooling and 0.53(3) for heating. From this analysis, it can be shown that there is a hysteresis effect on the phase transition temperature, as the T_c on heating is 6.5(4) K higher than it is on cooling.

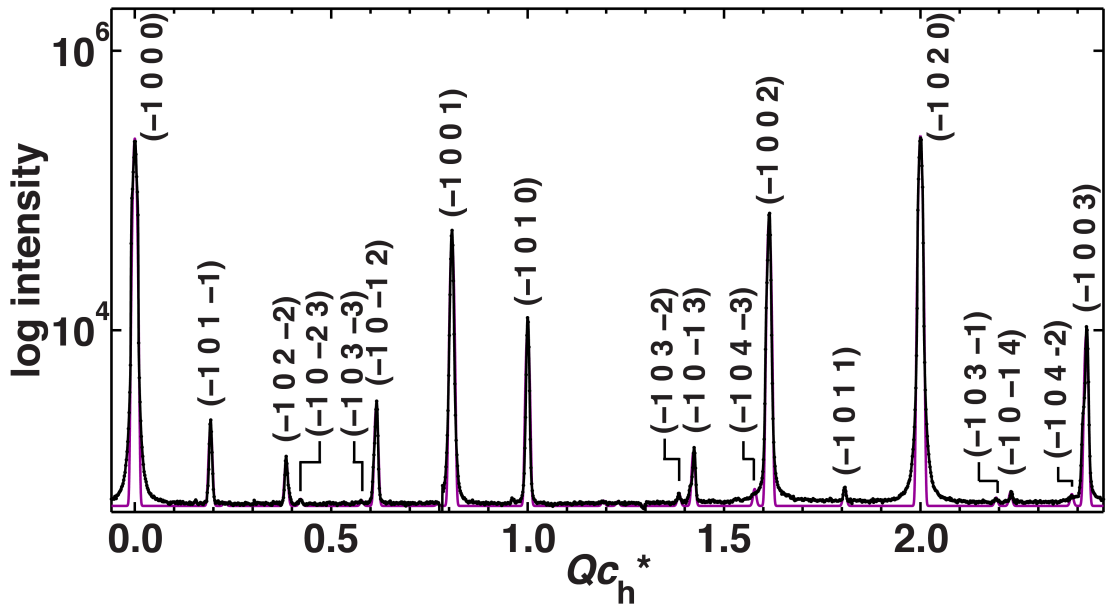

Figure 2.2.2.1. Profile analysis of the (-1 0 *l m*)$_h$ layer line of the unwarped synchrotron oscillation image of 2,8-nonanedione/urea-d_4 at 287 K. The profile was fit with γ = 0.80734(5). The measurement was made using a 60° ϕ rotation about the crystal ***c*** axis at a detector distance of 650.0 mm on ALS beamline 8.2.2 with λ = 0.999868 Å.[45]

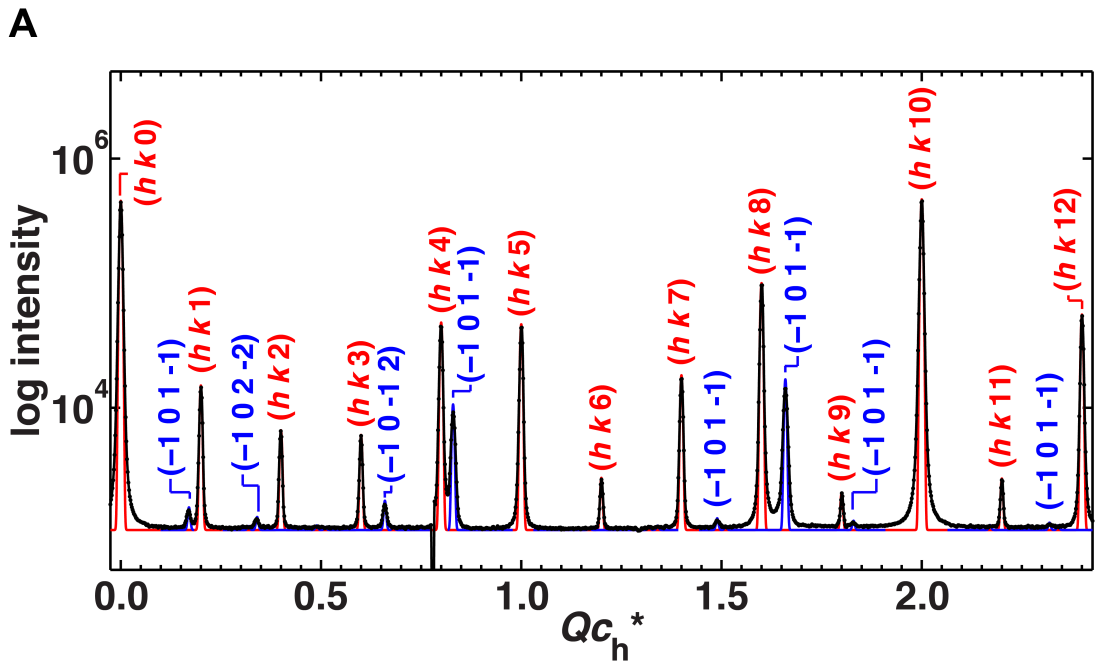

Figure 2.2.2.2. (A) Profile analysis of the (-1 -1 *l* *m*)$_o$ and (0 -2 *l* *m*)$_o$ layer lines of the unwarped synchrotron oscillation image of 2,8-nonanedione/urea-d_4 at 230 K. There are two components: one commensurate phase with $4c_g' = 5c_h'$ and a shortened phase that was fit with $\gamma = 0.8298(5)$. The measurement was made using a 60° ϕ rotation about the crystal ***c*** axis at a detector distance of 650.0 mm on beamline 8.2.2. at ALS with λ = 0.999868 Å.[46]

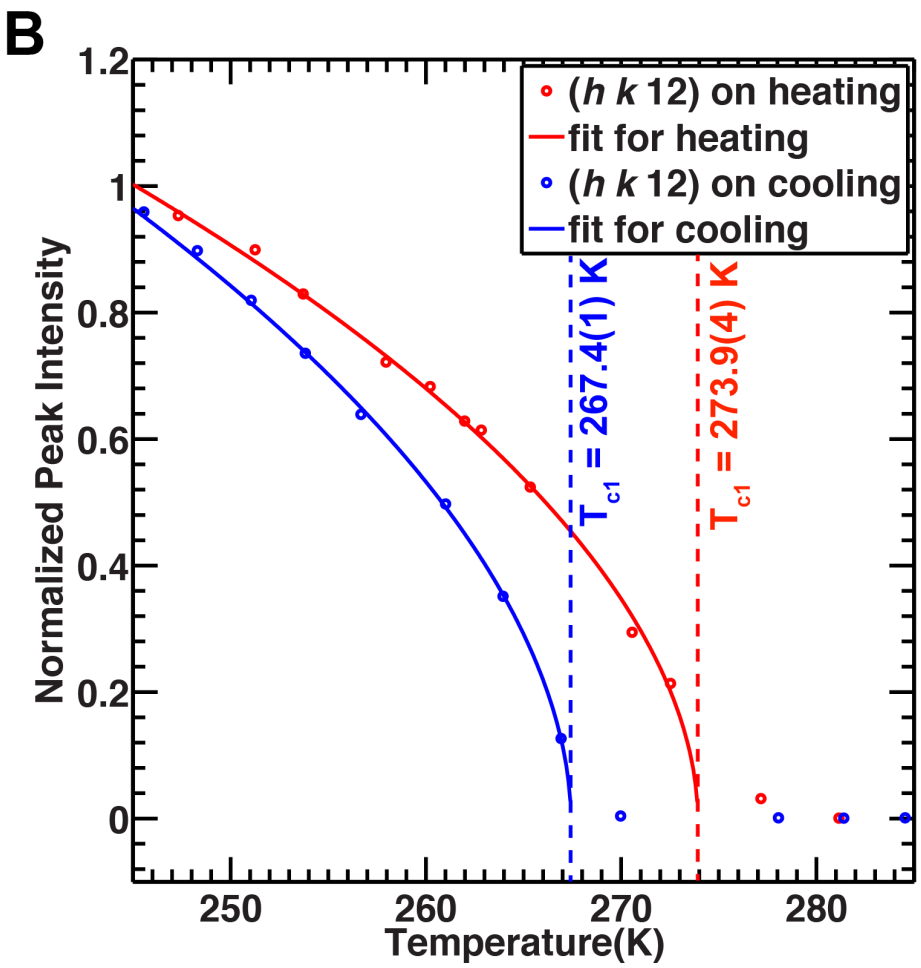

Figure 2.2.2.2. (B) Normalized peak intensities as a function of temperature. The measurements were made from the sum intensities of the $(0\ 2\ 12)_o$ and $(1\ 1\ 12)_o$ peaks from the phase with $4c_g' = 5c_h'$. Solid lines are fits to $A(T_c - T)^{\beta}$. The measurements were made using 60° ϕ rotations about the crystal ***c*** axis at a detector distance of 500.0 mm on APS beamline 14-BM-C with λ = 0.97870 Å.[44]

The behavior of this phase transition can be also explained with the self-compression mechanism. The lock-in phase transition observed for 2,8-nonanedione/urea-d_4 is very similar to that in the protiated UIC discussed in Section 2.2.1, except that the temperature of the transition is 2.0 K higher with the deuterated host during both heating and cooling. This isotope effect on the lock-in temperature is most likely due to the slight shortening of the host repeat in 2,8-nonanedione/urea-d_4 (c_h = 11.0075(16) Å versus c_h = 11.022(2) Å for the urea-h_4 analog). In the urea-d_4 host, the guest does not have to elongate as much to lock into the phase with $4c_g' = 5c_h'$. (The guest lengths are very similar in each case (13.634(3) Å in 2,8-nonanedione/urea-d_4 and 13.646(3) Å in 2,8-nonanedione/urea).

As the commensurate phase continued to grow below 267.4 K, the incommensurate phase was compressed more. The shortening of the guest is shown in Figures 2.2.2.7 and 2.2.2.9. As shown in Figure 2.2.2.3, at 218 K, the UIC has four phases, three commensurate phases with $4c_g' = 5c_h'$, $14c_g' = 17c_h'$, and $9c_g' = 11c_h'$, and an incommensurate phase with γ = 0.83620(11) (c_g = 13.150(3) Å, using c_h = 10.996(2) Å). As shown in Figure 2.2.2.4, at 170 K, the profile of the layer lines was modeled with five commensurate components: $4c_g' = 5c_h'$, $9c_g' = 11c_h'$, $14c_g' = 17c_h'$, $5c_g' = 6c_h'$, and $6c_g' = 7c_h'$. The phase with $6c_g' = 7c_h'$ will be discussed below.

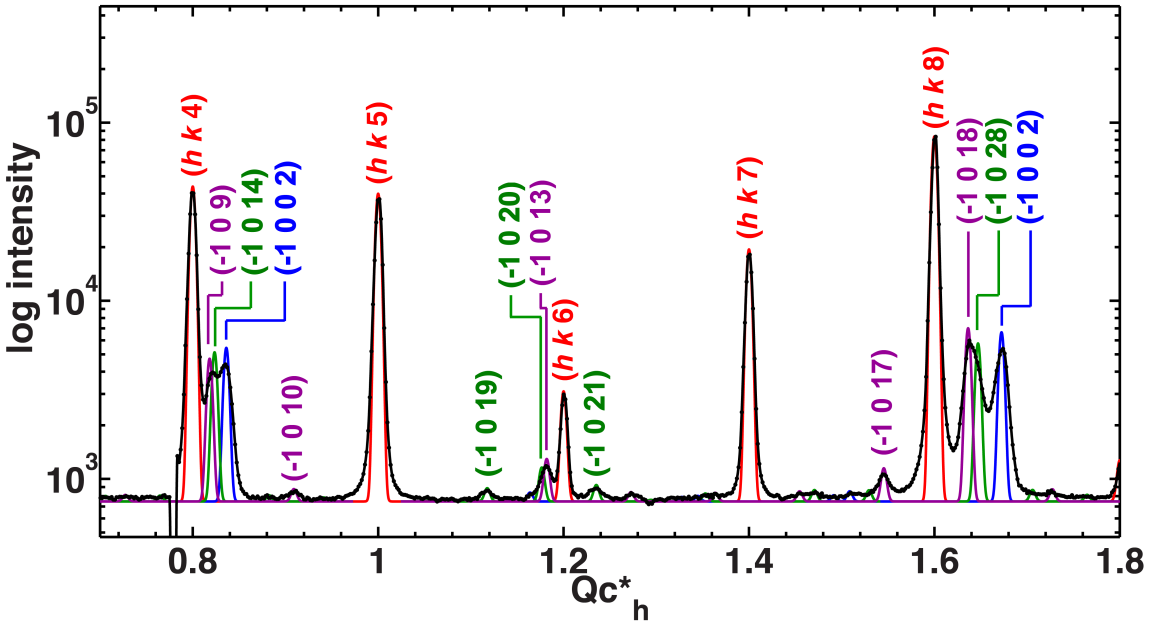

Figure 2.2.2.3. Profile analysis of the (-1 0 *l* *m*)$_o$ and (0 -2 *l* *m*)$_o$ layer lines of the unwarped synchrotron oscillation image of 2,8-nonanedione/urea-d_4 at 218 K. There are four components. The data were modeled with three commensurate phases with $4c_g' = 5c_h'$ (red), $9c_g' = 11c_h'$ (magenta), and $14c_g' = 17c_h'$ (green), and a shortened phase was fit with $\gamma = 0.83620(11)$ (blue). The measurement was made using a 60° ϕ rotation about the crystal ***c*** axis at a detector distance of 650.0 mm on ALS beamline 8.2.2 with λ = 0.999868 Å.[47]

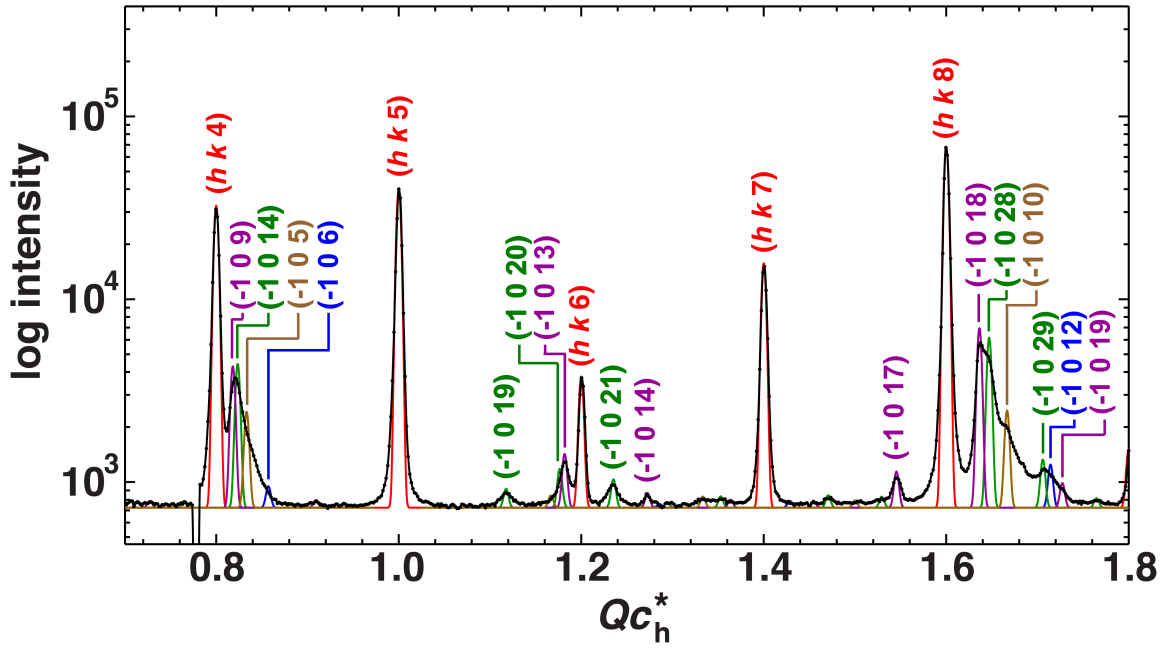

Figure 2.2.2.4. Profile analysis of the (-1 0 *l* *m*)$_o$ and (0 -2 *l* *m*)$_o$ layer lines of the unwarped synchrotron oscillation image of 2,8-nonanedione/urea-d$_4$ at 170 K. The data were modeled with five commensurate phases with $4c_g' = 5c_h'$ (red), $9c_g' = 11c_h'$ (magenta), $14\ c_g' = 17c_h'$ (green), $5c_g' = 6c_h'$ (brown), and $6c_g' = 7c_h'$ (blue). The measurement was made using a 60° ϕ rotation about the crystal ***c*** axis at a detector distance of 650.0 mm on ALS beamline 8.2.2 with λ = 0.999868 Å.[48]

To obtain accurate phase transition temperatures and to measure the evolution of the peak intensities of the commensurate phases with $9c_g' = 11c_h'$ and $14c_g' = 17c_h'$, normalized peak intensities around $\mathbf{Qc_h^*}$ = 2.45 were measured.[44] For the phase with $9c_g' = 11c_h'$, intensities of the (0 1 27)$_h$ peaks were fit to $A(T_c - T)^{\beta}$, as shown in Figure 2.2.2.5 (A). The phase transition temperatures were measured to be 227.9(3) K for cooling and 233.4(4) K for heating with critical exponents, β, of 0.32(4) for cooling and 0.35(5) for heating. From this analysis, it can be shown that there is a hysteresis effect on the phase transition temperatures, as the T_c on heating is 5.5(5) K higher than it on

cooling. For the phase with $14c_g' = 17c_h'$, sum intensities of the $(0\ 2\ 42)_o$ and $(1\ 1\ 42)_o$ peaks were fit to $A(T_c - T)^{\beta}$, as shown in Figure 2.2.2.5 (B). The phase transition temperatures were measured to be 223.5(5) K for cooling, and 229.3(3) K for heating, with critical exponents, β, of 0.43(5) for cooling and 0.38(3) for heating. Once again there is a hysteresis effect, as the T_c on heating is 5.8(6) K higher than it is on cooling. This analysis shows that the phase transition for the phase with $9c_g' = 11c_h'$ occurs about 4 K higher than for the phase with $14c_g' = 17c_h'$. This differs from the case with the protiated host, in which the phase transitions for both components occur at the same temperature, around 222.4 K on cooling and 230.2 K on heating.

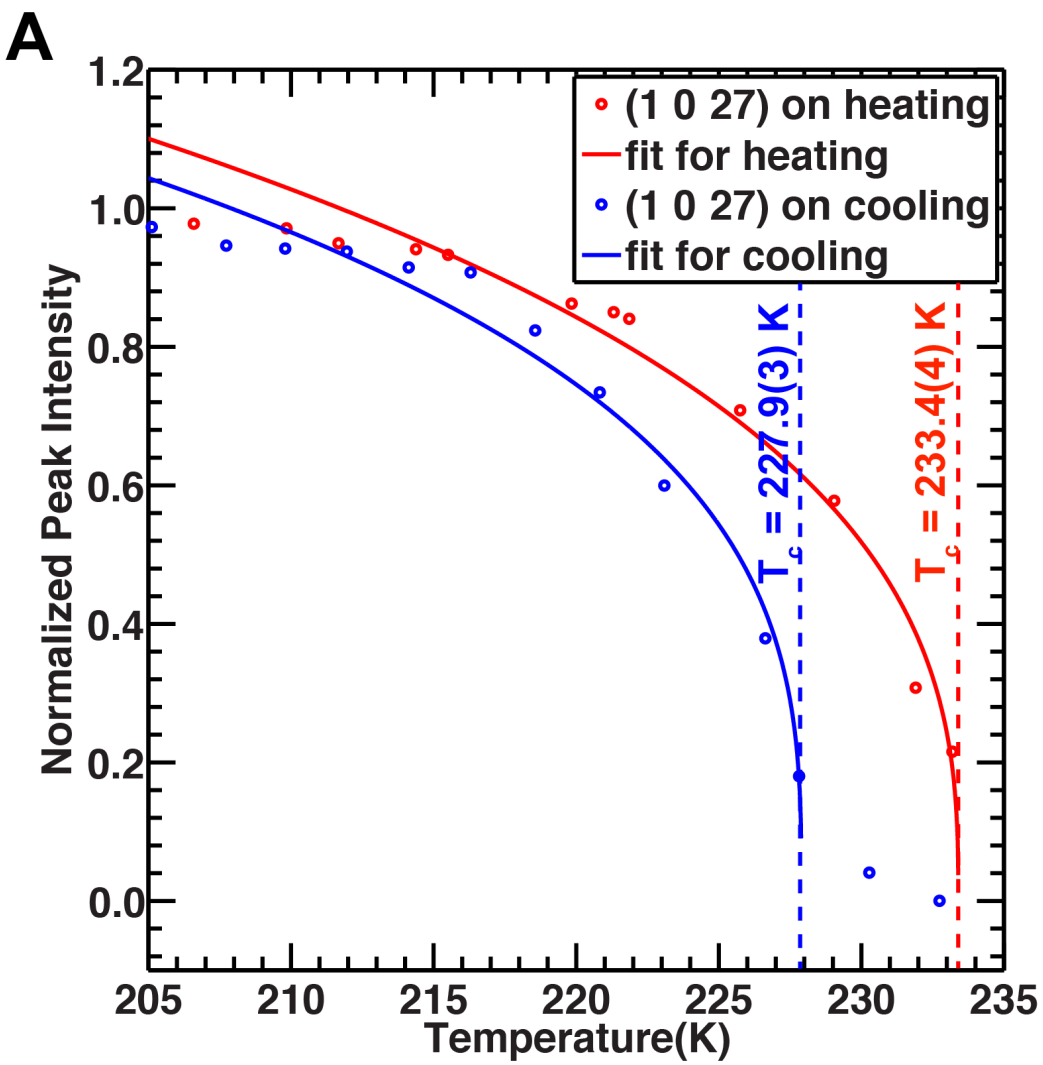

Figure 2.2.2.5. Normalized peak intensities as a function of temperature. (A) The measurements were made from intensities of the $(1\ 0\ 27)_h$ peaks from the phase with $9c_g' = 11c_h'$.

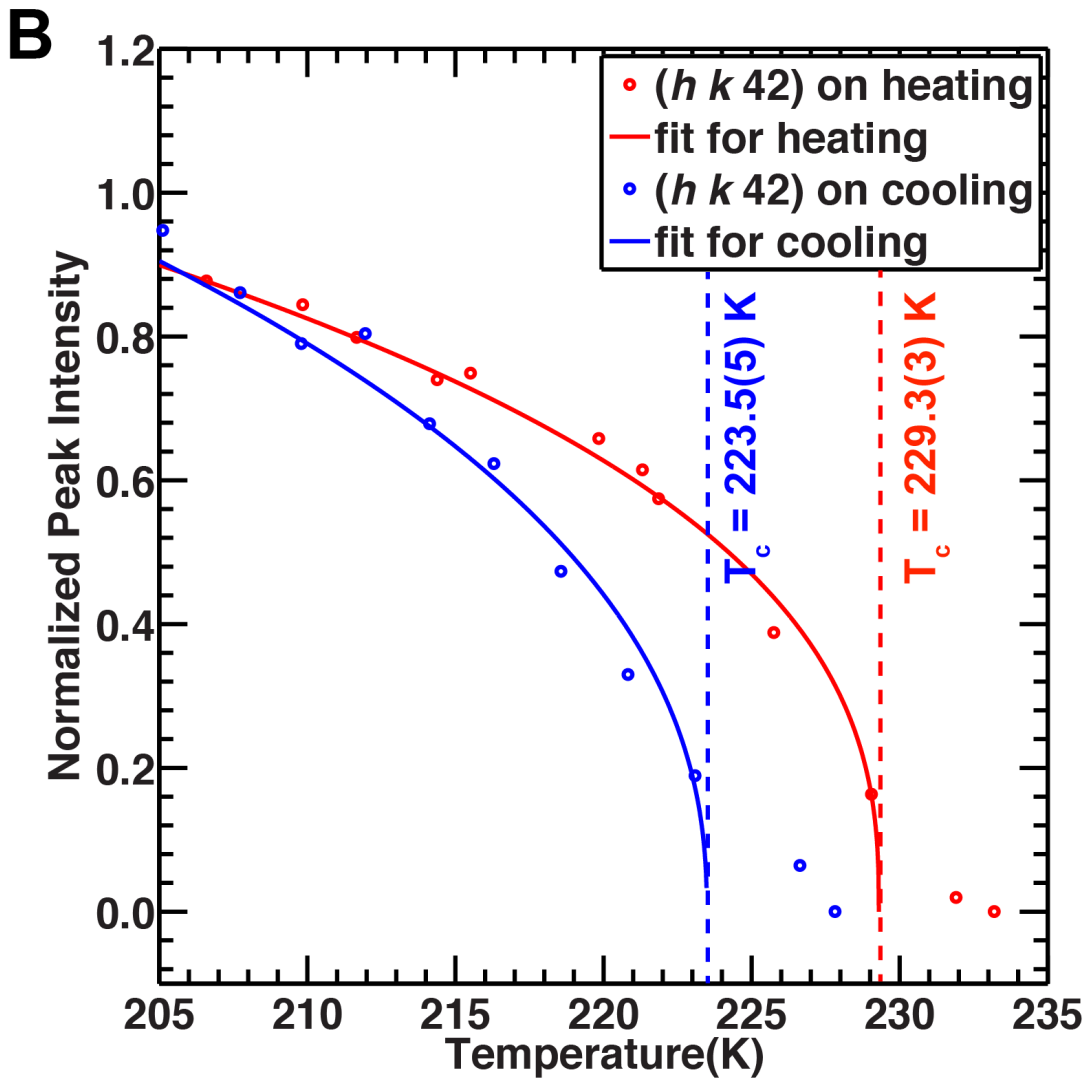

Figure 2.2.2.5. (B) The measurements were made from the sum intensities of $(0\ 2\ 42)_o$ and $(1\ 1\ 42)_o$ peaks from the phase with $14c_g' = 17c_h'$. Solid lines are fits to $A(T_c - T)^{\beta}$. The measurements were made using 60° ϕ rotations about the crystal ***c*** axis at a detector distance of 500.0 mm on APS beamline 14-BM-C with λ = 0.97870 Å.[44]

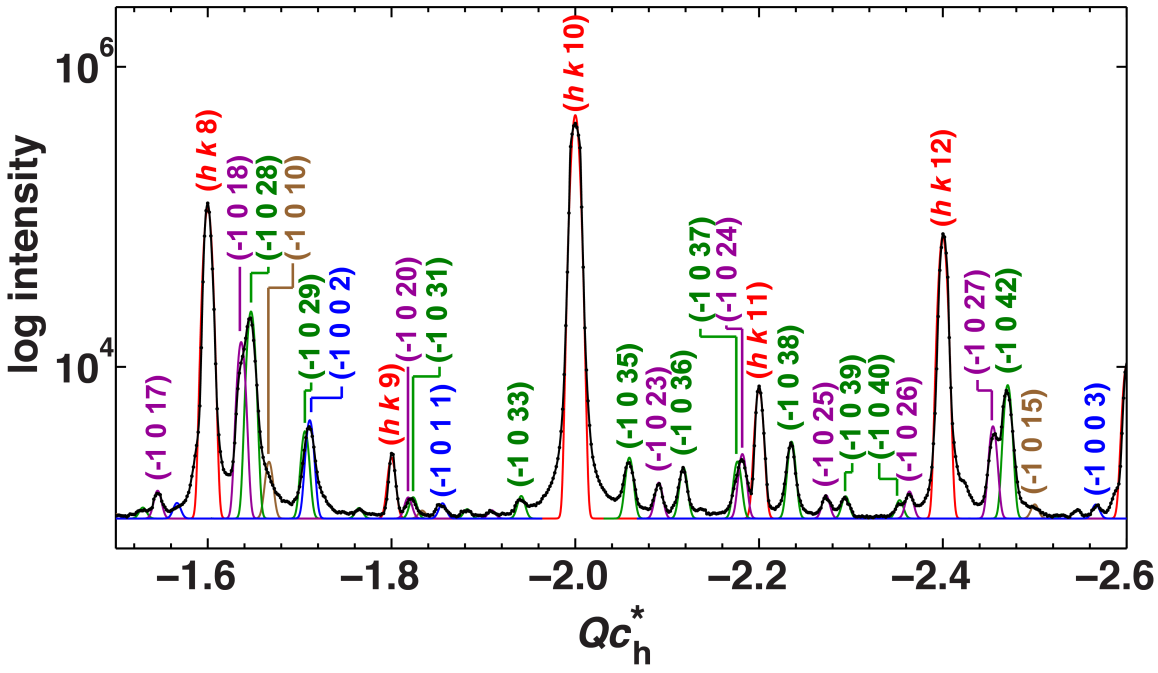

Figure 2.2.2.6. Profile analysis of the (-1 0 *l* *m*)$_o$ and (0 -2 *l* *m*)$_o$ layer lines of the unwarped synchrotron oscillation image of 2,8-nonanedione/urea-d$_4$ at 102 K. The data were modeled with four commensurate phases with $4c_g' = 5c_h'$ (red), $9c_g' = 11c_h'$ (magenta), $14c_g' = 17c_h'$ (green), $5c_g' = 6c_h'$(brown), and an incommensurate phase with $\gamma = 0.8555$ (blue). The measurement was made using a 60° ϕ rotation about the crystal ***c*** axis at a detector distance of 650.0 mm on ALS beamline 8.2.2 with $\lambda = 0.999868$ Å.[49]

As shown in Figure 2.2.2.6, at 102 K the profile of the (-1 0 *l* *m*)$_o$ and (0 -2 *l* *m*)$_o$ layer lines was modeled with five phases, four commensurate phases with $4c_g' = 5c_h'$, $9c_g' = 11c_h'$, $14c_g' = 17c_h'$, $5c_g' = 6c_h'$, and an incommensurate phase with $\gamma = 0.8555$. Note that the intensities from the phase with $5c_g' = 6c_h'$ are very weak, thus no intensity analysis was performed on that phase. The most compressed phase was modeled with $\gamma = 0.8555$ in Figure 2.2.2.6, which is very close to $6c_g' = 7c_h'$ ($\gamma = 0.8571$). The temperature evolution of the misfit parameter of the compressed component is shown in Figure 2.2.2.7. On cooling, the compression stops around 180 K, and on heating

expansion starts abruptly at 203.8(3) K, indicating hysteresis of the compressed phase of around 24 K.

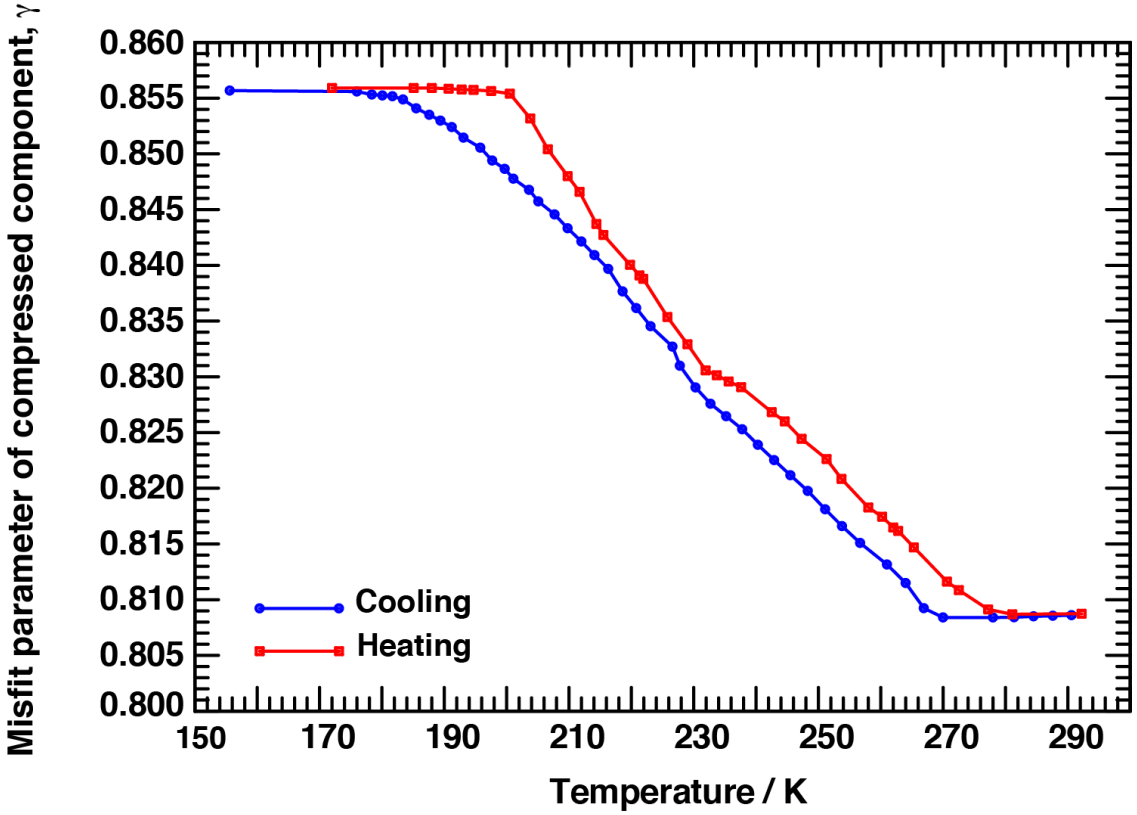

Figure 2.2.2.7. Temperature evolution of the misfit parameter, γ, of the compressed component in 2,8-nonanedione/urea-d_4. This was determined from least squares fits of the (1 1 0 ±(2, 3))$_o$ and (0 2 0 ±(2, 3))$_o$ peaks from oscillation images. The measurements were made using 60° ϕ rotations about the crystal ***c*** axis at a detector distance of 500.0 mm on APS beamline 14-BM-C with λ = 0.97870 Å. This figure is adapted from personal communication with Ilya Frantsuzov.[50]

Measurements of the most compressed state shown in Figures 2.2.2.6 and 2.2.2.7 are based on the *h* + *k* = even layer lines (in the orthorhombic basis) with five overlapping phases, where the most compressed state is again fit well with γ = 0.8555, just short of 6/7. As encountered in the unlabeled host case, a slight elongation of c_h in

the most compressed state compared to all the other phases occurs when it locks in to a structure with $6c_g' = 7c_h'$ The superstructure layer lines, with orthorhombic indices $h + k$ = odd, again contained only reflections from the most compressed phase, including host peaks, as shown in Figure 2.2.2.8. Fitting these gave an average γ = 0.8568(2) (which is within measurement uncertainty of 6/7 = 0.8571) and values of c_h that were on average 0.01 Å larger than in structure layer lines.[51]

In conclusion, 2,8-nonanedione/urea-d_4 also shows four to five lock-in phase transitions (the phase with $5c_g' = 6c_h'$ was not always observed), as well as self-compression. At 287 K, 2,8-nonanedione/urea-d_4 has an incommensurate phase with γ = 0.80734(5), c_g = 13.634(3) Å (using c_h = 11.007(2) Å). The incommensurate-to-commensurate lock-in at 267.43(14) K results in an elongation of c_g by 11.0037(16) × (5/4 - 1/0.80734) = 0.1251(16) Å. As the phase with $4c_g' = 5c_h'$ grows, stress accumulates and compresses leftover incommensurate regions along the channel, which leads to progressively shortened phases, as shown by progressively smaller values of c_g for the compressed phase below 267 K (see Figures 2.2.2.7 and 2.2.2.9). When cooled further to 227.9(3) K, the compressed incommensurate component locks-in to a commensurate phase with $9c_g' = 11c_h'$. Then, at 223.5(5) K, the compressed incommensurate component also locks into another commensurate phase with $14c_g' = 17c_h'$. More stress accumulates on cooling, and the c_g of the compressed component keeps decreasing. Finally, the compressed state reaches a commensurate plateau with $6c_g' = 7c_h'$ at around 180 K with c_g' = 10.9901(16)/0.8555 = 12.846(2) Å (using c_h and γ from structure layer lines). Overall, the guest repeat length shortens by 11.0037(16)/0.80734 - 10.9901(16)/0.8555 = 0.783(3) Å between 267.43(14) and 180 K, of which 10.9901(16) × (1/0.80734 - 1/0.8555) = 0.7663(1) Å is via self-compression and (11.0037(16) - 10.9901(16))/0.80734 = 0.017(3) Å is due to thermal shrinking of the host.

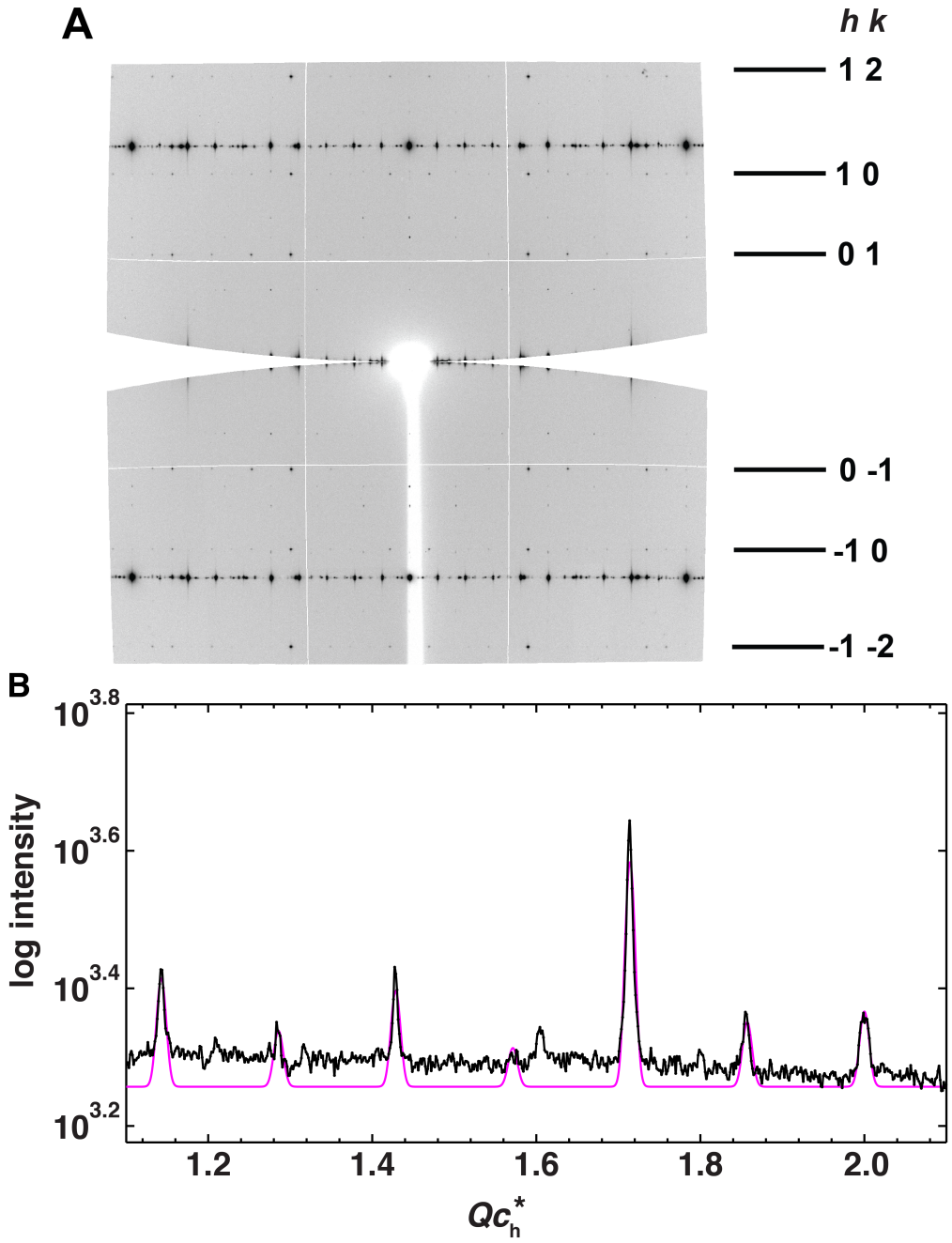

Figure 2.2.2.8. (A) Unwarped synchrotron oscillation image of 2,8-nonanedione/urea-d_4 taken on APS beamline 14-BM-C at 123.4 K with d = 800.0 mm, ϕ = 0-60°, exposure = 30 s, λ = 0.97870 Å.[52] (B) Profile analysis of the (-1 0 *l m*)$_o$ layer line of this image. The profile was modeled as a commensurate phase with $6c_g' = 7c_h'$.

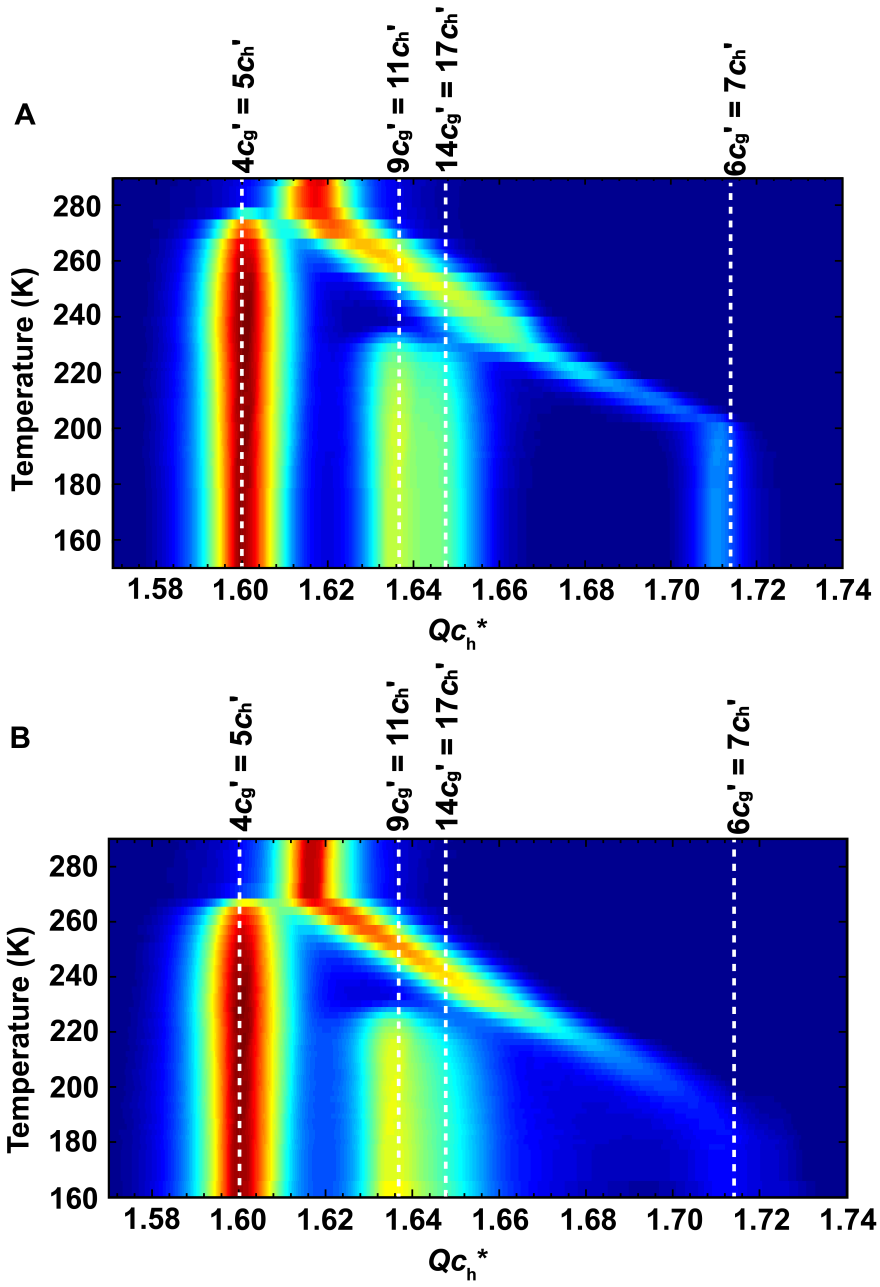

Figure 2.2.2.9. Temperature evolution of the (1 0 *l m*)$_h$ layer line and overlapping (0 2 *l m*)$_o$, and (1 1 *l m*)$_o$ layer lines of 2,8-nonanedione/urea-d$_4$. Layer line profiles are shown on a logarithmic color scale, with red being most intense. Measurements were made using 60° ϕ rotations about the ***c*** axis at a distance of 500.0 mm on APS beamline 14-BM-C with λ = 0.97870 Å.[44] (A) Upon heating from 150 K to 290 K. (B) Upon cooling from 290 K to 160 K. Four commensurate phases are labeled with mc_g' = nc_h'.[50]

2.2.3. Sequence with a UIC from a solution containing a 98.5:1.5 mixture of 2,8-nonanedione and 2-nonanone.

In the “self-compression” mechanism, the driving force is the lock-in transition of enthalpically favored commensurate phases that form. It is important to realize that a commensurate phase must be pinned to the host lattice more so than the remaining incommensurate phase. Otherwise, if the guest in the elongated commensurate phase can translate freely along the channel, no pressure can be held to generate “self-compression”. The degree of pinning of the guest to the host via hydrogen bonding, and hence the driving force of compression, can be tailored systematically by incorporation of impurities in the system. Mixed crystals with various ratios of 2-nonanone and 2,8-nonanedione/urea were grown from a stirred solution. Since the monoketone has only one carbonyl available to make hydrogen bonds to the host, this should lower the stability of the commensurate phases. In fact, in the study of mixed crystals of 2,10-undecanedione:2-undecanone/urea, 2-undecanone serves as a relaxive impurity that disrupts the specific hydrogen-bonding network in the ferroelastic system.[53] Similarly, in the mixed crystal of 2,8-nonanedione:2-nonanone/urea, it is expected that the higher the proportion of the monoketone, the less stable the commensurate phase would be. A less-stable commensurate phase has a higher free energy, thus making the lock-in phase transition less enthalpically favored. In this well-balanced “self-compression” system, if the driving force behind the formation of the elongated commensurate phase is impaired, a lesser percentage of the system is expected to lock in upon cooling, resulting in less compression.

A UIC crystal from a solution containing a 98.5:1.5 mixture of 2,8-nonanedione and 2-nonanone exhibits “self-compression” phase transitions. Profile analyses of the layer lines from the oscillation images of this mixed crystal at different states are presented here. From 281.0 K to 272.9 K, this mixed crystal has a single

incommensurate phase with $\gamma = 0.80889(14)$, as shown in Figure 2.2.3.1. The guest repeat length being c_g = 11.022(2)/0.80889(14) = 13.626(3) Å. Throughout this section it is assumed that the host repeat length is the same as in 2,8-nonanedione/urea, c_h = 10.977(2) + 1.555(9) × 10^{-4} *T*. Upon cooling, the commensurate phase with $4c_g' = 5c_h'$ was first observed at 269.1 K. By 263.7 K the phase with $4c_g' = 5c_h'$ had grown and self-compression was just starting, with the incommensurate component having a misfit parameter γ = 0.80916(11) with c_g = 13.621(3) Å, as shown in figure 2.2.3.2.

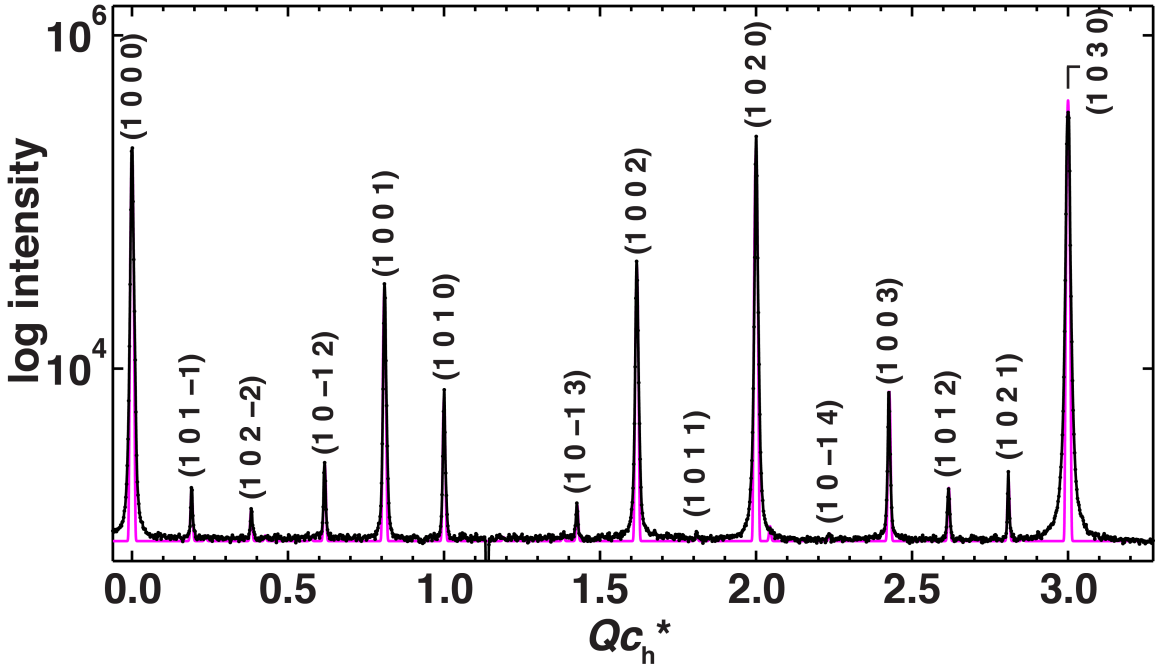

Figure 2.2.3.1. Profile analysis of the (1 0 *l m*)$_h$ layer line of the unwarped synchrotron oscillation image of a urea inclusion crystal from a solution containing a 98.5:1.5 mixture of 2,8-nonanedione and 2-nonanone. The profile was fit with γ = 0.80889(14). The measurement was made using a 60° ϕ rotation about the crystal ***c*** axis at a detector distance of 500.0 mm on beamline 14-BM-C at the APS with λ = 0.97870 Å at 281.0 K.[54]

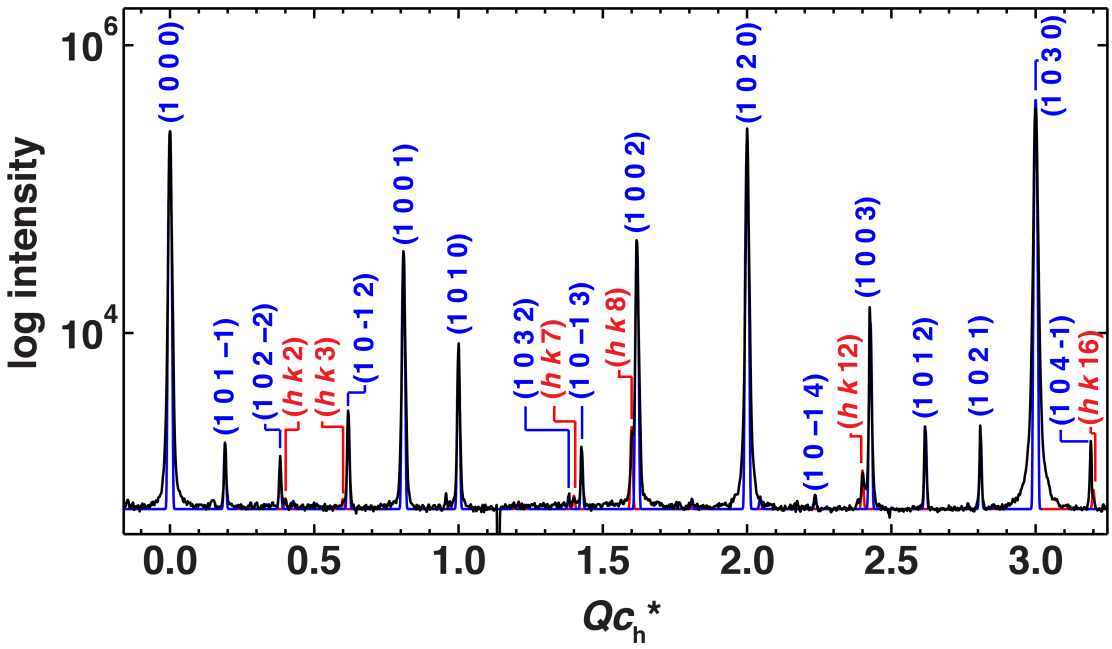

Figure 2.2.3.2. Profile analysis of the (1 0 *l m*)$_h$ layer line of an unwarped synchrotron oscillation image at 263.7 K of a urea inclusion crystal from a solution containing a 98.5:1.5 mixture of 2,8-nonanedione and 2-nonanone. The profile was modeled with a commensurate phase with $4c_g' = 5c_h'$ (red), and fit with an incommensurate phase with γ = 0.80916(11) (blue). The measurement was made using a 60° ϕ rotation about the crystal ***c*** axis at a detector distance of 500.0 mm on APS beamline 14-BM-C with λ = 0.97870 Å.[55]

Between 260.7 and 254.1 K three phases coexisted in the crystal. A growing commensurate phase with $4c_g' = 5c_h'$, a variably-compressed incommensurate phase and a shrinking uncompressed incommensurate phase. These are shown at 256.7 K in Figure 2.2.3.3, with the compressed phase having γ = 0.8130(2), c_g = 13.5509 Å. Clearly, the reduced compressive force generated by the commensurate phase is initially not enough to overcome host-guest pinning (likely due to hydrogen bonding) in some incommensurate regions of the crystal. Unlike the phase with $4c_g' = 5c_h'$, neither of the incommensurate phases showed ferroelastic distortion and a hexagonal basis is

used to index their peaks here. The intensity of the uncompressed incommensurate phase went to zero between 254.1 and 250.6 K, while the self-compression continued. Figure 2.2.3.4 shows a profile of the overlapped (1 0 *l m*)$_h$, (1 1 *l m*)$_o$, and (0 2 *l m*)$_o$ layer lines at 228.9K with the compressed incommensurate phase having γ = 0.8261(6), c_g = 13.331(9) Å.

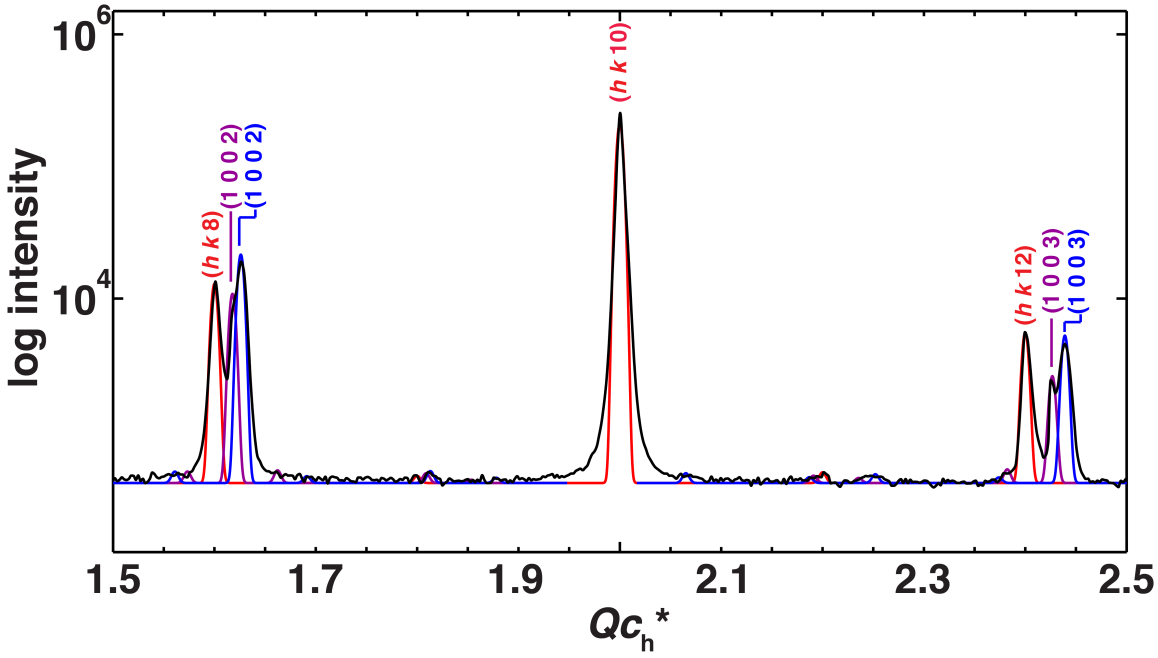

Figure 2.2.3.3. Profile analysis of (1 0 *l m*)$_h$, (1 1 *l m*)$_o$, and (0 2 *l m*)$_o$ layer lines of the unwarped synchrotron oscillation image at 256.7 K of a urea inclusion crystal from a solution containing a 98.5:1.5 mixture of 2,8-nonanedione and 2-nonanone. The profile was modeled with a commensurate phase with $4c_g' = 5c_h'$ (red), and fit with two incommensurate phases: one with γ = 0.8130(2) (blue), the other with γ = 0.8089(2) (magenta). The measurement was made using a 60° ϕ rotation about the crystal ***c*** axis at a detector distance of 500.0 mm on APS beamline 14-BM-C with λ = 0.97870 Å.[56]

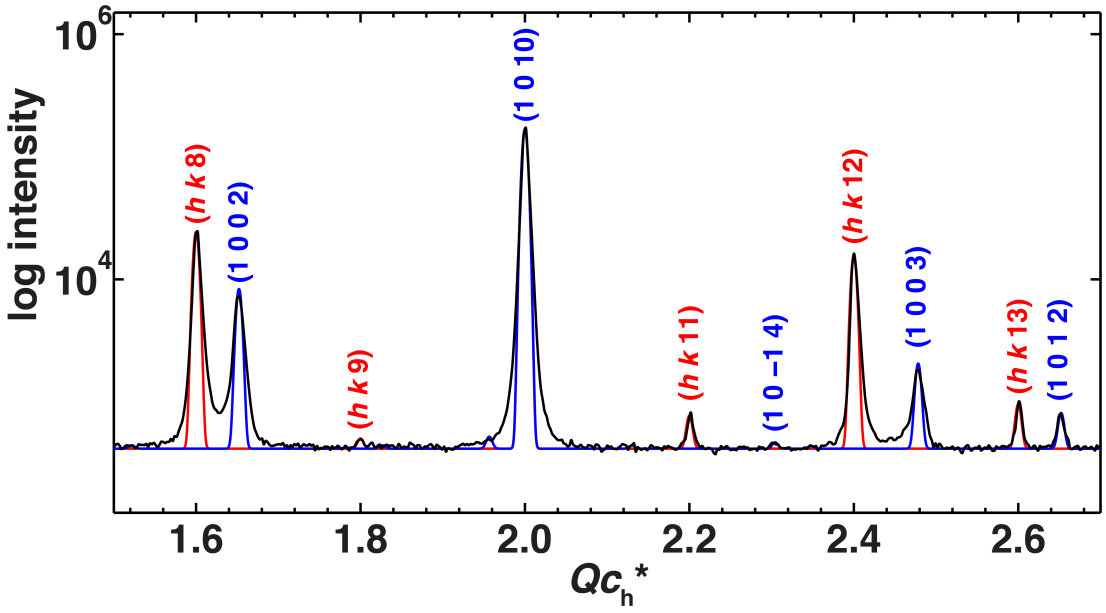

Figure 2.2.3.4. Profile analysis of $(1\ 0\ l\ m)_h$, $(1\ 1\ l\ m)_o$, and $(0\ 2\ l\ m)_o$ layer lines of the unwarped synchrotron oscillation image at 228.9 K of a urea inclusion crystal from a solution containing a 98.5:1.5 mixture of 2,8-nonanedione and 2-nonanone. The profile was modeled with a commensurate phase with $4c_g' = 5c_h'$ (red), and fit with an incommensurate phase with $\gamma = 0.8261(6)$ (blue). The measurement was made using a 60° ϕ rotation about the crystal ***c*** axis at a detector distance of 500.0 mm on APS beamline 14-BM-C with $\lambda = 0.97870$ Å.[57]

A second lock-in phase transition occurred at 225.8 K during cooling as the compressed incommensurate phase locked into a commensurate phase with $9c_g' = 11c_h'$, furhter compressing the remaining incommensurate phase to $\gamma = 0.8286(3)$. Note that only the commensurate phase with $4c_g' = 5c_h'$ is visibly distorted in the ***a*b**** plane. Also, this lock-in phase transition occurred 3.3 K higher compared to 2,8-nonanedione/urea (222.5 K). These temperatures are directly comparable, having been acquired only a day apart under the same beamline conditions. At 169.3 K, the lowest

temperature measured for this crystal, the compressed phase had γ = 0.853(3), c_g = 12.899(45) Å, as shown in Figure 2.2.3.6. This corresponds to a reduction in guest length of 13.626(3) - 12.899(45) = 0.727 Å, of which 11.0033 × (1/0.80889 - 1/0.853) = 0.7034 Å is via self-compression and (11.022(2) - 11.0033(2))/0.80889 = 0.0231 Å is due to thermal shrinking of the host. The peak for this most compressed phase is weak, which makes it difficult to evaluate whether it had reached the commensurate phase with $6c_g' = 7c_h'$. However, the absence of superstructure layer lines indicates that it remained incommensurate.

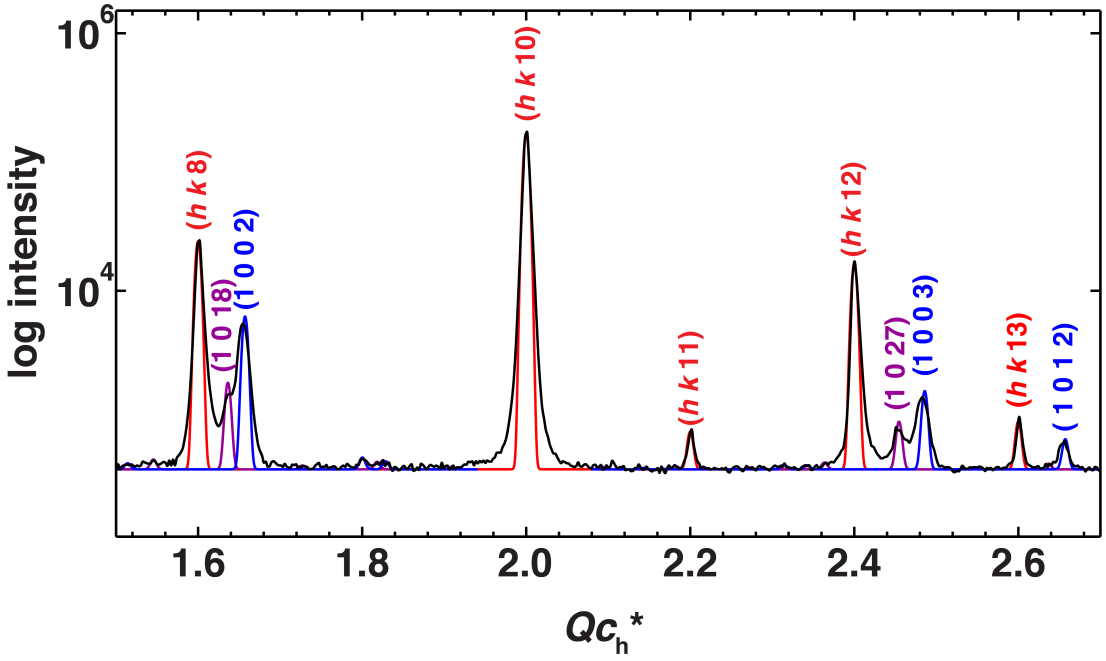

Figure 2.2.3.5. Profile analysis of $(1\ 0\ l\ m)_h$, $(1\ 1\ l\ m)_o$, and $(0\ 2\ l\ m)_o$ layer lines of the unwarped synchrotron oscillation image at 225.8 K of a urea inclusion crystal from a solution containing a 98.5:1.5 mixture of 2,8-nonanedione and 2-nonanone. The profile was modeled with two commensurate phases: one with $4c_g' = 5c_h'$ (red) and the other with $9c_g' = 11c_h'$ (purple). The compressed incommensurate phase was fit with γ = 0.8286(3) (blue). The measurement was made using a 60° ϕ rotation about the crystal ***c*** axis at a detector distance of 500.0 mm on APS beamline 14-BM-C with λ = 0.97870 Å.[58]

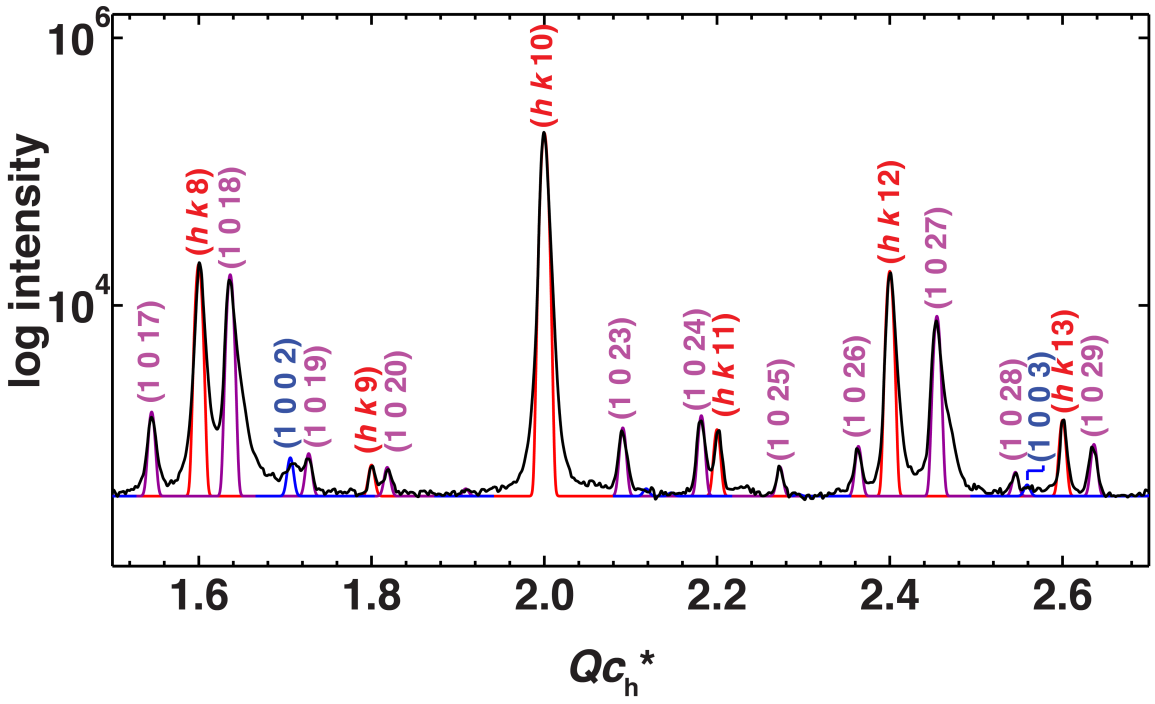

Figure 2.2.3.6. Profile analysis of (1 0 *l* *m*)$_h$, and (1 1 *l* *m*)$_o$, and (0 2 *l* *m*)$_o$ layer lines of the unwarped synchrotron oscillation image at 169.3 K of a urea inclusion crystal from a solution containing a 98.5:1.5 mixture of 2,8-nonanedione and 2-nonanone. The profile was modeled with two commensurate phases: one with $4c_g' = 5c_h'$ (red), and the other with $9c_g' = 11c_h'$ (purple). The compressed incommensurate phase was fit with γ = 0.853(3) (blue). The measurement was made using a 60° ϕ rotation about the crystal ***c*** axis at a detector distance of 500.0 mm on APS beamline 14-BM-C with λ = 0.97870 Å.[59]

From the above analysis, when only 1.5% monoketone is used in the growing solution, “self-compression” phase transitions still occur. As shown in Figure 2.2.3.7, two lock-in phase transitions trigger “self-compression”. As the temperature is lowered, the compressed state is continuously shortened. Although the “self-compression” phase transition behavior still holds true for this sample, a difference compared with the pure diketone sample is that the commensurate phase with $14c_g' = 17c_h'$ exhibits much

reduced intensities. (Notice the shoulder from this phase on the right of the (1 0 18) and (1 0 27) peaks shown in Figure 2.2.3.6.) In a commensurate phase with $14c_g' = 17c_h'$, a twofold screw axis might translate seven guest molecules to cover a whole unit cell. Thus, at a maximum, there are only two hydrogen bonds for every seven guest molecules. It is likely that a slight amount of monoketone inclusion is enough to reduce the formation of this commensurate phase with $14c_g' = 17c_h'$.

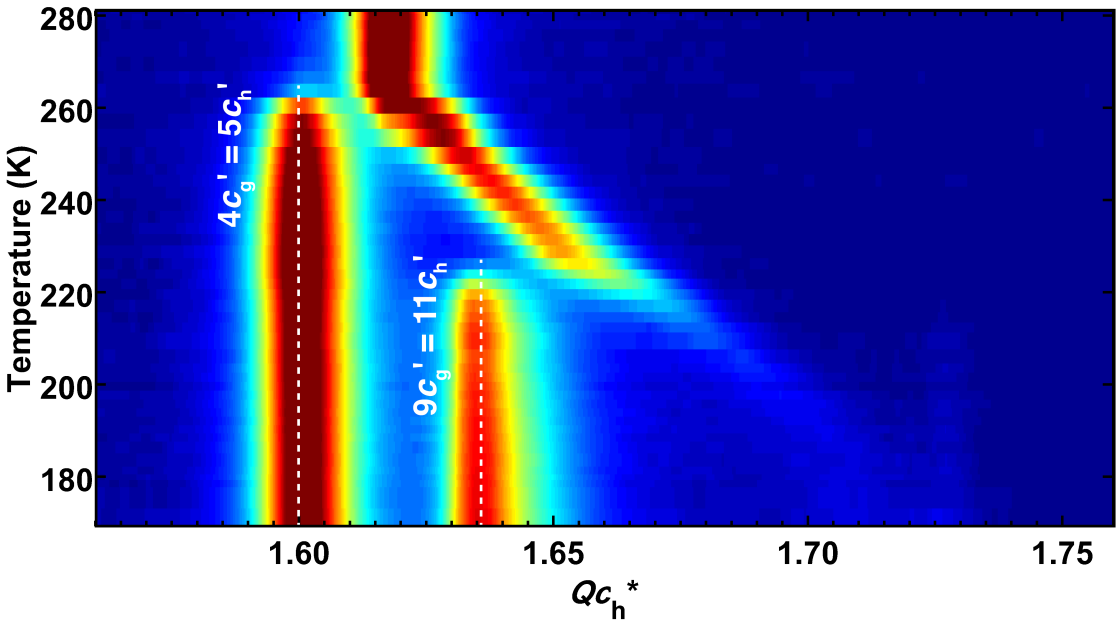

Figure 2.2.3.7. Temperature evolution of the (-1 0 *l m*)$_h$, (0 -2 *l m*)$_o$ and (-1 -1 *l m*)$_o$ layer lines of the unwarped synchrotron oscillation images of a urea inclusion crystal from a solution containing a 98.5:1.5 mixture of 2,8-nonanedione and 2-nonanone upon cooling from 280 to 170 K. Layer line profiles are shown on a logarithmic color scale, with red being most intense. Measurements were made using a 60° ϕ rotations about the crystal ***c*** axis at a detector distance of 500.0 mm on APS beamline 14-BM-C with λ = 0.97870 Å.[60] Two commensurate phases are labeled with $mc_g' = nc_h'$.

2.2.4. Sequence with a UIC from a solution containing a 97.0:3.0 mixture of 2,8-nonanedione and 2-nonanone

A UIC crystal from a solution containing a stirred 97.0:3.0 mixture of 2,8-nonanedione and 2-nonanone was measured on APS beamline 14-BM-C. The sample also showed "self-compression" from lock-in phase transitions at 263.1 K and 224.6 K. Details of these phase transitions are discussed here.

At 281.0 K the crystal had a single incommensurate phase with a misfit parameter γ = 0.8078(5), which corresponds to c_g = 11.022(2)/0.8078(5) = 13.643(9) Å, as shown in Figure 2.2.4.1. A lock-in phase transition occurred at 263.1 K upon cooling, indicated by reflections from the commensurate phase with $4c_g' = 5c_h'$ appearing in the synchrotron oscillation image. Similar to the 98.5:1.5 2,8-nonanedione:2-nonanone/urea crystal, this system had three coexisting phases between 263.1 and 226.9 K, a commensurate phase with $4c_g' = 5c_h'$, a compressed incommensurate phase and remnants of the starting uncompressed incommensurate phase. This is shown at 257.2 and 226.9 K in Figures 2.2.4.2 and 2.2.4.3, where the compressed incommensurate phase has γ = 0.8114(5) and 0.8250(5), respectively. Note that the uncompressed incommensurate phase with γ = 0.8083(5) started to distort in $\boldsymbol{a}^*\boldsymbol{b}^*$ plane below around 250.8 K. At 226.9 K, the uncompressed incommensurate phase has comparable peak intensities to the commensurate phase with $4c_g' = 5c_h'$. The reduced proportion of the crystal that locks in to the phase with $4c_g' = 5c_h'$ results in less driving force for "self-compression". A comparison of the degree of compression between different samples is shown in Section 2.2.6.

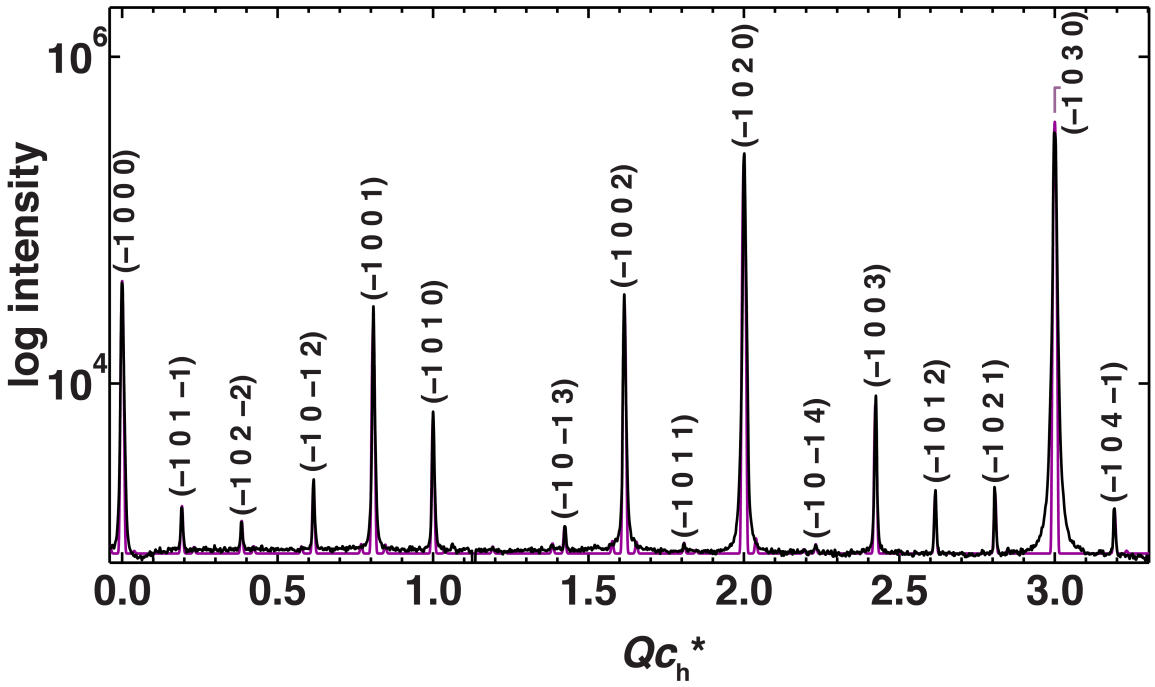

Figure 2.2.4.1. Profile analysis of the (1 0 *l m*)$_h$ layer line of the unwarped synchrotron oscillation image at 281.0 K of a UIC crystal from a solution containing a 97.0:3.0 mixture of 2,8-nonanedione and 2-nonanone. The profile was fit with γ = 0.8078(5). The measurement was made using a 60° ϕ rotation about the crystal ***c*** axis at a detector distance of 500.0 mm at APS beamline 14-BM-C with λ = 0.97870 Å.[61]

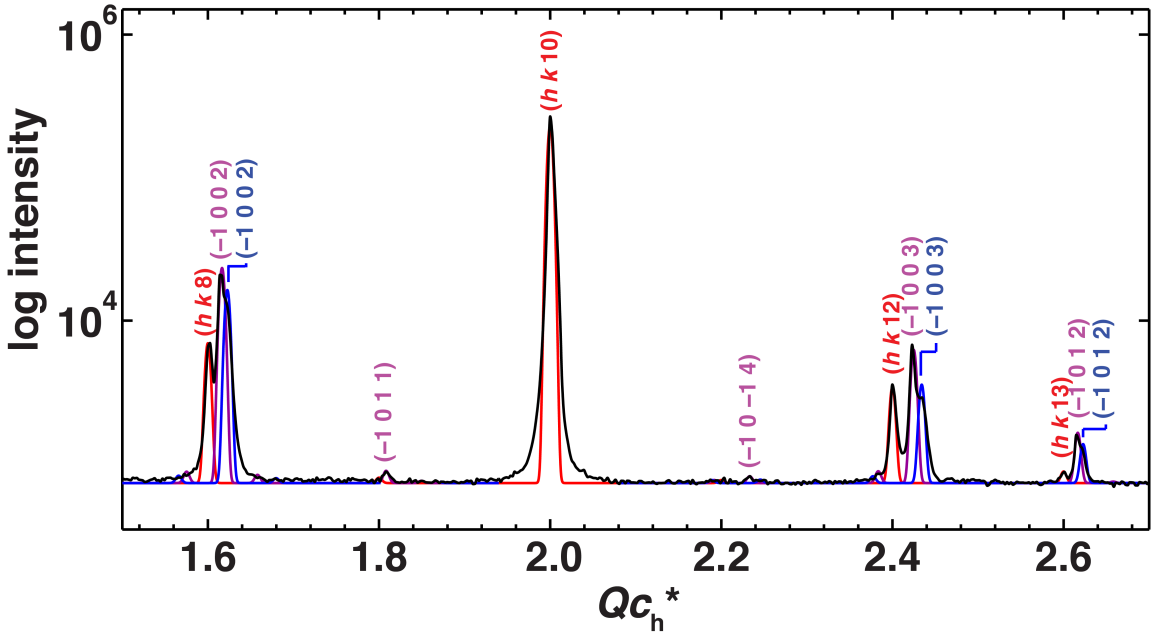

Figure 2.2.4.2. Profile analysis of the (1 0 *l* *m*)$_h$ layer line of the unwarped synchrotron oscillation image at 257.2 K of a urea inclusion crystal from a solution containing a 97.0:3.0 mixture of 2,8-nonanedione and 2-nonanone. The profile was modeled with three phases: a commensurate phase with $4c_g' = 5c_h'$ (red), and two incommensurate phases with $\gamma = 0.8114(5)$ (blue) and $\gamma = 0.8083(5)$ (magenta). The measurement was made using a 60° ϕ rotation about the crystal ***c*** axis at a detector distance of 500.0 mm on APS beamline 14-BM-C with $\lambda = 0.97870$ Å.[62]

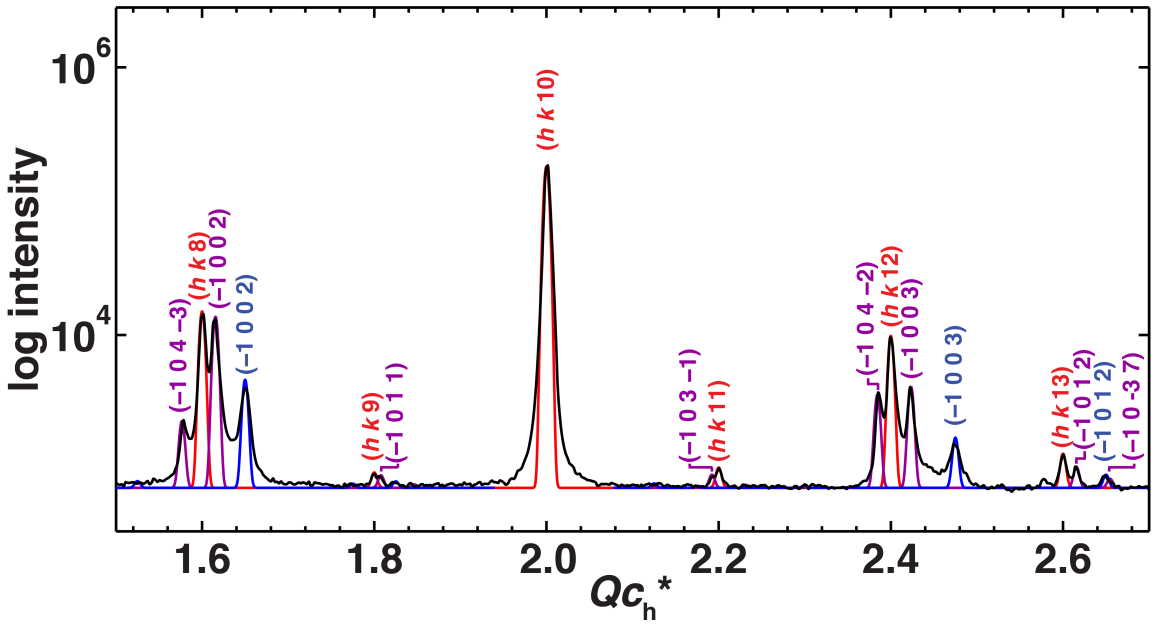

Figure 2.2.4.3. Profile analysis of the (1 0 *l m*)$_h$ layer line and the overlapping (1 1 *l m*)$_o$ and (0 2 *l m*)$_o$ layer lines of the unwarped synchrotron oscillation image of a urea inclusion crystal from a solution containing a 97.0:3.0 mixture of 2,8-nonanedione and 2-nonanone at 226.9 K. The profile was modeled with three phases: a commensurate phase with $4c_g' = 5\ c_h'$ (red), and two incommensurate phases with $\gamma = 0.8280(5)$ (blue) and $\gamma = 0.8078(5)$ (magenta). The measurement was made using a 60° ϕ rotation about the crystal ***c*** axis at a detector distance of 500.0 mm on APS beamline 14-BM-C with λ = 0.97870 Å.[63]

Upon further cooling, reflections from a commensurate phase with $9c_g' = 11c_h'$ first appeared at 224.6 K, driving further self-compression of the compressed incommensurate component while its intensity decreased. Note that the intensity of the remaining uncompressed incommensurate component, which had a guest repeat 0.1645 Å longer than that required for $9c_g' = 11c_h'$ at 226.9 K, did not decrease during this phase transition. This indicates that the phase with $9c_g' = 11c_h'$ was formed entirely from the

compressed component via extension of the guest repeat by 0.1596 Å. This topic will be covered in more detail in Chapter 3. It is difficult to tell at what temperature self-compression stopped, since the intensity of the compressed component was so low. At 186.0 K an oscillation image with prolonged exposure was acquired, a profile of which is shown in Figure 2.2.4.4. The shortest component had a misfit parameter of around γ = 0.848(5), corresponding to c_g = 12.98(8) Å. This is 13.643(9) - 12.98(8) = 0.66(9) Å shorter than at 281 K, of which 11.006 × (1/0.8078 - 1/0.848) = 0.6459 Å is from self-compression and (11.021 - 11.006)/0.8078 = 0.0186 Å is due to thermal shrinking of the host.

The overall phase transition sequence is shown in Figure 2.2.4.5. In summary, above 263.1 K, there is only one phase with γ = 0.8078(5). At 263.1 K the distorted commensurate phase with $4c_g' = 5c_h'$ appeared, growing and compressing some of the incommesurate phase as the temperature was lowered. Then at 244.6 K, the undistorted commensurate phase with $9c_g' = 11c_h'$ appeared. By 186.0 K the most compressed phase was estimated to have been shortened by 0.6459 Å via self-compression. During the whole cooling process, a substantial proportion of the initial uncompressed incommensurate phase persisted. As a result, with only 3.0% 2-nonanone added to the growth solution, the formation of the commensurate phase with $4c_g' = 5c_h'$ is hindered. With reduced formation of the extended commensurate phase with $4c_g' = 5c_h'$, there is less driving force for self compression.

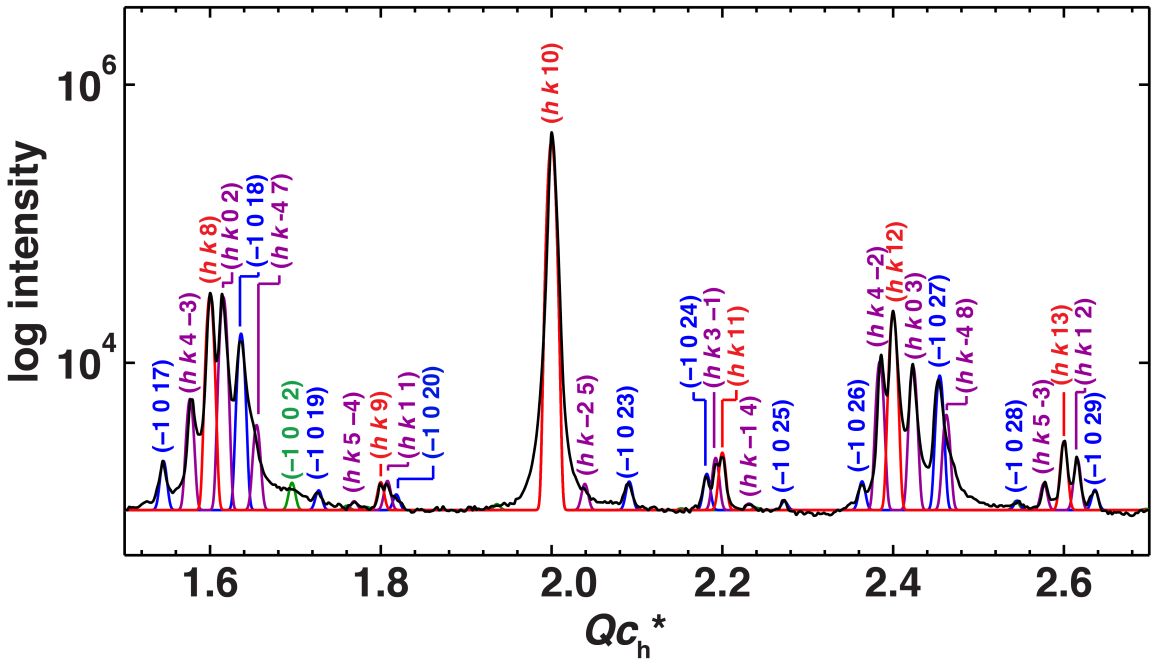

Figure 2.2.4.4. Profile analysis of the (1 0 *l m*)$_h$ layer line and the overlapping (1 1 *l m*)$_o$ and (0 2 *l m*)$_o$ layer lines of the unwarped synchrotron oscillation image of a urea inclusion crystal from a solution containing a 97.0:3.0 mixture of 2,8-nonanedione and 2-nonanone at 186.0 K. The profile is modeled with four phases: two commensurate phases with $4c_g' = 5c_h'$ (red) and $9c_g' = 11c_h'$ (blue), and two incommensurate phases with $\gamma = 0.8278(5)$ (magenta) and $\gamma = 0.848(5)$ (green). The measurement was made using a 60° ϕ rotation about the crystal ***c*** axis at a detector distance of 500.0 mm on APS beamline 14-BM-C with $\lambda = 0.97870$ Å.[64]

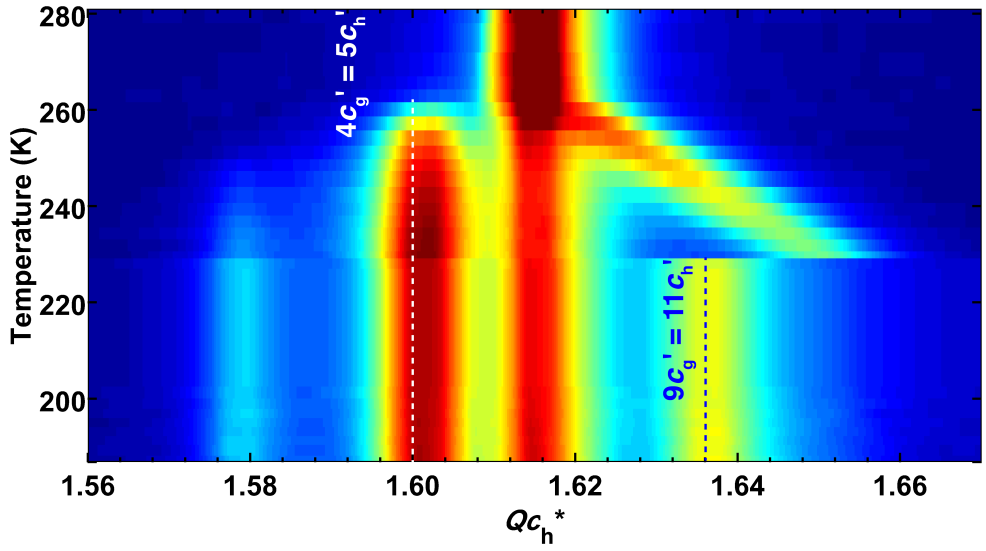

Figure 2.2.4.5. Temperature evolution of the (1 0 *l* *m*)$_h$ and overlapping (0 2 *l* *m*)$_o$ and (1 1 *l* *m*)$_o$ layer lines from the unwarped synchrotron oscillation images of a urea inclusion crystal grown from a solution containing a mixed crystal of a 97.0:3.0 mixture of 2,8-nonanedione and 2-nonanone upon cooling from 281 K to 186 K. Layer line profiles are shown on a logarithmic color scale, with red being most intense. Measurements were made using a 60° ϕ rotation about the crystal ***c*** axis at a detector distance of 500.0 mm on APS beamline 14-BM-C with λ = 0.97870 Å.[65] The two commensurate phases are indicated with dashed lines. Notice that the phase with γ = 0.8083 is persists throughout the temperature scan.

2.2.5. Phase transition sequence with a UIC from a solution containing a 94.0:6.0 mixture of 2,8-nonanedione and 2-nonanone

A UIC crystal from a stirred solution containing a 96.0:4.0 mixture of 2,8-nonanedione and 2-nonanone was studied at APS beamline 14-BM-C. With this ratio of diketone to monoketone, no lock-in phase transition was observed from 280.0 K to 170.0 K. The profile analysis of the $(-1\ 0\ l\ m)_h$ layer line at 280.0 K, shown in Figure 2.2.6.1, gives a misfit parameter of $\gamma = 0.80813(2)$, corresponding to $c_g = 13.637(2)$ Å. When the crystal was cooled below 245.5 K, a ferroelastic phase transition occurred without lock-in to a commensurate structure. The separation of the $(-1\ -1\ l\ m)_o$ and $(0\ -2\ l\ m)_o$ layer lines due to the ferroelastic distortion is shown at 179.7 K in Figure 2.2.5.2 (A). The misfit parameter at that temperature was the same as at 280 K (Figure 2.2.5.2 (B)), corresponding to $c_g = 11.005(2)/0.80814(2) = 13.618(2)$ Å; the reduction in c_g being entirely due to thermal contraction of the host.

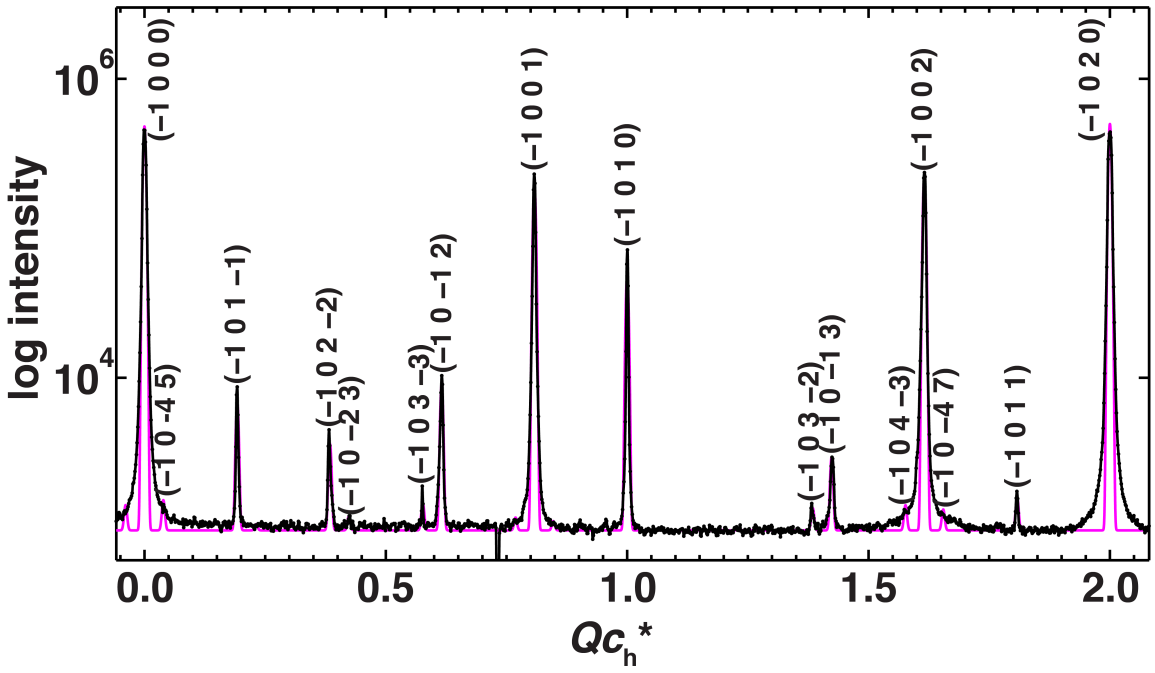

Figure 2.2.5.1. The (-1 0 *l m*)$_h$ layer line of the unwarped synchrotron oscillation image of a urea inclusion crystal from a solution containing a 94.0:6.0 mixture of 2,8-nonanedione and 2-nonanone at 280.0 K. The profile of this layer line was fit with γ = 0.80813(2). The measurement was made using a 60° ϕ rotation about the crystal ***c*** axis at a detector distance of 800.0 mm on beamline 14-BM-C at the APS with λ = 0.97870 Å.[66]

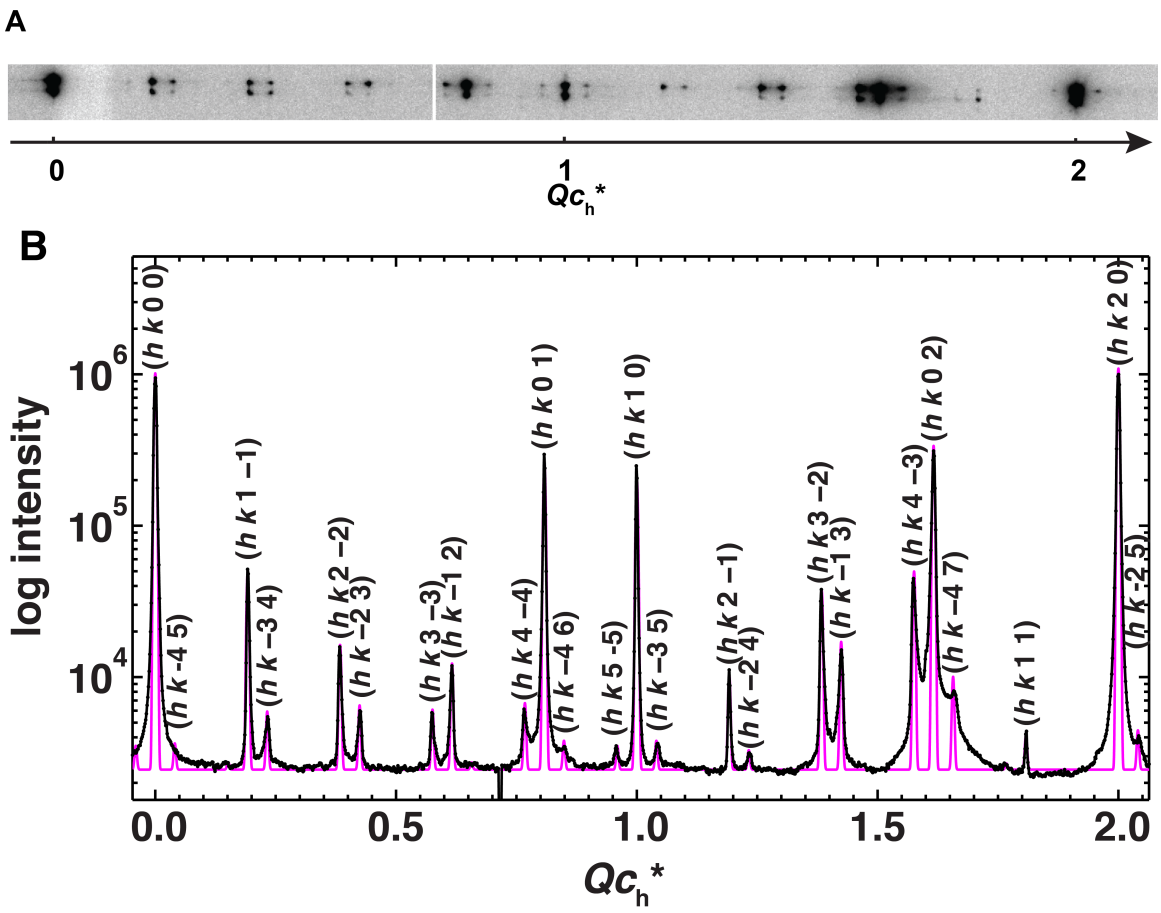

Figure 2.2.5.2. (A) The (-1 -1 *l* *m*)$_o$ and (0 -2 *l* *m*)$_o$ layer lines of an unwarped synchrotron oscillation image of a urea inclusion crystal from a solution containing a 94.0:6.0 mixture of 2,8-nonanedione and 2-nonanone at 179.7 K. (B) The profile of these layer lines was fit with γ = 0.80814(2). The measurement was made using a 60° ϕ rotation about the crystal ***c*** axis at a detector distance of 800.0 mm on APS beamline 14-BM-C with λ = 0.97870 Å.[67]

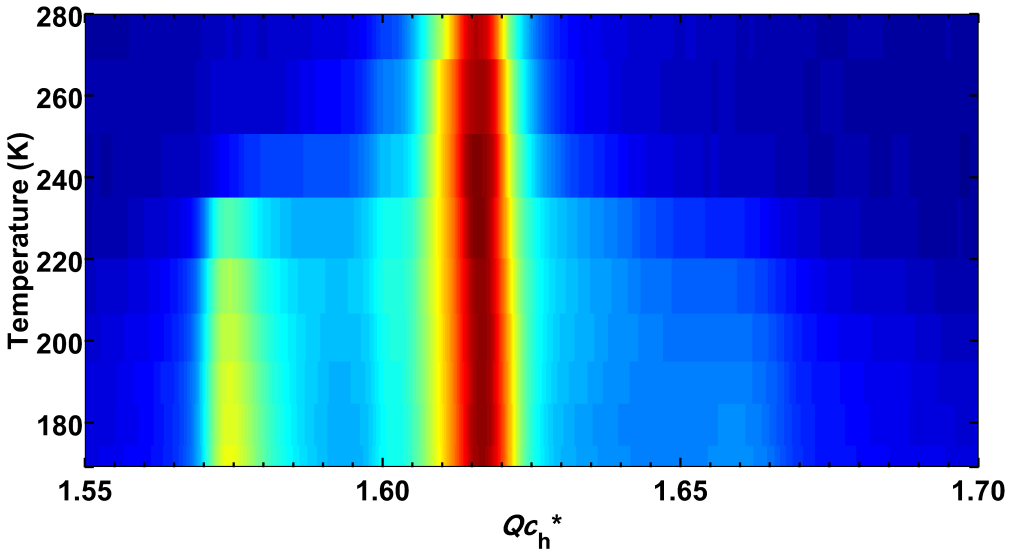

Figure 2.2.5.3. Temperature evolution of the (1 0 *l m*)$_h$ ((-1 -1 *l m*)$_o$ and (0 -2 *l m*)$_o$ below 245.5 K) layer line(s) of unwarped synchrotron oscillation images of a urea inclusion crystal from a solution containing a 94.0:6.0 mixture of 2,8-nonanedione and 2-nonanone. The intensity at $\boldsymbol{Qc}_h^*$ = 1.6163 is for (*h k* 0 2), at $\boldsymbol{Qc}_h^*$ = 1.5756 is for (*h k* 4 -3), and at $\boldsymbol{Qc}_h^*$ = 1.6570 is for (*h k* -4 7). Layer line profiles are shown on a logarithmic color scale, with red being most intense. The measurements were made using 60° ϕ rotations about the crystal ***c*** axis at a detector distance of 800.0 mm on APS beamline 14-BM-C with λ = 0.97870 Å.[68]

As shown in Figure 2.2.5.3, the misfit parameter of this UIC is constant upon cooling from 280.0 to 170 K without any lock-in phase transitions. This result further supports the self-compression mechanism: without elongation of guest molecules in commensurate regions of the crystal, no pressure is generated to compress regions left in between.

2.2.6. Comparison of 2,8-nonanedione/urea with varying proportions of 2-nonanone

In the above sections, “self-compression” phase transitions are discussed in crystals of 2,8-nonanedione/urea, 2,8-nonanedione/urea-d_4, and mixed crystals of 2,8-nonanedione:2-nonanone/urea. A brief summary of the phase transitions is shown in Table 2.2.6. Significant reductions in the degree of compression are observed with small amounts of 2-nonanone included as a relaxive impurity. Since the monoketone can only hydrogen bond to the host at one end, this reduces the enthalpic driving force for the formation of commensurate phases that produce self-compression. This also reduces the proportion of the crystal that experiences self-compression, a quantitative study of which is needed for future research.

Sample	Misfit parameters in the high temperature phase, and c_g (Å)	First lock in temperature (K), on cooling	Second lock in temperature (K), on cooling	Degree of self-compression (Å)
2,8-nonanedione /urea	0.80768(7), 13.646(3)	265.4(5)	222.5(9) and 222.2(4)	0.761(2)
2,8-nonanedione /urea-d_4	0.80734(5), 13.634(3)	267.4(1)	227.9(3) and 223.5(5)	0.7663
*98.5:1.5 UIC	0.80889(14), 13.626(3)	269.1	225.8	0.7034
*97.0:3.0 UIC	0.8078(5), 13.643(9)	263.1	224.6	0.6459
*94.0:6.0 UIC	0.80813(2) 13.634(3)	NA	NA	0

Table 2.2.6. Compiled phase transition temperatures and misfit parameters in the high temperature phase (above first lock-in) for each sample. *The ratio represents 2,8-nonanedione:2-nonanone in the crystal growth solutions, not necessarily in the actual crystal.

2.2.7. Sequence for 2,8-nonanedione/urea grown at low temperature

Given that the phase transition temperature for the formation of the phase with $4c_g' = 5c_h'$ is 265.4(5) K (-7.8(5) ºC) on cooling, it was attampted to grow crystals of 2,8-nonanedione/urea below this phase transition temperature in order to generate crystals that were commensurate at growth. A dilute solution containing 2,8-nonanedione (0.289 g, 1.85 mmol, synthesized and purified with column chromatography) and urea (0.966 g, 16.1 mmol, Sigma-Aldrich puriss) in 15.42 mL methanol (Sigma-Aldrich, HPLC grade) was prepared. The solution was placed in a HAAKE refrigeration bath circulator, filled with a mixture of water and ethylene glycol, set to perform a 24 hour cooling ramp from 258.15 K to 248.15 K. Crystallization was observed at around 252 K. The circulator was at that point reset to a more gradual 24-hour cooling ramp from 251.45 K to 243.15 K to grow large crystals, and harvesting occurred when it had reached approximately 246 K.

The crystal growth solution was transferred outside in a precooled bath of ethylene glycol/water mixture at -25 ºC (248 K). Harvesting was performed on a cold winter morning (Jan 09, 2015) when the outside temperature was measured with a thermocouple to be between -12.4 and -10 ºC (260.75–263.15 K). The crystals were kept on dry ice (194.7 K) until harvesting on Jan 13, 2015 when the outside temperature was measured with a thermocouple to be between -12.9 and -13.0 ºC (260.25–260.15 K). A crystal that appeared as a sectored hexagonal plate was selected from the batch (500 μm wide, 350 μm high, and about 40 μm thick). The sectoring, as shown in Figure 2.2.7.1, indicates that the system is biaxial, i.e., with a symmetry lower than hexagonal/trigonal, as is expected for the ferroelastically distorted phase with $4c_g' = 5c_h'$.[69] The crystal was then mounted on a glass fiber with Super Glue.

The mounted sample was transported on dry ice to ALS Beamline 8.2.1. This macromolecular crystallography beamline is equipped with a 3x3 ADSC Quantum 315R CCD detector, which facilitates obtaining X-ray oscillation images with high spatial

resolution. The crystal was mounted in the cryostream (from Oxford Cryosystems Ltd.) at 230.0 K. After orienting the crystal's channel axis to be perpendicular to the beam, a series of oscillation images were obtained during a cooling ramp from 230 to 100 K.[70]

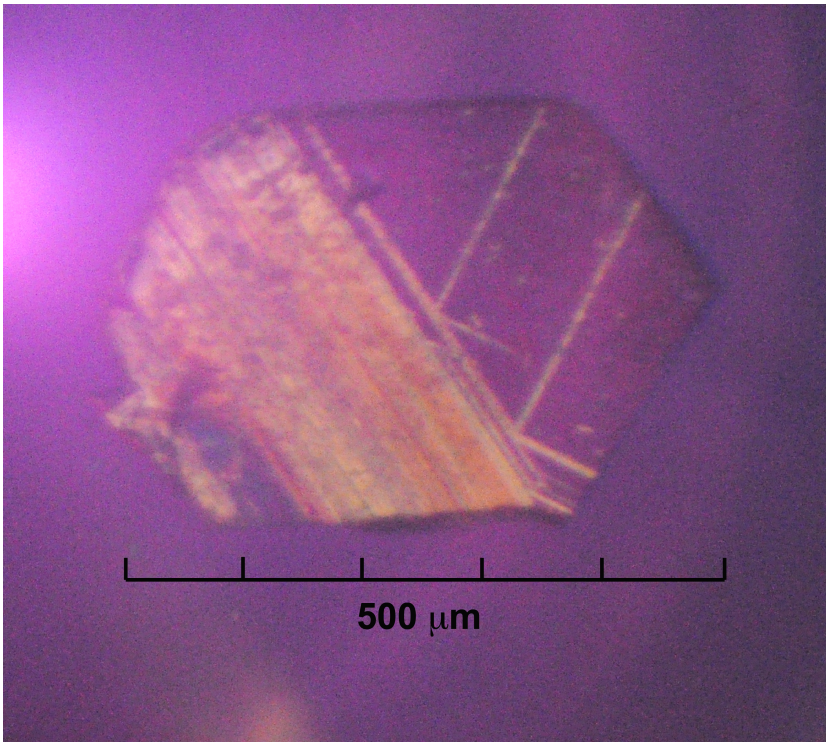

Figure 2.2.7.1. Photomicrograph of 2,8-nonanedione/urea grown in methanol from 258.15 to approximately 246 K, taken at -13.0 ºC (260.15 K) using crossed polars and a 1st order red compensator at 50-fold magnification.[71] The crystal measures 500 μm wide, 350 μm high, and about 40 μm thick.

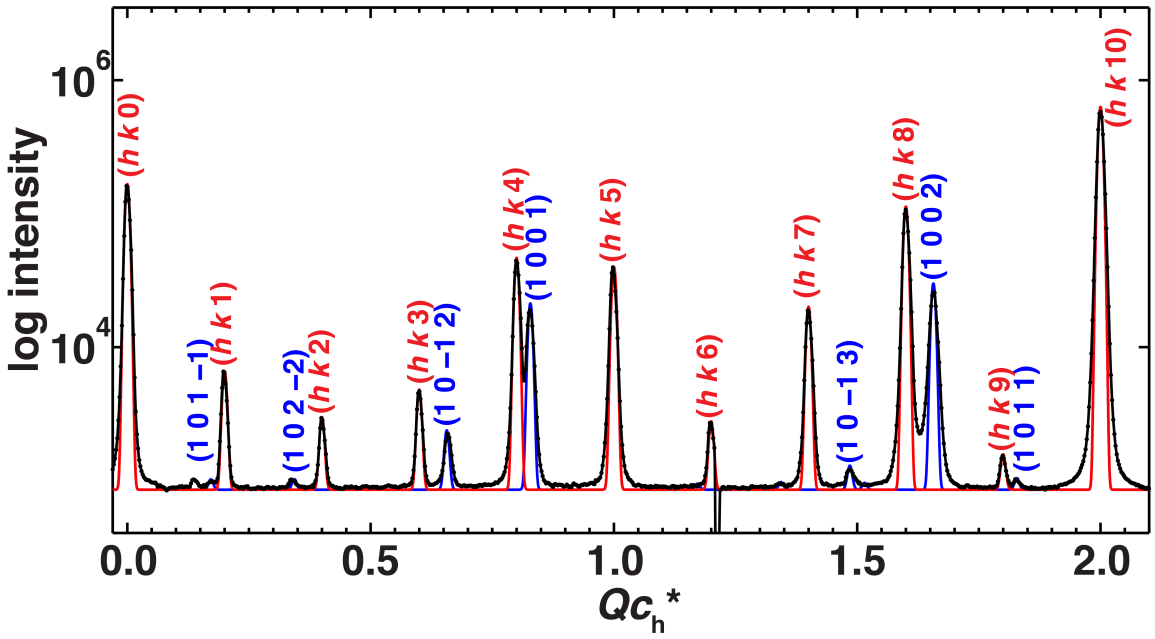

Figure 2.2.7.2. Profile analysis of the (1 0 *l* *m*)$_h$ and the overlapping (1 1 *l* *m*)$_o$ and (0 2 *l* *m*)$_o$ layer lines of the unwarped synchrotron oscillation image taken at 230.0 K of a crystal of 2,8-nonanedione/urea grown from 258.15 to approximately 246 K. The profile was modeled as a commensurate structure with $4c_g' = 5c_h'$ (red), and fit with an incommensurate phase with $\gamma = 0.82828(4)$ (blue). The measurement was made using a 60° ϕ rotation about the crystal ***c*** axis at a detector distance of 480.0 mm on ALS beamline 8.2.1 with $\lambda = 0.999925$ Å.[72]

As shown in Figure 2.2.7.2, the crystal contained two phases at 230.0 K, a commensurate phase with $4c_g' = 5c_h'$ and an incommensurate phase with $\gamma = 0.82828(4)$, $c_g = 13.296(7)$ (using $c_h = 11.013(2)$ Å). For reference, crystals of 2,8-nonanedione/urea grown above the first lock-in phase transition temperature have a compressed incommensurate component with a similar repeat length of $c_g = 13.315(10)$ at 230 K (see Table 2.2.1.1). It is unclear how the shortened structure in the present crystal was formed. One suspicion is that the crystal was not kept cold enough during

crystal harvesting or transferring. The highest outside temperature was -10 ºC (263.15 K) during harvesting, which is close to the incommensurate-to-commensurate phase transition temperature of 271.9(3) K on heating. Even if the crystal formed entirely in the commensurate phase with $4c_g' = 5c_h'$ during growth, the crystal might still undergo a commensurate-to-incommensurate phase transition slowly during harvesting close to the phase transition temperature. If, during this process, the guest molecules contracted along the channel, the voids propagated to the ends of the channel would lead to partial collapse of the UIC at the crystal faces. Thus, when lock-in occurred upon subsequent cooling, it would result in self-compression, as the channels would then be too short to accommodate all the guests in their extended conformation with $4c_g' = 5c_h'$.

Upon further cooling, a lock-in phase transition was first observed at 215.8 K. The profile analysis in Figure 2.2.7.3 clearly shows that at 204.0 K, there are three commensurate phases: $4c_g' = 5c_h'$, $9c_g' = 11c_h'$, and $14c_g' = 17c_h'$. The compressed incommensurate state was measured to have γ = 0.840(5) at 204.0 K, c_g = 11.01(2)/0.840(5) = 13.11(8) Å. Further cooling produced more self-compression, but the intensity of the compressed component became too small to measure accurately, as shown in Figure 2.2.7.4, at 100.0 K.

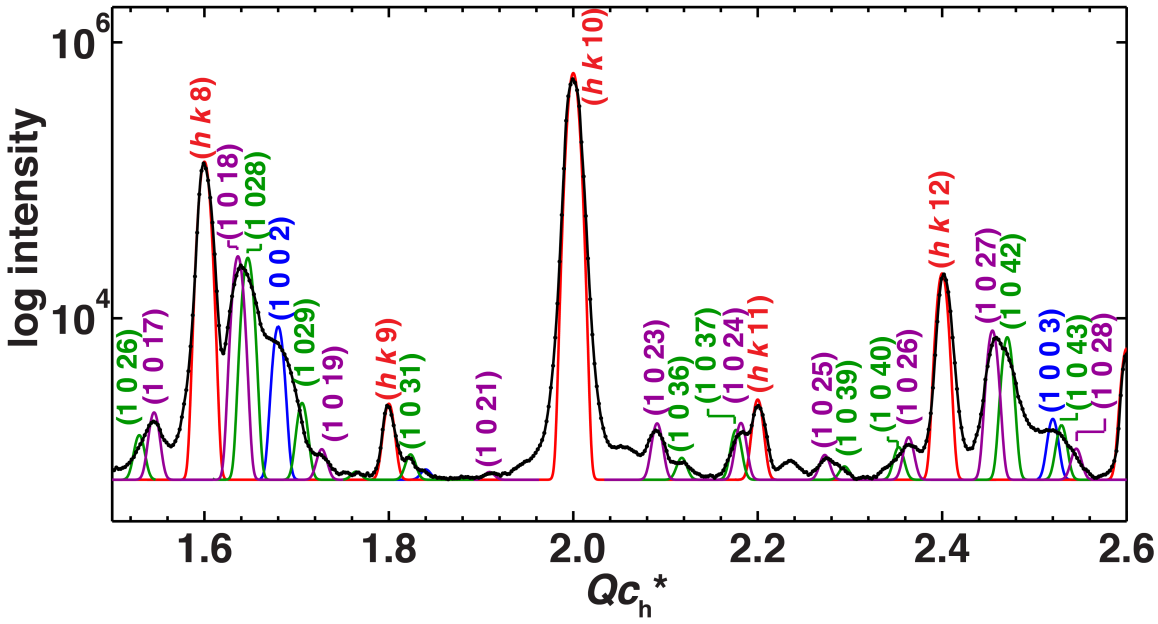

Figure 2.2.7.3. Profile analysis of the (1 0 *l* / *m*)$_h$ and the overlapping (1 1 *l* / *m*)$_o$ and (0 2 *l* / *m*)$_o$ layer lines of the unwarped synchrotron oscillation image taken at 204.0 K of a crystal of 2,8-nonanedione/urea grown from 258.15 to approximately 246 K. The profile is modeled with three commensurate phases: $4c_g' = 5c_h'$ (red), $9c_g' = 11c_h'$ (magenta), and $14c_g' = 17c_h'$ (green), as well as an incommensurate phase with $\gamma = 0.840(5)$ (blue). The measurement was made using a 60° ϕ rotation about the crystal ***c*** axis at a detector distance of 480.0 mm on beamline 8.2.1 at the ALS with $\lambda = 0.999925$ Å at 204.0 K.[73]

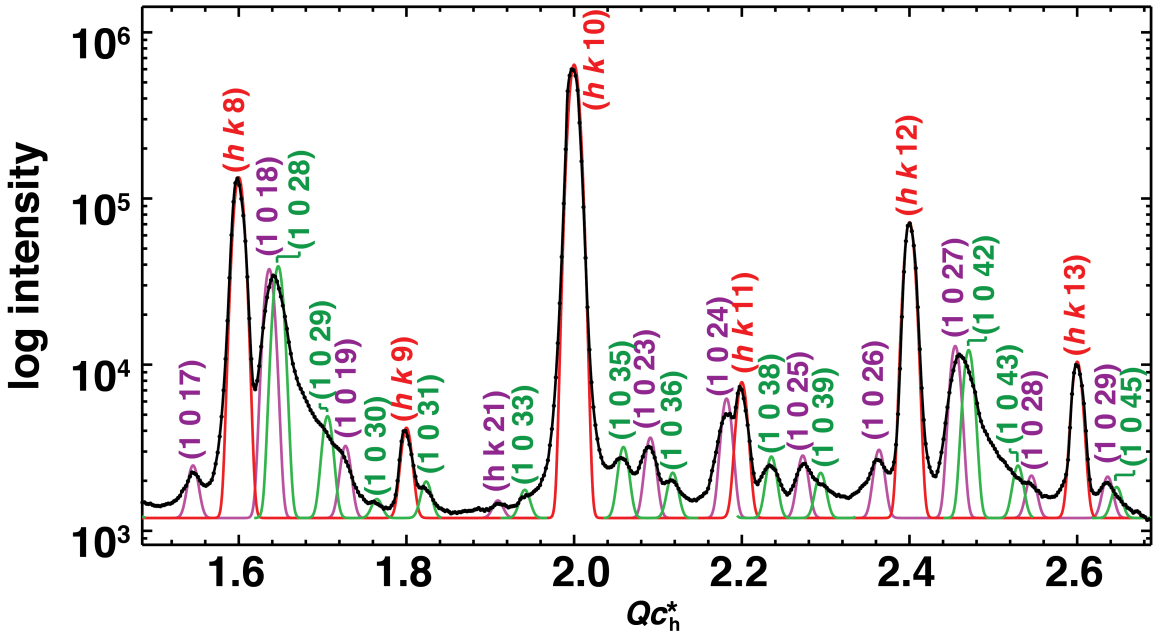

Figure 2.2.7.4. Profile analysis of the (1 0 *l m*)$_h$ and the overlapping (1 1 *l m*)$_o$ and (0 2 *l m*)$_o$ layer lines of the unwarped synchrotron oscillation image taken at 100.0 K of a crystal of 2,8-nonanedione/urea grown from 258.15 to approximately 246 K. The profile was modeled with three commensurate phases: $4c_g' = 5c_h'$ (red), $9c_g' = 11c_h'$ (magenta), and $14c_g' = 17c_h'$ (green). The measurement was made using a 60° ϕ rotation about the crystal ***c*** axis at a detector distance of 480.0 mm on ALS beamline 8.2.1 with λ = 0.999925 Å.

From this temperature scan of a crystal grown from 258.15 to 243.15 K, below the highest lock-in phase transition temperature, it is shown that self-compression still occurred. It is likely that the crystal had partially converted to an incommensurate phase from being held above the lock-in phase transition temperature of 271.9(3) K.

2.2.8. Reversibility test with cooling-heating cycles

To test whether the “self-compression” phase transitions of crystals of 2,8-nonanedione/urea are reversible, three cooling-heating cycles were conducted on the same crystal of 2,8-nonanedione/urea. To avoid potential beam damage, a high degree of attenuation was applied. Temperature scans were conducted on APS beamline 14-BM-C. The synchrotron oscillation image parameters were: distance = 450.0 mm, focus = 400.0 mm, ϕ = 60º-120º, exposure = 4.0 s, beam size = 0.30 × 0.40 mm, attenuation = 16 aluminum sheets, λ = 0.97870 Å.[74]

An identical sequence of phase transitions was observed in the three cooling and heating cycles. The misfit parameters of the compressed phase in each cycle are compiled in the Figure 2.2.8. The results show that the slopes of γ (and hence c_g) are the same in repeated cycles. Furthermore, the start and end γ at the extremes of temperature are the same in each cycle. Both of these indicate that the degrees of compression in the three cycles are the same, and that the phase transitions are reversible.

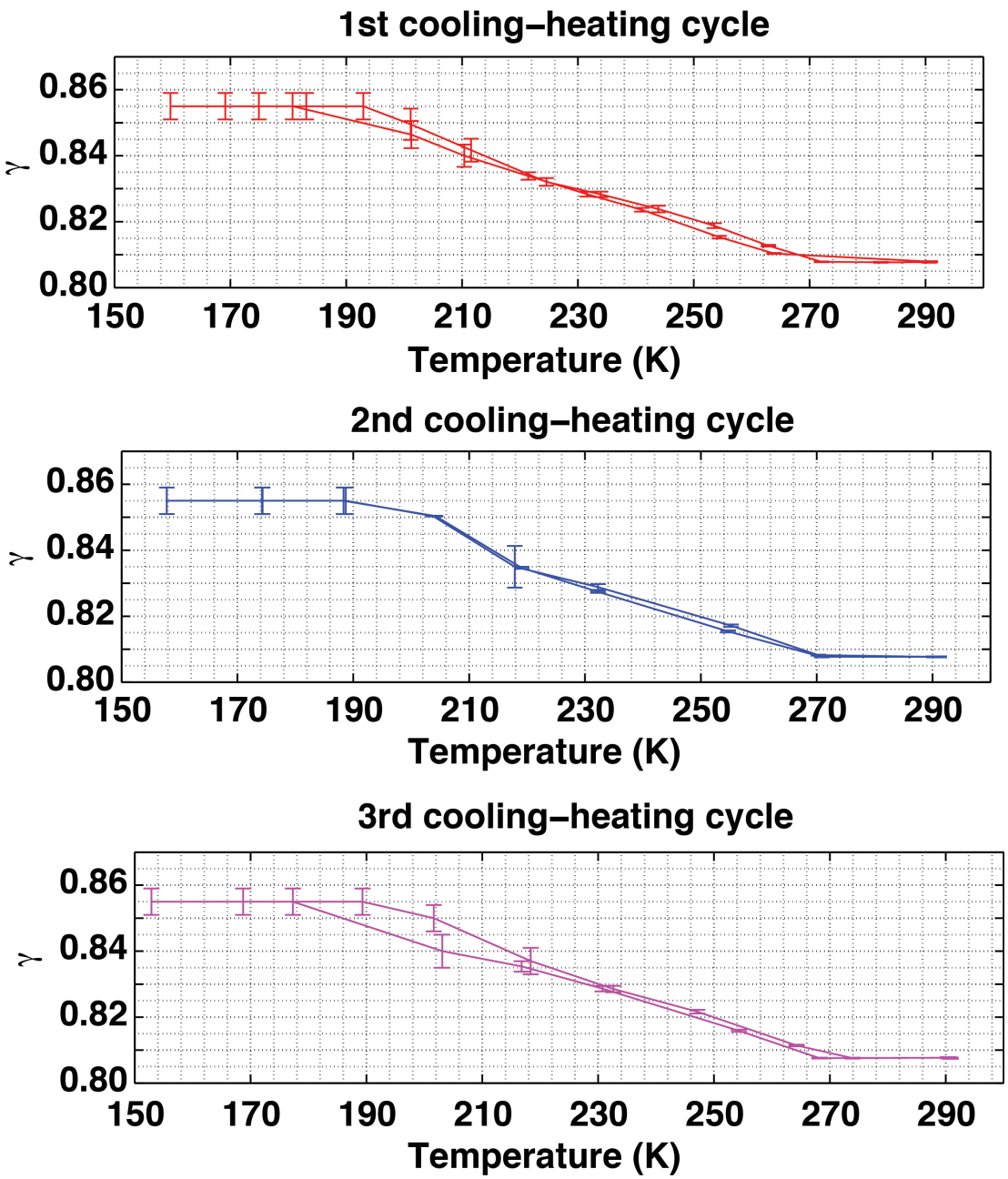

Figure 2.2.8. Reversibility test of the phase transitions of 2,8-nonanedionere/urea. The misfit parameter, γ, of the compressed structure as a function of temperature for three consecutive cycles done on the same crystal is compiled. The misfit parameters were measured from profile analysis of the (1 1 *l m*)$_o$ and (0 2 *l m*)$_o$ layer lines of unwarped synchrotron oscillation images.[74]

2.2.9. Oscillation images of 4,4'-oxybis(2-butanone)/urea

Another way to probe the self-compression mechanism is by modifying the guest. Since it is expected that the driving force for the lock-in phase transition is the relatively strong hydrogen bonding network between the host and 2,8-nonanedione, an analogous molecule, 4,4'-oxybis(2-butanone), was investigated. At 290 K it was established that the value of c_g in 2,8-nonanedione/urea was 13.646(3) Å. To estimate the room-temperature c_g of the analog, semi-empirical AM1 calculations were performed on both 4,4'-oxybis(2-butanone) and 2,8-nonanedione.[75] The methyl-methyl distance in 2,8-nonanedione was calculated to be 10.07 Å, so a constant offset of 13.646(3) - 10.07 = 3.576(3) Å should be added to the methyl-methyl distance of the analog to give its predicted value of c_g. The methyl-methyl distance in 4,4'-oxybis(2-butanone) was calculated to be 9.83 Å, and c_g of this analog is predicted to be 9.83 + 3.576(3) = 13.406(3) Å. Thus, 4,4'-oxybis(butan-2-one)/urea has a predicted value of c_g in between those for structures with $14c_g' = 17c_h'$ (c_g' = 13.3839 Å) and $9c_g' = 11c_h'$ (c_g' = 13.4713 Å). This guest was synthesized and crystallized via evaporation at room temperature.[76] A hexagonal crystal (size 0.3×0.6×1.0 mm) was selected, as shown in Figure 2.2.9.1. Synchrotron X-ray oscillation images were then recorded at ALS beamline 8.2.2.

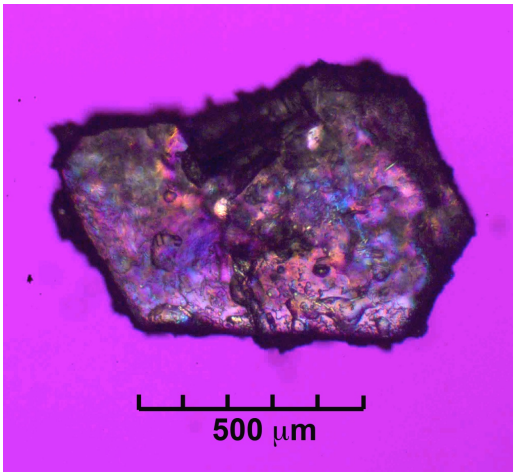

Figure 2.2.9.1. Photomicrograph of 4,4'-oxybis(2-butanone)/urea with crossed polars and a 1st order red compensator taken at 4-fold magnification.[76]

The profile analysis of the (-1 0 *l* *m*)$_h$ layer line at 290.0 K is shown in Figure 2.2.9.2. The misfit parameter was fit to γ = 0.81797(8), c_g = 13.475(3) Å (using c_h = 11.022(2) Å), which is indistinguishable from a commensurate phase with $9c_g' = 11c_h'$ (c_g' = 13.471(2)). Further evidence for the commensurability of this phase is provided by the crystal structure below. Surprisingly, the profile analysis of the (-1 -1 *l* *m*)$_h$ layer line at 290.0 K shows that there are two components: a major component modeled as a commensurate phase with $9c_g' = 11c_h'$, and a minor incommensurate component modeled with γ = 0.8205, as shown in Figure 2.2.9.2 (B).

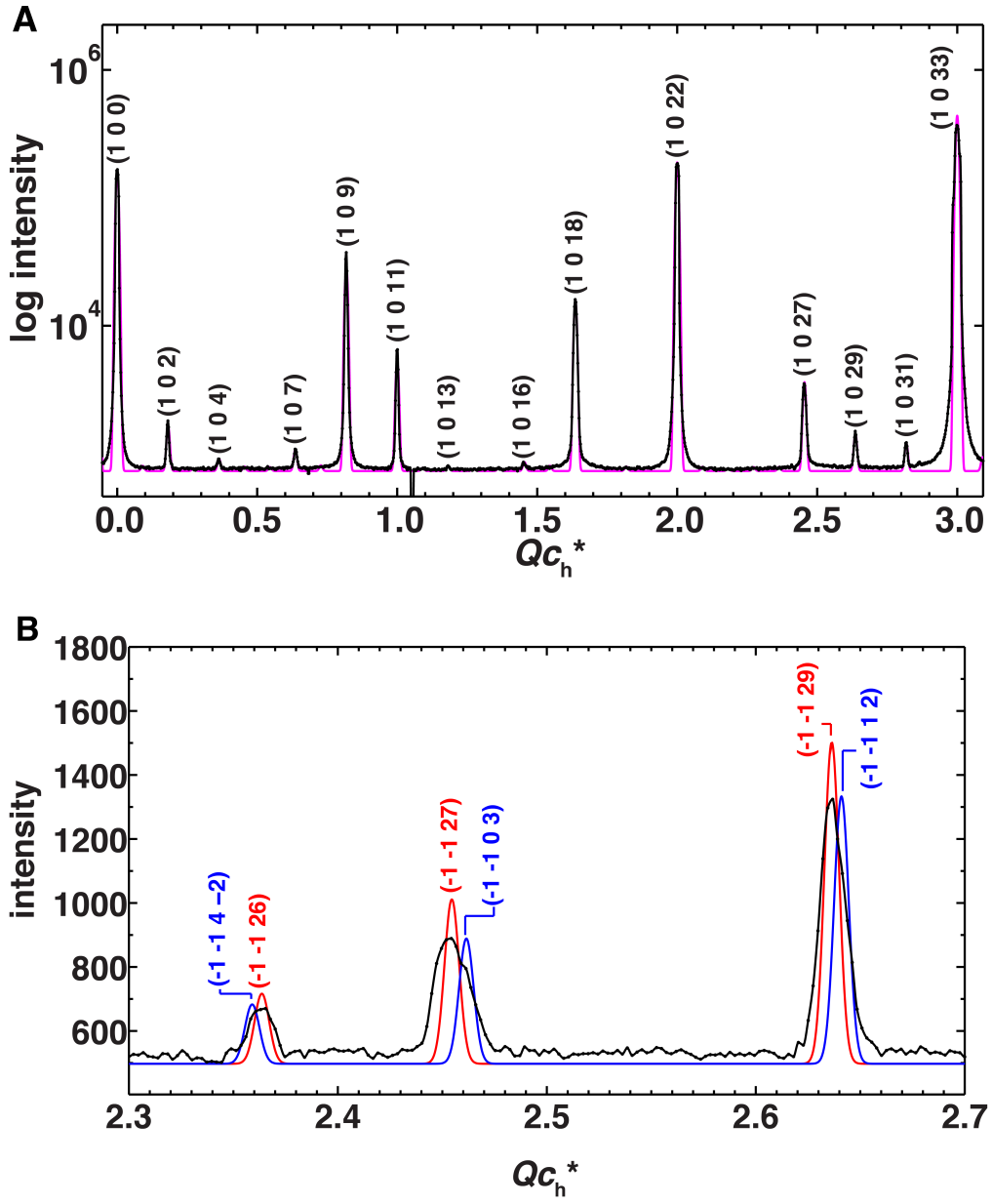

Figure 2.2.9.2. (A) Profile analysis of the (1 0 *l* *m*)$_h$ layer line of the unwarped synchrotron oscillation image of 4,4'-oxybis(2-butanone)/urea at 290.0 K. The profile was modeled with commensurate phase with $9c_g' = 11c_h'$. (B) Profile analysis of the (-1 -1 *l* *m*)$_h$ layer line. The major component was modeled with $9c_g' = 11c_h'$ (red) and the minor component was modeled with $\gamma = 0.8205$ (blue). The measurement was made using a 60° ϕ rotation about the crystal ***c*** axis at a detector distance of 480.0 mm on beamline 8.2.2 at the ALS with $\lambda = 0.999979$ Å.[77]

A ferroelastic phase transition of the commensurate phase with $9c_g' = 11c_h'$ occurred at 196 K. Below 196 K, the commensurate phase with $9c_g' = 11c_h'$ is distorted in the ***ab*** plane, as shown in Figure 2.2.9.3 (B). However, the minor component did not distort and its misfit parameter remained constant as a function of temperature, as shown for 187.0 K in Figure 2.2.9.3 (A). Although the major component is distorted in the ***ab*** plane, indicating symmetry lower than hexagonal/trigonal, the $h+k$ = odd layer lines were not observed. Thus it is likely to be a C-centered cell. Upon cooling below 159 K, superstructure lines with $h+k$ = odd appeared, suggesting a transition to a primitive cell. The profile analysis of the image taken at 101.0 K is shown in Figure 2.2.9.3. In the analysis, only the commensurate phase with $9c_g' = 11c_h'$ is modeled.

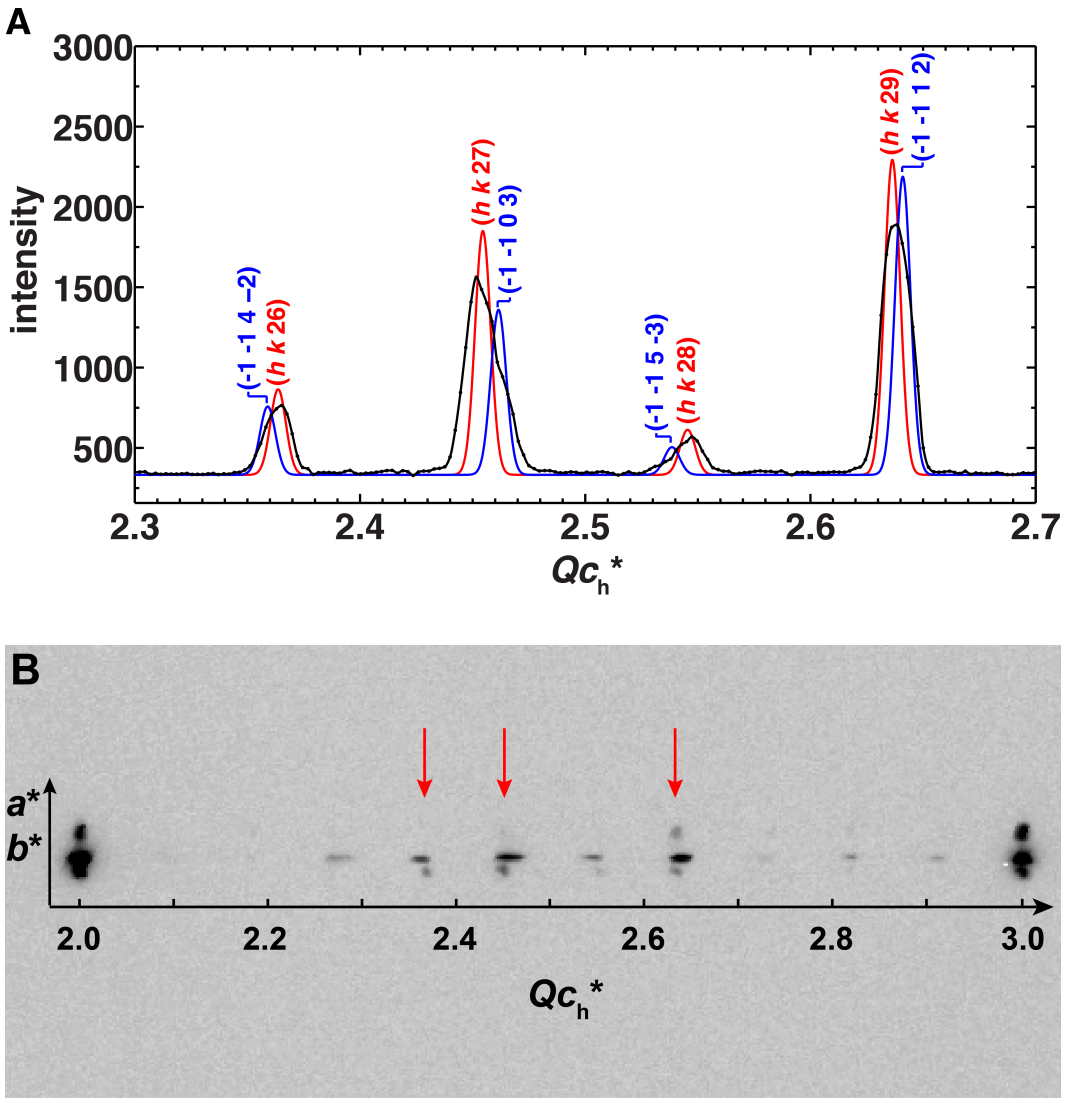

Figure 2.2.9.3. (A) Profile analysis of the (-1 -1 *l m*)$_h$ and the overlapping (-1 -3 *l m*)$_o$ and (-2 0 *l m*)$_o$ layer lines of the unwarped synchrotron oscillation image of 4,4'-oxybis(2-butanone)/urea at 187.0 K. The major component was modeled with $9c_g' = 11c_h'$ (red). The incommensurate minor component (not distorted) was modeled with $\gamma = 0.8205$ (blue). (B) Section of the unwarped oscillation image used in part (A). Peaks indicated by red arrows are the largest peaks in part (A). The layer lines of the commensurate component only are separated along ***a*b**** due to ferroelastic distortion. The measurement was made using a 60° ϕ rotation about the crystal ***c*** axis at a detector distance of 480.0 mm on beamline 8.2.2 at the ALS with $\lambda = 0.999979$ Å.[78]

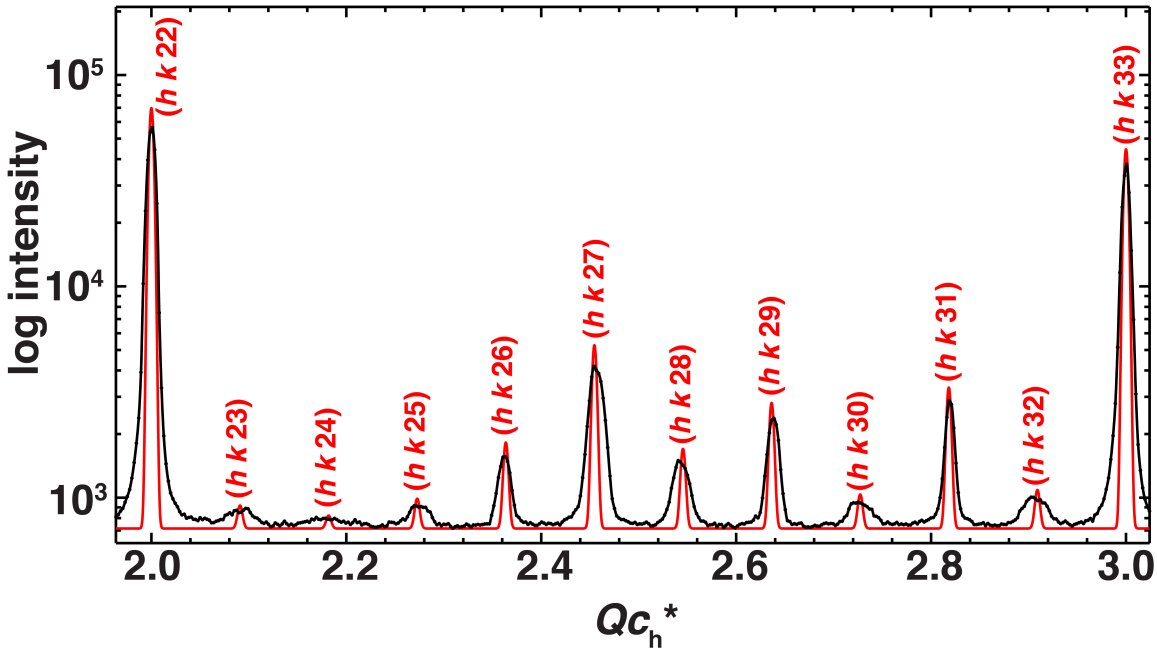

Figure 2.2.9.4. Profile analysis of the (-1 -3 *l* *m*)$_o$ and (-2 0 *l* *m*)$_o$ layer lines of the unwarped synchrotron oscillation image of 4,4' -oxybis(2-butanone)/urea at 101.0 K. The profile was modeled with the commensurate phase with $9c_g' = 11c_h'$. The measurement was made using a 60° ϕ rotation about the crystal ***c*** axis at a detector distance of 480.0 mm on beamline 8.2.2 at the ALS with λ = 0.999979 Å.[79]

From the above analysis, it was learned that this system is mainly commensurate with $9c_g' = 11c_h'$ and not ferroelastically distorted above 197 K. Another crystal from the same batch was then picked to collect an X-ray dataset on ALS beamline 8.2.2 at 210.0 K, using λ = 0.885601 Å, distance = 130.0 mm.[39] It was integrated using APEX2,[80] and solved by the XS method using Olex2.[81,82]

A

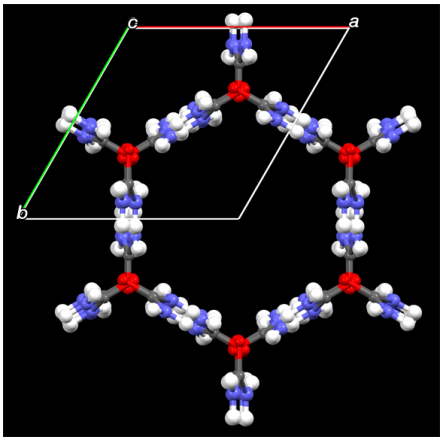

B

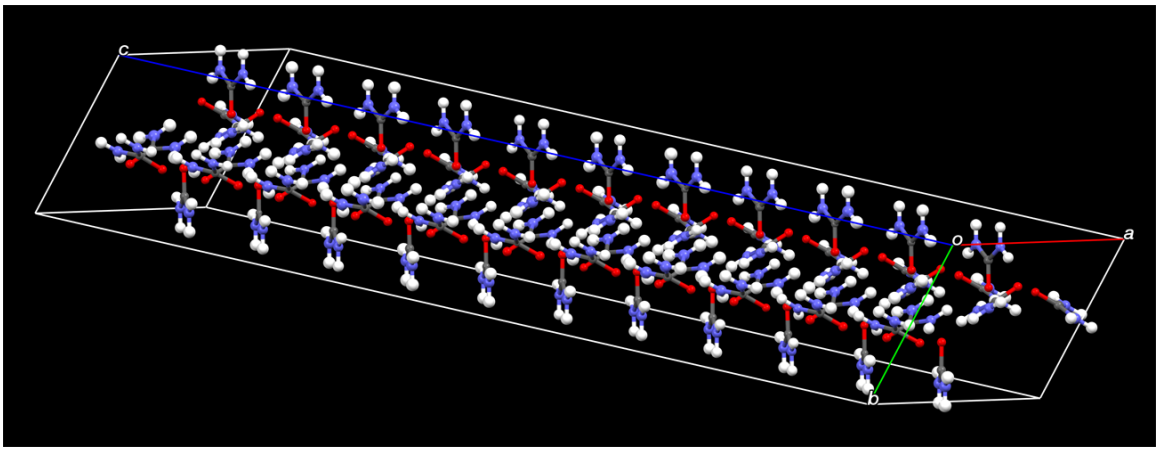

Figure 2.2.9.5. (A) Host structure of 4,4'-oxybis(2-butanone)/urea view along ***c***. (B) A side view of the channel, the axes are shown. This host structure was solved in $P3_112$, with $R_1 = 0.2835$. The guest could not be located.[83]

Cell constants and an orientation matrix for data collection were obtained from a least-squares refinement of 9979 reflections.[80]

a = 8.1628(2) Å	α = 90°
b = 8.1628(2) Å	β = 90°
c = 120.881(3) Å	γ = 120°
V = 6975.4(3) Å^3	

In a hexagonal setting, the R_{sym} was estimated to be 0.177. The systematic absence exceptions for a threefold screw axis generated within the .prp file are: 50 out of 591 observed reflections that have $I>3\sigma$, with an average intensity = 0.2 and intensity over σ = 0.6. From these statistics, although there are violations for the threefold screw axis, they are quite weak. Thus the UIC has a threefold screw axis. For a commensurate $9c_g' = 11c_h'$ relationship, the threefold screw axis can translate three guest molecules along the channel to fill the unit cell. The highest symmetry allowed in this case would be $P3_112$, where a twofold axis perpendicular to the channel can relate one and half guest molecules. Although the host structure was found, as shown in Figure 2.2.9.4, the guest molecules could not be located. Test solutions in $P3_1$ also failed in locating the guest. The difficulties in resolving the guest molecules could be for several reasons. First, there is diffuse scattering along the guest layer lines, indicating that the guest molecules are disordered. Since only two hydrogen bonds can theoretically be made by every three guest molecules, they might have high thermal vibration. Second, as shown in the profile analyses, there is a minor component that is not commensurate. A mixture of phases influences the value of F_{obs} of a pure commensurate system. Furthermore, with a minor incommensurate phase incorporated in the channel, the commensurate guest domains might be disordered spatially along the channel, *e.g.* screw-like disordered sites. This issue is similar to that in mixed crystals of 2,9-decanedione:2-decanone/urea, where one crystal has two components: a commensurate phase with $3c_g' = 4c_h'$ and an incommensurate phase. In that case, a multiple disordered model was proposed.[60]

In summary, data analysis of 4,4’-oxybis(2-butanone)/urea crystals shows that the UIC is mainly commensurate with $9c_g' = 11c_h'$. The single crystal structure can only be resolved to the host structure, which has a threefold screw axis along the channel.

Identification code	4,4'-oxybis(2-butanone)/urea
Empirical formula	CH_4N_2O
Formula weight	60.06
Temperature/K	210.0
Crystal system	Trigonal
Space group	$P3_112$
a/Å	8.1628(2)
b/Å	8.1628(2)
c/Å	120.881(3)
α/°	90
β/°	90
γ/°	120
Volume/Å^3	6975.4(3)
Z	66
ρ_{calc} g/cm^3	0.944
μ/mm^{-1}	0.143
F(000)	2114.3
Crystal size/mm^3	0.6 × 0.4 × 0.1
Radiation	Synchrotron (λ = 0.885601)
2ϕ range for data collection/°	1.26 to 52.56
Index ranges	-8 ≤ h ≤ 8, -7 ≤ k ≤ 7, -116 ≤ l ≤ 116
Reflections collected	94749
Independent reflections	4856 [R_{int} = 0.0973, R_{sigma} = 0.0299]
Data/restraints/parameters	4856/0/176
Goodness-of-fit on F^2	3.543
Final R indexes [I>=2σ (I)]	R_1 = 0.2835, wR_2 = 0.7440
Final R indexes [all data]	R_1 = 0.2990, wR_2 = 0.7668
Largest diff. peak/hole / e Å^{-3}	1.40/-1.64
Flack parameter	-2(2)
Temperature (K)	210.0

Table 2.9.1. Crystallographic parameters of the host structure of 4,4'-oxybis(2-butanone)/urea.[83]

2.3. Crystal structure of 2,8-nonanedione/urea

In order to determine the crystal structure of the phase with $4c_g' = 5c_h'$, ideally a single domain of the ferroelastically-distorted crystal needs to be isolated. This is not possible for a crystal grown above the lock-in phase transtion and subsequently cooled, since the crystal then contains 6 non-merohedral twins as well as the compressed incommensurate component.

A crystal was taken from the same batch as described at the start of Section 2.2.7. Harvesting and mounting occurred on Jan 09, 2015 while the outside temperature was measured with a thermocouple to be between -12.4 and -11.7 ºC (260.75–261.45 K). The starting crystal (shown in Figure 2.3.1) exhibited sectoring, indicating that it was biaxial with a symmetry lower than hexagonal/trigonal. This is a signature of ferroelastic deformation of the unit cell, as expected for the phase with $4c_g' = 5c_h'$.[69] Furthermore, the flat plate morphology is consistent with zero offset between guests in adjacent channels.[1]

The section of the crystal shown in Figure 2.3.1 was cut out and mounted on a 75 µm MiTeGen MicroLoop™ with low viscosity cryo-oil (MiTeGen LV CryoOil™). The trimmed sector, a trapezoid measuring about 200 by 200 µm wide and 25 µm thick, was almost clear and appeared to be a single domain. This crystal was then transported on dry ice (194.7 K) to ALS beamline 11.3.1.[84] It was transferred to a helium cryostrem at 240.0 K, and then cooled to 18.0 K before data collection. The synchrotron beam was set to 14999.8223 eV (wavelength = 0.82657 Å). Beamline 11.3.1 employs a Bruker PHOTON100 CMOS detector running in shutterless mode. A Cryocool 3-in 1 Unit helium cryostream from Cryo Industries of America, Inc. and a LakeShore 336 Temperature Controller from Lakeshore Cryotronics, Inc. were used to maintain the crystal at temperatures as low as 18.0 K in this study. To acquire low angle data, heavy

attenuation was applied (48% + 78% + 38% beam attenuators and 16 aluminum sheets). For high-angle data, only eight aluminum sheets were used.

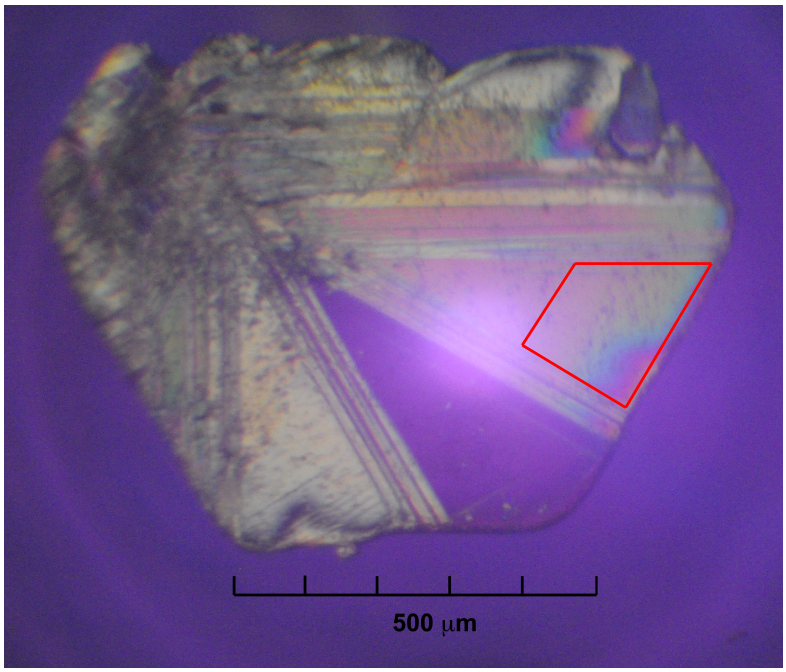

Figure 2.3.1. Photomicrograph of 2,8-nonanedione/urea grown in methanol from 258.15 K to approximately 246 K, taken at -12.4 ºC (260.75 K) with crossed polars and a 1st order red compensator. The image was taken at 50-fold magnification, with the crystal measuring 950 μm wide, 670 μm high and about 25 μm thick. The indicated trapezoid section, measuring about 200 by 200 μm, was cut out and used for the experiments in this section.

The following discussion concerns the crystal structure determination.[85] The dataset was processed using the Bruker APEX2 software package.[80] Cell constants and an orientation matrix were obtained from a least-squares refinement of 73273 reflections. This corresponded to a C-centered orthorhombic cell with the following dimensions:

a = 8.102(4) Å α = 90°

b = 14.043(7) Å β = 90°

c = 54.85(3) Å γ = 90°

V = 6241(5) Å^3

For Z = 4 and F.W. = 1213.36, the calculated density is 1.291 g/cm^3. Based on the systematic absences of:

hkl: *h*+*k* ≠ 2n

a statistical analysis of intensity distributions, and the successful solution and refinement of the structure uniquely determined the space group to be:

$C222_1$ (# 20)

The data were collected at a temperature of 18.0 K using ω and φ scans using the Bruker APEX2 software package.[80] Of the 73273 reflections (1.726° ≤ 2θ ≤ 67.17°) that were collected, 7799 were unique (R_{int} = 0.0818, R_{sigma} = 0.0373); equivalent reflections were merged using SADABS 2014/5.[86] Because different settings of attenuation had been applied, datasets with the same attenuation were integrated together.[87] Later, all of the data was scaled with SADABS software.[86] The linear absorption coefficient, μ, for the synchrotron radiation is 0.153 mm^{-1}.[85b]

Using Olex2,[81] the structure was solved with the XS structure solution program using direct methods and refined with the XL refinement package using least squares minimization.[82] In the final cycles of refinement, all non-hydrogen atoms were refined anisotropically. The position of each hydrogen atom was refined using a riding model, with values of U_{iso} that were 1.2 or 1.5 times the U_{eq} for the heavy atom to which the hydrogen is bonded, depending on the position of the heavy atom. The final cycle of full-matrix least-squares refinement[88] was based on 7476 observed reflections (I > 4.00σ(I)), 220 variable parameters, 265 restraints, and converged with unweighted and weighted

agreement factors of:

$R1 = \Sigma||Fo|-|Fc|| / \Sigma|Fo| = 0.1261$

$wR2 = \{\Sigma[w(Fo^2-Fc^2)]^2 / \Sigma[w(Fo^2)]^2\}^{1/2} = 0.3555$

where

$w = 1/[\sigma^2(Fo^2)+(aP)^2+bP]$,

and

$P = [2Fc^2+Max(Fc^2,0)]/3$

Here, a and b were set to 0.10 and 20.0, respectively.

The goodness of fit was 1.461.[89] The maximum and minimum peaks in the final difference Fourier map corresponded to 0.56 e/Å^3 (0.50 Å from O2) and -0.53 e/Å^3 (0.12 Å from O1), respectively. Neutral atom scattering factors were taken from International Tables for Crystallography.[90]

Note that the R1 and wR2 values are quite high. One possible cause is that the crystal contained phases other than the single domain with $4c_g' = 5c_h'$. Although only one commensurate phase with $4c_g' = 5c_h'$ was expected, it was shown in Section 2.2.7 that there were at least three commensurate phases for the same batch of crystals: $4c_g' = 5c_h'$, $9c_g' = 11c_h'$, and $14c_g' = 17c_h'$ at 100 K.[85b] Figure 2.3.2 shows a portion of a frame form this dataset in which peaks with a different periodicity than the predominant commensurate structure are observed along a section of the $(5\ 1\ l)_o$ layer line. These are likely from another commensurate phase with $9c_g' = 11c_h'$ or $14c_g' = 17c_h'$ within the crystal. Peaks from an additional phase could easily be overlapped with those from the dominant phase with $4c_g' = 5c_h'$, contaminating the intensity measurements, and resulting in a deviation of F_o of the pure commensurate phase with $4c_g' = 5c_h'$. Luckily, the percentage of this type of contamination was relatively low, so that the crystal structure could still be solved.

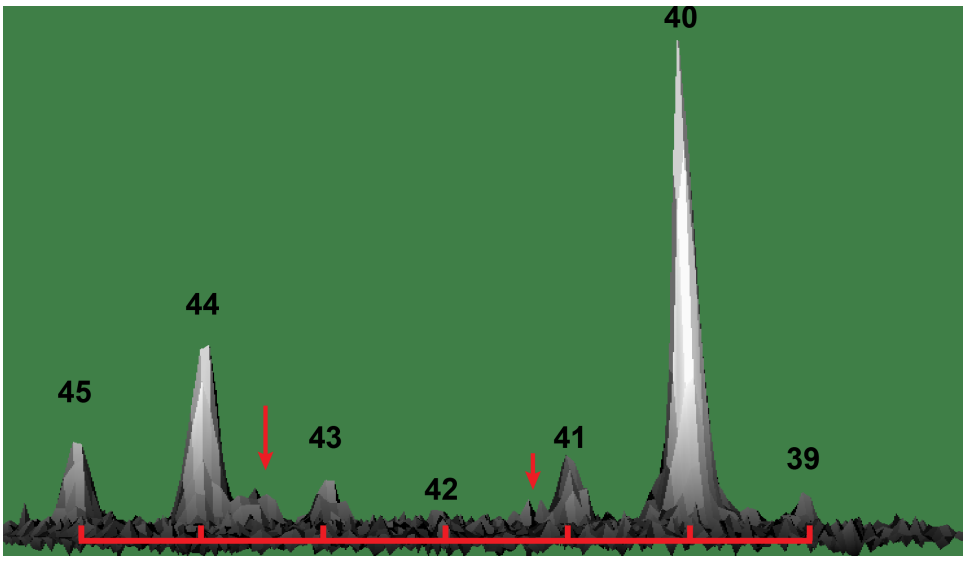

Figure 2.3.2. A 3-D view of a slice of the synchrotron X-ray diffraction image. This layer line has indices h = 5, k = 1, and l is labeled. The red arrows show peaks belonging to a phase other than the phase with $4c_g' = 5c_h'$, very likely to be the phases with $9c_g' = 11c_h'$ or $14c_g' = 17c_h'$.[91]

For the weighting scheme with $w = 1/[\sigma^2(Fo^2)+(aP)^2+bP]$, a and b were set to 0.10 and 20.0, respectively. The XL program suggested a WGHT scheme with a = 0.140 and b = 53.130. A survey of different matrix of weighting schemes was conducted to find an optimized combination. As shown in Table 2.3.1, three factors were considered; Goof (smaller than two is suggested by IUCr),[92] R1, and the esds of atomic positions. A suitable WGHT of a = 0.15 and b = 20 was chosen as a compromise between the optimization metrics. This weighting scheme also gave a flat analysis of variance, K, over the whole range of resolutions, as shown in Table 2.3.2.

	a	b	Goof	R1	esds
WGHT	0.140	53.130	1.088	12.420	0.132
WGHT	0.100	0.000	2.830	12.700	0.127
WGHT	0.200	0.000	1.817	12.860	0.120
WGHT	0.150	0.000	2.211	12.780	0.122
WGHT	0.150	10.000	1.689	12.570	0.128
WGHT	0.150	20.000	1.461	12.126	0.129
WGHT	0.150	30.000	1.290	12.470	0.130
WGHT	0.200	0.000	1.817	12.860	0.120

Table 2.3.1. Compiled weighting scheme results using $w=1/[\sigma^2(Fo^2)+(aP)^2+bP]$. For each combination of a and b the dataset was refined to convergence to provide the Goof, R1, and esds metrics.

Resolution (Å)	0.75-0.78	0.78-0.81	0.81-0.85	0.85-0.89	0.89-0.95	0.95-1.01	1.01-1.12	1.12-1.28	1.28-1.60	1.60-Inf.
Reflections	802	761	808	761	780	765	788	774	775	785
Goof	1.077	1.103	1.059	1.303	1.292	1.403	1.459	1.683	1.699	2.166
K	1.093	1.023	1.017	1.034	1.010	1.020	0.992	1.019	1.042	1.001
R1	0.177	0.173	0.152	0.154	0.125	0.126	0.119	0.129	0.117	0.106

Table 2.3.2. Compiled analyses of Goof, K, and R1 values over a range of resolutions.

To improve the 2,8-nonanedione/urea structure model, 265 restraints were applied during refinement as follows:

1. An earlier model without twinning was checked using Platon[93] and a possible twin law was suggested by the TwinRotMat algorithm. Based on the F_c calculated from coordinates in the .cif file, a twofold axis was found along either the [1 -3 0] direct lattice direction, or along the [1 -1 0] direction in reciprocal space. The calculated difference

between the two directions is = 0.03°. The suggested twin law was:

$$\begin{bmatrix} -0.499 & -0.500 & 0.000 \\ -1.502 & 0.499 & 0.000 \\ 0.000 & 0.000 & -1.000 \end{bmatrix} \times \begin{bmatrix} h1 \\ k1 \\ l1 \end{bmatrix} = \begin{bmatrix} h2 \\ k2 \\ l2 \end{bmatrix}$$

Since the reflections are too overlapped to be integrated individually, the data was integrated as totally overlapped pseudo-merohedral twins. Shelx XL calculates F_c^2 values as :

$$(F_c^2)^* = \mathrm{osf}^2 \sum_{m=1}^{n} k_m F_{cm}^2$$

where osf is the overall scale factor, k_m is the fractional contribution from the twin, (which is refined by the BSAF command in Shelx XL), and F_{cm} is the calculated structure factor of twin domain *m*. The following two commands were therefore used in Shelx XL:

BASF 0.503

TWIN -0.5 -0.5 0 -1.5 0.5 0 0 0 -1 2

By applying this twin law, R1 was reduced by 7%.

2. The U_{iso} of the hydrogen atoms was set to be either 1.2 or 1.5 times the corresponding value of the heavy atoms to which they were bonded, for atoms in non-terminal and terminal positions, respectively.

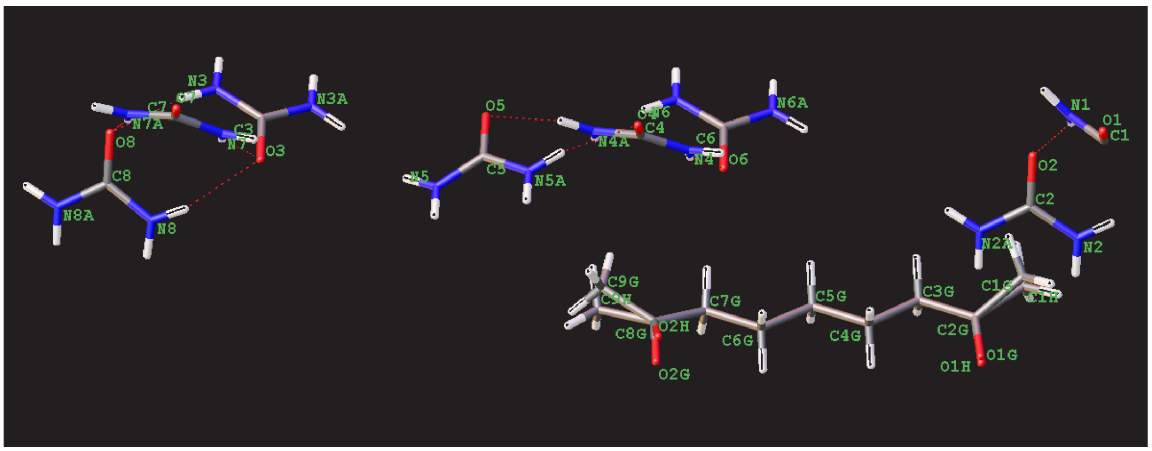

Figure 2.3.3. Labeled diagram of one asymmetric unit of the crystal structure of 2,8-nonanedione/urea in the phase with $4c_g' = 5c_h'$.

3. 1,2- and 1,3-distances were restrained as described below. For atom labels refer to Figure 2.3.3.

The SADI command was used with sigma = 0.01 on 1,2-distances:

a. The C_{sp3}-C_{sp2} bond distance of the guest carbonyl groups was restrained.

C1G-C2G ≈ C1H-C2G ≈ C9G-C8G ≈ C2G-C3G ≈ C8G-C7G ≈ C8G-C9H≈ C2G-C3G ≈ C8G-C7G

b. The C_{sp3}-C_{sp3} bond distance in the guest was restrained.

C3G-C4G ≈ C4G-C5G ≈ C5G-C6G ≈ C6G-C7G

c. The C=O bond distance in the guest was restrained.

O2G-C8G ≈ O1G-C2G ≈ C8G-O2H ≈ O1H-C2G

d. The C-N bond distance in each urea molecule was restrained.

C1-N1 ≈ C2-N2 ≈ C2-N2A ≈ C3-N3 ≈ C3-N3A ≈ C4- N4 ≈ C4-N4A ≈ C5

N5 ≈ C5-N5A ≈C6-N6 ≈ C6-N6A ≈ C7-N7 ≈ C7-N7A ≈ C8-N8 ≈ C8-N8A

e. The C=O bond distance in each urea molecule was restrained.

C1-O1 ≈ C2-O2 ≈ C3-O3 ≈ C4-O4 ≈ C5-O5 ≈ C6-O6 ≈ C7-O7 ≈ C8-O8

The SADI command was used with sigma = 0.02 on 1,3-distances:

C1G-C3G ≈ C9G-C7G

C2G-C4G ≈ C8G-C6G

C7G-C5G ≈ C6G-C4G ≈ C5G-C3G

O2G-C9G ≈ O2G-C7G ≈ O1G-C3G ≈ O1G-C1G ≈ O2H-C9H ≈ O2H-C7G≈ O1H-C1H ≈ O1H-C3G

4. The FLAT command was used to restrain planarity, with sigma = 0.1.

C7G, C8G, C9H, O2H
C7G, C8G, C9G, O2G
C1G, C2G, C3G, O1G
C1H, C2G, C3G, O1H
O2, C2, N2, N2A
O5, C5, N5, N5A

5. U_{iso}/U_{aniso} restraints and constraints were applied in disordered sites.

U_{aniso} of the following atoms were restrained to make them behave more isotropically by using the ISOR command:

Sigma	Atoms
0.02	O1G O1H O2G O2H C9G C1G C9H C1H N1
0.01	C3 C6

U_{aniso} of the following atoms were refined to be the same by using the EADP command:

C2G C3G C4G C5G C6G C7G C8G

C9G C1G C9H C1H
O1G O1H O2G O2H
N4 N4A N7 N7A
C1 C4 C7
O1 O4 O7
C3 C6
O3 O6
N3 N3A N6 N6A
O2 O5 O8
C2 C5 C8
N2 N5 N8 N2A N5A N8A

6. Site occupancy factors (s.o.f.) were tied in two disordered sites of the guest, using the FVAR and PART commands.

Sof(C1G)=Sof(H1GA)=Sof(H1GB)=Sof(H1GC)=Sof(O1G)=FVAR(1)
Sof(C1H)=Sof(H1HA)=Sof(H1HB)=Sof(H1HC)=Sof(O1H)=1-FVAR(1)
Sof(C9G)=Sof(H9GA)=Sof(H9GB)=Sof(H9GC)=Sof(O2G)=FVAR(2)
Sof(C9H)=Sof(H9HA)=Sof(H9HB)=Sof(H9HC)=Sof(O2H)=1-FVAR(2)

7. The geometries of hydrogen atoms were restrained with the AFIX and HFIX commands:

a. Secondary CH_2 groups were refined with riding-model coordinates, using AFIX 23. C3G(H3GA,H3GB), C4G(H4GA,H4GB), C5G(H5GA,H5GB), C6G(H6GA,H6GB), C7G(H7GA,H7GB)

b. Hydrogen atoms of urea molecules were refined with riding-model coordinates, using

AFIX 93.

N3(H3A,H3B), N3A(H3AA,H3AB), N4(H4A,H4B), N4A(H4AA,H4AB), N5A(H5AA,H5AB), N5(H5A,H5B), N2(H2A,H2B), N2A(H2AA,H2AB), N1(H1A,H1B), N8(H8A,H8B), N8A(H8AA,H8AB), N6(H6A,H6B), N6A(H6AA,H6AB), N7(H7A,H7B), N7A(H7AA,H7AB)

c. The idealized methyl groups of the guest molecules were refined as rotating groups with AFIX 137

C1G(H1GA,H1GB,H1GC), C1H(H1HA,H1HB,H1HC), C9G(H9GA,H9GB,H9GC), C9H(H9HA,H9HB,H9HC).

With the above data treatment, a successful model of 2,8-nonanedione/urea was refined, as shown in Figure 2.3.4. The structure shows several important features. Firstly, the commensurability of the phase with $4c_g' = 5c_h'$ is proven, with four guest molecules corresponding to the length of five urea helices. Secondly, a diagonal hydrogen bonding network is shared between host and guest molecules, with one carbonyl group from each guest molecule forming a hydrogen bond with the host. This causes the guest molecules to be aligned in the ***ac*** plane, as well as tilting the urea molecules to which they are bound along the ***a*** axis (Figure 2.3.5). These factors are expected to result in an elongated ***a*** axis (***a*** > ***b***/√3), as observed in oscillation images (Figure 2.2.1.6). However, the unit cell parameters determined from this dataset have a slight elongation along the ***b*** axis instead, with ***a*** = 8.102(4) and ***b***/√3 = 8.108(4) Å. This is likely an anomaly due to the two twins being integrated together. The structure substantiates the earlier hypothesis that the formation of host-guest hydrogen bonds is the driving force behind the lock-in phase transition. As a result, the exothermic peak observed at 260.6 K in the DSC cooling scan (Figure 2.2.1.1) should be attributed to the formation of this hydrogen bond network. Thirdly, guest molecules show disorder at the carbonyl and terminal methyl positions. When refining the guest molecules without

disorder, those atoms showed unrealistic thermal ellipsoids. In the disordered model, two sets of terminal methyl groups and two oxygen atoms in each of the carbonyl groups were used. The two terminal methyl ketones were each modeled as two sites. This allowed them to adopt the most extended zig-zig geometries and to avoid torsions of the carbon skeleton. The refined s.o.f. values of the two sites are 60(7)% for C1G, O1G (40(7)% for C1H and O1H) and 55(2)% for O2G, C9G (45(2)% for O2H and C9H).

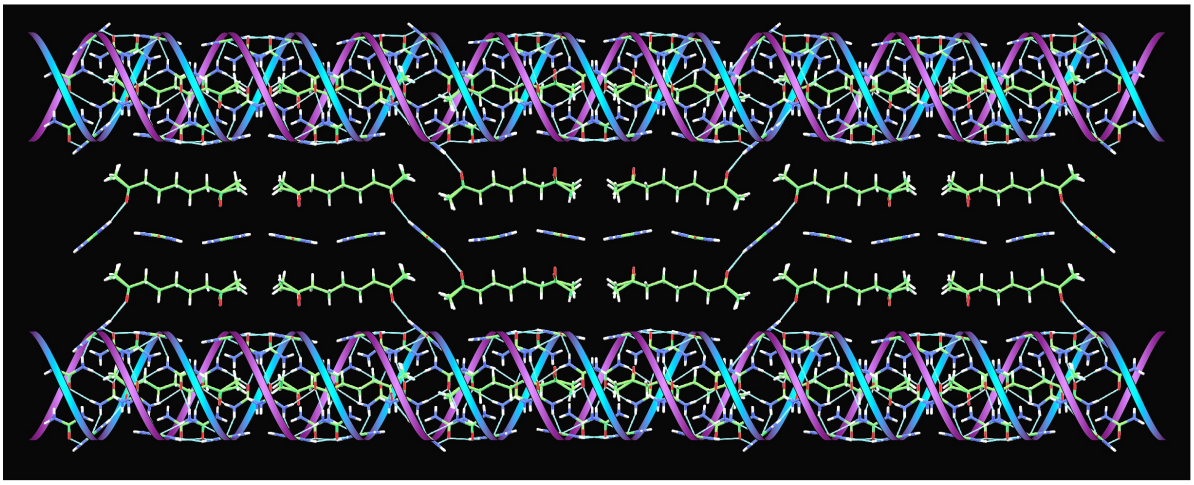

Figure 2.3.4. A schematic drawing of the crystal structure of 2,8-nonanedione/urea from the phase with $4c_g' = 5c_h'$ at 18.0 K, view along ***b***.

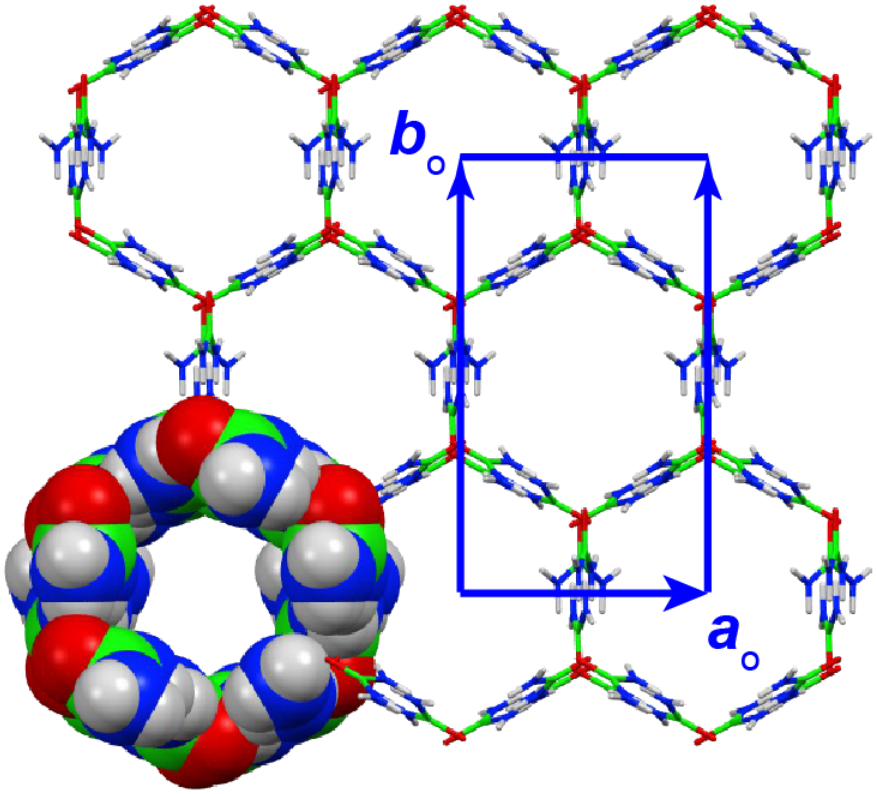

Figure 2.3.5. Host structure of 2,8-nonanedione/urea from the phase with $4c_g' = 5c_h'$ at 18.0 K, view along ***c***.

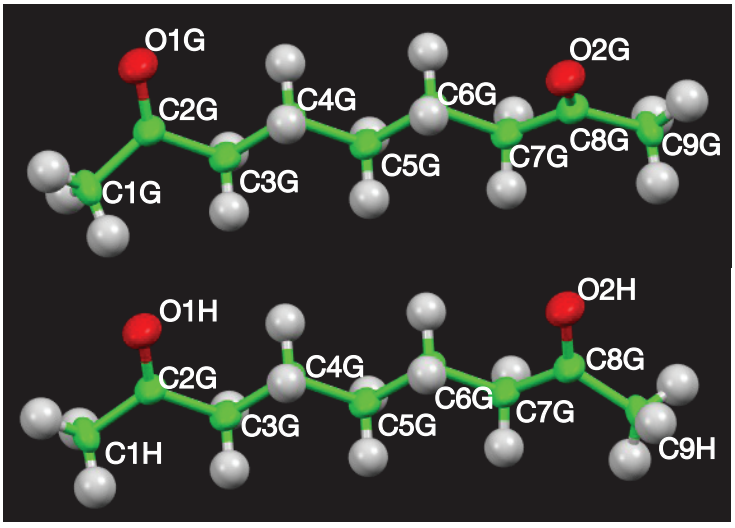

Figure 2.3.6. Disordered model in the carbonyl oxygen atoms and methyl groups of the structure of 2,8-nonanedione/urea from the phase with $4c_g' = 5c_h'$ at 18.0 K, view along ***b***.

Supplemental data for the crystal structure refinement:

Table 2.3.3. Crystal data and structure refinement for BW_F_281_09_C2221-c14.	
Identification code	BW_F_281_09_C2221-c14
Empirical formula	$C_{33}H_{92}N_{30}O_{19}$
Formula weight	1213.36
Temperature/K	18.0
Crystal system	orthorhombic
Space group	$C222_1$
a/Å	8.102(4)
b/Å	14.043(7)
c/Å	54.85(3)
α/°	90
β/°	90
γ/°	90
Volume/Å^3	6241(5)
Z	4
ρ_{calc}g/cm^3	1.291
μ/mm^{-1}	0.153
F(000)	2608.0
Crystal size/mm^3	0.2 × 0.2 × 0.025
Radiation	Synchrotron (λ = 0.82657)
2θ range for data collection/°	1.726 to 67.17
Index ranges	-10 ≤ h ≤ 10, -18 ≤ k ≤ 18, -72 ≤ l ≤ 73
Reflections collected	73273
Independent reflections	7799 [R_{int} = 0.0818, R_{sigma} = 0.0373]
Data/restraints/parameters	7799/270/220
Goodness-of-fit on F^2	1.461
Final R indexes [I>=2σ (I)]	R_1 = 0.1261, wR_2 = 0.3555
Final R indexes [all data]	R_1 = 0.1285, wR_2 = 0.3572
Largest diff. peak/hole /eÅ^{-3}	0.56/-0.53
Flack parameter	-5.6(10)
Diffractometer	Bruker PHOTON100 CMOS
Crystal to detector distance	60.0 mm

Table 2.3.4. Fractional atomic coordinates (×10^4) and equivalent isotropic displacement parameters (Å^2×10^3) for BW_F_281_09_C2221-c14. U_{eq} is defined as 1/3 of of the trace of the orthogonalized U_{ij} tensor.

Atom	*x*	*y*	*z*	U(eq)
C1G	1180(20)	5050(30)	2845(3)	41(4)
C1H	930(50)	5390(40)	2832(3)	41(4)
C2G	-80(12)	5069(8)	3045.4(14)	45.0(11)
C3G	507(14)	5378(10)	3292.5(15)	45.0(11)
C4G	-360(15)	4933(10)	3503.4(14)	45.0(11)
C5G	222(15)	5258(10)	3751.2(13)	45.0(11)
C6G	-598(15)	4793(10)	3965.5(14)	45.0(11)
C7G	-9(15)	5143(9)	4211.1(15)	45.0(11)
C8G	-562(13)	4570(8)	4424.9(14)	45.0(11)

C9H	440(30)	4590(20)	4655(3)	41(4)
C9G	-110(30)	4931(17)	4674(2)	41(4)
O1G	-1505(19)	4790(20)	3009(3)	55(3)
O1H	-1380(30)	4620(30)	3017(5)	55(3)
O2H	-1870(20)	4114(19)	4411(4)	55(3)
O2G	-1240(30)	3785(11)	4402(3)	55(3)
C3	6044(9)	7036(5)	6163.0(12)	15.2(10)
C4	4805(11)	4067(5)	4501.1(11)	19.4(11)
N3	6935(10)	7169(6)	6365.2(11)	23.2(8)
N3A	6561(10)	7440(6)	5955.1(11)	23.2(8)
N4	4548(11)	4551(5)	4293.5(10)	22.8(9)
N4A	5069(11)	4558(5)	4708.6(10)	22.8(9)
O3	4687(7)	6590(4)	6162.2(9)	16.7(8)
O4	4824(8)	3169(4)	4506.7(9)	20.5(9)
C5	3747(9)	2969(6)	5167.7(12)	19.3(9)
N5A	3185(10)	2536(7)	4966.7(11)	29.0(8)
N5	2807(10)	2957(7)	5368.7(12)	29.0(8)
N2	3090(10)	7434(7)	2630.6(11)	29.0(8)
N2A	3266(10)	7479(7)	3053.8(12)	29.0(8)
N1	5903(12)	4848(7)	2657.1(14)	40(2)
O5	5089(7)	3403(5)	5166.3(10)	19.4(7)
C2	3933(9)	7234(5)	2836.7(11)	19.3(9)
O2	5297(7)	6800(4)	2828.4(10)	19.4(7)
C8	3983(9)	6936(6)	6824.7(12)	19.3(9)
N8	2968(10)	7071(7)	6629.5(12)	29.0(8)
N8A	3377(11)	7256(7)	7037.6(12)	29.0(8)
O8	5348(7)	6505(5)	6813.9(10)	19.4(7)
C1	5000	4349(6)	2500	19.4(11)
O1	5000	3447(6)	2500	20.5(9)
C6	6040(9)	7033(5)	4167.0(11)	15.2(10)
N6	6861(9)	7100(6)	4376.2(11)	23.2(8)
N6A	6655(10)	7398(6)	3961.0(11)	23.2(8)
O6	4691(8)	6580(4)	4160.2(9)	16.7(8)
C7	5097(11)	4028(5)	6513.6(11)	19.4(11)
N7	4784(11)	4552(5)	6311.2(10)	22.8(9)
N7A	5281(11)	4486(5)	6723.9(10)	22.8(9)
O7	5035(8)	3131(5)	6501.6(9)	20.5(9)

Table 2.3.5. Anisotropic displacement parameters ($Å^2 \times 10^3$) for BW_F_281_09_C2221-c14. The anisotropic displacement factor exponent takes the form: $-2\pi^2[h^2a^{*2}U_{11}+2hka^*b^*U_{12}+\ldots]$.

Atom	U_{11}	U_{22}	U_{33}	U_{23}	U_{13}	U_{12}
C1G	45(6)	50(9)	28(4)	-6(5)	9(4)	-18(6)
C1H	45(6)	50(9)	28(4)	-6(5)	9(4)	-18(6)
C2G	33(2)	65(3)	36(2)	-6(2)	-4.2(17)	-17.5(19)
C3G	33(2)	65(3)	36(2)	-6(2)	-4.2(17)	-17.5(19)
C4G	33(2)	65(3)	36(2)	-6(2)	-4.2(17)	-17.5(19)
C5G	33(2)	65(3)	36(2)	-6(2)	-4.2(17)	-17.5(19)

C6G	33(2)	65(3)	36(2)	-6(2)	-4.2(17)	-17.5(19)
C7G	33(2)	65(3)	36(2)	-6(2)	-4.2(17)	-17.5(19)
C8G	33(2)	65(3)	36(2)	-6(2)	-4.2(17)	-17.5(19)
C9H	45(6)	50(9)	28(4)	-6(5)	9(4)	-18(6)
C9G	45(6)	50(9)	28(4)	-6(5)	9(4)	-18(6)
O1G	46(5)	64(7)	54(4)	6(4)	-8(4)	-19(5)
O1H	46(5)	64(7)	54(4)	6(4)	-8(4)	-19(5)
O2H	46(5)	64(7)	54(4)	6(4)	-8(4)	-19(5)
O2G	46(5)	64(7)	54(4)	6(4)	-8(4)	-19(5)
C3	24(3)	8(2)	14(2)	-2.4(17)	1(2)	-5(2)
C4	21(3)	21(3)	16(3)	3.3(19)	-1(2)	-2(2)
N3	21.7(19)	37(2)	10.8(14)	4.7(15)	-2.1(14)	-10.0(16)
N3A	21.7(19)	37(2)	10.8(14)	4.7(15)	-2.1(14)	-10.0(16)
N4	41(2)	18.6(19)	9.0(14)	-0.5(12)	-2.3(16)	-0.6(16)
N4A	41(2)	18.6(19)	9.0(14)	-0.5(12)	-2.3(16)	-0.6(16)
O3	26(2)	15(2)	9.1(15)	1.3(13)	-2.5(16)	-7.9(16)
O4	26(2)	22(2)	13.6(18)	-0.2(14)	-1.2(17)	-4.7(17)
C5	28(2)	19(2)	10.6(18)	-2.1(16)	-1.1(16)	1.1(18)
N5A	23.3(16)	52(2)	11.4(12)	-0.3(14)	2.7(11)	4.4(15)
N5	23.3(16)	52(2)	11.4(12)	-0.3(14)	2.7(11)	4.4(15)
N2	23.3(16)	52(2)	11.4(12)	-0.3(14)	2.7(11)	4.4(15)
N2A	23.3(16)	52(2)	11.4(12)	-0.3(14)	2.7(11)	4.4(15)
N1	49(6)	48(5)	23(4)	-9(4)	-7(4)	19(5)
O5	18.4(17)	26.8(18)	13.0(14)	-1.9(14)	2.4(11)	0.4(14)
C2	28(2)	19(2)	10.6(18)	-2.1(16)	-1.1(16)	1.1(18)
O2	18.4(17)	26.8(18)	13.0(14)	-1.9(14)	2.4(11)	0.4(14)
C8	28(2)	19(2)	10.6(18)	-2.1(16)	-1.1(16)	1.1(18)
N8	23.3(16)	52(2)	11.4(12)	-0.3(14)	2.7(11)	4.4(15)
N8A	23.3(16)	52(2)	11.4(12)	-0.3(14)	2.7(11)	4.4(15)
O8	18.4(17)	26.8(18)	13.0(14)	-1.9(14)	2.4(11)	0.4(14)
C1	21(3)	21(3)	16(3)	3.3(19)	-1(2)	-2(2)
O1	26(2)	22(2)	13.6(18)	-0.2(14)	-1.2(17)	-4.7(17)
C6	24(3)	8(2)	14(2)	-2.4(17)	1(2)	-5(2)
N6	21.7(19)	37(2)	10.8(14)	4.7(15)	-2.1(14)	-10.0(16)
N6A	21.7(19)	37(2)	10.8(14)	4.7(15)	-2.1(14)	-10.0(16)
O6	26(2)	15(2)	9.1(15)	1.3(13)	-2.5(16)	-7.9(16)
C7	21(3)	21(3)	16(3)	3.3(19)	-1(2)	-2(2)
N7	41(2)	18.6(19)	9.0(14)	-0.5(12)	-2.3(16)	-0.6(16)
N7A	41(2)	18.6(19)	9.0(14)	-0.5(12)	-2.3(16)	-0.6(16)
O7	26(2)	22(2)	13.6(18)	-0.2(14)	-1.2(17)	-4.7(17)

Table 2.3.6. Bond lengths for BW_F_281_09_C2221-c14.

Atom	Atom	Length/Å		Atom	Atom	Length/Å
C1G	C2G	1.497(10)		C4	O4	1.261(7)
C1H	C2G	1.497(11)		C5	N5A	1.338(7)
C2G	C3G	1.501(9)		C5	N5	1.340(7)
C2G	O1G	1.235(13)		C5	O5	1.247(7)

C2G	O1H	1.234(14)		N2	C2	1.350(7)
C3G	C4G	1.490(9)		N2A	C2	1.352(7)
C4G	C5G	1.509(9)		N1	C1	1.330(7)
C5G	C6G	1.500(9)		C2	O2	1.263(7)
C6G	C7G	1.511(9)		C8	N8	1.363(7)
C7G	C8G	1.492(9)		C8	N8A	1.344(7)
C8G	C9H	1.501(11)		C8	O8	1.263(7)
C8G	C9G	1.504(10)		C1	N1[1]	1.330(7)
C8G	O2H	1.237(13)		C1	O1	1.266(9)
C8G	O2G	1.236(13)		C6	N6	1.329(7)
C3	N3	1.336(7)		C6	N6A	1.337(7)
C3	N3A	1.341(7)		C6	O6	1.266(7)
C3	O3	1.265(7)		C7	N7	1.356(7)
C4	N4	1.342(7)		C7	N7A	1.329(7)
C4	N4A	1.348(7)		C7	O7	1.263(8)

[1]1-X,+Y,1/2-Z

Table 2.3.7. Bond Angles for BW_F_281_09_C2221-c14.

Atom	**Atom**	**Atom**	**Angle/˚**		**Atom**	**Atom**	**Atom**	**Angle/˚**
C1G	C2G	C3G	116.8(10)		O4	C4	N4A	119.3(6)
O1G	C2G	C1G	121.0(11)		N5A	C5	N5	118.6(7)
O1G	C2G	C3G	122.2(11)		O5	C5	N5A	120.9(7)
O1H	C2G	C1H	121.5(13)		O5	C5	N5	120.4(7)
C4G	C3G	C2G	115.5(8)		N2	C2	N2A	118.8(7)
C3G	C4G	C5G	115.2(8)		O2	C2	N2	120.9(7)
C6G	C5G	C4G	115.8(9)		O2	C2	N2A	120.3(7)
C5G	C6G	C7G	114.7(8)		N8A	C8	N8	114.6(7)
C8G	C7G	C6G	115.5(8)		O8	C8	N8	123.9(7)
C7G	C8G	C9H	119.1(11)		O8	C8	N8A	121.4(7)
C7G	C8G	C9G	117.4(10)		N1	C1	N1[1]	116.4(11)
O2H	C8G	C7G	119.2(10)		O1	C1	N1	121.8(5)
O2H	C8G	C9H	121.6(12)		O1	C1	N1[1]	121.8(5)
O2G	C8G	C7G	122.3(10)		N6	C6	N6A	121.0(7)
O2G	C8G	C9G	120.0(11)		O6	C6	N6	119.6(6)
N3	C3	N3A	118.6(6)		O6	C6	N6A	119.3(6)
O3	C3	N3	122.8(7)		N7A	C7	N7	118.0(7)
O3	C3	N3A	118.5(7)		O7	C7	N7	119.4(6)
N4	C4	N4A	118.8(7)		O7	C7	N7A	122.2(6)
O4	C4	N4	121.9(6)					

[1]1-X,+Y,1/2-Z

Table 2.3.8. Torsion Angles for BW_F_281_09_C2221-c14.										
A	**B**	**C**	**D**	**Angle/˚**		**A**	**B**	**C**	**D**	**Angle/˚**
C1G	C2G	C3G	C4G	-149(2)		C6G	C7G	C8G	C9H	155.7(18)
C1H	C2G	C3G	C4G	-171(3)		C6G	C7G	C8G	C9G	-175.6(16)
C2G	C3G	C4G	C5G	-179.2(12)		C6G	C7G	C8G	O2H	-27(2)
C3G	C4G	C5G	C6G	-178.0(12)		C6G	C7G	C8G	O2G	11(2)
C4G	C5G	C6G	C7G	-179.1(12)		O1G	C2G	C3G	C4G	27(3)
C5G	C6G	C7G	C8G	-168.8(11)		O1H	C2G	C3G	C4G	13(3)

Table 2.3.9. Hydrogen Atom Coordinates (Å×10^4) and Isotropic Displacement Parameters (Å^2×10^3) for BW_F_281_09_C2221-c14.				
Atom	***x***	***y***	***z***	**U(eq)**
H1GA	821	4612	2717	62
H1GB	2242	4844	2911	62
H1GC	1293	5695	2777	62
H1HA	2097	5250	2862	62
H1HB	792	6081	2810	62
H1HC	564	5061	2685	62
H3GA	1699	5232	3306	54
H3GB	382	6078	3305	54
H4GA	-222	4234	3493	54
H4GB	-1554	5072	3489	54
H5GA	1425	5141	3763	54
H5GB	49	5954	3763	54
H6GA	-408	4098	3956	54
H6GB	-1802	4902	3954	54
H7GA	1212	5156	4210	54
H7GB	-397	5806	4233	54
H9HA	665	3943	4709	62
H9HB	-182	4932	4782	62
H9HC	1481	4927	4625	62
H9GA	-737	4578	4798	62
H9GB	-383	5610	4686	62
H9GC	1071	4842	4702	62
H3A	6583	6942	6505	28
H3B	7873	7483	6358	28
H3AA	5960	7392	5822	28
H3AB	7501	7753	5952	28
H4A	4387	4242	4156	27
H4B	4541	5178	4295	27
H4AA	5253	4252	4846	27
H4AB	5058	5185	4707	27
H5AA	3764	2557	4831	35
H5AB	2235	2232	4970	35
H5A	3136	3258	5501	35
H5B	1861	2649	5369	35
H2A	3490	7262	2488	35

H2B	2141	7737	2639	35
H2AA	3783	7337	3190	35
H2AB	2315	7781	3059	35
H1A	6522	4552	2765	48
H1B	5881	5474	2653	48
H8A	3252	6851	6485	35
H8B	2029	7378	6648	35
H8AA	3934	7166	7173	35
H8AB	2423	7556	7041	35
H6A	6465	6831	4509	28
H6B	7800	7414	4382	28
H6AA	6121	7323	3823	28
H6AB	7592	7714	3964	28
H7A	4541	4267	6173	27
H7B	4825	5178	6318	27
H7AA	5365	4163	6861	27
H7AB	5320	5112	6726	27

Table 2.3.10. Atomic Occupancy for BW_F_281_09_C2221-c14.

Atom	***Occupancy***		**Atom**	***Occupancy***		**Atom**	***Occupancy***
C1G	0.60(7)		H1GA	0.60(7)		H1GB	0.60(7)
H1GC	0.60(7)		C1H	0.40(7)		H1HA	0.40(7)
H1HB	0.40(7)		H1HC	0.40(7)		C9H	0.45(2)
H9HA	0.45(2)		H9HB	0.45(2)		H9HC	0.45(2)
C9G	0.55(2)		H9GA	0.55(2)		H9GB	0.55(2)
H9GC	0.55(2)		O1G	0.60(7)		O1H	0.40(7)
O2H	0.45(2)		O2G	0.55(2)			

2.4. Conclusions

In summary, to rationalize the observation of the series of phase transitions of 2,8-nonanedione/urea and 2,8-nonanedione/urea-d_4, the stress-induced "self-compression" mechanism is proposed. The incommensurate-to-commensurate lock-in phase transitions, that occur upon cooling, generate commensurate phases ($4c_g' = 5c_h'$, $9c_g' = 11c_h'$, and $14c_g' = 17c_h'$,) with guest conformations that are longer than the parent incommensurate phase. As the commensurate phases grow, incommensurate regions in between are compressed until they reach a commensurate phase with $6c_g' = 7c_h'$.

These “self-compression” phase transitions are shown to be reversible over the course of three complete cool-heat cycles. In the phase transitions of UIC crystals grown from a mixed solution of 2,8-nonanedione and 2-nonanone, the degree of compression is adversely affected by increasing amounts of 2-nonanone included. Data analysis of 4,4’-oxybis(2-butanone)/urea (an analog of 2,8-nonanedione/urea with a shorter guest length) shows that the UIC is mainly commensurate with $9c_g' = 11c_h'$, but only the host structure could be resolved from the current data at 210 K. The host exhibits a 3-fold screw axis along the channel (maximal space group $P3_112$), which is expected to relate three guest molecules along the length of the unit cell.

Finally, the crystal structure of the commensurate phase of 2,8-nonanedione/urea with $4c_g' = 5c_h'$ was solved using synchrotron data. This was achieved using a section from a single ferroelastic domain of a crystal grown from 258.15 to roughly 246 K, and harvested at 260.8-261.5 K. The structure provides valuable information on the system, confirming the hypothesis that formation of host-guest hydrogen bonds drives the formation of the commensurate phase.

2.5. References

1. Hollingsworth, M. D.; Brown, M. E.; Hillier, A. C.; Santarsiero, B. D.; Chaney, J. D., Superstructure control in the crystal growth and ordering of urea inclusion compounds. *Science* **1996,** *273*, 1355-1359.
2. Brown, M. E.; Chaney, J. D.; Santarsiero, B. D.; Hollingsworth, M. D., Superstructure topologies and host-guest interactions in commensurate inclusion compounds of urea with bis(methyl ketone)s. *Chem. Mater.* **1996,** *8*, 1588-1591.
3. Notebook BW_D_143_33.
4. Notebook BW_F_304 and APS_B_204_08.
5. Notebook APS_B_226, temperature calibrations of APS using E type thermocouple.
6. FibonacciBuild s3 Ver. 5.11, a Matlab program which was originally written by Laurent Guérin and modified by Philippe Rabiller and Ilya Frantsuzov.
7. Mannsfeld, S. C. B.; Tang, M. L.; Bao, Z. A., Thin film structure of triisopropylsilylethynyl-functionalized pentacene and tetraceno[2,3-b]thiophene from grazing incidence X-ray diffraction. *Adv. Mater.* **2011,** *23*, 127-131.
8. Notebook APS_A_098_03_004.

9. Notebook APS_B_204_05, temperature scans of 2,8-nonanedione/urea at beamline 14-BM-C at APS.
10. Notebook BW_G_12, BW_G_24.
11. Mariette, C.; Frantsuzov, I.; Wang, B.; Guerin, L.; Rabiller, P.; Hollingsworth, M. D.; Toudic, B., Frustrated pretransitional phenomena in aperiodic composites. *Phys. Rev. B* **2016,** *94*, 184105.
12. Guerin, L.; Mariette, C.; Rabiller, P.; Huard, M.; Ravy, S.; Fertey, P.; Nichols, S. M.; Wang, B.; Mannsfeld, S. C. B.; Weber, T.; Hollingsworth, M. D.; Toudic, B., Long-range modulation of a composite crystal in a five-dimensional superspace. *Phys. Rev. B* **2015,** *91* (18).
13. Huard, M.; Toudic, B.; Rabiller, P.; Ecolivet, C.; Guerin, L.; Bourges, P.; Breczewski, T.; Hollingsworth, M. D., Confined linear molecules inside an aperiodic supramolecular crystal: The sequence of superspace phases in n-hexadecane/urea. *J. Chem. Phys.* **2011,** *135*, 204505.
14. Forst, R.; Jagodzinski, H.; Boysen, H.; Frey, F., Diffuse-scattering and disorder in urea inclusion-compounds $OC(NH_2)_2 + C_nH_{2n+2}$. *Acta Crystallogr. Sect. B* **1987,** *43*, 187-197.
15. Lefort, R.; Etrillard, J.; Toudic, B.; Guillaume, F.; Breczewski, T.; Bourges, P., Incommensurate intermodulation of an organic intergrowth compound observed by neutron scattering. *Phys. Rev. Lett.* **1996,** *77*, 4027-4030.
16. Mariette, C.; Huard, M.; Rabiller, P.; Nichols, S. M.; Ecolivet, C.; Janssen, T.; Alquist, K. E.; Hollingsworth, M. D.; Toudic, B., A molecular "phase ordering" phase transition leading to a modulated aperiodic composite in n-heptane/urea. *J. Chem. Phys* **2012,** *136*, 104507.
17. Brown, M. E.; Hollingsworth, M. D., Stress-induced domain reorientation in urea inclusion-compounds. *Nature* **1995,** *376*, 323-327.
18. Hollingsworth, M. D.; Brown, M. E.; Dudley, M.; Chung, H.; Peterson, M. L.; Hillier, A. C., Template effects, asymmetry, and twinning in helical inclusion compounds. *Angew. Chem. Int. Ed.* **2002,** *41*, 965–969.
19. Notebook APS_A_098_03_011.
20. Mariette, C.; Guerin, L.; Rabiller, P.; Ecolivet, C.; Garcia-Orduna, P.; Bourges, P.; Bosak, A.; de Sanctis, D.; Hollingsworth, M. D.; Janssen, T.; Toudic, B., Critical phenomena in higher dimensional spaces: The hexagonal-to-orthorhombic phase transition in aperiodic n-nonadecane/urea. *Phys. Rev. B* **2013,** *87*, 104101.
21. Mariette, C.; Guerin, L.; Rabiller, P.; Chen, Y. S.; Bosak, A.; Popov, A.; Hollingsworth, M. D.; Toudic, B., The creation of modulated monoclinic aperiodic composites in n-alkane/urea compounds. *Z. Kristallogr. Cryst.* **2015,** *230*, 5-11.
22. Guerin, L.; Mariette, C.; Rabiller, P.; Huard, M.; Ravy, S.; Fertey, P.; Nichols, S. M.; Wang, B.; Mannsfeld, S. C. B.; Weber, T.; Hollingsworth, M. D.; Toudic, B., Long-range modulation of a composite crystal in a five-dimensional superspace. *Phys. Rev. B* **2015,** *91*, 184101.
23. Rush, J. R., Crystal growth, guest ordering and ferroelastic properties of urea inclusion compounds. Ph.D. thesis, Kansas State University **2007**.
24. Notebook BW_G_44_04 for data analysis, and data is from APS_A_098_03 series.
25. Toudic, B.; Aubert, F.; Ecolivet, C.; Bourges, P.; Breczewski, T., Pressure-induced lock-in in an aperiodic nanoporous crystal. *Phys. Rev. Lett.* **2006,** *96*, 145503.
26. Adxv (2013). Adxv – a program to display X-ray diffraction images, http://www.scripps.edu/~arvai/adxv.html.
27. Notebook BW_G_052_01.
28. Unpublished work by Bo Wang, Mark D. Hollingsworth and John Bacsa.

29. Notebook APS_A_098_03.
30. Notebook APS_A_098_03_017.
31. Peak intensities were obtained from Dr. Ilya Frantsuzov.
32. Notebook BW_G_59.
33. Notebook APS_A_098_03_024.
34. Crystal structure of 2,15-hexadecanedione/urea, unpublished work by Bo Wang, Michael E. Brown, and Mark D. Hollingsworth.
35. Notebook APS_A_098_03_082.
36. Notebook BW_G_41_01, data taken on APS_B_204.
37. Pynn, R., Incommensurable structures. *Nature* **1979,** *281*, 433-437.
38. Bak, P., Commensurate phases, incommensurate phases and the devils staircase. *Rep. Prog. Phys.* **1982,** *45*, 587-629.
39. Notebook ALS_A_210.
40. Notebook ALS_A_214_03.
41. Notebook APS_B_209_09 and APS_B_209_12.
42. Notebook APS_B_209_05.
43. Notebook BW_G_54.
44. Notebook APS_B_209_03 and 05 series.
45. Notebook ALS_A_214_03_010.
46. Notebook ALS_A_214_03_026.
47. Notebook ALS_A_214_03_027.
48. Notebook ALS_A_214_03_034.
49. Notebook ALS_A_214_03_045.
50. Data from APS_B_209_03, and APS_B_209_05series.
51. Unpublished work by Dr. Ilya Frantsuzov, and Bo Wang. .
52. Notebook APS_B_209_03_004.
53. Hollingsworth, M. D.; Peterson, M. L.; Rush, J. R.; Brown, M. E.; Abel, M. J.; Black, A. A.; Dudley, M.; Raghothamachar, B.; Werner-Zwanziger, U.; Still, E. J.; Vanecko, J. A., Memory and perfection in ferroelastic inclusion compounds. *Cryst. Growth. Des.* **2005,** *5*, 2100-2116.
54. Notebook APS_B_219_03_001.
55. Notebook APS_B_216_03_009.
56. Notebook APS_B_216_03_011.
57. Notebook APS_B_216_03_022.
58. Notebook APS_B_216_03_023.
59. Notebook APS_A_216_03_048.
60. Reference: Unpublished work by Bo Wang, Mark D. Hollingsworth and John Bacsa.
61. Notebook APS_B_220_03_001.
62. Notebook APS_B_220_03_008.
63. APS_B_221_03_019.
64. Notebook APS_B_220_03_038.
65. Notebook APS_B_220_03.
66. Notebook APS_B_068_03_003 and Notebook BW_F_290_02.
67. Notebook APS_B_068_03_040 and Notebook BW_F_290_05.
68. Notebook APS_B_068_03 and Notebook BW_F_290.
69. Brown, M. E.; Hollingsworth, M. D., Stress-Induced Domain Reorientation in Urea Inclusion-Compounds. *Nature* **1995,** *376* (6538), 323-327.
70. Notebook ALS_A_194.
71. Notebook BW_E_239_1_21 and 26.jpg.
72. Notebook ALS_A_194_02_001.

73. Notebook ALS_A_194_02_005.
74. Notebook APS_B_199.
75. Dewar, M. J. S.; Zoebisch, E. G.; Healy, E. F.; Stewart, J. J. P., The Development and Use of Quantum-Mechanical Molecular-Models .76. AM1 - a New General-Purpose Quantum-Mechanical Molecular-Model. *J. Am. Chem. Soc* **1985,** *107*, 3902-3909.
76. Notebook BW_E_270_07.
77. Notebook ALS_A_205_07_001.
78. Notebook ALS_A_205_07_037.
79. Notebook ALS_A_205_07_071.
80. Bruker (2012). APEX2. Bruker AXS Inc., Madison, Wisconsin, USA.
81. Dolomanov, O. V., Bourhis, L. J., Gildea, R. J., Howard, J. A. K. & Puschmann, H., OLEX2: a complete structure solution, refinement and analysis program. *J. Appl. Cryst.* **2009,** *42*, 339–341.
82. Sheldrick, G. M., A short history of SHELX. *Acta Crystallogr. Sect. A* **2008,** *64*, 112-122.
83. Notebook BW_E_302_7.
84. The Advanced Light Source is supported by the Director, Office of Science, Office of Basic Energy Sciences, of the U.S. Department of Energy under Contract No. DE-AC02-05CH11231.
85. (a) Notebook ALS_A_196, the structure file used is BW_F_281_09_C2221-c12.res/cif; (b) Notebook BW_F_218.
86. Bruker (2001). SADABS. Bruker AXS Inc., Madison, Wisconsin, USA.
87. Personal communication from Kevin Gagnon.
88. Least-Squares function minimized: $\Sigma w (|Fo| - |Fc|)^2$, where: $w = 1/\sigma^2(Fo)$.
89. Standard deviation as observation of weight.
90. Cromer, D. T.; Waber, J. T., International Tables for Crystallography, Vol. C; Table 4.2.4.2. The Kynoch Press: Birmingham, U.K., 1991.
91. Notebook ALS_A_176_08_03_262.
92. http://checkcif.iucr.org.
93. Spek, A. L., Structure validation in chemical crystallography - Platon. *Acta Crystallogr. Sect. B* **2009**, 148-155.

Chapter 3. Phase transitions of 2,11-dodecanedione/urea

3.1. Earlier work on 2,11-dodecanedione/urea

The UIC of 2,11-dodecanedione posed an interesting challenge because it could potentially have at least three different structures. These include two commensurate structures, one with $12c_g' = 19c_h'$ ($\gamma = 0.6316$, $c_g' = 17.477$ Å using $c_h' = 11.038$ Å - see below), the other with $7c_g' = 11c_h'$ ($\gamma = 0.6364$, $c_g' = 17.345$ Å using $c_h' = 11.038$ Å), and possibly more than one incommensurate structure. Due to equipment limitations, earlier X-ray oscillation images of 2,11-dodecanedione/urea could not be used to distinguish between these possibilities. In 1996, Hollingsworth and coworkers measured c_g to be 17.31(3) Å at room temperature and proposed that this UIC has a commensurate phase of $12c_g' = 19c_h'$, but stated that they could not exclude a structure with $7c_g' = 11c_h'$. An AFM image of this UIC showed that the {001} face of the crystal was rough, consistent with a poor match between host and guest substructures.[1] In the same year, Brown and coworkers published an infrared absorption spectrum of this UIC that contained a broad peak at 1723 cm^{-1} (FWHM = 15 cm^{-1}). This suggested two different environments for the carbonyl groups of the guest, one with hydrogen bonding to the host, and the other without it.[2] High-resolution X-ray diffraction studies were therefore used to discern between these possibilities.

The initial variable-temperature synchrotron X-ray scans of crystals of 2,11-dodecanedione/urea revealed two types of phase transitions. As shown in Figure 3.1.1

(A), for the batch grown by cooling from -15.0 °C to -23.0 °C (as well as many other crystals grown above the phase transition), a lock-in phase transition to a commensurate structure was observed around 265 K, as indicated by the appearance of regularly-spaced Bragg peaks. For a batch grown by cooling from 40 °C to room temperature, a transition to a phase with a long-range modulation was observed around 262 K, as indicated by additional satellite peaks in Figure 3.1.1 (B).

To establish the relationship between the structure of the crystal and the nature of the phase transitions, a systematic study of crystals grown under different conditions was conducted. This chapter describes synchrotron X-ray studies of crystals of 2,11-dodecanedione/urea grown at -20.0 °C, -10.0 °C, 0.0 °C, 10.0 °C, 20.0 °C, 30.0 °C, 40.0 °C, 46 °C, and by cooling from 40 °C to room temperature. This chapter concludes with a discussion of the crystal structure determination of the commensurate phase of 2,11-dodecanedione/urea in which $12c_g' = 19c_h'$.

Before layer line profile analysis, the channel axis length, ***c***, and its temperature dependence needs to be established. For the structure with $12c_g' = 19c_h'$ at 170.0 K, ***c*** is determined to be 209.21(10) Å, as discussed in Section 3.3.[3] Using this very accurate value and the separation between the $(1\ 0\ -2\ 0)_h$ and $(1\ 0\ 2\ 0)_h$ peaks during a temperature scan from 160 K to 290 K of a crystal grown at -20.0 °C, a linear fit of the thermal expansion along the channel axis was determined to be: c_h = 10.9913(5) + 0.000161(10) T Å.[4] The host repeat lengths used below are all from this relationship. For example, c_h = 11.0380(5) at 290.0 K. (See Section 5.2.1.)

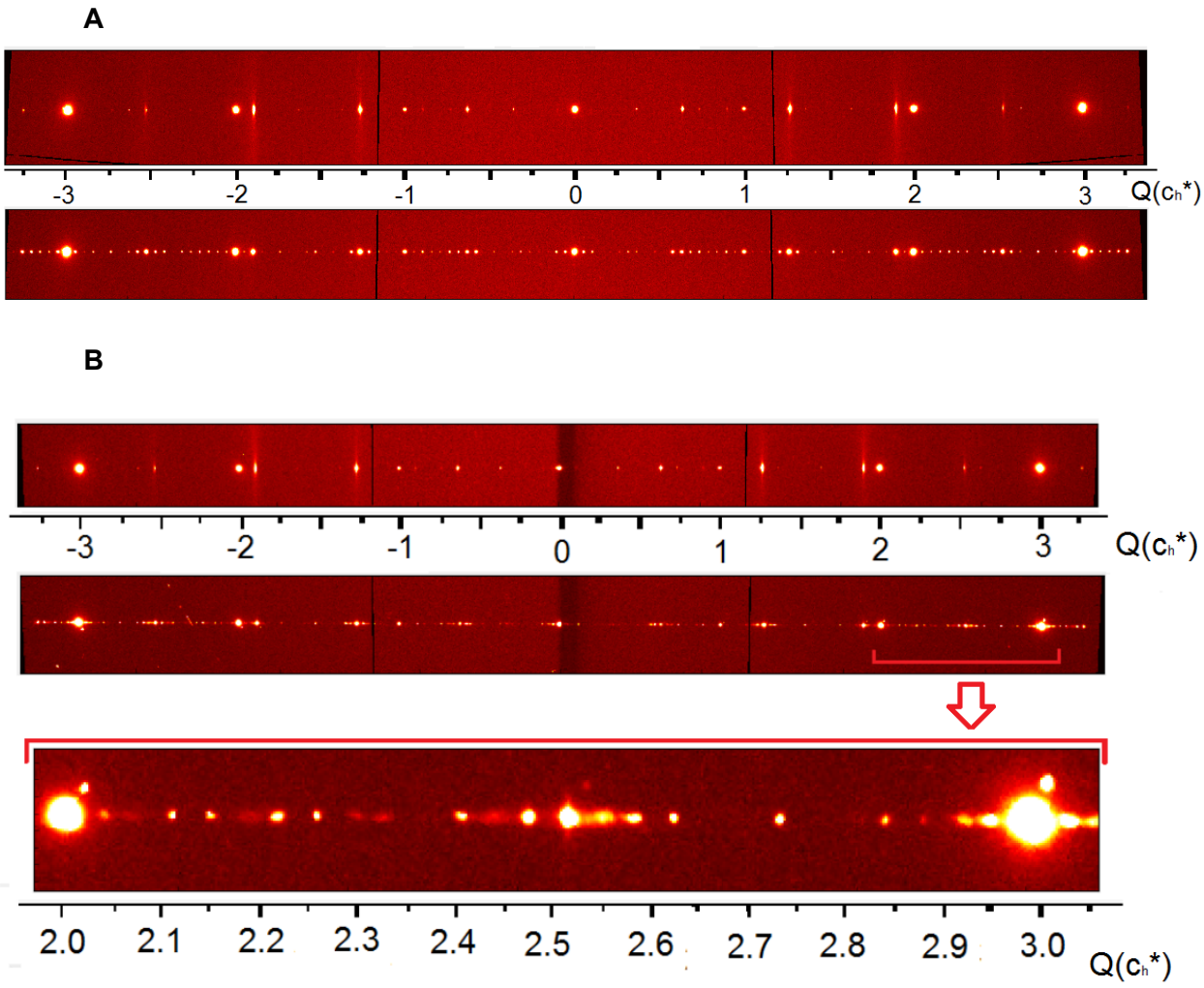

Figure 3.1.1. Synchrotron oscillation images using a 60° ϕ rotation about the crystal ***c*** axis showing the (-1 0 *l m*) layer line of a crystal of 2,11-dodecanedione/urea. (A) A crystal grown by cooling from -15 °C to -23 °C. The upper image was taken at 280 K, whereas the lower one was taken at 210 K.[5] (B) A crystal grown by cooling from 40 °C to room temperature. The top image was taken at 290 K, the middle one was taken at 212 K, and the bottom one is an enlargement of the image at 212 K (indicated with a red line).[6] The measurements were made on APS beamline 14-BM-C with d = 500 mm, φ = 0-60°, and λ = 0.97870 Å.

3.2.1. Synchrotron X-ray studies of 2,11-dodecanedione/urea grown at -20.0 °C

The sample was crystallized by evaporation while purging with argon in a HAKKE (C40) temperature controller set at -20.0 °C.[7] As shown in Figure 3.2.1.1, the DSC trace of this sample shows an exothermic phase transition at 263.0 K on cooling (ΔH = -0.62 J/g), and an endothermic phase transition at 264.7 K on heating (ΔH = 0.63 J/g). In oscillation X-ray images collected from 290.0 K to 119.3 K on ALS beamline 8.2.2, a phase transition was observed between 263 K and 259 K on cooling. The guest repeat length (c_g) and type of phase transition were studied by analyzing unwarped synchrotron oscillation images taken at 290.0, 236.0, 200.6, and 162.4 K. These profiles were first unwarped with WxDiff[8] and were then analyzed with FibonacciBuild in Matlab R2014.[9] A 10-fold interpolation was used in generating all of the profiles in FibonacciBuild. Note that this method of interpolation artificially reduces the standard error of the mean of the fit by sqrt(10). (See Section 2.2.1.)

The indexing of the unwarped oscillation image at 290.0 K is shown in Figure 3.2.1.2. The layer lines observed coincide with those expected from a hexagonal basis, and since there is no peak distortion in the ***a***b**** plane, this crystal is likely hexagonal at 290.0 K, similar to 2,8-nonanedione/urea. In the profile analysis of the $(1\ 0\ l\ m)_h$ layer line, the predominant misfit parameter was γ= 0.63462(3), as shown in Figure 3.2.1.2 (B). Thus c_g = 11.0380(5)/0.63462(3) = 17.3931(11) Å, and this UIC is incommensurate. This is measurably different from the two nearest commensurate phases ($7c_g' = 11c_h'$, in

which c_g' = 17.3454(8) Å for this host repeat, and $12c_g' = 19c_h'$, in which c_g' = 17.4768(8) Å). Note that judging by the sloping side of the guest peaks in Figure 3.2.1.2 (B) there appears to be a distribution of c_g values in the sample, with some being shorter than the peak at γ = 0.63462(3).

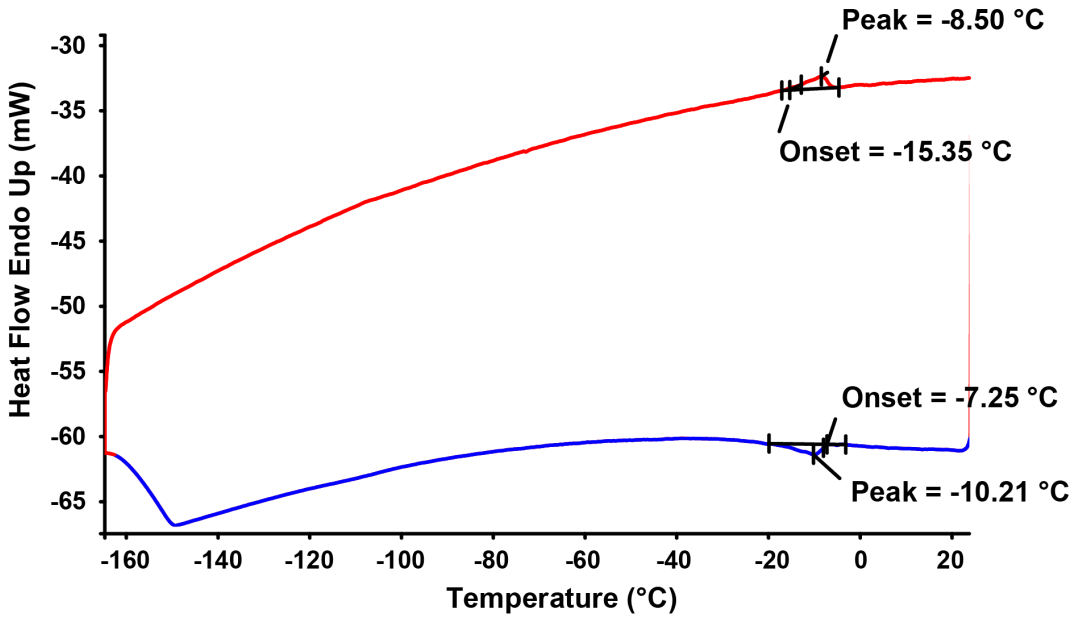

Figure 3.2.1.1. DSC trace (using a Perkin Elmer Pyris 1 DSC) of 2,11-dodecanedione/urea grown at -20.0 ºC.[10] The blue line is the cooling scan, and the red line is the heating scan. The scan rate was 20 K/min, and the scan ranges were from 298 K (25 ºC) to -108 K (-165 ºC) and then back to 298 K. An exothermic phase transition was observed at a peak position of 263.0 K (-10.2 ºC) in the cooling curve, and a corresponding endothermic phase transition occurred at a peak position of 264.7 K (-15.4 K) upon heating.

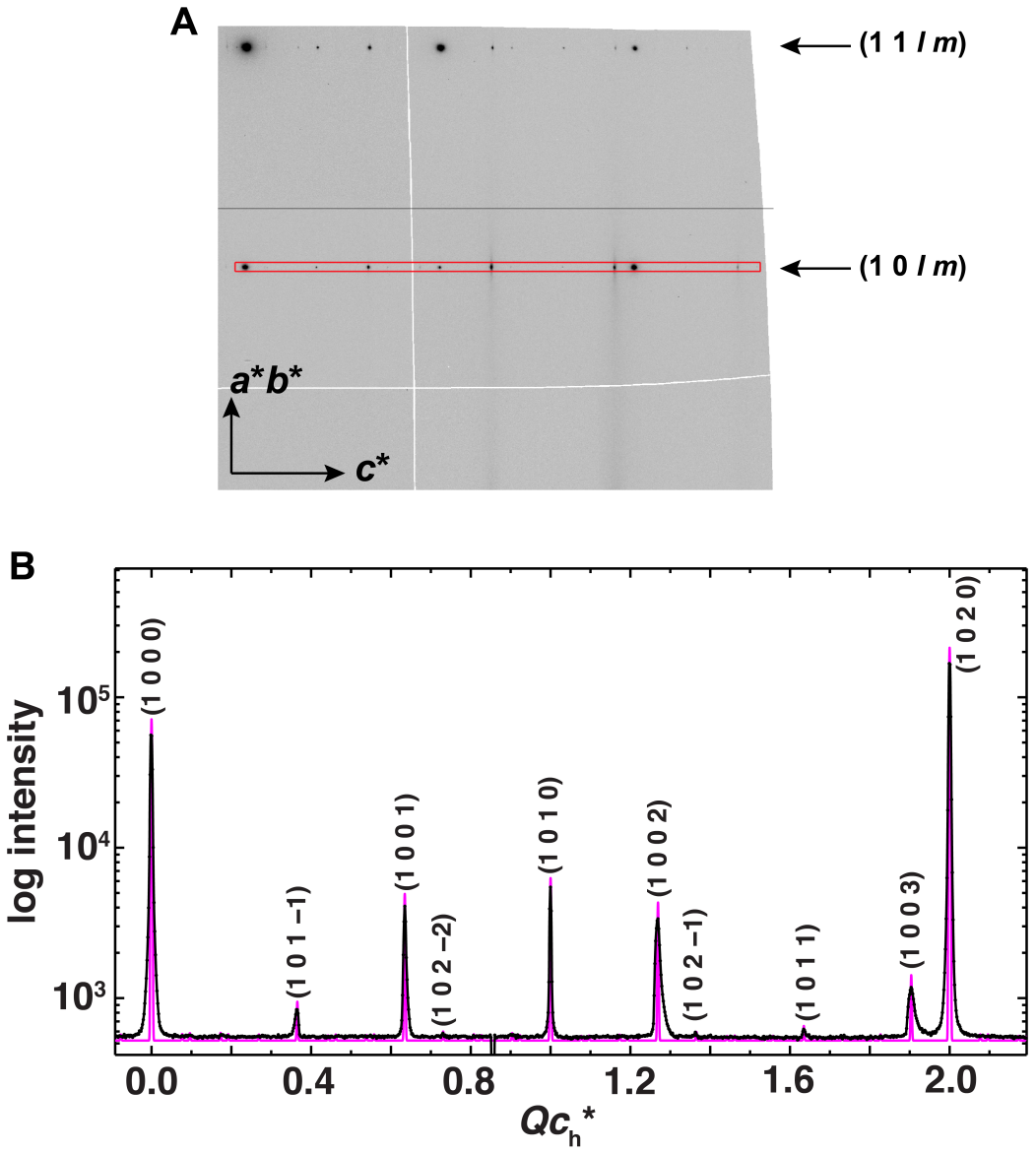

Figure 3.2.1.2. (A) An unwarped synchrotron oscillation image of 2,11-dodecanedione/ urea grown at -20.0 °C. The measurement was made on ALS beamline 8.2.2 using a 60° ϕ rotation about the crystal ***c*** axis at 290.0 K with a detector distance of 500.0 mm, an exposure time of 8.0 s, and λ of 1.18080 Å.[11] The red rectangle shows the (1 0 *l m*)$_h$ layer line, which is analyzed here. (B) Profile analysis of the (1 0 *l m*)$_h$ layer line of the image shown in (A). The misfit parameter at 290.0 K was fit to γ = 0.63462(3).

Judging by the appearance of Bragg peaks from a commensurate phase in the oscillation images, a lock-in phase transition occurred in the temperature range of 263.0 K to 259.1 K. Unfortunately, evaluation of the X-ray images in the first cooling run of this sample is not straightforward because of beam damage to the crystal. This discussion, therefore, will begin with frames collected at low temperatures after crystal translation.

Figure 3.2.1.3 shows an oscillation image taken at 162.4 K after a translation of the crystal. The profile analysis of the image shows there are two commensurate phases, one with $12c_g' = 19c_h'$ (c_g' = 17.4443(8) Å), and a compressed commensurate phase with $2c_g' = 3c_h'$ (c_g' = 16.5261(8) Å). The overall shortening of the guest repeat length from 290 to 162.4 K is therefore Δc_g = 17.3931(11) - 16.5261(8) = 0.8670(14) Å, of which 11.0174(5) × (1/0.63462 - 3/2) = 0.83453(4) Å is via self-compression, and (11.0380(5) - 11.0174(5))/0.63462 = 0.0325(7) Å is due to thermal shrinkage of the host.

In the oscillation image at 162.4 K, there are extra layer lines from the most compressed phase (with $2c_g' = 3c_h'$). The indices of those extra layer lines are shown in Figure 3.2.1.3 (A). By measuring the separations between peaks in those layer lines, the cell parameters of this compressed phase were determined to be $\boldsymbol{a}$ = 8.270 Å and $\boldsymbol{b}$ = 13.957 Å. (See Appendix 5.2.2.) This corresponds to a 2.6% distortion from hexagonal metric symmetry. For comparison, the cell parameters of the commensurate phase with $12c_g' = 19c_h'$ were determined to be $\boldsymbol{a}_h = \boldsymbol{b}_h$ = 8.130 Å, using the same procedure. With its lowered symmetry, the most compressed state with $2c_g' = 3c_h'$ most

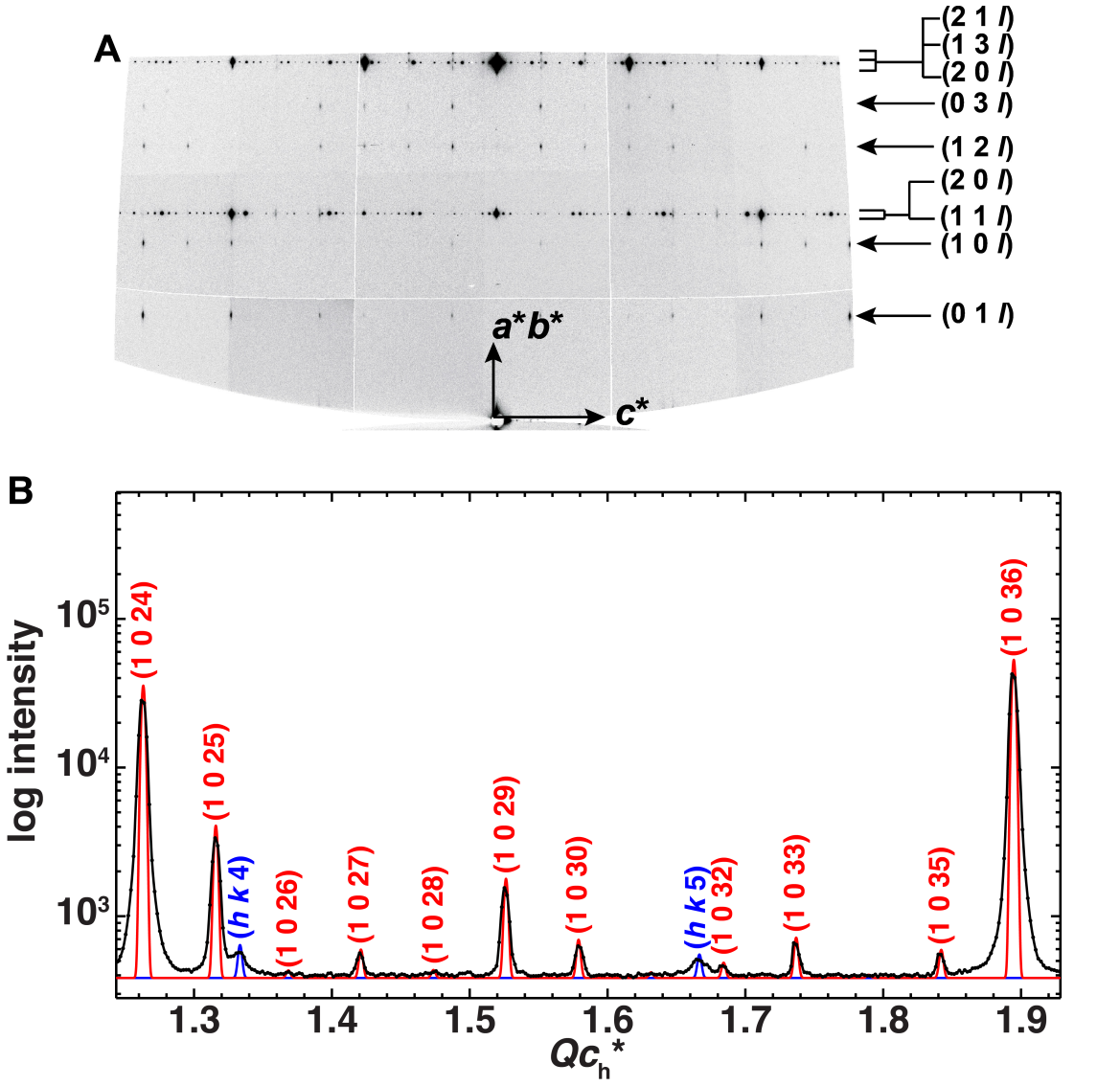

Figure 3.2.1.3. (A) Unwarped synchrotron oscillation image of 2,11-dodecanedione/urea grown at -20.0 °C. The measurement was made on ALS beamline 8.2.2 using a 60° ϕ rotation about the crystal ***c*** axis at 162.4 K, with the following parameters: distance = 500.0 mm, φ = 60-120°, time = 8.0 s, and λ = 1.18080 Å, and beam size (x,y) = (100,200) μm.[12] (B) Profile analysis of the (1 0 l)$_h$ and overlapping (1 1 l)$_o$, and (2 0 l)$_o$ layer lines of the oscillation image shown in (A). The profile was modeled with a commensurate phase with $12c_g' = 19c_h'$ (red), and a commensurate phase with $2c_g' = 3c_h'$ (blue).

likely has a primitive orthorhombic cell. Since the guest molecules in the structure with $2c_g' = 3c_h'$ are likely related along the channel axis by a two-fold screw axis (as in 2,10-undecanedione/urea),[13] this ferroelastic distortion is reasonable. The commensurate phase with $12c_g' = 19c_h'$ is still undistorted at 162.4 K, as evidenced by the absence of displaced layer lines in the ***a***b**** plane of the oscillation

Because the peaks from the compressed phase with $2c_g' = 3c_h'$ are quite broad along ***a***b**** in oscillation images with φ ranges of 60º, it is not clear from this data if this phase is truly crystalline. However, synchrotron data collected at DLS beamline I04 on a fresh crystal at 170 K showed clear evidence of Bragg peaks, as shown in Figure 3.2.1.4.

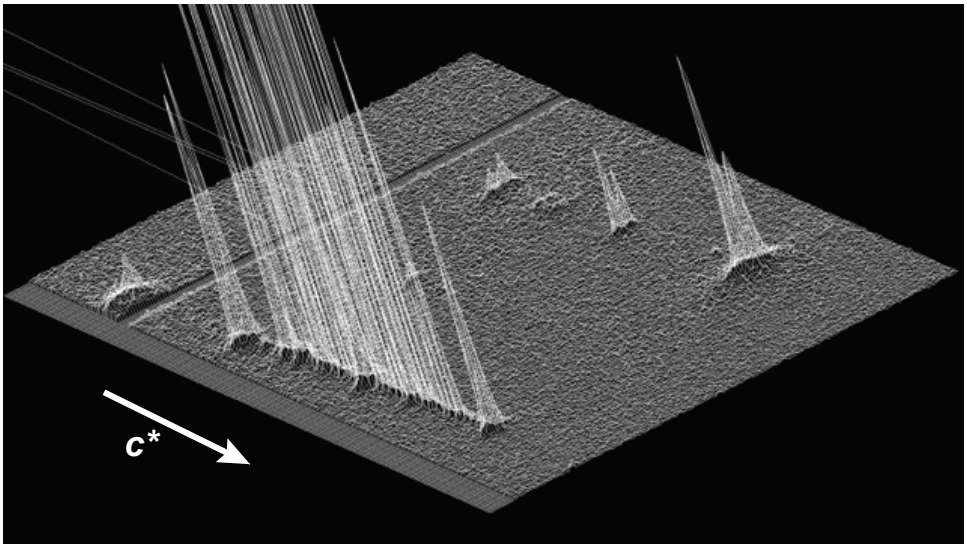

Figure 3.2.1.4. 3D profile of a synchrotron image of a crystal of 2,11-dodecanedione/urea grown by cooling from -13.0 to -23.0 °C.[14] The data was collected at 170 K on a misoriented crystal on beamline I04 at the Diamond Light Source (DLS), Oxford.[15] The Bragg peaks on the right are from the phase with $2c_g' = 3c_h'$.

Due to the weak intensities of the Bragg peaks from the most compressed phase and the nature of this initial experiment, the transition temperature for its formation is unclear. Upon heating this same crystal, an incommensurate phase appears at 216 K and coexists with the two commensurate phases until 245 K. The profile analysis of the $(1\ 0\ l\ m)_h$ and overlapping $(1\ 1\ l)_o$, and $(2\ 0\ l)_o$ layer lines of the oscillation image taken at 236.0 K (Figure 3.2.1.5) shows these three phases. In this profile, the incommensurate phase was modeled with a γ value of 0.64286. Above 245 K, the commensurate phase with $2c_g' = 3c_h'$ disappears. When further heated above 245 K, the misfit parameter (γ) of this compressed, incommensurate phase continuously decreases (Figure 3.2.1.6).

As the temperature of the crystal was raised from 245 K to 262 K, the peak intensities from the reflections of the commensurate phase with $12c_g' = 19c_h'$ slowly decreased and finally collapsed at 262 K. Concomitantly, the peaks from the compressed phase gradually return to the values found in the original uncompressed phase. The evolution of peaks in the oscillation images during heating is shown in Figure 3.2.1.6. At 290.0 K, the final misfit parameter is predominantly $\gamma = 0.63467(4)$, which equates to $c_g = 17.3917(8)$ Å using $c_h = 11.0380(5)$ Å, as shown in Figure 3.2.1.7. The similarity between this value and the c_g of 17.3931(11) Å in the initial state at 290 K before cooling suggests that the phase sequence is reversible through this cooling-and-heating cycle. The guest peaks are still asymmetric in Figure 3.2.1.7, so a distribution of guest repeat lengths is again present, as it was before cooling.

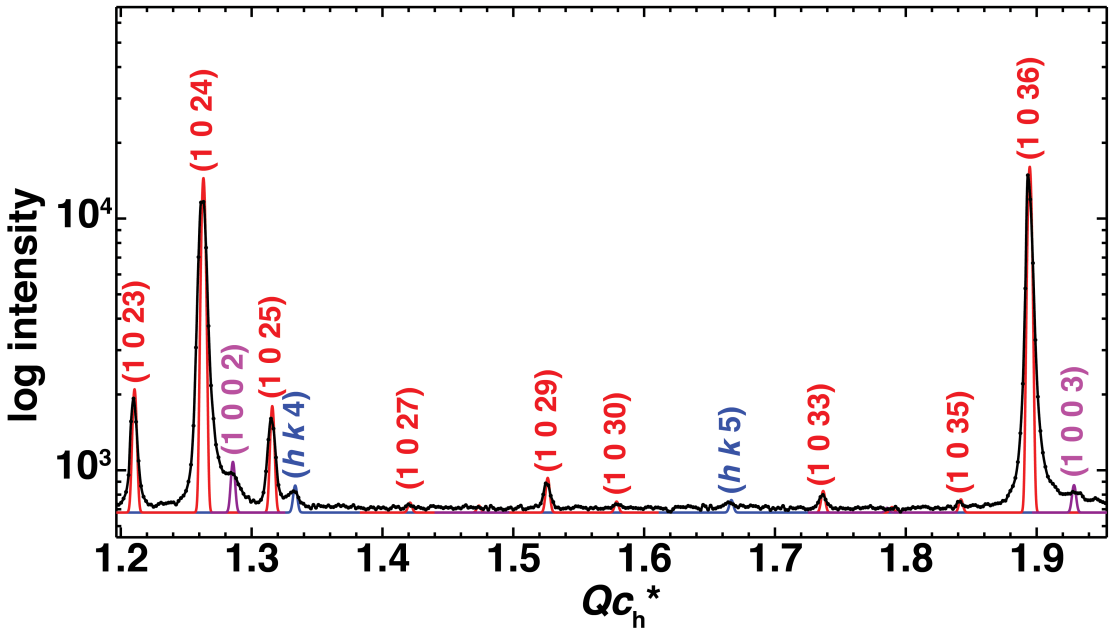

Figure 3.2.1.5. Profile analysis of the (1 0 *l* *m*)$_h$, overlapping (1 1 l)$_o$, and (2 0 l)$_o$ layer lines in the unwarped synchrotron oscillation image of 2,11-dodecanedione/urea grown at -20.0 °C. The measurement was made on ALS beamline 8.2.2 using a 60° ϕ rotation about the crystal ***c*** axis at 236.0 K with the following parameters: distance = 500.0 mm, φ = 60-120°, time = 8.0 s, λ = 1.18080 Å, and beam size (x,y) = (100,200) μm.[16] The profile was modeled with three commensurate phases: $12c_g' = 19c_h'$ (red), $2c_g' = 3c_h'$ (blue), and an incommensurate phase with a γ value of 0.64286 (magenta).

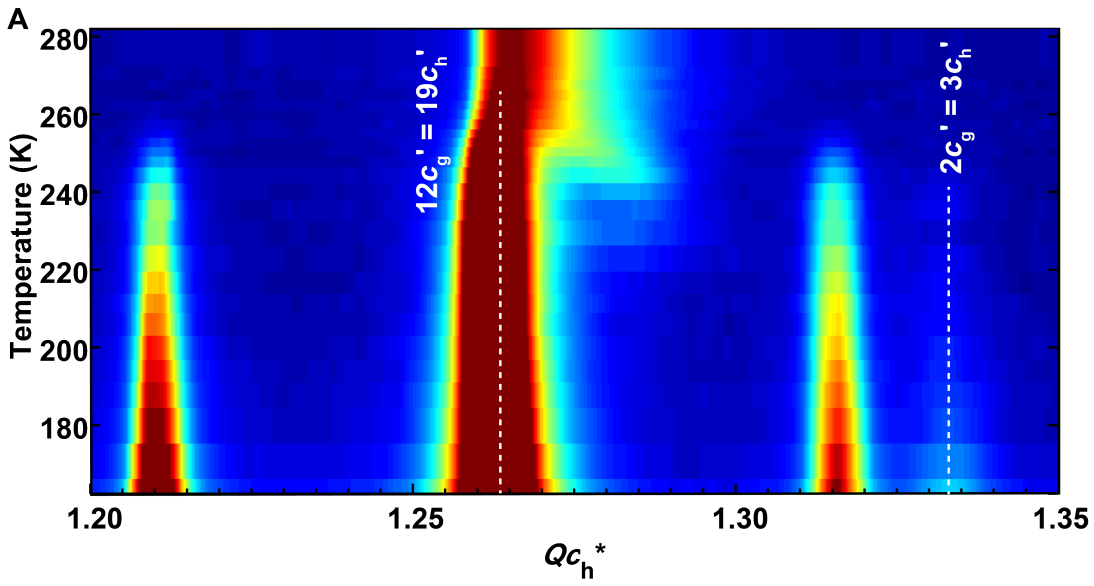

Figure 3.2.1.6. (A) Temperature evolution upon heating from 163 to 290 K of the (-1 0 *l* *m*)$_h$ and overlapping (0 -2 *l* *m*)$_o$ and (-1 -1 *l* *m*)$_o$ layer lines of 2,11-dodecanedione/urea grown at -20.0 °C. Measurements were made on ALS beamline 8.2.2 using 60° ϕ rotations about the crystal ***c*** axis from 162.4 to 290.0 K with the following parameters: distance = 500.0 mm, time = 8.0 s, λ = 1.18080 Å, and beam size (x,y) = (100, 200) μm.[17] Layer line profiles are shown on a logarithmic color scale, with red being most intense. The dashed lines denote the commensurate phases with $12c_g' = 19c_h'$ and $2c_g' = 3c_h'$.

B

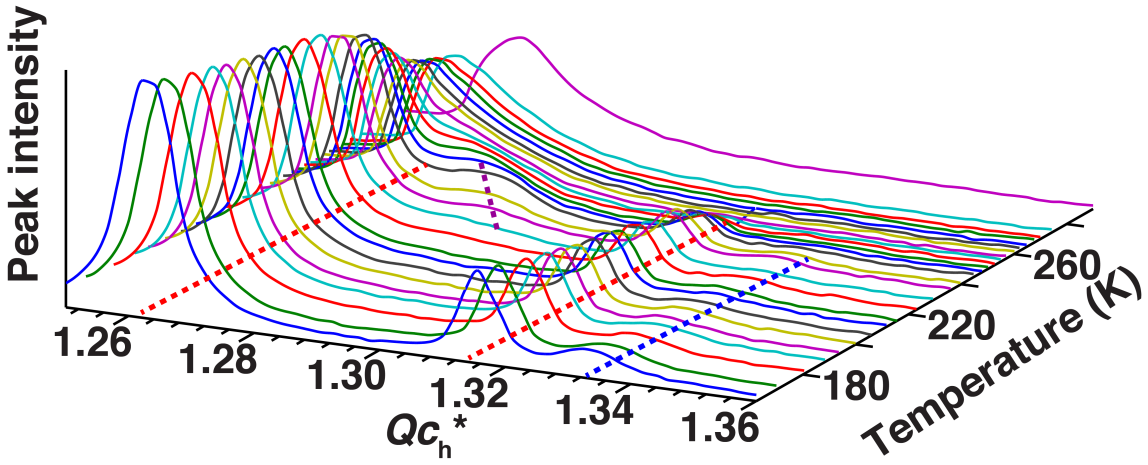

Figure 3.2.1.6. (B) Stacked profiles of synchrotron oscillation images from $\mathbf{Qc_h^*}$ = 1.256 to 1.36 of the (-1 0 *l m*)$_h$ and overlapping (0 -2 *l m*)$_o$ and (-1 -1 *l m*)$_o$ layer lines. The dashed lines denote the phases with $12c_g' = 19c_h'$ (red), $2c_g' = 3c_h'$ (blue), and a variably compressed phase (magenta).

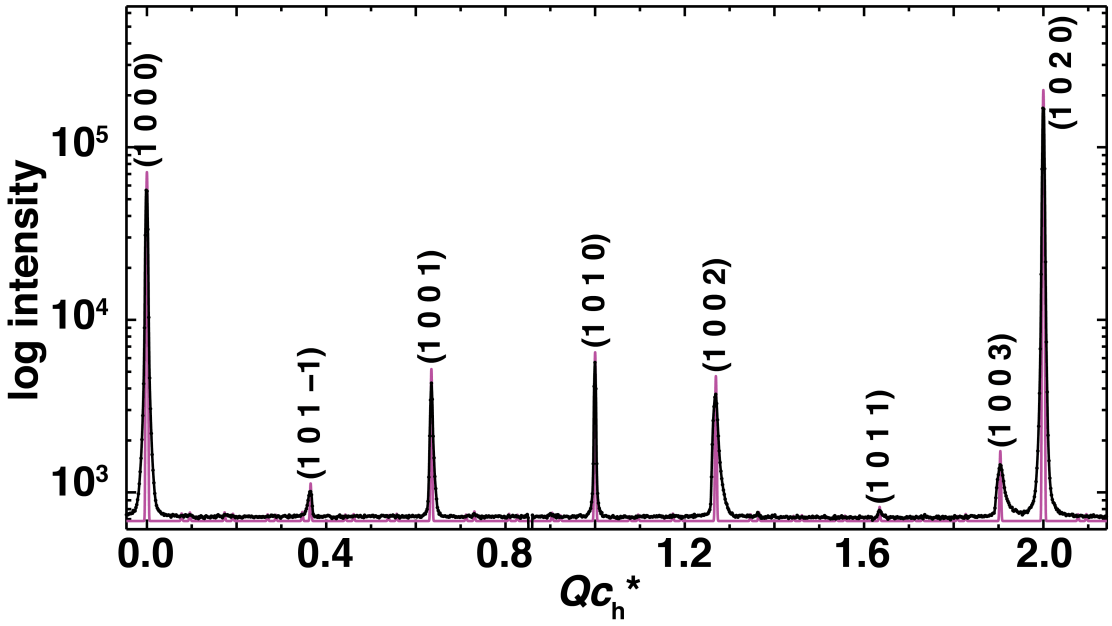

Figure 3.2.1.7. Profile analysis of the (1 0 *l m*)$_h$ layer line in the unwarped synchrotron oscillation image of 2,11-dodecanedione/urea grown at -20.0 °C. The measurement was made on ALS beamline 8.2.2 using a 60° ϕ rotation about the crystal ***c*** axis with *T* = 290.0 K, distance = 500.0 mm, φ = 60-120°, time = 8.0 s, λ = 1.18080 Å, and beam size (x,y) = (100,200) μm.[18] The profile was fit with γ = 0.63467(4).

The sequence of phases observed while warming 2,11-dodecanedione/urea grown at -20.0 °C is summarized in Figure 3.2.1.8. There are three phase transitions. Below 216 K, the system contains an undistorted commensurate phase with 12*c*' = 19c_h' and a distorted commensurate phase with 2c_g' = 3c_h'. Between 216 K and 245 K, three

phases coexist: $12c_g' = 19c_h'$, $2c_g' = 3c_h'$, and a incommensurate, compressed phase. Upon warming to 245 K, the phase with $2c_g' = 3c_h'$ disappears, leaving a commensurate phase with $12c_g' = 19c_h'$ and a compressed phase. Above 262 K, the system contains a single incommensurate phase with $\gamma = 0.63467(4)$. The phase transitions are rationalized with the self-compression mechanism, with the emergence of a commensurate phase with $12c_g' = 19c_h'$ on cooling driving the formation of shortened structures.

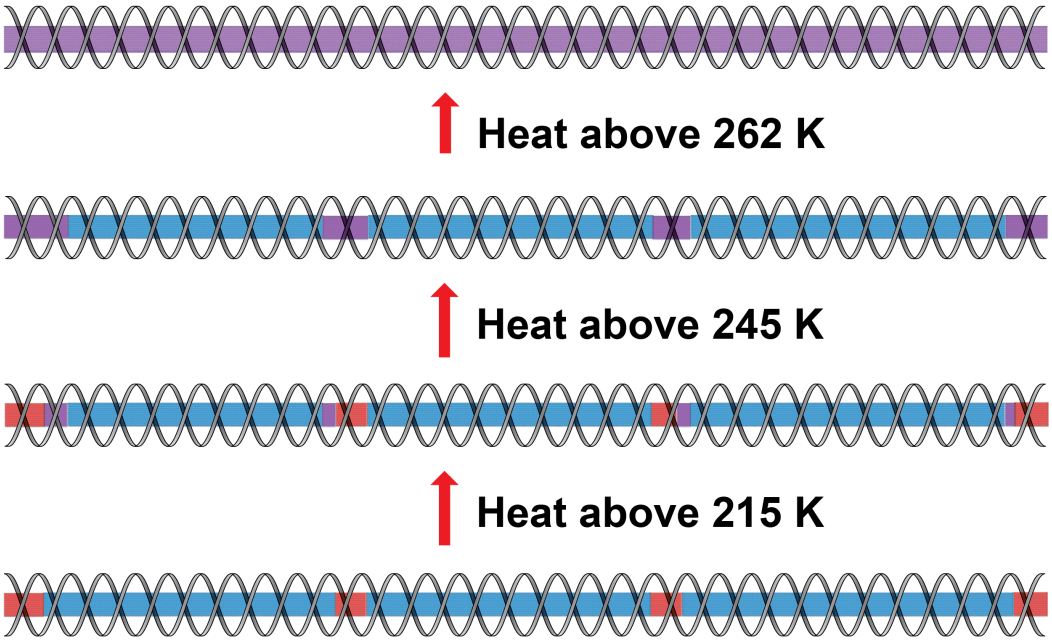

Figure 3.2.1.8. Schematic representations of phase transitions of 2,11-dodecanedione/urea (grown at -20 °C) during heating. Several phases are indicated with colored blocks: $12c_g' = 19c_h'$ (blue, $c_g' = 17.464$ Å), $2c_g' = 3c_h'$ (red, $c_g' = 16.545$ Å), and a compressed phase ($0.63467 < \gamma < 0.64286$, $c_g' = 17.158$-17.379 Å), using $c_h = 11.030$ Å (for T = 240 K).

3.2.2. Synchrotron X-ray studies of 2,11-dodecanedione/urea grown at -10.0 °C

The sample was crystallized by evaporation while purging with argon in a HAKKE (C40) temperature controller set at -10.0 °C.[19] The DSC trace of this sample shows an exothermic phase transition on cooling at 257.5 K (ΔH = -0.89 J/g), and an endothermic phase transition on heating at 261.0 K (ΔH = 1.06 J/g), as shown in Figure 3.2.2.1.

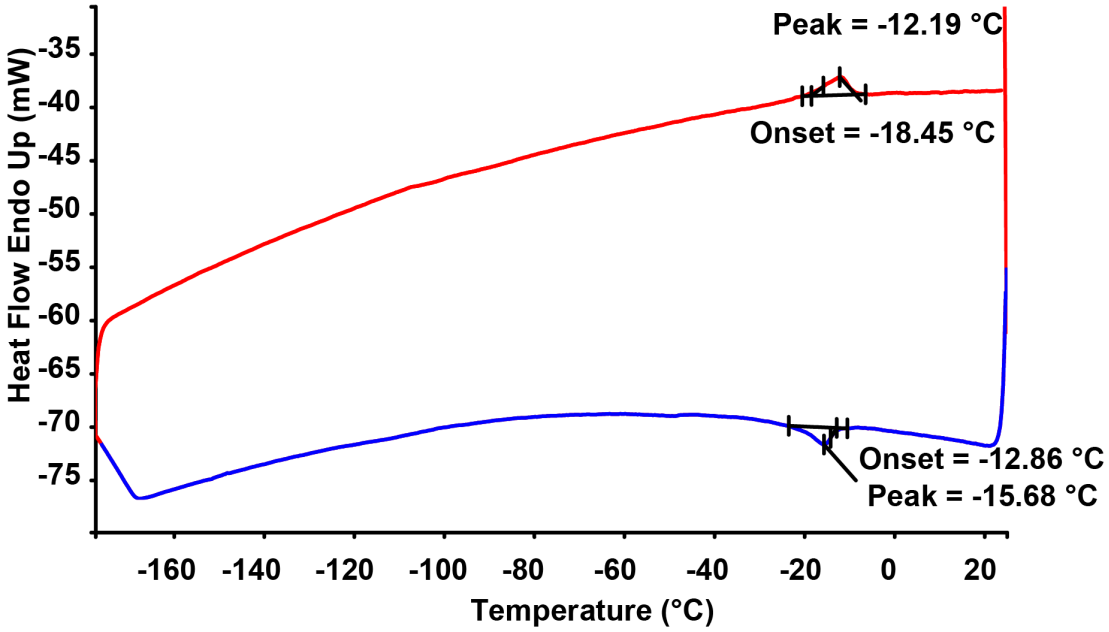

Figure 3.2.2.1. DSC trace (using a Perkin Elmer Pyris 1 DSC) of 2,11-dodecanedione/urea grown at -10.0 ºC.[20] The blue line is the cooling scan, and the red line is the heating scan. The scan rate was 20 K/min, and the scan ranges were from 298 K (25 ºC) to -108 K (-165 ºC) and then back to 298 K. An exothermic phase transition was observed with a peak position of 257.5 K (-15.7 ºC) on the cooling curve, and a corresponding endothermic phase transition was observed with a peak position of 261.0 K (-12.2 ºC) upon heating.

A variable temperature X-ray scan from 290.8 K to 200.3 K was conducted on APS beamline 14-BM-C. By comparing the temperatures from the Oxford Cryostream (Oxford Cryosystems Ltd.) at 100.0 K and 290.0 K with those from a calibrated thermocouple at the sample position, a temperature calibration with T_{actual} = 0.984861 × T_{cryo} + 5.24 was obtained.[21] Data analysis shows that this sample has phase transitions that are very similar to those observed in the crystal grown at -20.0 °C. At 290.8 K this UIC has an undistorted lattice with a misfit parameter γ = 0.63335(5), as shown in Figure 3.2.2.2. Thus c_g = 11.0380(5)/0.63335(5) = 17.4279(16) Å. This is 0.0489(18) Å shorter than the value of c_g' (17.4768(8) Å) required for a commensurate phase with $12c_g' = 19c_h'$, using c_h' = 11.0380(5) Å.

Upon cooling, a lock-in phase transition occurred at 267(3) K.[22] As shown in Figure 3.2.2.3, the commensurate phase with $12c_g' = 19c_h'$ was used to model the profile extracted from the $(1\ 0\ l\ m)_h$ layer line in the oscillation image taken at 261.0 K. Although an expected compressed structure can be seen in the diffraction image as diffuse bands, it has very little intensity and is not observed in this profile analysis.

The very low concentration of the compressed phase is likely a consequence of the guest repeat at 290.8 K being only 0.0489(18) Å shorter than the value required for a phase with $12c_g' = 19c_h'$ (compared with 17.4768(8) - 17.3931(11) = 0.0837(14) Å in the crystal grown at -20.0 ºC). To see this, it is necessary to understand that because the strongly hydrogen-bonded host has such a rigid structure, the overall length of the

crystal (along the channel axis) remains essentially constant through this lock-in phase transition. This is evidenced by the relatively fixed positions of the host reflections during the phase transition. In the phase transition in this crystal grown at -10 ºC, an elongation of only 0.0489(18) Å is needed for the guest to lock into the structure with $12c_g' = 19c_h'$. For a fixed channel length, the total amount of compression, which is the population of the compressed state times its compressive strain, must be proportional to the overall amount of guest elongation (its population times its extensive strain). In this crystal, almost all of the guest molecules lock into the commensurate structure, so the amount by which other guests are compressed, and the population of such phases, is limited. The domain sizes of these compressed regions are clearly too small to diffract coherently. At 198.1 K, the crystal is mostly commensurate with $12c_g' = 19c_h'$.

The lock-in phase transition of this crystal of 2,11-dodecanedione/urea on cooling can be better observed with the aid of the color map shown in Figure 3.2.2.4.

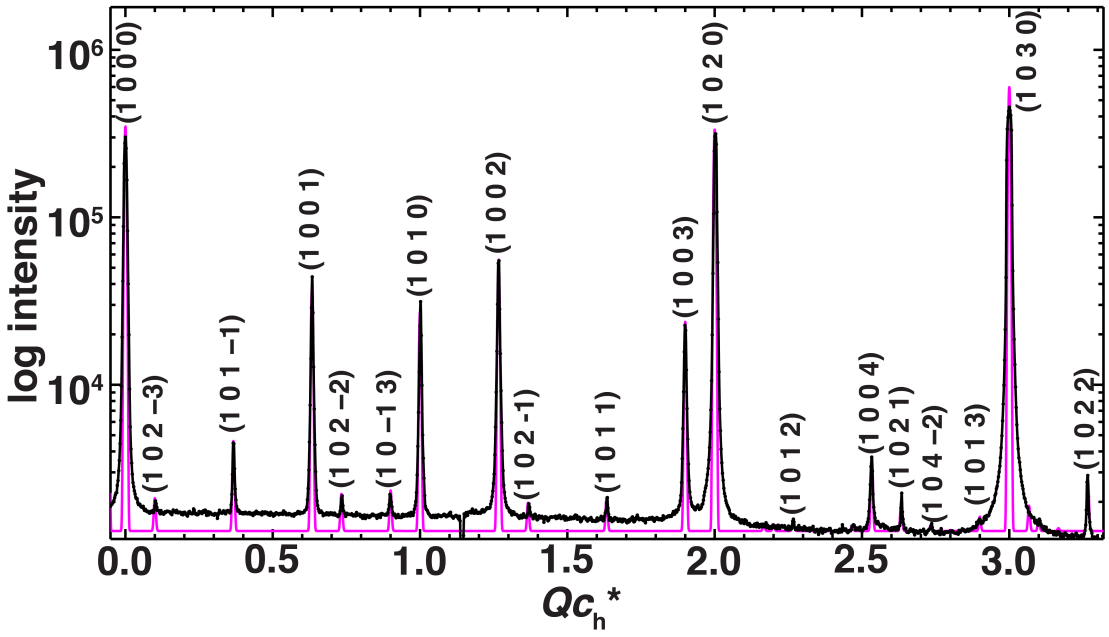

Figure 3.2.2.2. Profile analysis of the (1 0 *l* *m*)$_h$ layer line in the unwarped synchrotron oscillation image of 2,11-dodecanedione/urea grown at -10.0 °C. The measurement was made on a fresh crystal using a 60° ϕ rotation about the crystal ***c*** axis at 290.8 K on APS beamline 14-BM-C with the following parameters: distance = 500.0 mm, φ = 60-120°, time = 6 s, λ = 0.97870 Å.[23] The profile was fit with a misfit parameter of γ = 0.63335(5).

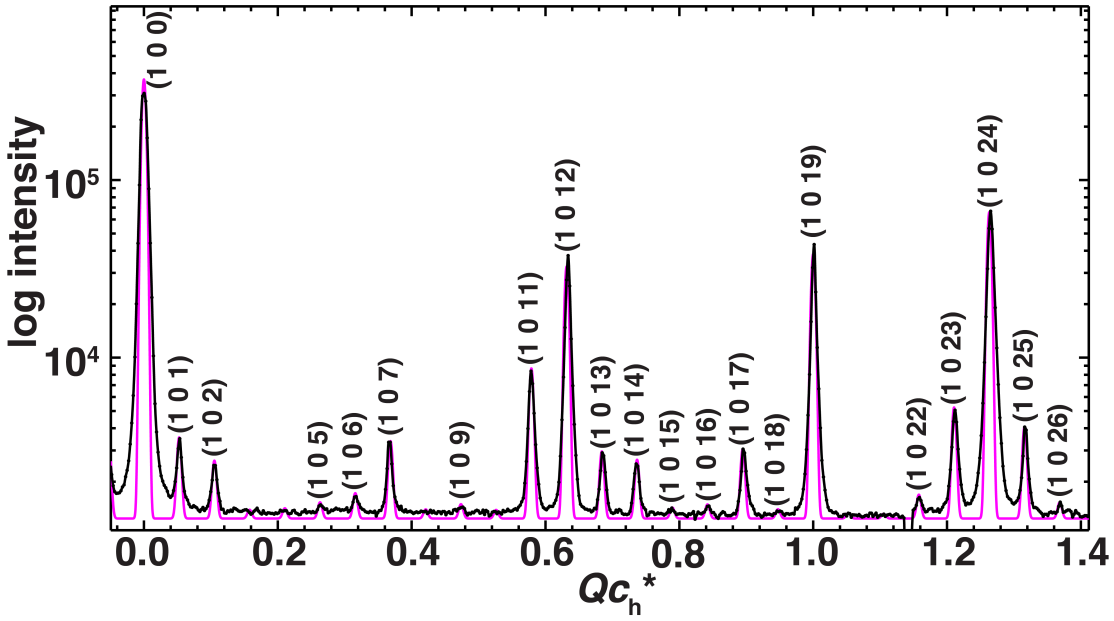

Figure 3.2.2.3. Profile analysis of the (1 0 l)$_h$ layer line in the unwarped synchrotron oscillation image of 2,11-dodecanedione/urea grown at -10.0 °C. The measurement was made using a 60° ϕ rotation about the crystal ***c*** axis at 261.0 K on APS beamline 14-BM-C with the following parameters: distance = 500.0 mm, φ = 60-120°, time = 6 s, λ = 0.97870 Å.[24] The profile was modeled as a commensurate phase with $12c_g' = 19c_h'$.

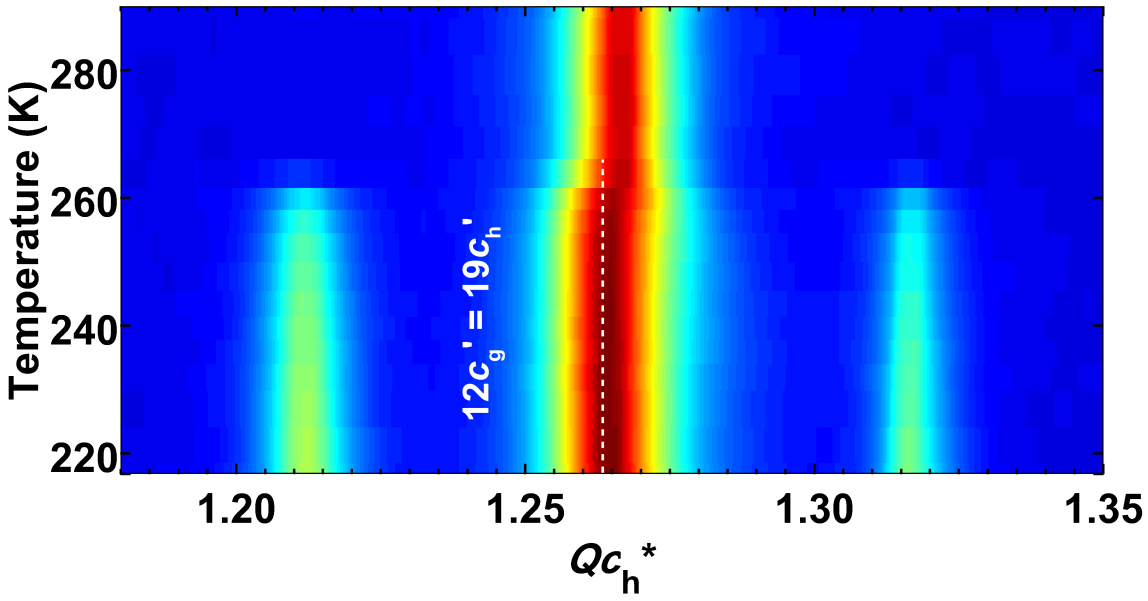

Figure 3.2.2.4. Temperature evolution of the (1 0 *l m*)$_h$ layer line in oscillation images of 2,11-dodecanedione/urea grown at -10.0 °C upon cooling from 290.8 K to 218.8 K. Measurements were made on APS beamline 14-BM-C using 60° ϕ rotations about the crystal ***c*** axis from 290.8 to 218.8 K with the following parameters: distance = 500.0 mm, time = 6 s, λ = 0.97870 Å, and beam size (x,y) = (300, 400) μm.[25] Layer line profiles are shown on a logarithmic color scale, with red being most intense. The dashed line shows the (1 0 24) peak of the commensurate phase with $12c_g' = 19c_h'$. The temperatures used in this color map should be adjusted to include temperature calibration.

After translation of the crystal to observe a fresh region at 200.3 K, some evidence of a compressed phase with $2c_g' = 3c_h'$ is observed, as shown in Figure 3.2.2.5. The reverse of a self-compression sequence of events can be observed in the subsequent

heating run, as shown in Figure 3.2.2.6. At 281.0 K, this UIC is back to the initial incommensurate phase with γ = 0.63333(2), as shown in Figure 3.2.2.8. This is nearly identical to starting value of γ = 0.63335(5) at 290.0 K, as shown in Figure 3.2.2.2.

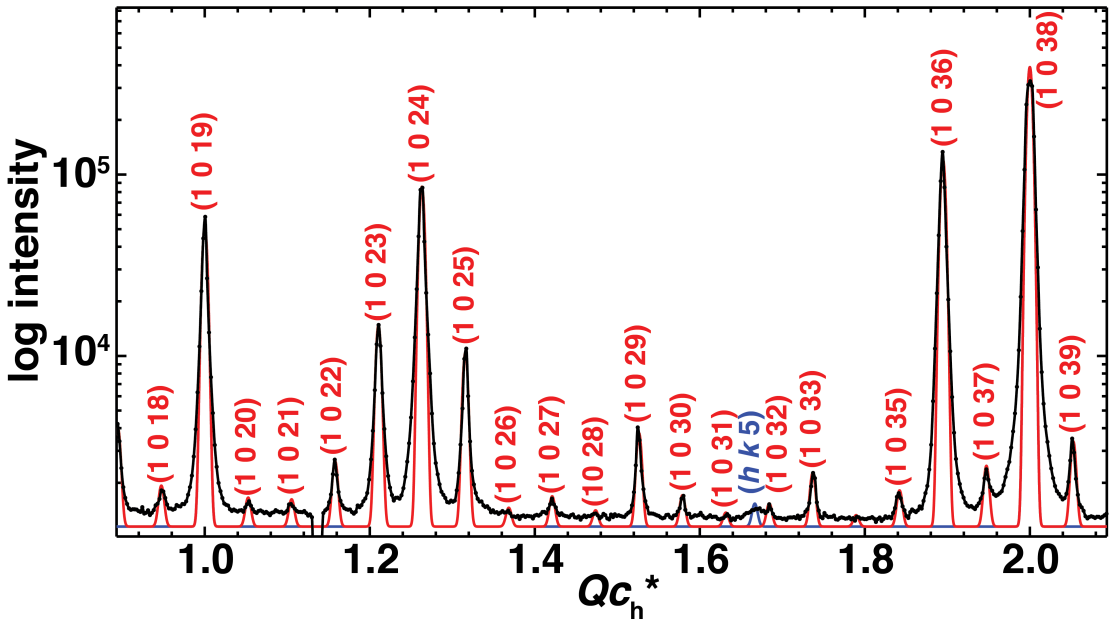

Figure 3.2.2.5. Profile analysis of the (1 0 l)$_h$ layer line in the unwarped synchrotron oscillation image of 2,11-dodecanedione/urea grown at -10.0 °C. The measurement was made using a 60° ϕ rotation about the crystal ***c*** axis at 200.3 K on APS beamline 14-BM-C with the following parameters: distance = 500.0 mm, φ = 60-120°, time = 6 s, λ = 0.97870 Å.[26] The profile was modeled as a commensurate phase with $12c_g' = 19c_h'$ (red) and as a commensurate phase with $2c_g' = 3c_h'$ (blue).

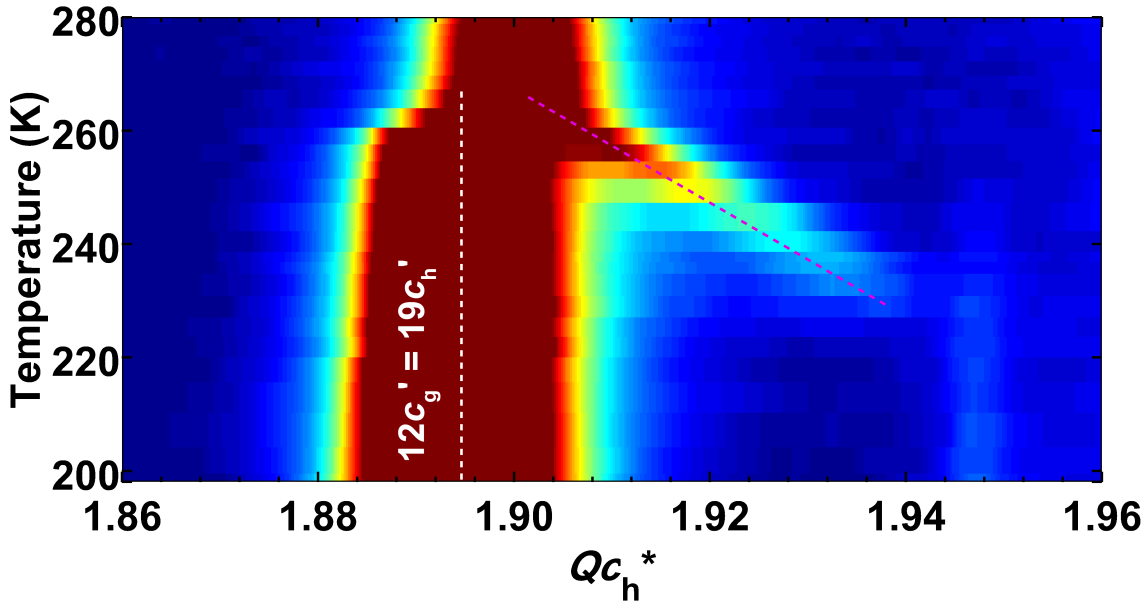

Figure 3.2.2.6. Temperature evolution of the (1 0 *l m*)$_h$ layer line in the oscillation image of 2,11-dodecanedione/urea grown at -10.0 °C upon heating from 200.3 to 281.0 K. Measurements were made on APS beamline 14-BM-C using 60° ϕ rotations about the crystal ***c*** axis from 200.3 to 281.0 K with the following parameters: distance = 500.0 mm, time = 6 s, λ = 0.97870 Å, and beam size (x,y) = (300, 400) μm.[27] Layer line profiles are shown on a logarithmic color scale, with red being most intense. The white dashed line shows the (1 0 24) peak of the commensurate phase with $12c_g' = 19c_h'$. The pink dashed line shows the (1 0 2 0) peak of the compressed state. The temperatures used in this color map should be adjusted to include temperature calibration.

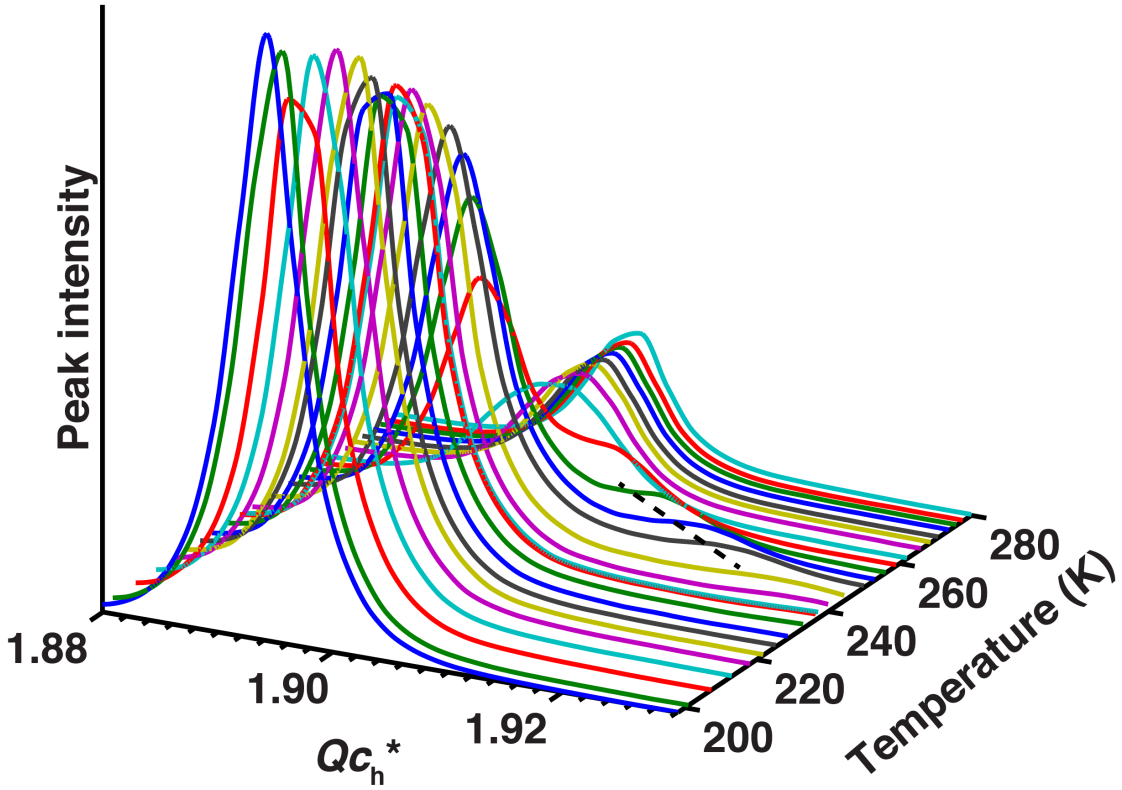

Figure 3.2.2.7. Stacked plot for the same region shown in Figure 3.2.2.6.

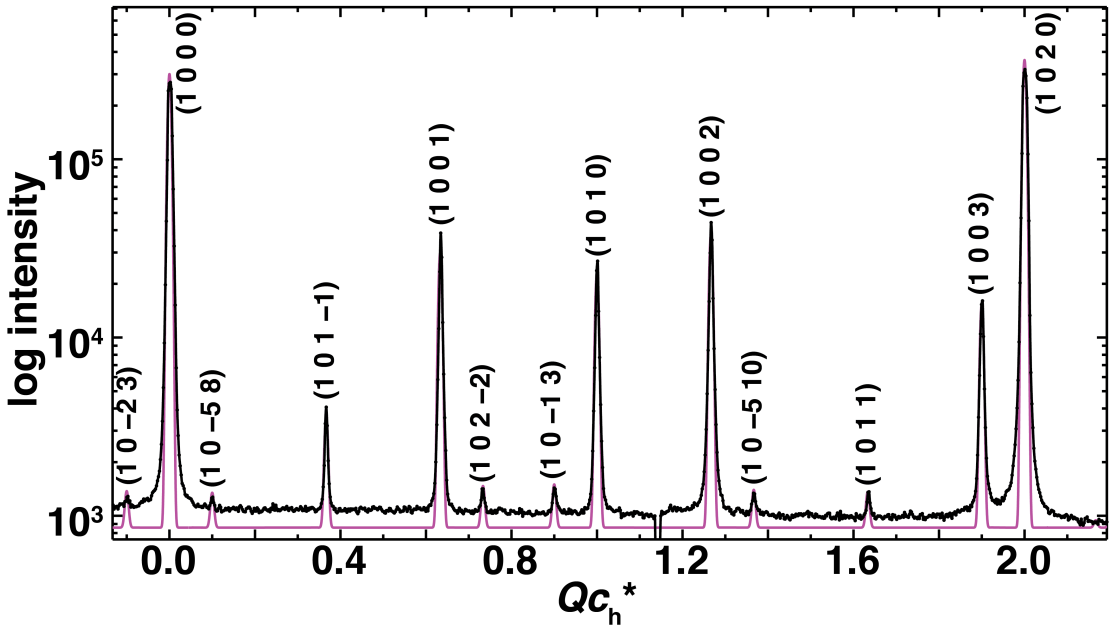

Figure 3.2.2.8. Profile analysis of the (1 0 *l* *m*)$_h$ layer line in the unwarped synchrotron oscillation image of 2,11-dodecanedione/urea grown at -10.0 °C. The measurement was made on APS beamline 14-BM-C after cooling from 290.8 to 198.1 K and then warming to 281.0 K, using a 60° ϕ rotation about the crystal ***c*** axis at a detector distance of 500.0 mm, φ = 60-120°, time = 6.0 s, and λ = 0.97870 Å.[28] The profile was fit as an incommensurate phase with γ = 0.63333(2).

Another sample from this batch grown at -10.0 °C was measured on beamline 8.2.2 at the ALS. This sample had an initial misfit parameter of γ = 0.63332(9) at 290.0 K (not shown). To maintain crystal integrity during cooling, the crystal was translated to a fresh region four times while collecting oscillation images between 270.1 K and 227.9 K. This

allowed the self-compression to be observed during this cooling run, as shown in Figure 3.2.2.9.

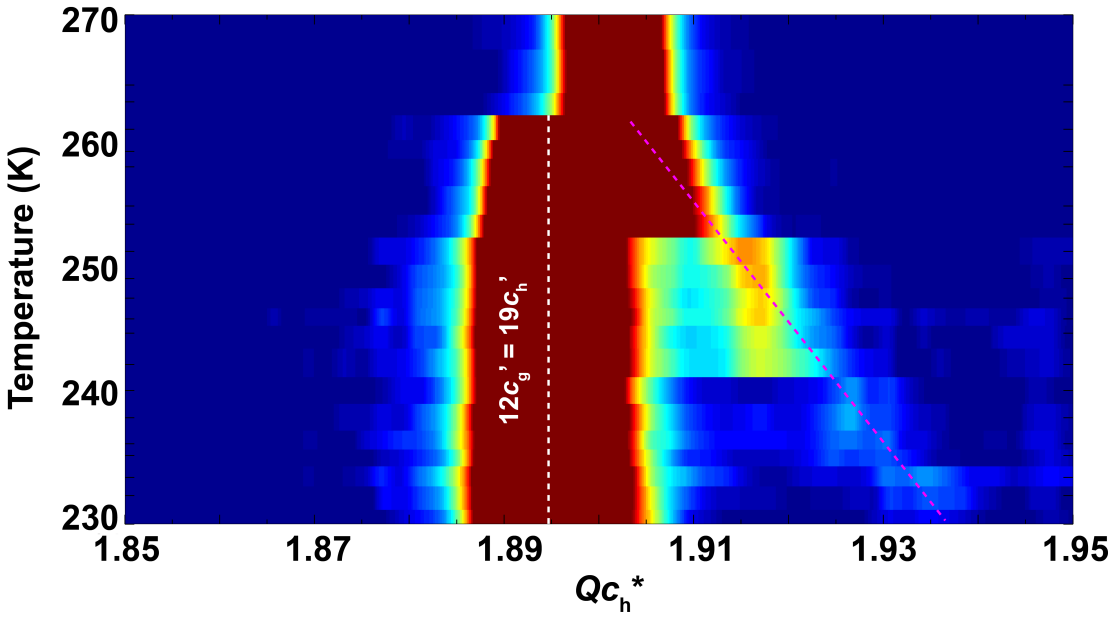

Figure 3.2.2.9. Temperature evolution of the (1 0 *l m*)$_h$ layer line in oscillation images of 2,11-dodecanedione/urea grown at -10.0 °C upon cooling from 270 K to 230 K. Layer line profiles are shown on a logarithmic color scale, with red being most intense. The white dashed line shows the (1 0 24) peak of the commensurate phase with $12c_g' = 19c_h'$. The pink dashed line shows the (1 0 2 0) peak of the compressed phase. The measurements were made using 60° ϕ rotations about the crystal ***c*** axis on ALS beamline 8.2.2 with the following parameters: distance = 500.0 mm, φ = 0-60°, time = 6.0 s, λ = 0.999957 Å, beam size (x,y) = (100,100) μm.[29]

In summary, 2,11-dodecanedione/urea grown at -10.0 °C has a mean γ of 0.63333(3) above 280.0 K. Upon cooling below 267(3) K, this incommensurate structure undergoes a self-compression phase transition by locking in to a phase with $12c_g' = 19c_h'$. There is some evidence to suggest that the shortest compressed state in this sample is commensurate with $2c_g' = 3c_h'$ below approximately 226 K. Compared with the UIC grown at -20.0 °C, the compressed phase from the -10.0 °C batch had weaker intensities. This can be rationalized by noting that for the sample grown at -10.0 °C, the guest repeat was required to extend by only 0.0489(18) Å to lock into the structure with $12c_g' = 19c_h'$. On the other hand, in the sample grown at -20.0 °C, the guest repeat elongated by 0.0837(14) Å in the same lock-in transition. As a result, a larger amount of compression was generated in the sample grown at -20.0 °C.

3.2.3. Synchrotron X-ray studies of 2,11-dodecanedione/urea grown at 0.0 °C

The sample was crystallized by evaporation while purging with argon in a HAKKE (C40) temperature controller set at 0.0 °C.[30] The DSC trace of this sample shows an exothermic phase transition on cooling at 259.3 K (ΔH = -0.89 J/g), and an endothermic phase transition on heating at 262.8 K (ΔH = 1.4 J/g), as shown in Figure 3.2.3.1.

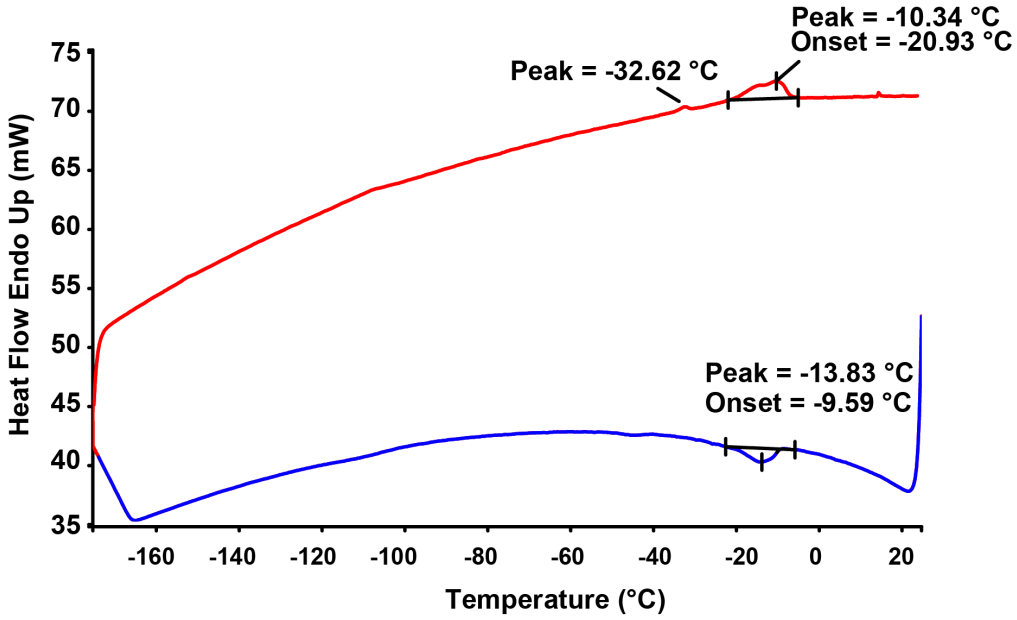

Figure 3.2.3.1. DSC trace (using a Pyris 1 DSC) of 2,11-dodecanedione/urea grown at 0.0 ºC. [31] The blue line is the cooling scan, and the red line is the heating scan. The scan rate was 20 K/min, and the scan ranges were from 298 K (25 ºC) to -108 K (-165 ºC) and then back to 298 K. An exothermic transition was observed at 259.3 K (-13.8 ºC) on the cooling curve, and a corresponding endothermic transition was observed at 260.8 K (-10.3 ºC) upon heating. A weak exotherm was observed near 230 K (-43 ºC) upon cooling. Its corresponding endotherm was observed at 240.5 K (-32.6 ºC) upon warming.

A variable temperature X-ray scan was conducted from 290.0 K to 119.0 K on ALS beamline 8.2.2. At 290.0 K, this UIC has an undistorted lattice, and the profile of the $(1\ 0\ l\ m)_h$ layer line was fit with $\gamma = 0.631219(14)$, as shown in Figure 3.2.3.2. Thus $c_g = 11.0380(5)/0.631219(14) = 17.4868(9)$ Å. This misfit parameter (γ) is very close to the commensurate relationship of $12c_g' = 19c_h'$ ($\gamma = 0.63158$), with $c_g' = 17.4768(8)$ Å. Three other profiles from different regions of the detector gave the following values of γ: $(1\ 0\ l\ m)_h$ layer line (negative $\mathbf{Q}\boldsymbol{c}_h^*$) = 0.6315(2), $(-1\ 0\ l\ m)_h$ layer line (positive $\mathbf{Q}\boldsymbol{c}_h^*$) = 0.63087(10), $(-1\ 0\ l\ m)_h$ layer line (negative $\mathbf{Q}\boldsymbol{c}_h^*$) = 0.63070(9).[32] The average value (0.6311(4)) corresponds to a guest repeat of 17.491(11) Å, which is only 0.014(11) Å longer than the value required for a commensurate structure with $12c_g' = 19c_h'$.

Because of the variation in γ across the detector, it is difficult to tell if the phase observed at 290 K is commensurate or not. (See the summary of this section for further discussion.) For each of the phase transitions reported in the crystals discussed previously, guest extension during the lock-in transition was the driving force for self-compression. However, because the misfit parameters are so close to the one expected for a commensurate phase with $12c_g' = 19c_h'$, no self-compression is expected upon cooling this sample.

Upon cooling below 261(3) K,[33] a number of Bragg peaks appeared in the layer lines with $h + k$ = even; these showed no distortion from hexagonal metric symmetry. The profile of the $(-1\ 0\ l\ m)_h$ layer line from the oscillation image taken at 222.3 K was

modeled as a commensurate phase with $12c_g' = 19c_h'$, as shown in Figure 3.2.3.3. No compressed phase was observed. Because of the uncertainties in the misfit parameter at 290 K, it is not known if the emergence of the new peaks below 261(3) K occurs because of a lock-in phase transition or whether they merely correspond to ordering of a phase that is already commensurate.

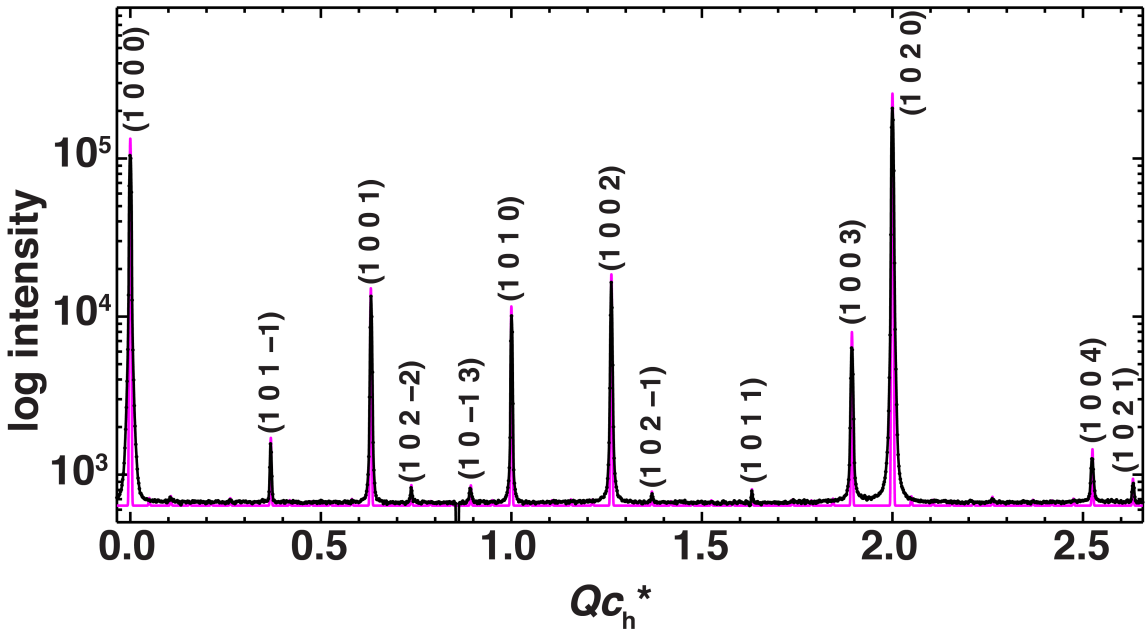

Figure 3.2.3.2. Profile analysis of the (1 0 *l m*)$_h$ layer line in the unwarped synchrotron oscillation image of 2,11-dodecanedione/urea grown at 0.0 °C. The measurement was made using a 60° ϕ rotation about the crystal ***c*** axis at 290.0 K on ALS beamline 8.2.2 with a detector distance of 500.0 mm and λ = 1.18080 Å.[34] The profile was fit as an incommensurate phase with γ = 0.631219(14).

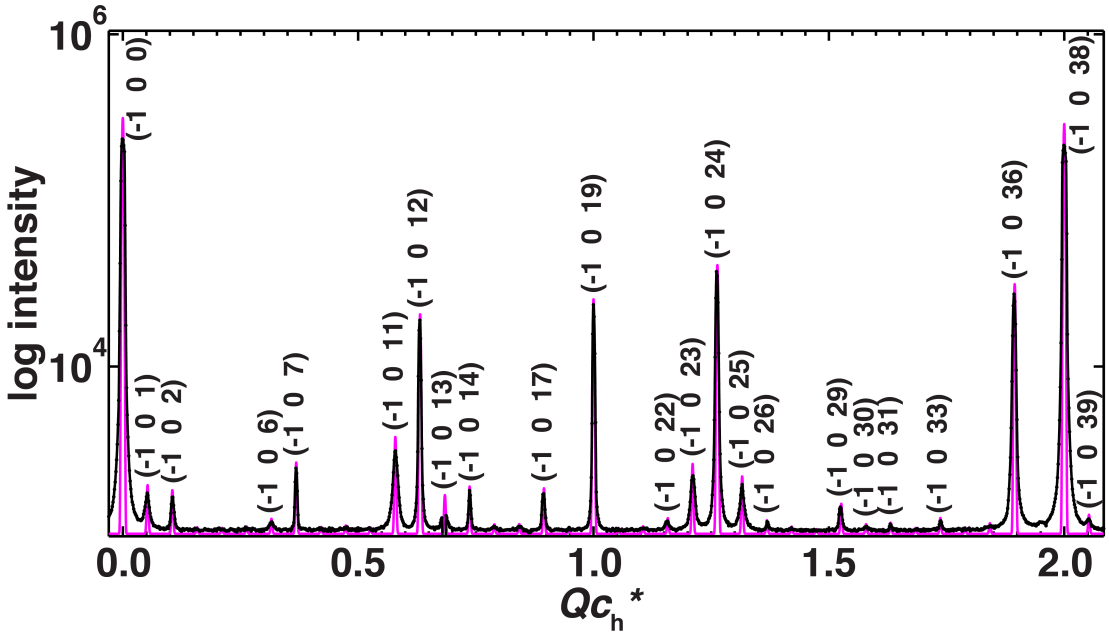

Figure 3.2.3.3. Profile analysis of the (-1 0 *l m*)$_h$ layer line in the unwarped synchrotron oscillation image of 2,11-dodecanedione/urea grown at 0.0 °C. The measurement was made using a 60° ϕ rotation about the crystal ***c*** axis at 222.3 K on ALS beamline 8.2.2 with a detector distance of 500.0 mm and λ = 1.18080 Å.[35] The profile was fit as a commensurate phase with $12c_g' = 19c_h'$.

Surprisingly, after this crystal was translated to a fresh region at low temperature, the reverse of a self-compression sequence was observed on heating. Below 209.5 K, there are weak and diffuse peaks from the commensurate phase with $2c_g' = 3c_h'$ (not shown here). As shown in Figure 3.2.3.4, at 228.0 K, the system has two components: a commensurate phase with $12c_g' = 19c_h'$ and a compressed incommensurate phase with a misfit parameter of γ = 0.6450. Upon warming above 260(2) K, this crystal consisted

only of an incommensurate phase with γ = 0.63254(3), as shown for 290.5 K in Figure 3.2.3.5. Unlike in the initial crystal region observed during cooling, here the guest repeat was c_g = 17.4503(11) Å, 0.0265(14) Å shorter than that for a commensurate crystal with $12c_g' = 19c_h'$. The reverse self-compression behavior during this heating run can be observed with the aid of the color map shown in Figure 3.2.3.6.

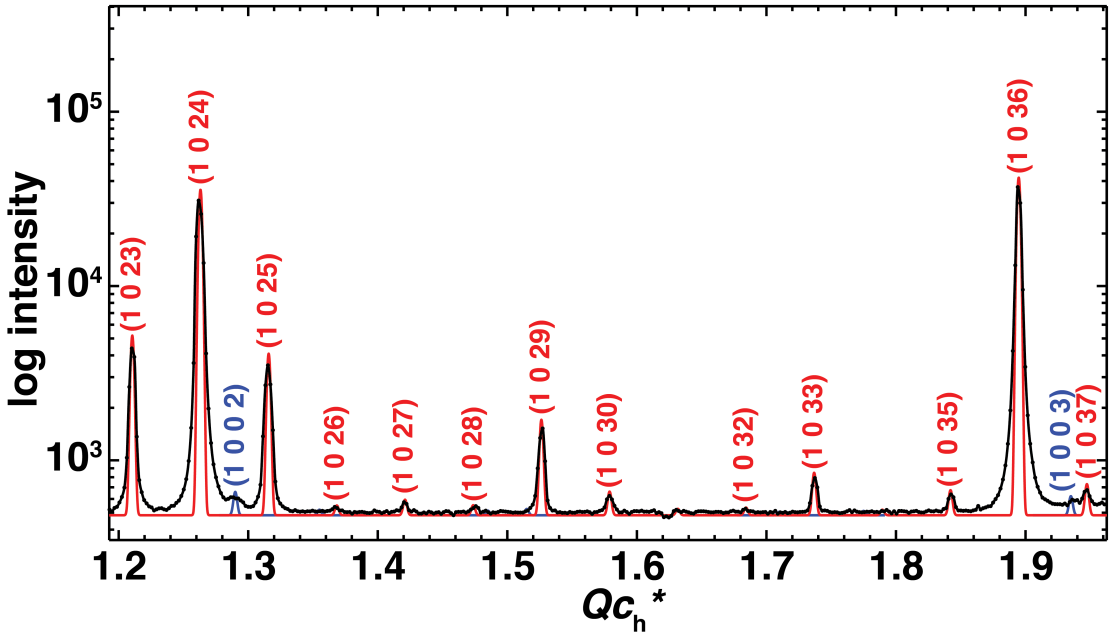

Figure 3.2.3.4. Profile analysis of the (1 0 *l m*)$_h$ layer line in the unwarped synchrotron oscillation image of 2,11-dodecanedione/urea grown at 0.0 °C. The measurement was made using a 60° ϕ rotation about the crystal ***c*** axis at 228.0 K on ALS beamline 8.2.2 with a detector distance of 500.0 mm and λ = 1.18080 Å.[36] The profile was modeled with two components: a commensurate phase with $12c_g' = 19c_h'$ (red), and a compressed incommensurate phase with misfit parameter γ = 0.6450(5) (blue).

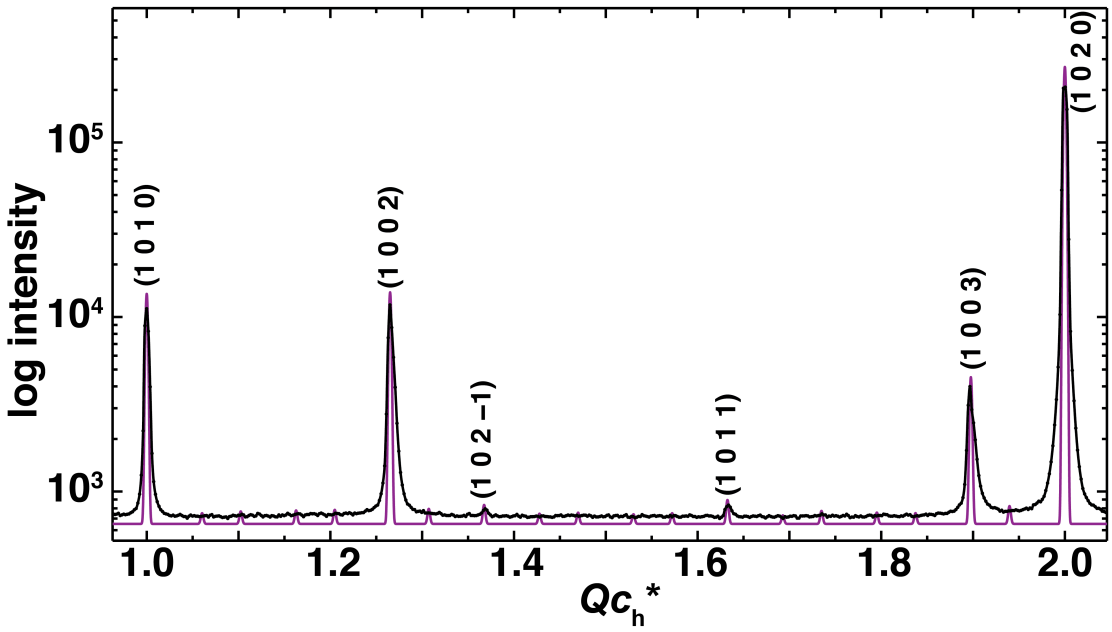

Figure 3.2.3.5. Profile analysis of the (1 0 *l m*)$_h$ layer line in the unwarped synchrotron oscillation image of 2,11-dodecanedione/urea grown at 0.0 °C. The measurement was made using a 60° ϕ rotation about the crystal ***c*** axis at 290.5 K on ALS beamline 8.2.2 with a detector distance of 500.0 mm and λ = 1.18080 Å.[37] The profile was fit as an incommensurate phase with γ = 0.63254(3). This corresponds to a guest repeat of 17.4503(11) Å.

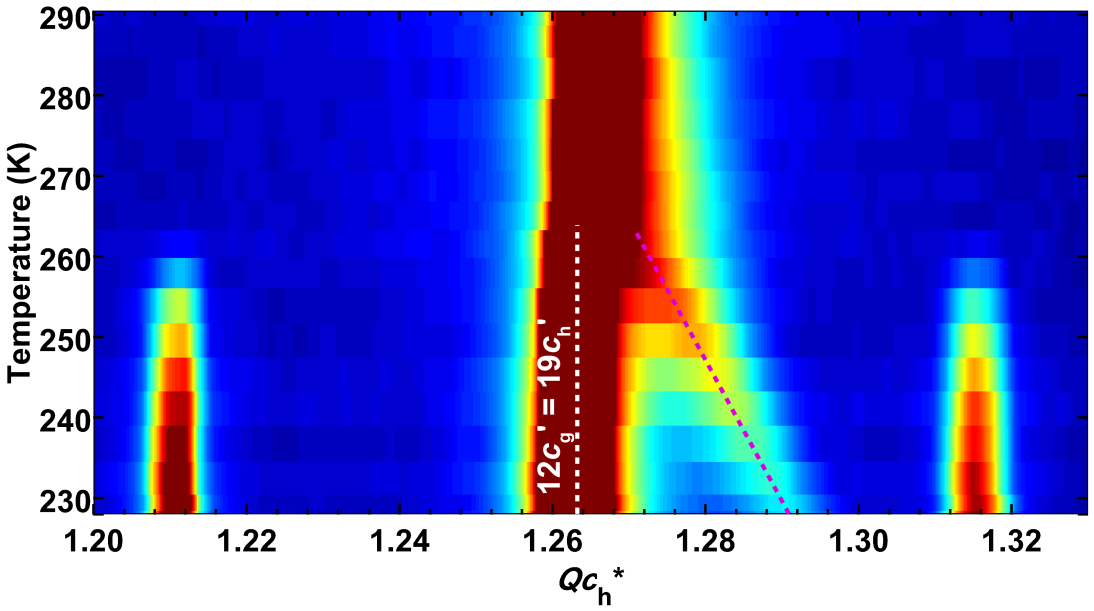

Figure 3.2.3.6. Temperature evolution of the (1 0 *l m*)$_h$ layer line in the oscillation images of 2,11-dodecanedione/urea grown at 0.0 °C upon heating from 228 K to 290 K. Layer line profiles are shown on a logarithmic color scale, with red being most intense. The data was collected on ALS beamline 8.2.2 using 60° ϕ rotations about the crystal ***c*** axis with a detector distance of 500.0 mm and λ = 1.18080 Å. Two phases are indicated: commensurate with $12c_g' = 19c_h'$ (white dashed line) and variably-compressed incommensurate (magenta dashed line).

In summary, this crystal of 2,11-dodecanedione/urea grown at 0.0 °C exhibits a surprising result in which the guest repeat length is not constant along the ***c*** axis. In the first region that was examined, the guest repeat was indistinguishable from that expected for a commensurate structure with $12c_g' = 19c_h'$. This region shows no

evidence for self-compression upon cooling. In a region of the crystal in which the guest, after warming through the lock-in transition, had a repeat length of c_g = 17.4503(11) Å at 290.5 K (0.0265(14) Å shorter than it would be with $12c_g' = 19c_h'$), reverse self-compression behavior is observed during warming. Although, in this case, the initial guest repeat was not measured for this region of the crystal, data from other crystals suggests that the equilibrium length of a guest at 290 K is the same before and after cooling through the lock-in phase transition. It is likely that the observed exotherm in the DSC cooling curve was caused by the regions of the crystal that locked into the commensurate phase with $12c_g' = 19c_h'$.

3.2.4. Synchrotron X-ray studies of 2,11-dodecanedione/urea grown at 10.0 °C

The sample was crystallized by evaporation while purging with argon in a Neslab (RTE-140) temperature controller set at 10.0 °C.[38] The DSC trace of this sample shows an exothermic phase transition on cooling at 255.3 K (ΔH = -0.99 J/g), and an endothermic phase transition on heating at 258.1 K (ΔH = 1.2 J/g), as shown in Figure 3.2.4.1.

A variable temperature X-ray scan from 290.0 K to 110.0 K was conducted on ALS beamline 8.2.2. In this run, the crystal to detector distance was 630.00 mm, λ = 1.180787 Å (10.5000 keV), and the beam size = 100 × 100 μm. At 290.0 K, this UIC has an undistorted lattice, and the profile of the $(1\ 0\ l\ m)_h$ layer line in the oscillation image

was fit with γ = 0.63315(2), as shown in Figure 3.2.4.2. Thus c_g = 11.0380(5)/0.63315(2) = 17.4334(10) Å, which is 0.0434(13) Å shorter than c_g' for the commensurate phase with $12c_g' = 19c_h'$.

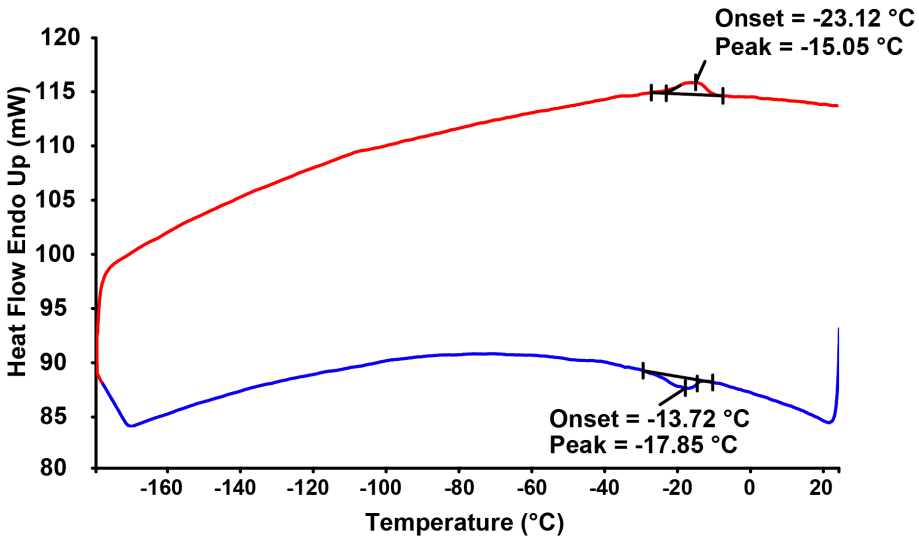

Figure 3.2.4.1. DSC trace (using a Perkin Elmer Pyris 1 DSC) of 2,11-dodecanedione/urea grown at 10.0 ºC.[31] The blue line is the cooling scan, and the red line is the heating scan. The scan rate was 20 K/min, and the scan ranges were from 298 K (25 ºC) to -108 K (-165 ºC) and then back to 298 K. An exothermic phase transition was observed with a peak position of 255.3 K (-17.9 ºC) on the cooling curve, and a corresponding endothermic phase transition was observed with a peak position of 258.1 K (-15.1 ºC) upon heating.

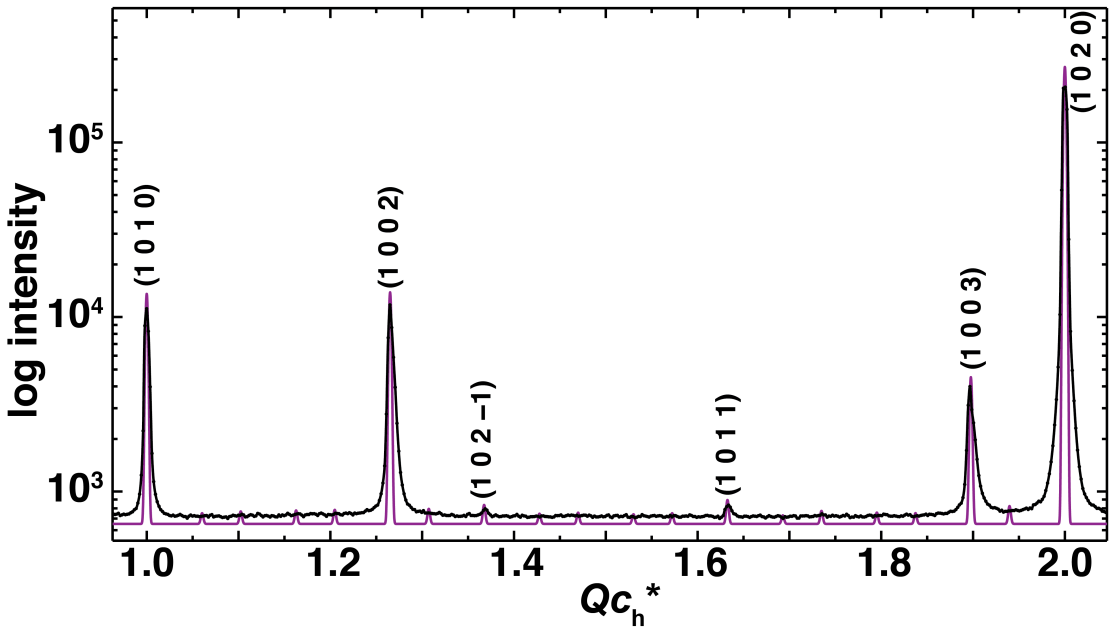

Figure 3.2.4.2. Profile analysis of the (1 0 *l m*)$_h$ layer line in the unwarped synchrotron oscillation image of 2,11-dodecanedione/urea grown at 10.0 °C. The measurement was made using a 60° ϕ rotation about the crystal ***c*** axis at 290.0 K on ALS beamline 8.2.2 with a detector distance of 630.0 mm and λ = 1.180787 Å.[39] The profile was fit as an incommensurate phase with γ = 0.63315(2).

Upon cooling, the onset of a lock-in phase transition occurred from 259.0 to 257.5 K, followed by self-compression. At 110.0 K the crystal contained two commensurate components: an undistorted phase with $12c_g' = 19c_h'$ and a distorted phase with $2c_g' = 3c_h'$, as shown in Figure 3.2.4.2. Upon heating, the sequence of phases is essentially identical to that described for the batch grown at -20.0 °C (Section

3.2.1). In both cases, two commensurate phases (with $12c_g' = 19c_h'$ and $2c_g' = 3c_h'$) and a less compressed phase coexisted from 219 K to 230 K.

On heating, the shortened phase kept elongating until the commensurate-to-incommensurate phase transition occurred at 262.4 K. Above 230 K, the intensity of the phase with $2c_g' = 3c_h'$ went to zero, while guest repeat length in the compressed incommensurate phase increased. At 262.4 K a commensurate-to-incommensurate phase transition occurred for the phase with $12c_g' = 19c_h'$, resulting in a single incommensurate phase in the crystal. In the final state, measured at 290.0 K, c_g = 11.0380(5)/0.6335(2) = 17.424(6) Å (0.009(6) Å shorter than the value measured before cooling). Within error, this is essentially the same value as before cooling.

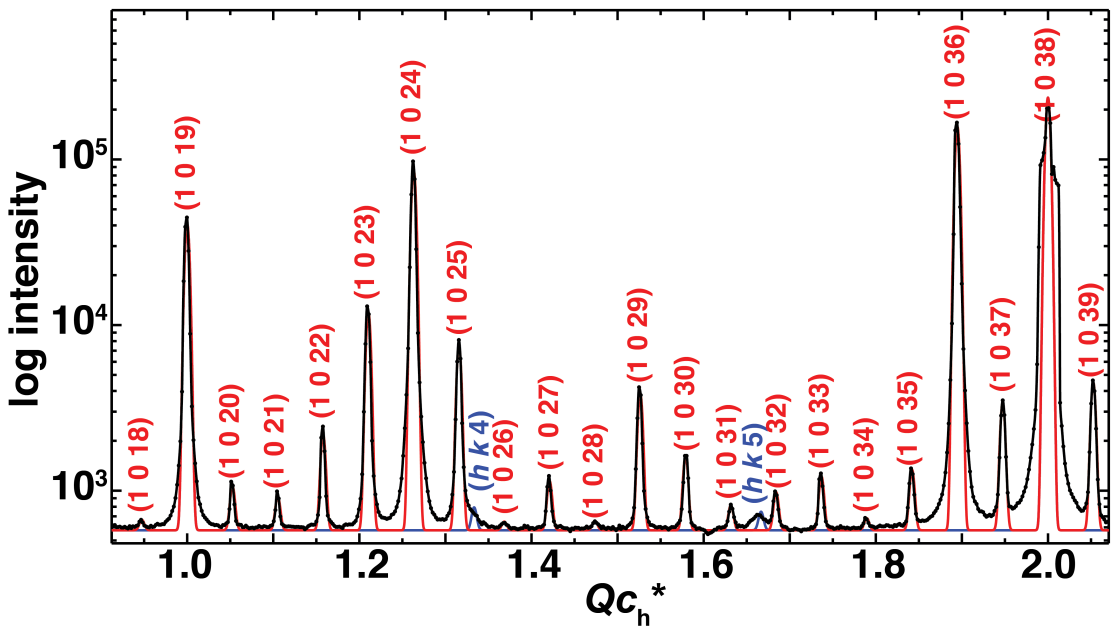

Figure 3.2.4.3. Profile analysis of the (1 0 *l m*)$_h$ layer line in the unwarped synchrotron oscillation image of 2,11-dodecanedione/urea grown at 10.0 °C. The measurement was made using a 60° ϕ rotation about the crystal ***c*** axis at 110.0 K on ALS beamline 8.2.2 with a detector distance of 630.0 mm and λ = 1.180787 Å.[40] The profile was modeled as two commensurate phases, one with $12c_g' = 19c_h'$ (red) and the other with $2c_g' = 3c_h'$ (blue).

3.2.5. Synchrotron X-ray studies of 2,11-dodecanedione/urea grown at 20.0 °C

The sample was crystallized by evaporation while purging with argon in a Neslab (RTE-140) temperature controller set at 20.0 °C.[41] The DSC trace of this sample shows an exothermic phase transition on cooling at 256.3 K (ΔH = -0.94 J/g), and an

endothermic phase transition on heating at 260.3 K (ΔH = 1.1 J/g), as shown in Figure 3.2.5.1. Weaker transitions are also observed at 224.3 K (-48.8 ºC) on the cooling curve and at 237.4 K (-35.7 ºC) on the heating curve.

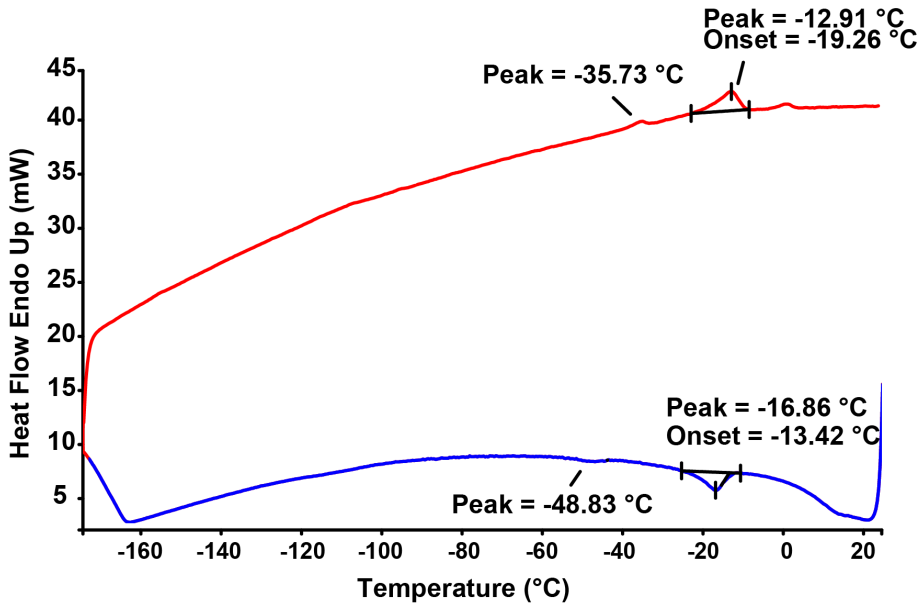

Figure 3.2.5.1. DSC trace (using a Perkin Elmer Pyris 1 DSC) of 2,11-dodecanedione/urea grown at 20.0 ºC.[42] The blue line is the cooling scan, and the red line is the heating scan. The scan rate was 20 K/min, and the scan ranges were from 298 K (25 ºC) to -108 K (-165 ºC) and then back to 298 K. Two exothermic phase transitions were observed at peak positions of 256.3 K (-16.9 ºC) and 224.3 K (-48.8 ºC) on the cooling curve, and two corresponding endothermic phase transitions were observed at peak positions of 260.3 K (-12.9 ºC) and 237.4 K (-35.7 ºC) on the heating curve. Weaker transitions are also noted.

A variable temperature X-ray scan was conducted from 290.0 K to 121.6 K on ALS beamline 8.2.2. At 290.0 K, this UIC has an undistorted lattice, and the profile of the $(1\ 0\ l\ m)_h$ layer line was fit with $\gamma = 0.63254(2)$, as shown in Figure 3.2.5.2. Thus c_g = 11.0380(5)/0.63254(2) = 17.4503(10) Å, which is 0.0266(8) Å shorter than the value required for a commensurate structure with $12c_g' = 19c_h'$. Upon cooling, a lock-in phase transition occurred at 260(1) K. As shown in Figure 3.2.5.3, the profile of the $(1\ 0\ l\ m)_h$ layer line at 239.0 K was modeled with two components, a commensurate phase with $12c_g' = 19c_h'$, and a compressed incommensurate phase with c_g = 11.0298(5)/0.6420(5) = 17.180(13) Å. At the lowest temperatures studied (122 K), there were no Bragg reflections for a compressed phase with $2c_g' = 3c_h'$. The only signature of such a phase came from difuse bands that were extremely broad along $\boldsymbol{c^*}$ in the layer lines with $h + k$ = odd.

In conclusion, crystals of 2,11-dodecanedione/urea grown at 20.0 °C have guest repeats that are 0.027(6) Å shorter than that required for a commensurate structure with $12c_g' = 19c_h'$ (at 290.0 K), and self-compression occurs as this commensurate phase grows below 260(1) K.

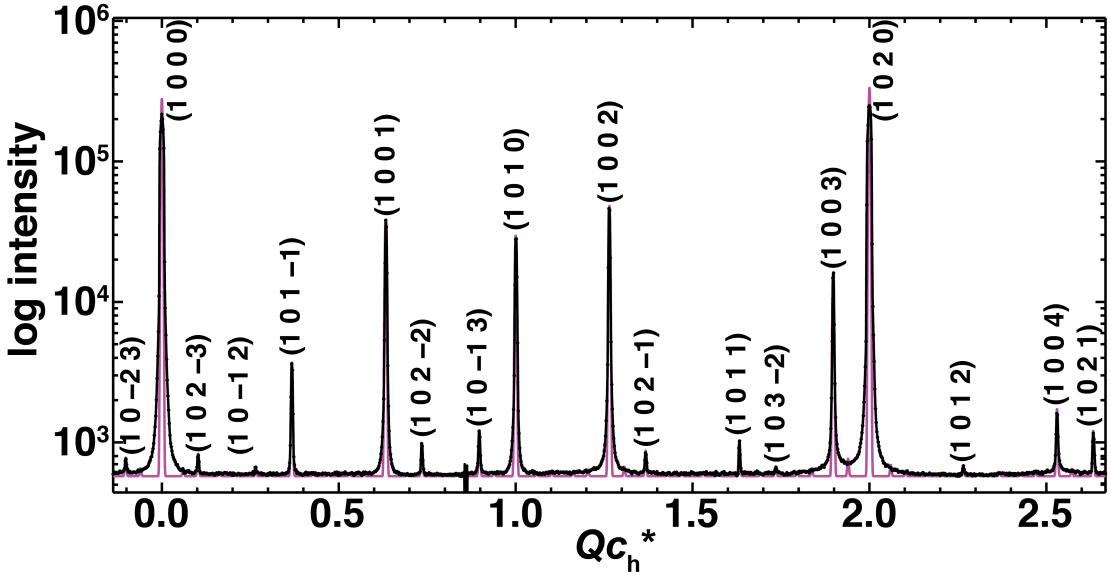

Figure 3.2.5.2. Profile analysis of the (1 0 *l* *m*)$_h$ layer line in the unwarped synchrotron oscillation image of 2,11-dodecanedione/urea grown at 20.0 °C. The measurement was made using a 60° ϕ rotation about the crystal ***c*** axis at 290.0 K on ALS beamline 8.2.2 a detector distance of 500.0 mm and λ = 1.18080 Å.[43] The profile was fit as an incommensurate phase with γ = 0.63254(2).

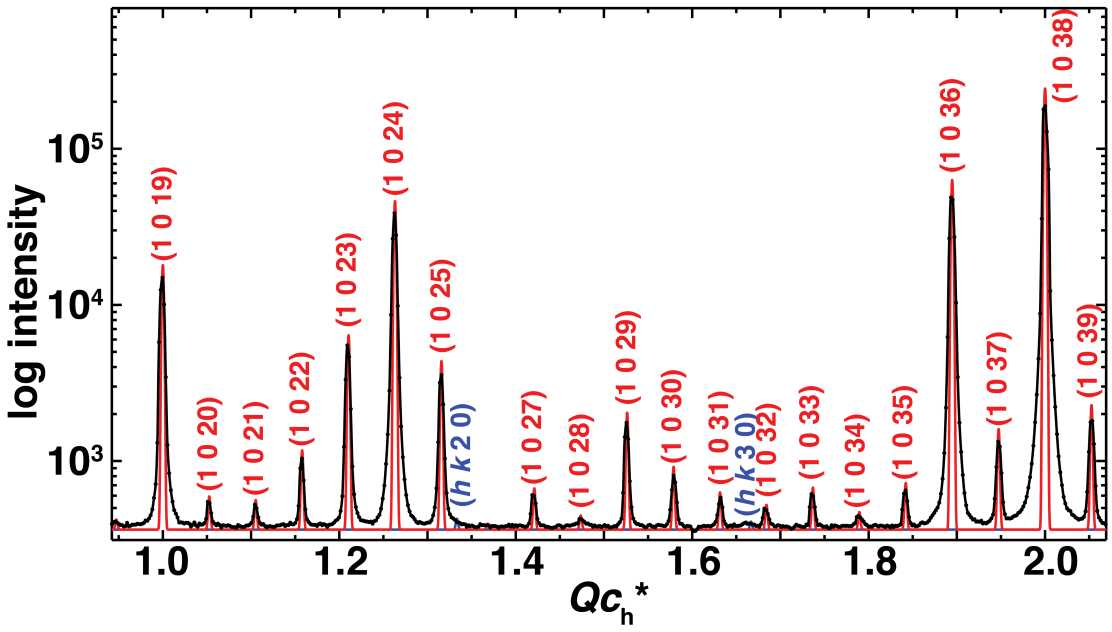

Figure 3.2.5.3. Profile analysis of the (1 0 *l* *m*)$_h$ layer line in the unwarped synchrotron oscillation image of 2,11-dodecanedione/urea grown at 20.0 °C. The measurement was made using a 60° ϕ rotation about the crystal ***c*** axis at 239.0 K on ALS beamline 8.2.2 with a detector distance of 500.0 mm and λ = 1.18080 Å.[44] The profile was modeled as a commensurate phase with $12c_g' = 19c_h'$ (red) and an incommensurate phase with γ = 0.63254(2) (blue).

3.2.6. Synchrotron X-ray studies of 2,11-dodecanedione/urea grown at 30.0 °C

The sample was crystallized by evaporation while submerged in a 4 liter Dewar filled with water. The temperature of the water bath was maintained at 30.0 °C by a Lakeshore DRC 91C temperature controller.[45] The DSC trace of this sample shows an

exothermic phase transition on cooling at 255.3 K (ΔH = -0.82 J/g), and an endothermic phase transition on heating at 258.5 K (ΔH = 1.02 J/g), as shown in Figure 3.2.6.1.

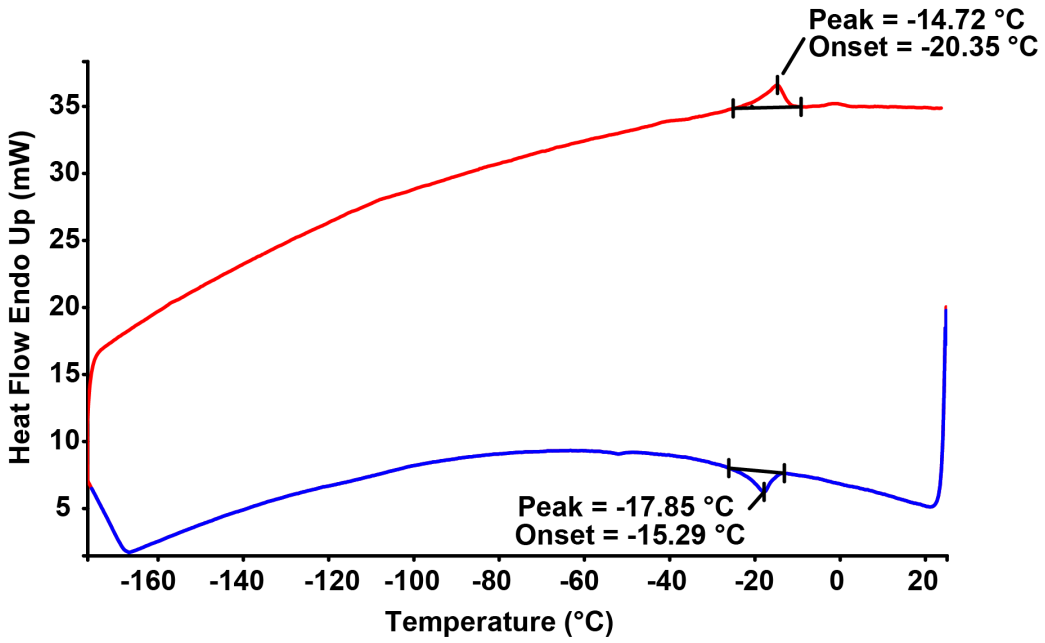

Figure 3.2.6.1. DSC trace (using a Perkin Elmer Pyris 1 DSC) of 2,11-dodecanedione/urea grown at 30.0 ºC.[46] The blue line is the cooling scan, and the red line is the heating scan. The scan rate was 20 K/min, and the scan ranges were from 298 K (25 ºC) to -108 K (-165 ºC) and then back to 298 K. An exothermic phase transition was observed at a peak position of 255.3 K (-17.9 ºC) in the cooling curve, and a corresponding endothermic phase transition occurred at a peak position of 258.5 K (-14.7 ºC) upon heating.

A variable temperature X-ray scan from 290.0 K to 119.1 K was conducted on ALS beamline 8.2.2. Here, the crystal to detector distance was 500.0 mm, λ = 1.18080 Å (10.5000 keV), and the beam size = 100 × 200 μm. At 290.0 K, this UIC has an undistorted lattice, and the profile of the (1 0 *l m*)$_h$ layer line in the oscillation image was fit with γ = 0.63375(2), as shown in Figure 3.2.6.2. Thus c_g = 11.0380(5)/0.63375(2) = 17.4170(10) Å. This is 0.0599(13) Å shorter than the guest repeat required for the commensurate phase with $12c_g' = 19c_h'$. Upon cooling, a lock-in phase transition occurred at 260(1) K. As shown in Figure 3.2.6.3, the profile of the (1 0 *l m*)$_h$ layer line in the oscillation image taken at 220.1 K could be modeled with two components: a commensurate phase with $12c_g' = 19c_h'$, and a incommensurate phase with c_g = 11.0267(5)/0.6335(5) = 17.406(14) Å. (The minor component seems to be beam damaged.) Once again, the incommensurate structure was compressed to a phase with $2c_g' = 3c_h'$ when cooled further. This phase with $2c_g' = 3c_h'$, which was observed after the crystal was translated by 50 μm below 208 K, has no apparent long-range order in the ***ab*** plane. Figure 3.2.6.4 shows the profile of the (1 0 *l m*)$_h$ layer line at 175.1 K modeled with two commensurate phases: one with $12c_g' = 19c_h'$, and the other with $2c_g' = 3c_h'$.

In conclusion, 2,11-dodecanedione/urea grown at 30.0 °C undergoes self-compression phase transitions upon cooling. The relatively large population of the compressed phase may be due to the significant difference (0.0599(13) Å) between the

incommensurate guest repeat at 290.0 K and that required for a commensurate structure with $12c_g' = 19c_h'$.

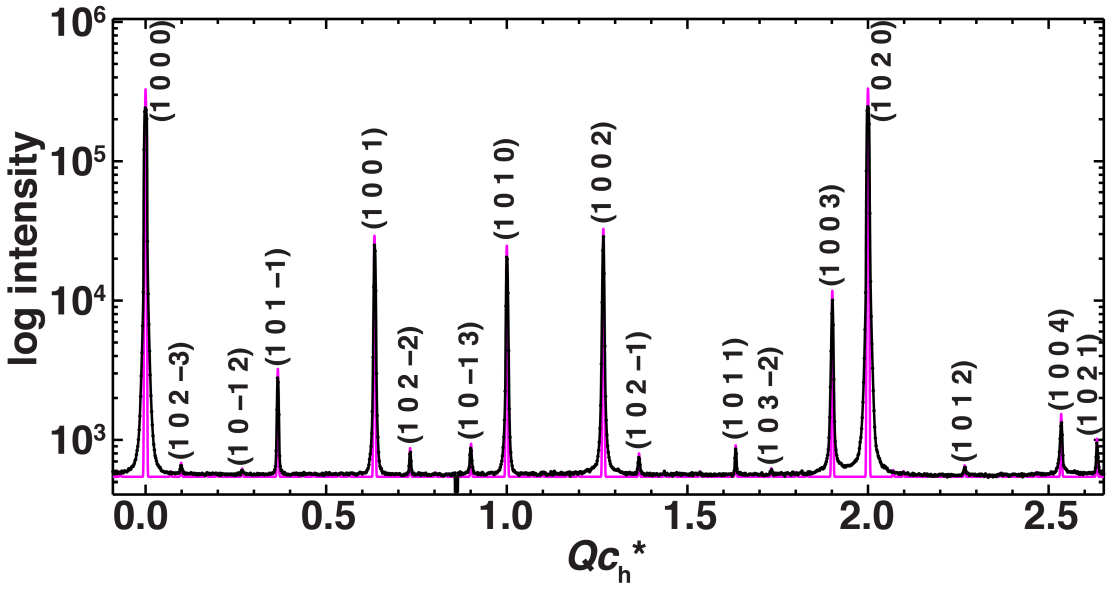

Figure 3.2.6.2. Profile analysis of the (1 0 *l m*)$_h$ layer line in the unwarped synchrotron oscillation image of 2,11-dodecanedione/urea grown at 30.0 °C. The measurement was made using a 60° ϕ rotation about the crystal ***c*** axis at 290.0 K on ALS beamline 8.2.2 at ALS with a detector distance of 500.0 mm and λ = 1.18080 Å.[47] The profile was fit as an incommensurate phase with γ = 0.63375(2).

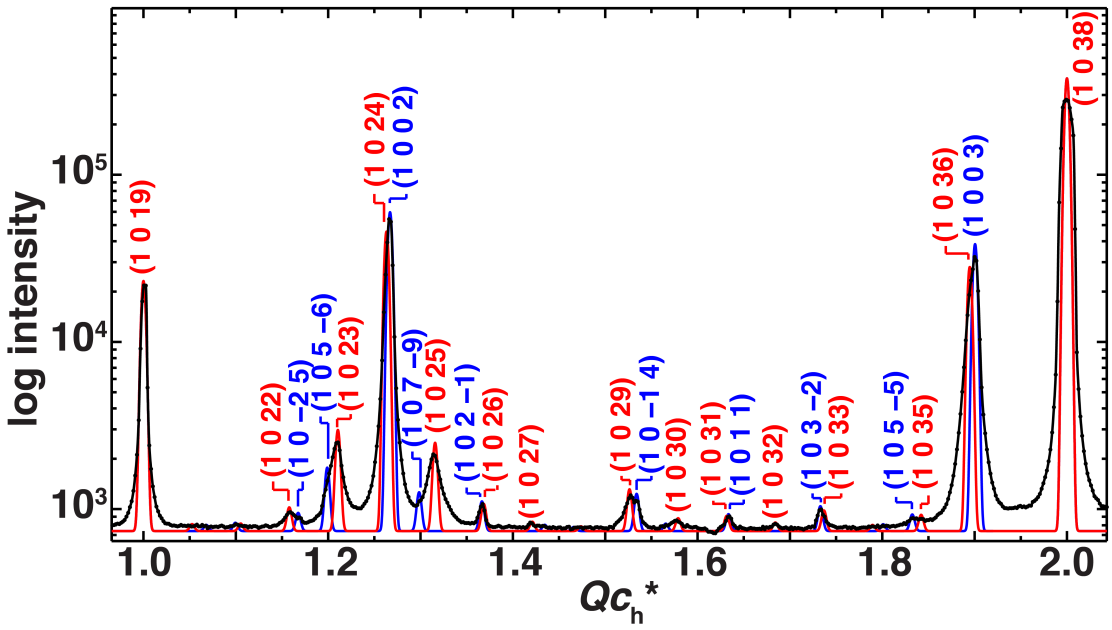

Figure 3.2.6.3. Profile analysis of the (1 0 *l m*)$_h$ layer line in the unwarped synchrotron oscillation image of 2,11-dodecanedione/urea grown at 30.0 °C. The measurement was made using a 60° ϕ rotation about the crystal ***c*** axis at 220.1 K on ALS beamline 8.2.2 with a detector distance of 500.0 mm and λ = 1.18080 Å. The profile was modeled as a commensurate phase with $12c_g' = 19c_h'$ (red) and as an incommensurate phase with γ = 0.6335 (blue).[48]

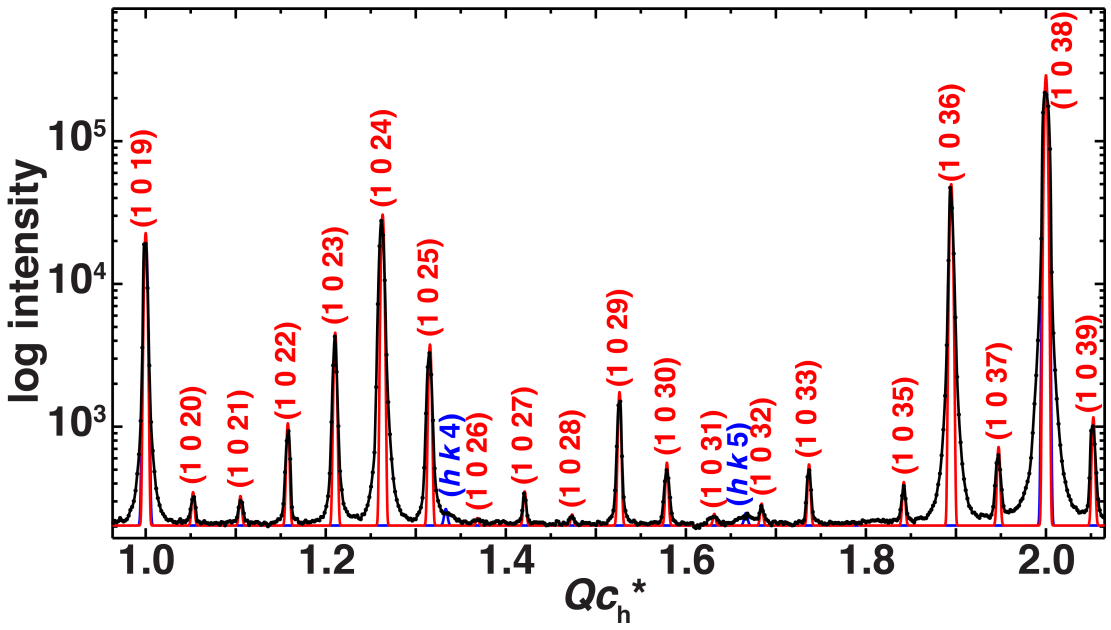

Figure 3.2.6.4. Profile analysis of the (1 0 *l m*)$_h$ layer line in the unwarped synchrotron oscillation image of 2,11-dodecanedione/urea grown at 30.0 °C. The measurement was made using a 60° ϕ rotation about the crystal ***c*** axis at 175.1 K on ALS beamline 8.2.2 with a distance of 500.0 mm and λ = 1.18080 Å. The profile was modeled with two commensurate phases with $12c_g' = 19c_h'$ (red), and $2c_g' = 3c_h'$ (blue).[49]

3.2.7. Synchrotron X-ray studies of 2,11-dodecanedione/urea grown at 35.0 °C

The sample was crystallized by evaporation over 3 days in an ethylene glycol/water bath maintained at 35.0 °C with a Neslab (RTE-140) temperature controller.[50] Variable temperature scans were conducted at ALS beamline 8.2.2 on two different crystals. As shown in Figure 3.2.7.1, at 290.0K, the profile of the $(1\ 0\ l\ m)_h$ layer line in the first crystal was fit as an incommensurate phase with γ = 0.63238(5), giving c_g = 11.0380(5)/0.63238(5) = 17.4546(16) Å. This is 0.0221(18) Å shorter than the guest repeat required for a commensurate phase with $12c_g' = 19c_h'$. Upon cooling, a lock-in phase transition occurred at 260(3) K. As shown in Figure 3.2.7.2, the profile of the $(1\ 0\ l\ m)_h$ layer line of an oscillation image taken at 188.0 K contained only a commensurate phase with $12c_g' = 19c_h'$. In a second sample, the $(1\ 0\ l\ m)_h$ layer line was fit to γ = 0.63298(5) at 290.0 K, giving c_g = 11.0380(5)/0.63298(5) = 17.4381(16) Å, which is 0.0387 Å shorter than the guest repeat required for a commensurate phase with $12c_g' = 19c_h'$. This sample also underwent a lock-in phase transition below 259(2) K.[51] In both cases, the crystal habit was that of a thin hexagonal plate, the faces of which were parallel to the {001} plane, and could therefore not be translated along the ***c*** axis to observe a fresh region. This is most likely why a compressed commensurate phase with $2c_g' = 3c_h'$, which in the previous sections was shown to be sensitive to beam damage, was not observed. However, from these two experiments, it can be concluded that

crystals of 2,11-dodecanedione/urea grown at 35.0 °C undergo incommensurate-to-commensurate phase transitions upon cooling below approximately 260 K.

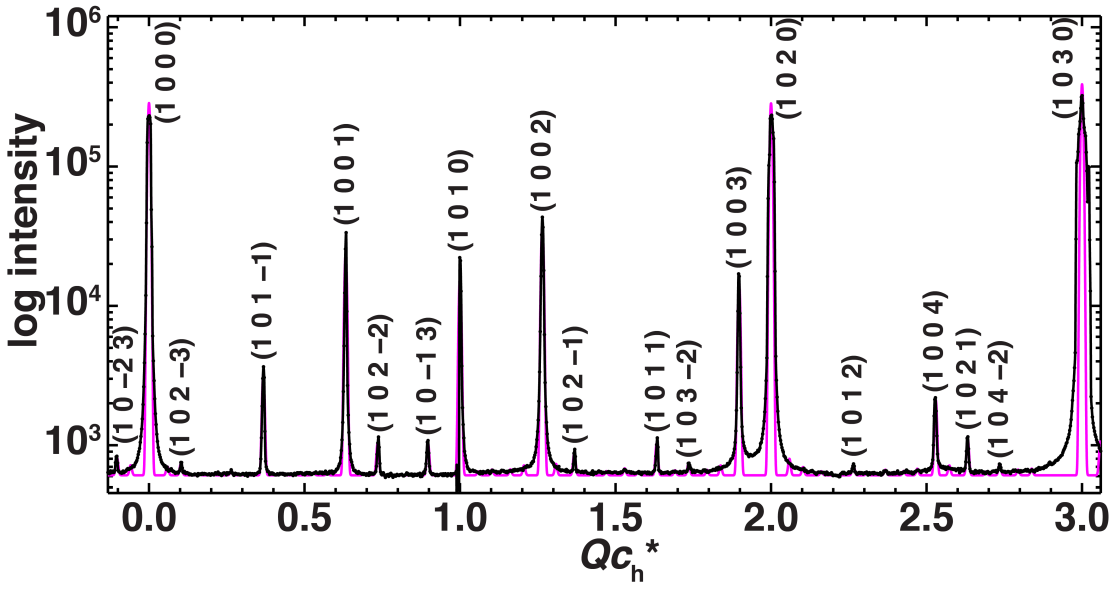

Figure 3.2.7.1. Profile analysis of the (1 0 *l* *m*)$_h$ layer line in the unwarped synchrotron oscillation image of 2,11-dodecanedione/urea grown at 35.0 °C. The measurement was made using a 60° ϕ rotation about the crystal ***c*** axis at 290.0 K on ALS beamline 8.2.2 with a distance of 500.0 mm and λ = 0.99991 Å. The profile was fit with a incommensurate phase with γ = 0.63238(5).[52]

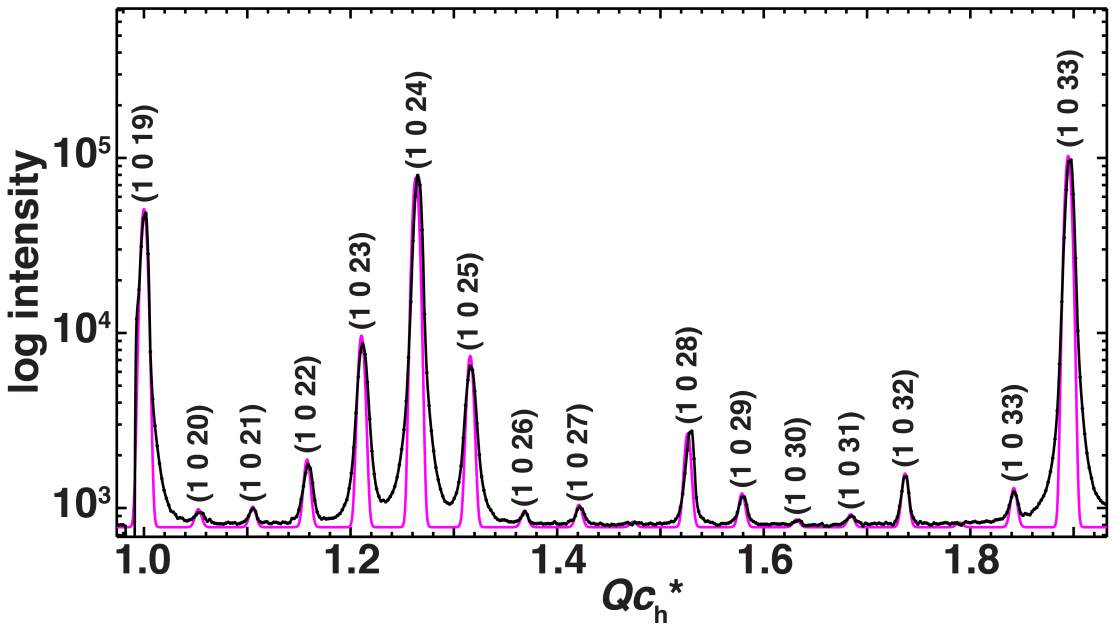

Figure 3.2.7.2. Profile analysis of the (1 0 *l m*)$_h$ layer line in the unwarped synchrotron oscillation image of 2,11-dodecanedione/urea grown at 35.0 °C. The measurement was made using a 60° ϕ rotation about the crystal ***c*** axis at 188.0 K on ALS beamline 8.2.2 with a distance of 500.0 mm and λ = 0.99991 Å. The profile was modeled with a commensurate phase with $12c_g' = 19c_h'$.[53]

3.2.8. Synchrotron X-ray studies of 2,11-dodecanedione/urea grown at 40.0 °C

The sample was crystallized by evaporation in a Neslab (RTE-140) temperature controller set to 40.0 °C.[54] The DSC trace of this sample shows an exothermic phase transition on cooling at 253.5 K (ΔH = -0.94 J/g), and an endothermic phase transition on heating at 256.4 K (ΔH = 0.92 J/g), as shown in Figure 3.2.8.1. The phase transition temperatures are especially low in this system, but the enthalpies are similar to those observed in other cases, where incommensurate-to-commensurate lock-in phase transitions occurred.

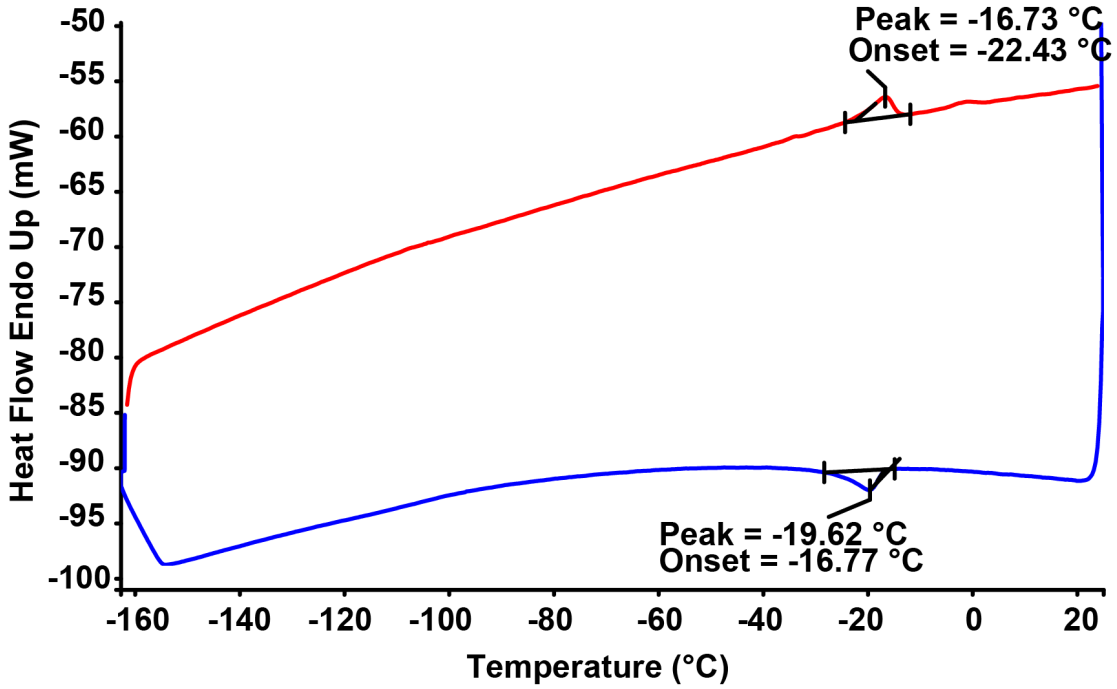

Figure 3.2.8.1. DSC trace of 2,11-dodecanedione/urea grown at 40.0 ºC.[55] The blue line is the cooling scan, and the red line is the heating scan. The scan rate was 20 K/min, and the scan ranges were from 298 K (25 ºC) to -108 K (-165 ºC) and then back to 298

K. An exothermic phase transition was observed at a peak position of 253.5 K (-19.6 ºC) in the cooling curve, and a corresponding endothermic phase transition occurred at a peak position of 256.4 K (-16.7 ºC) upon heating.

A variable temperature X-ray scan from 290.0 K to 119.0 K was conducted at ALS beamline 8.2.2. Surprisingly, at 290.0 K, the profile of the $(1\ 0\ l\ m)_h$ layer line in the oscillation image contained two components, a larger one with γ = 0.62940(2), and a much smaller one with γ = 0.6320(6), as shown in Figure 3.2.8.2. Both conformed to hexagonal metric symmetry. Most of the intensity come from the phase with γ = 0.62940(2), but a shoulder on the third guest layer line cannot be ignored and was therefore fit (using PeakFit[56]) as shown in Figure 3.2.8.1 (B). (A distribution of guest repeat lengths at 290.0 K was also observed in the crystal grown at -20.0 ºC (Figures 3.2.1.2 (B) and 3.2.1.7).)

The major component is 0.054(5) Å longer than the guest repeat required for a structure with $12c_g' = 19c_h'$. The minor component had c_g = 11.0380(5)/0.6325(5) = 17.465(17) Å, which is 0.012(17) Å shorter than required for $12c_g' = 19c_h'$. (This larger error occurs because only one very weak peak was deconvoluted.)

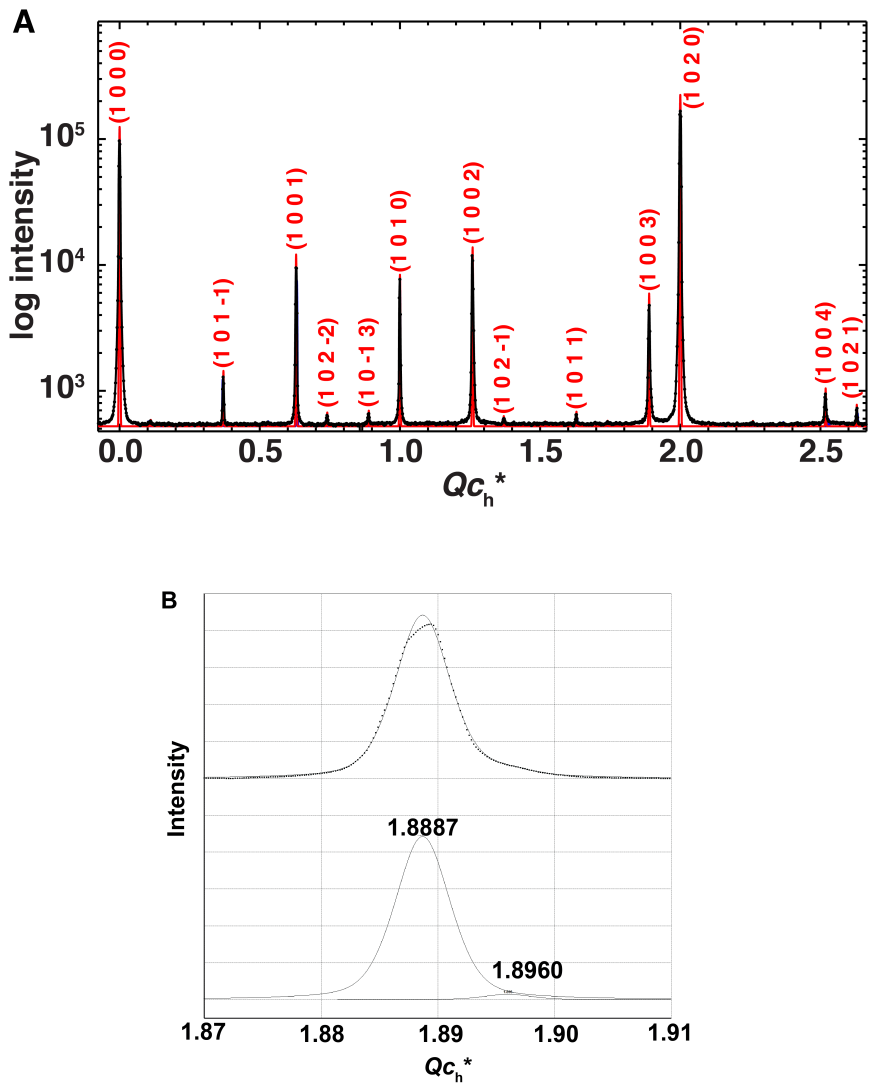

Figure 3.2.8.2. (A) Profile analysis of the (1 0 l m)$_h$ layer line in the unwarped synchrotron oscillation image of 2,11-dodecanedione/urea grown at 40.0 °C. The measurement was made using a 60° ϕ rotation about the crystal ***c*** axis at 290.0 K on ALS beamline 8.2.2 with a distance of 500.0 mm and λ = 1.18080 Å. The profile was fit with an incommensurate phase with γ of 0.62940(2). (B) The asymmetric peak in the vicinity of the third guest layer line was deconvoluted into two components, a major phase with γ = 0.6296(3) and a minor phase with γ = 0.6320(6), using PeakFit.[57]

Upon cooling below 259(3) K, extra Bragg peaks appeared in the layer lines for this hexagonal structure. At 165.9 K, as shown in Figure 3.2.8.3, two components were used to describe all of the Bragg peaks in the $(1\ 0\ l\ m)_h$ layer line: the major component was fit with γ = 0.629453(10), and the minor one was modeled as a phase with $12c_g' = 19c_h'$. Thus upon cooling, the major component with γ = 0.62940(2) preserved its guest repeat length relative to the host. Appearance of new Bragg peaks belonging to this component and increased intensities from those already present indicates pronounced 3-D ordering of this phase. On the other hand, the minor component that started with γ = 0.6320(6) at 290.0 K appears to have locked into a structure with $12c_g' = 19c_h'$ during this phase transition.

In summary, this experiment suggests that when a guest crystalizes with a repeat length that is substantially longer (0.054(5) Å) than that required for the commensurate structure with $12c_g' = 19c_h'$, it will not shorten to lock into that structure. On the other hand, the component with a guest repeat that was slightly shorter than the value required for the phase with $12c_g' = 19c_h'$ did lock into the commensurate structure.

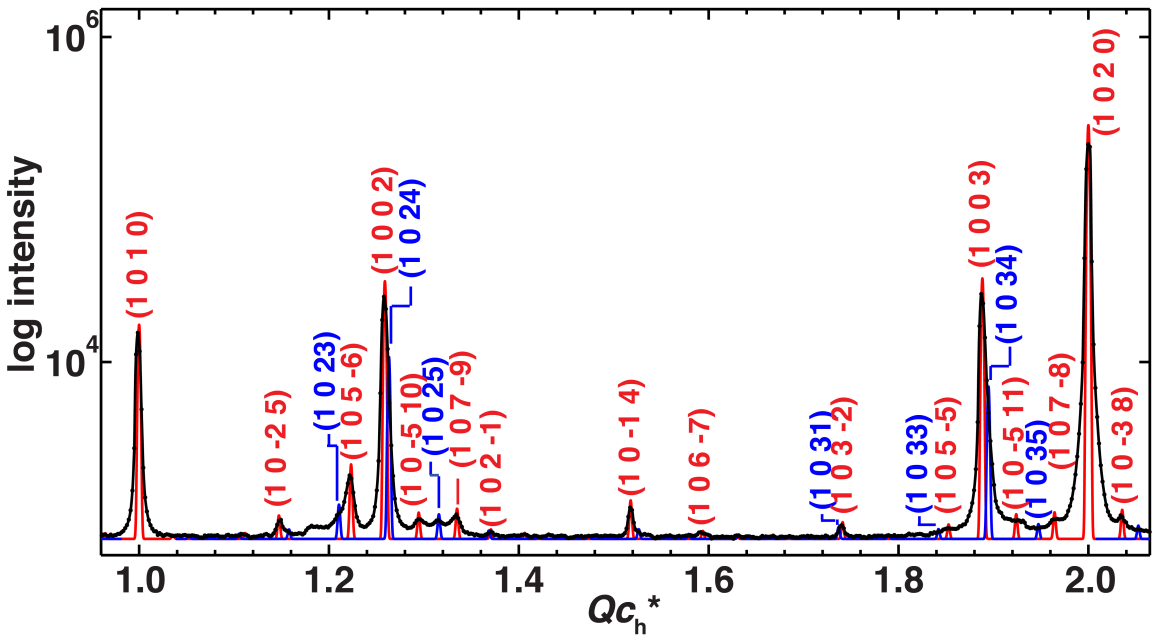

Figure 3.2.8.3. Profile analysis of the (1 0 *l* *m*)$_h$ layer line in the unwarped synchrotron oscillation image of 2,11-dodecanedione/urea grown at 40.0 °C. The measurement was made using a 60° ϕ rotation about the crystal ***c*** axis at 165.9 K on ALS beamline 8.2.2 with a distance of 500.0 mm and λ = 1.18080 Å.[58] The profile was modeled as a commensurate phase with γ = 0.631579 (12c_g' = 19c_h', blue) and fit to an incommensurate phase with γ = 0.629453(10) (red).

3.2.9. Synchrotron X-ray studies of 2,11-dodecanedione/urea grown at 46 °C

The sample was crystallized by evaporation in an oil bath held at 46(2) °C.[59] A variable temperature X-ray scan from 290.0 K to 190.0 K was conducted on beamline 8.2.2 at the ALS. At 290.0 K, the profile of the (1 0 *l* *m*)$_h$ layer line was fit with γ = 0.63155(2), which is almost exactly 12/19 = 0.63158, as shown in Figure 3.2.9.1. This

sample offered an excellent opportunity of probing the sequence of events as a function of temperature. Since it is apparently commensurate with $12c_g' = 19c_h'$ at room temperature, cooling should not generate any self-compression.

Indeed, when the crystal was cooled below 258(2) K, extra Bragg peaks from the existing phase with $12c_g' = 19c_h'$ appeared, but the value of γ did not change.[60] As shown in Figure 3.2.9.2, the profile of the $(1\ 0\ l\ m)_h$ layer line in the oscillation image taken at 201.2 K was modeled as a commensurate phase with $12c_g' = 19c_h'$. No compressed phase was observed. However, at 248.7 K and below, this crystal exhibited a Bragg peak of unknown origin at $\mathbf{Q}\boldsymbol{c}_h^* = 0.6$, which corresponds to a guest repeat of approximately $c_g = 18.36$ Å.

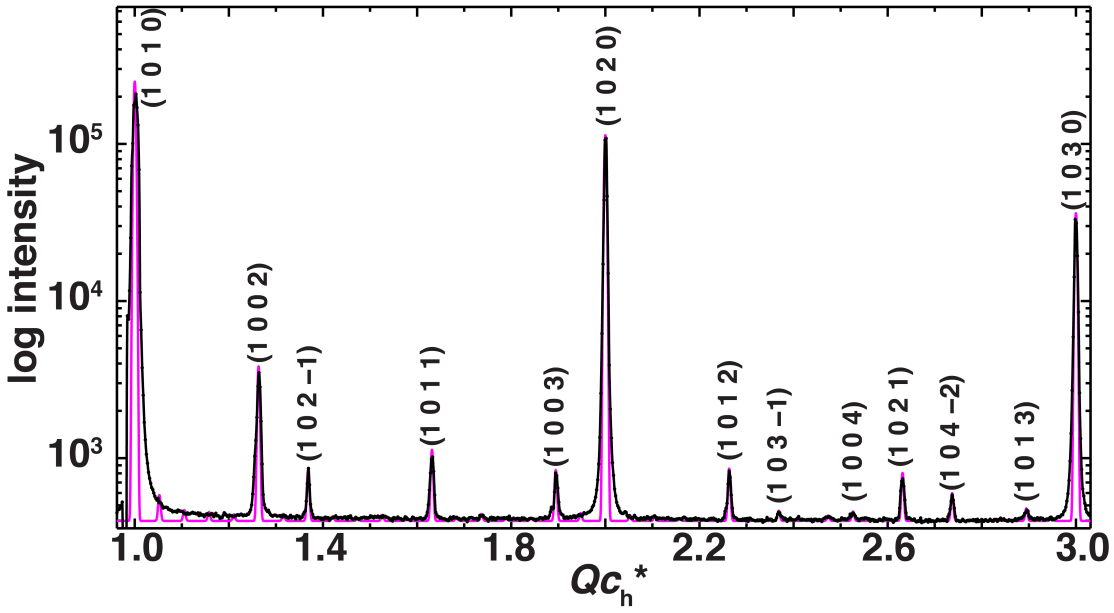

Figure 3.2.9.1. Profile analysis of the (1 0 *l* *m*)$_h$ layer line in the unwarped synchrotron oscillation image of 2,11-dodecanedione/urea grown at 46(2) °C. The measurement was made using a 60° ϕ rotation about the crystal ***c*** axis at 290.0 K on ALS beamline 8.2.2 with a distance of 500.0 mm, ϕ = 0 - 60°, beam size = 100×100 μm, exposure = 4 s, and λ = 0.999927 Å (12.39933 keV).[61] The profile was fit with γ = 0.63155(2).

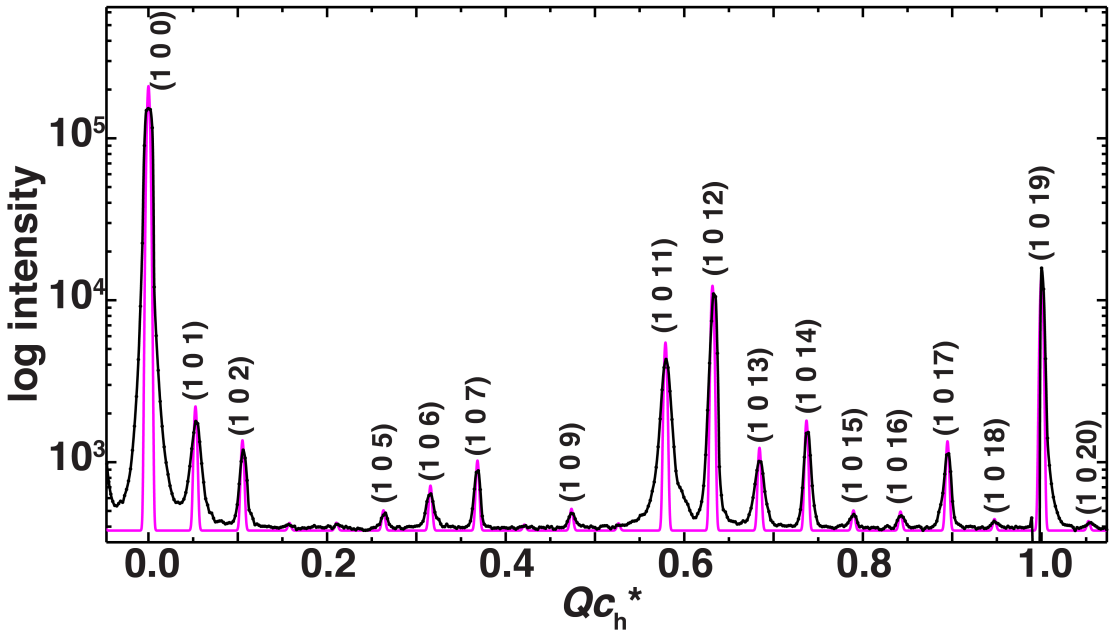

Figure 3.2.9.2. Profile analysis of the (1 0 *l m*)$_h$ layer line in the unwarped synchrotron oscillation image of 2,11-dodecanedione/urea grown at 46(2) °C. The measurement was made using a 60° ϕ rotation about the crystal ***c*** axis at 201.1 K on ALS beamline 8.2.2 with a distance of 500.0 mm, ϕ = 0 - 60°, beam size = 100×100 μm, exposure = 4 s, and λ = 0.999927 Å (12.39933 keV).[62] The profile was modeled as a commensurate phase with $12c_g' = 19c_h'$. Note the presence of an additional peak of unknown origin at $\mathbf{Q}c_h^*$ = 0.6.

3.2.10. Synchrotron X-ray studies of 2,11-dodecanedione/urea grown from 40 °C to r.t.

The sample was crystallized by cooling from 40 °C to room temperature in a 4 liter Dewar of water.[63] The DSC trace of this sample shows an exothermic phase transition

on cooling at 262.2 K (ΔH = -1.25 J/g), and an endothermic phase transition on heating at 264.3 K (ΔH = 1.43 J/g), as shown in Figure 3.2.10.1.

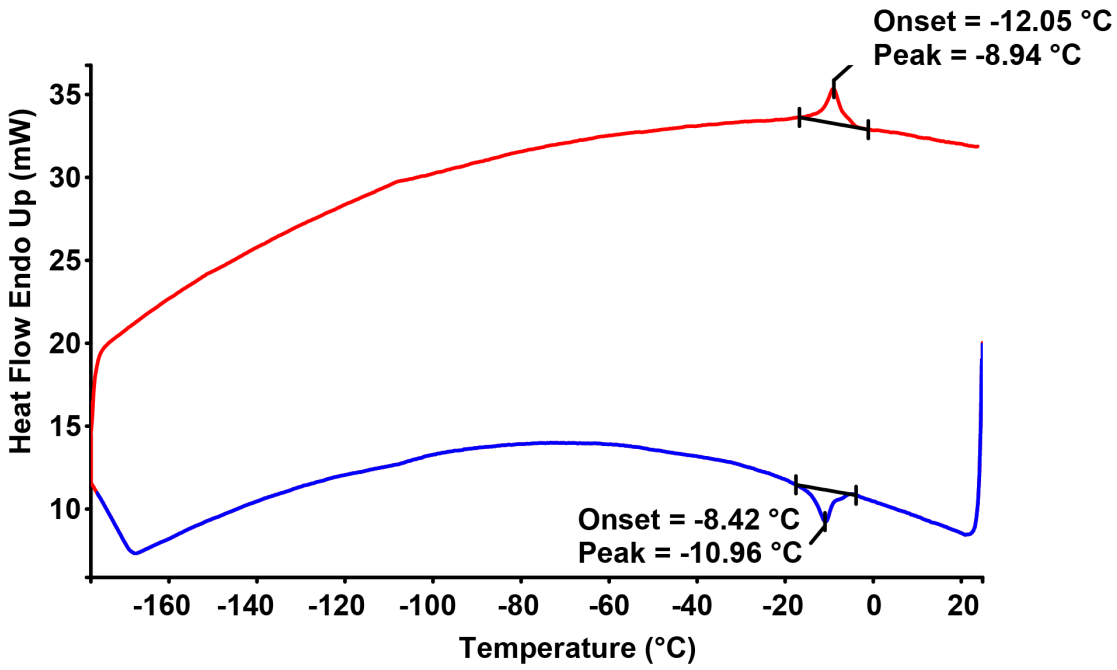

Figure 3.2.10.1. DSC trace (using a Perkin Elmer Pyris 1 DSC) of 2,11-dodecanedione/urea grown by cooling from 40 °C to room temperature.[64] The blue line is the cooling scan, and the red line is the heating scan. The scan rate was 20 K/min, and the scan ranges were from 298 K (25 ºC) to -108 K (-165 ºC) and then back to 298 K. An exothermic phase transition was observed at a peak position of 262.2 K (-11.0 ºC) in the cooling curve, and a corresponding endothermic phase transition occurred at a peak position of 264.3 K (-8.9 ºC) upon heating.

A variable temperature X-ray scan from 290.0 K to 113.0 K was conducted on APS beamline 14-BM-C. At 290.0 K, this UIC had a misfit parameter γ = 0.63007(2), with c_g = 11.0380(5)/0.63007(2) = 17.5187(10) Å, as shown in Figure 3.2.10.2. This is 0.0419(13) Å longer than the guest repeat required for a commensurate phase with $12c_g' = 19c_h'$. Least squares fits of the misfit parameter, γ, from 290.0 to 199.8 K show that it stays constant with a mean of 0.63016(10), as shown in Figure 3.2.10.3. This is expected in systems that do not undergo lock-in phase transitions.

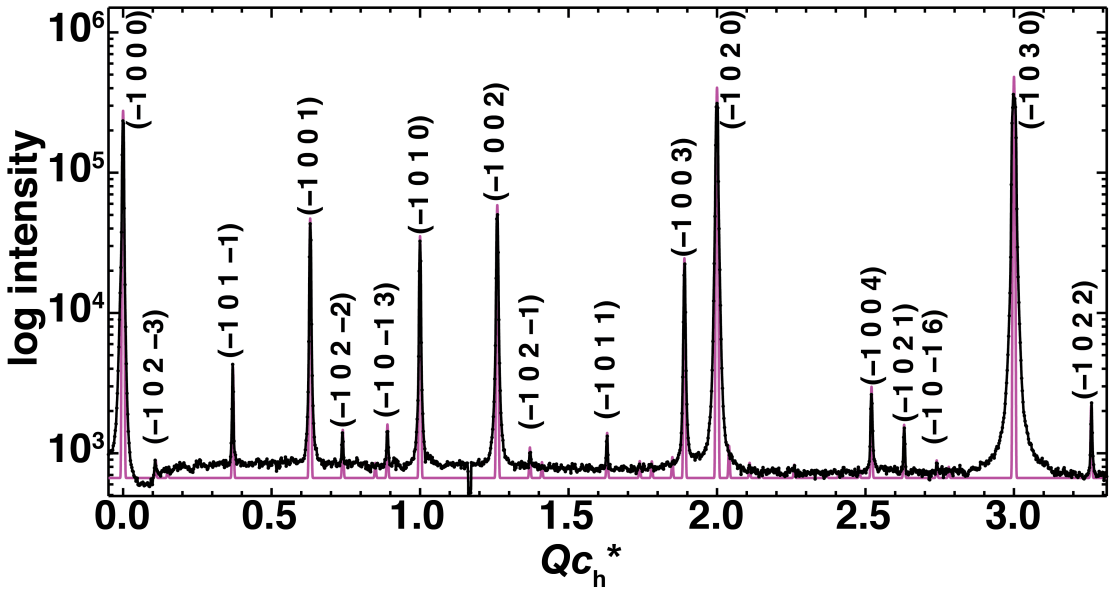

Figure 3.2.10.2. Profile analysis of the (1 0 *l m*)$_h$ layer line in the unwarped synchrotron oscillation image of 2,11-dodecanedione/urea grown by cooling from 40 °C to room temperature. The image was collected using a 60° ϕ rotation about the crystal ***c*** axis at 290.0 K on APS beamline 14-BM-C with a detector distance of 500.0 mm, ϕ = 0 - 60°, exposure = 6.0 s, beam size = 200×200 μm, and λ = 0.97870 Å.[65] The profile was fit as an incommensurate phase with γ = 0.63007(2).

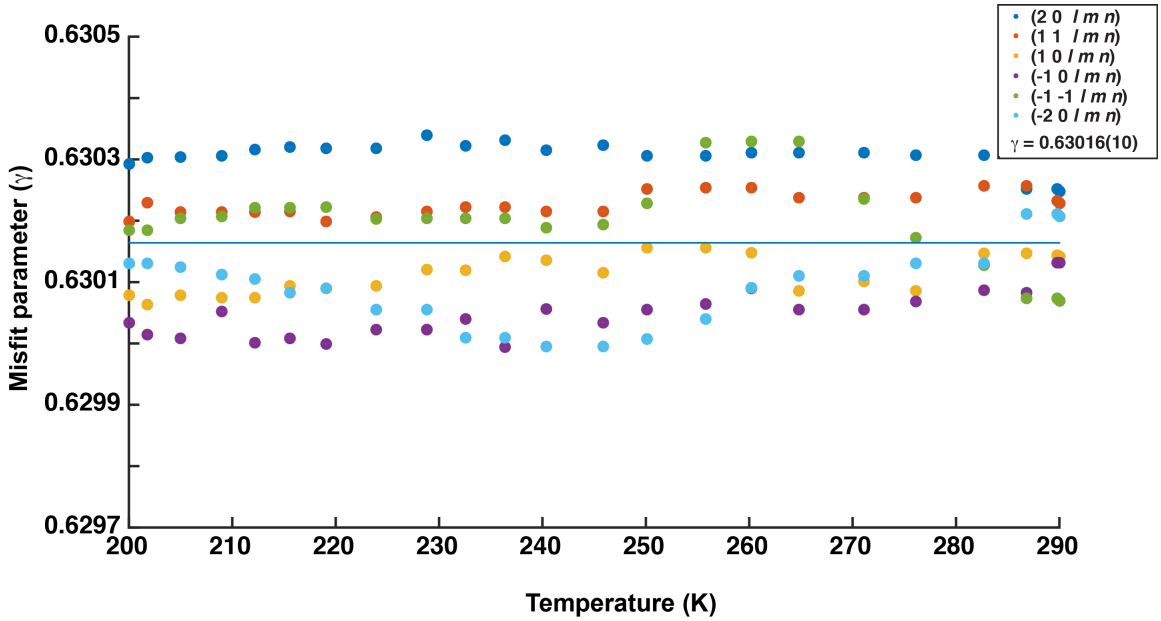

Figure 3.2.10.3. Temperature evolution of the misfit parameter (γ) of 2,11-dodecanedione/urea grown by cooling from 40 °C to room temperature. Measurements were made on APS beamline 14-BM-C using 60° ϕ rotations about the crystal ***c*** axis from 290.0 to 199.8 K with the following parameters: distance = 500.0 mm, time = 6 s, λ = 0.97870 Å, and beam size (x,y) = (200, 200) μm.[6] The reported values were obtained from least squares refinements of the misfit parameter for various layer lines in unwarped oscillation images through the temperature scan. The misfit parameter stayed constant, with a mean γ of 0.63016(10) (e.s.d) as shown by the horizontal blue line.

Upon cooling, extra Bragg peaks appeared below 262(2) K that did not correspond to the incommensurate phase with γ = 0.63016(10) (e.s.d.) or a new commensurate phase.[66] Therefore, the profiles of the layer lines were modeled with an

extra long-range modulation using a supplementary reciprocal unit cell vector, $\boldsymbol{c}_{\mathbf{m}}^*$, parallel to $\boldsymbol{c}_{\mathbf{h}}^*$.[67] This required a five dimensional description of the reciprocal image using the following basis:

$\mathbf{Q}_{hklmn} = h\cdot\boldsymbol{a}^* + k\cdot\boldsymbol{b}^* + l\cdot\boldsymbol{c}_{\mathrm{h}}^* + m\cdot\boldsymbol{c}_{\mathbf{g}}^* + n\cdot\boldsymbol{c}_{\mathbf{m}}^*$.

The supplementary misfit parameter (δ) is defined as $\delta = c_{\mathrm{h}}/c_{\mathrm{m}} = \boldsymbol{c}_{\mathbf{m}}^*/\boldsymbol{c}_{\mathrm{h}}^*$. As shown in Figure 3.2.10.4, the profile of the $(-1\ 0\ l\ m\ n)_{\mathrm{h}}$ layer line at 205.0 K was modeled with a misfit parameter γ = 0.63007 and fit with a supplementary misfit parameter δ = 0.0418(10).

As shown Figure 3.2.10.5, temperature evolution of the $(-1\ 0\ l\ m\ n)_{\mathrm{h}}$ layer line shows that the peak positions remain the same through the phase transition at 262(2) K. Indeed, least squares refinements of the supplementary misfit parameter (δ) in six layer lines shows that it is constant with a mean of 0.0410(3), as shown in Figure 3.2.10.6.

We note here that γ/δ = 0.63007(2)/0.0418(10) = 15.1(4). If there is a long-range modulation with a wavelength of fifteen guest molecules (approximately 263 Å), then this phase would more correctly be described as a four-dimensional structure. At this time, such an assessment is difficult, but further analysis might distinguish these two possibilities.

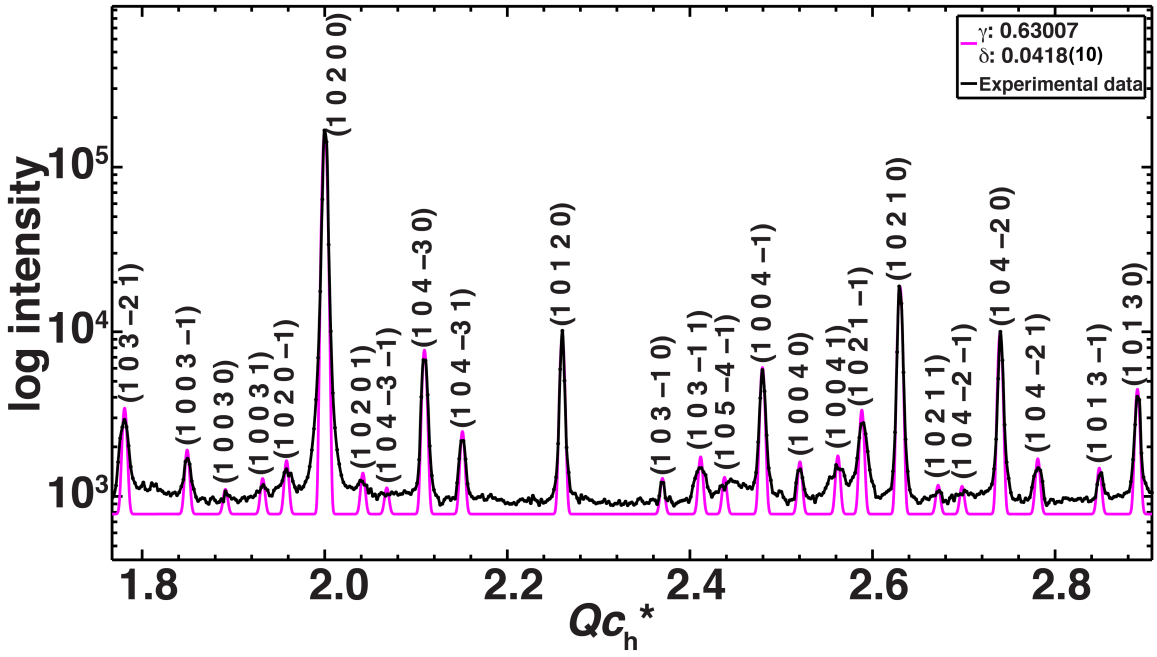

Figure 3.2.10.4. Profile analysis of the (-1 0 *l* *m*)$_h$ layer line of unwarped oscillation image of 2,11-dodecanedione/urea grown by cooling from 40 °C to room temperature. The image was collected using a 60° ϕ rotation about the crystal ***c*** axis at 205.0 K on APS beamline 14-BM-C at APS with a detector distance of 500.0 mm, exposure time of 6 sec, λ = 0.97870 Å, 200×200 μm. The profile was modeled with γ = 0.63007 and fit with δ = 0.0418(10).[68]

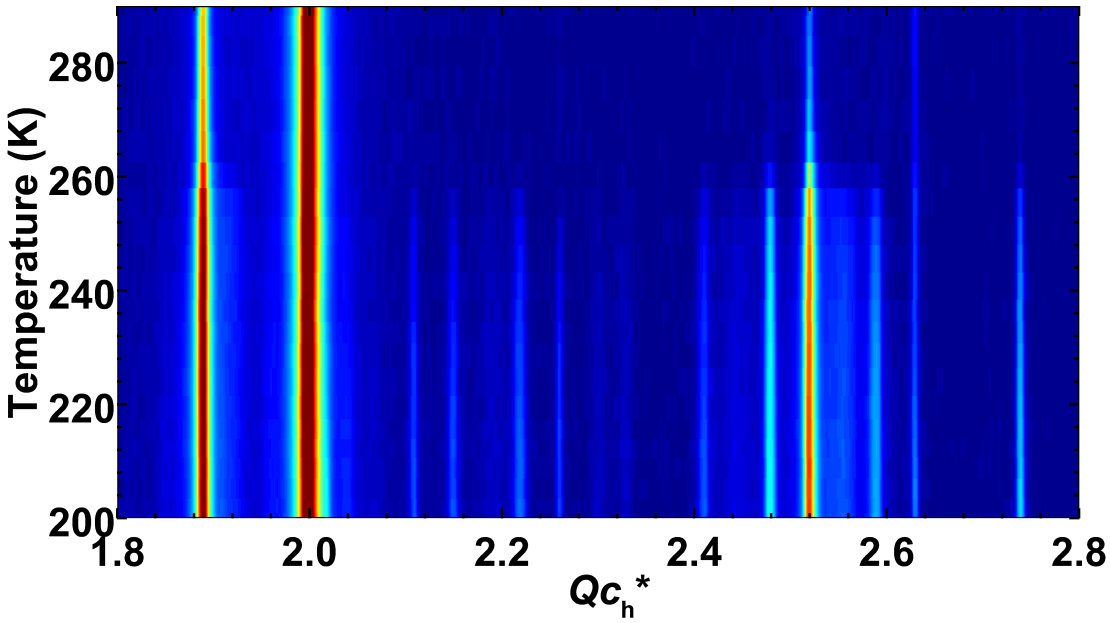

Figure 3.2.10.5. Temperature evolution of the (-1 0 *l m n*)$_h$ layer line in oscillation images of a crystal of 2,11-dodecanedione/urea grown by cooling from 40 °C to room temperature upon cooling from 290 K to 200 K. Measurements were made on APS beamline 14-BM-C using 60° ϕ rotations about the crystal ***c*** axis from 290.0 to 199.8 K with the following parameters: distance = 500.0 mm, time = 6 s, λ = 0.97870 Å, and beam size (x,y) = (200, 200) μm.[6] Layer line profiles are shown on a logarithmic color scale, with red being most intense.

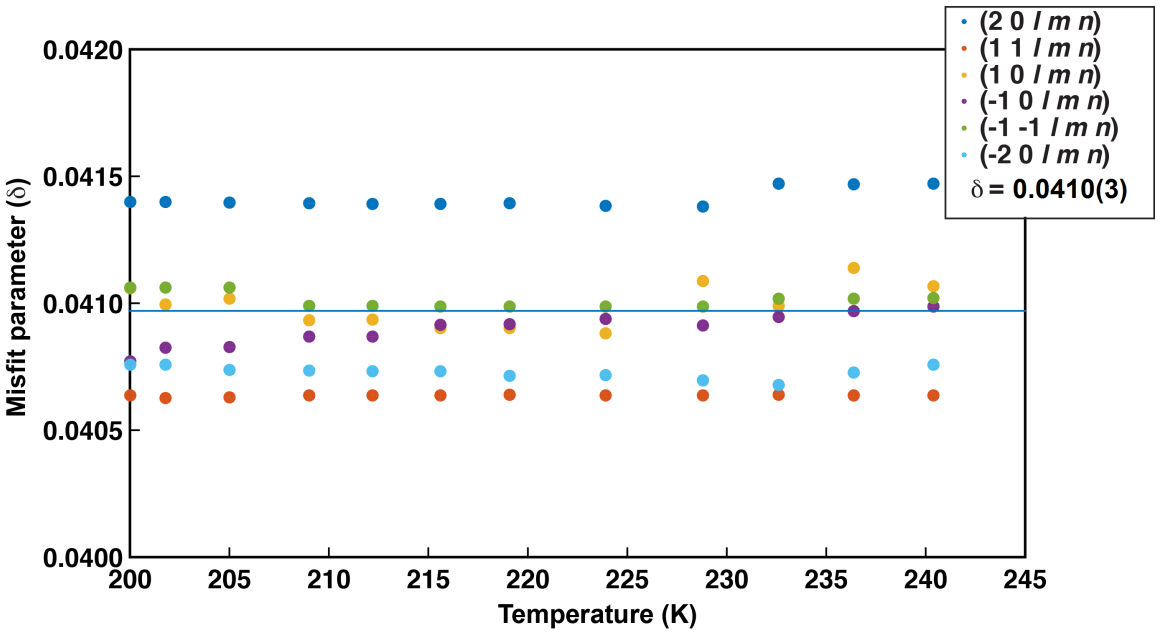

Figure 3.2.10.6. Temperature evolution of the supplementary misfit parameter (δ) of 2,11-dodecanedione/urea grown by cooling from 40 °C to room temperature. Measurements were made on APS beamline 14-BM-C using 60° ϕ rotations about the crystal ***c*** axis from 262.2 to 199.8 K with the following parameters: distance = 500.0 mm, time = 6 s, λ = 0.97870 Å, and beam size (x,y) = (200, 200) μm.[69] The reported values were obtained from least squares refinements of the misfit parameter for various layer lines in unwarped oscillation images through the temperature scan. The supplementry misfit parameter stayed constant, with an average value of δ = 0.0410(3) (e.s.d.) as shown by the horizontal blue line.

3.2.11. Summary of phase transitions of 2,11-dodecanedione/urea grown at different temperatures

From the above analyses, it is clear that phase transitions of 2,11-dodecanedione/urea depend on the growth conditions. As shown in Table 3.2.11.1,

the initial guest repeat length (c_g) directly affects the behavior of the phase transitions. When the value of c_g is shorter than that for the commensurate phase with $12c_g' = 19c_h'$, the crystal undergoes a lock-in phase transition accompanied by self-compression behavior. A rough comparison of peak intensities of the most compressed state in the batches grown at -20.0 °C. -10.0°C, and 0.0 °C revealed that the more the guest expands during the lock-in phase transition, the greater the proportion of the most compressed state relative to the commensurate phase with $12c_g' = 19c_h'$. Further work needs to be done to establish this quantitatively.

In the cases where the guest repeat is very close to the value expected for the commensurate phase with $12c_g' = 19c_h'$, self-compression is either reduced or absent. observed. From the available data, when the guest repeat is at least 0.0419(13) Å longer than that for the commensurate phase with $12c_g' = 19c_h'$, no lock-in phase transition occurred, as exhibited by the crystals grown at 40.0 °C and from 40 °C to room temperature. This can be explained by noting that if the guest shrinks during a lock-in phase transition, void space in the channel would be produced.[70] The resulting loss of attractive interactions between the guest and host leads to a high energetic barrier for the formation of a void. Thus, at least in the urea inclusion compounds, a lock-in phase transition involving significant shrinkage of the guest is unfavorable.

Note that the phase with $7c_g' = 11c_h'$ that was originally hypothesized was not observed in any of the experiments. Instead, incommensurate phases and a significantly shortened phase with $2c_g' = 3c_h'$ were the products of self-compression generated by locking into the phase with $12c_g' = 19c_h'$.

Growth Temperature (°C)	γ @290K	c_g (Å)	c_g compared with c_g' (Å)	T_c, X-ray (K)	T_c, DSC cool (K)	T_c, DSC heat (K	Lock-in?
-20.0	0.63462(3)	17.3931(11)	-0.0837(14)	261(2)	263.0	264.7	Yes
-10.0	0.63335(5)	17.4279(16)	-0.0489(18)	266(3)	257.5	261.0	Yes
0.0	0.6311(4) and 0.63254(3)	17.491(11) and 17.4503(11)	0.014(11) and -0.0265(14)	261(3) and *260(2)	259.3	260.8	Yes
10.0	0.63315(2)	17.4335(10)	-0.0434(13)	258(1)	255.3	258.1	Yes
20.0	0.63254(2)	17.4503(10)	-0.0266(13)	260(1)	256.3	260.3	Yes
30.0	0.63375(2)	17.4170(10)	-0.0599(13)	260(1)	255.3	258.5	Yes
35.0	0.63238(5)	17.4546(16)	-0.0221(18)	260(3)			Yes
40.0	0.62940(2) and 0.6320(6)	17.531(5) and 17.465(17)	0.054(5) and -0.012(17)	259(3)	253.5	256.4	No and Yes
46	0.63155(2)	17.4476(10)	0.00080(12)	258(2)			Yes
40 - r.t.	0.63007(2)	17.5187(10)	0.0419(13)	262(2)	262.2	264.3	No

Table 3.2.11.1. Compiled parameters of 2,11-dodecanedione/urea grown under different conditions. *This temperature refers to a warming run. The value of c_g' shown in the fourth column is for the commensurate phase with $12c_g' = 19c_h'$.

3.3. Crystal structure of 2,11-dodecanedione

Although almost all alkane/urea inclusion compounds are incommensurate, there are a number of crystal structures of commensurate UICs. Due to a reliable host-guest hydrogen bonding pattern, bis(methylketone)s tend to form commensurate systems with urea. The crystal structures of 2,7-octanedione/urea,[2] 2,9-decanedione/urea,[1] 2,10-undecanedione/urea,[71] and 2,12-tridecanedione[72] have been published.

Determination of the crystal structure of 2,11-dodecanedione/urea has presented a difficult challenge due to the complexity of the phases that occur in this UIC upon cooling. As described in the above sections, when the guest repeat in this UIC is smaller than that for the commensurate phase with $12c_g' = 19c_h'$, the system locks into the commensurate phase with $12c_g' = 19c_h'$. Thus the unit cell length along the channel axis

(***c***) can be estimated to be as long as 19 × 11.02 = 209.38 Å. Such a long channel axis results in very closely spaced reflections in diffraction images.

A preliminary crystal structure of the phase of 2,11-dodecanedione/urea[73] with $12c_g' = 19c_h'$ was solved using synchrotron data obtained at 246.0 K on APS beamline 14-BM-C, using λ = 0.97870 Å, a detector distance of 200.00 mm, and 0.20° ϕ scans that spanned 360° over a 2θ range of $4.818° \leq 2\theta \leq 58.266°$.[74] This beamline utilizes a Quantum 315 r area detector that has a dynamic range of 0 to 2^{16}. The hexagonal unit cell parameters of this $P6_122$ structure were found to be ***a*** = ***b*** = 8.1953(12) Å, and ***c*** = 209.54(4) Å. The resolution of this data set was too low for the crystal structure to be solved with direct methods using XS.[75]

To solve the crystal structure, a molecular replacement method was used in which the host structure was modeled with coordinates from the crystal structure of heptane/urea.[76] The guest was then located and refined using the program XL.[75] Using 82055 reflections (3930 unique reflections), the final preliminary structure had R_1 = 0.1385 and wR_2 = 0.4670, with the asymmetric unit shown in Figure 3.3.1. The numbers of data/restraints/and parameters are 3930/291/213. In this preliminary structure, the hydrogen bonding between the host and the guest can be readily seen. Every guest molecule makes one hydrogen bond to the host, as indicated by the red arrow shown in the Figure 3.3.1. Notice that the host molecule that hydrogen bonds to the guest turns into the channel. Interestingly, when the turned urea molecule was modeled as two sites, the site occupancy factors (*s.o.f*) of the turned and unturned sites were refined to 52 % versus 48%, respectively.

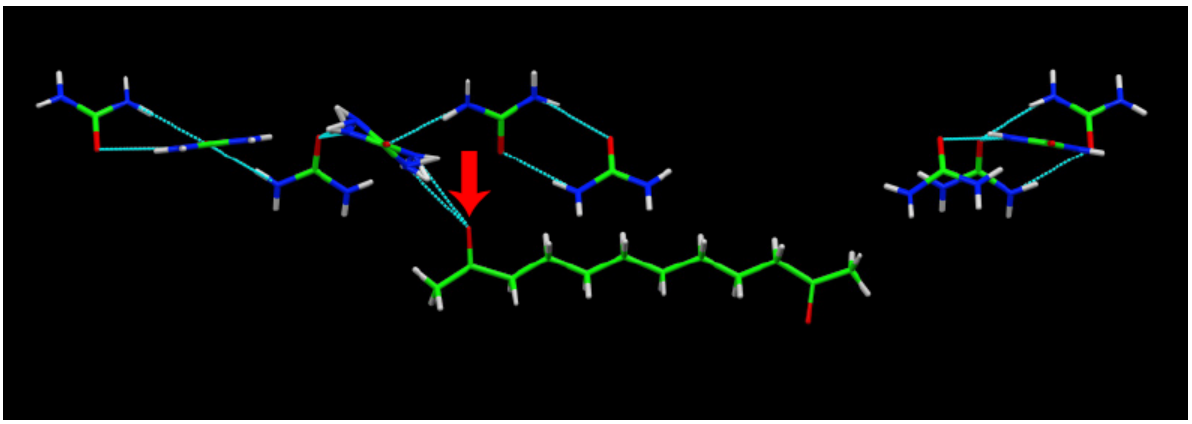

Figure 3.3.1.1. Preliminary crystal structure (at 246.0 K) of a crystal of 2,11-dodecanedione/urea grown above 268 K. The turned urea molecule, which makes hydrogen bonds to the guests, is indicated by a red arrow.

A more accurate structure was subsequently obtained from beamline I04 at the Diamond Light Source (DLS), Oxford. A hexagonal block (with dimensions 0.40 × 0.25 × 0.25 mm^3) of a crystal of 2,11-dodecanedione/urea grown by cooling from -13.0 to -23.0 °C was selected and mounted.[14] The crystal was kept cold until the experiments. Beamline I04 has a miniKappa goniometer with a PILATUS-6M detector which has a dynamic range of 0-2^{20}. The parameters of this dataset are: λ = 0.97949 Å, temperature = 170.0 K, distances = 170.00 and 220.00 mm, 180° ω scans in steps of 0.25° with Kappa at 0 and 70°.[3] In order to process the data using the Bruker APEX2 software package[77] the frames needed to be converted from miniCBF to SFRM format. During the conversion, the geometry of the miniKappa type goniometer needed to be converted into a Eulerian geometry setting. A conversion method was devised.[78] Without this conversion, the data could not be indexed. The dataset was then processed using the Bruker APEX2 software package.[77] Cell constants and an orientation matrix for data

integration were obtained from a least-squares refinement of 9978 reflections. This corresponded to a hexagonal cell with the following dimensions:

a = 8.1855(4) Å, α = 90°

b = 8.1855(4) Å, β = 90°

c = 209.210(10) Å, γ = 120°

V = 12139.6(13) Å^3

For Z = 6 and F.W. = 1537.75, the calculated density is 1.262 g/cm^3. Based on the systematic absences of:

00l: $l \neq 6n$

a statistical analysis of intensity distributions and the successful solution and refinement of the structure uniquely determined the space group to be:

$P6_122$ (# 178)

Of the 192094 reflections (4.83° ≤ 2θ ≤ 90.144°) that were collected, 11439 were unique (R_{int} = 0.0815, R_{sigma} = 0.0327); equivalent reflections were merged using SADABS 2014/5.[79] Later, all of the data was scaled with SADABS software.[79] The linear absorption coefficient, μ, for λ = 0.97949 Å is 0.248 mm^{-1}.

Using Olex2,[80] molecular replacement of the preliminary structure was used as the starting model. The model was refined with the XL refinement package using least squares minimization.[75] In the final cycles of the refinement, all non-hydrogen atoms were refined anisotropically. The position of each hydrogen atom was refined using a riding model, and values of U_{iso} that were 1.2 or 1.5 times the U_{eq} for the heavy atom to

which the hydrogen was bonded were used, depending on the position of the heavy atom. The final cycle of full-matrix least-squares refinement[81] was based on 11120 observed reflections ($I > 2.00\sigma(I)$), 513 variable parameters, 479 restraints, and converged with unweighted and weighted agreement factors of:

$R_1=\Sigma||Fo|-|Fc|| / \Sigma|Fo|= 0.0889$

$wR_2=\{\Sigma[w(Fo^2-Fc^2)]^2 / \Sigma[w(Fo^2)]^2\}^{1/2}= 0.2040$

where

$w=1/[\sigma^2(Fo^2)+(aP)^2+bP]$,

and

$P=[2Fc^2+Max(Fc^2,0)]/3$

Here, a and b were set to 0.1240 and 3.5668, respectively.

The goodness of fit was 1.079.[82] The maximum and minimum peaks in the final difference Fourier map corresponded to 0.43 e/Å^3 (1.37 A from H1ED) and -1.41 e/Å^3 (0.72 Å from C1A), respectively. Neutral atom scattering factors were taken from International Tables for Crystallography.[83]

As shown by the crystal structure in Figure 3.3.1.2, twelve guest molecules fit within nineteen repeats of the host helix in a single unit cell. This unambiguously proves the commensurate relationship of this phase of the UIC. The sixfold screw axis along the channel direction operates on two guest molecules, which are also related by a twofold axis perpendicular to the ***c*** direction. This DLS dataset provides much better resolution than the dataset from APS beamline 14-BM-C, and a large number of high-quality reflections enabled exploration of the structural model in much greater detail.

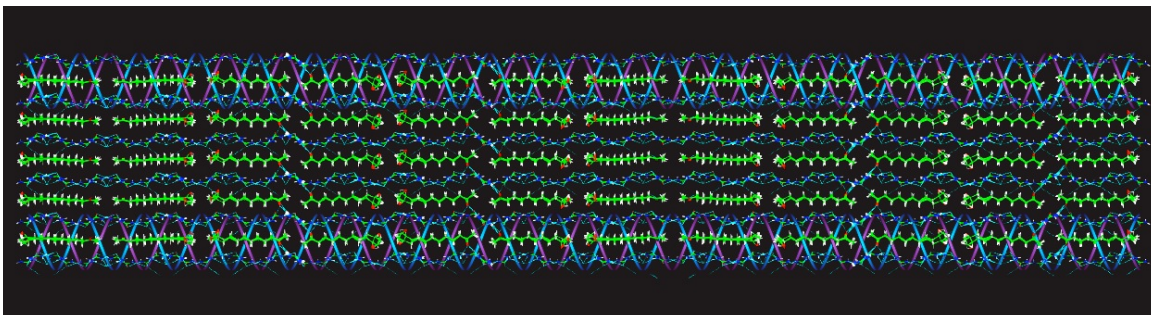

Figure 3.3.1.2. Crystal structure of 2,11-dodecanedione/urea from the data acquired on beamline I04 at the DLS, view along ***b***.

As shown in Figure 3.3.1.3, the guest was modeled with three sites: the major guest site has site occupancy factor (*s.o.f.*) = 54%, the second site has *s.o.f.* = 24%, and the minor site has *s.o.f.* = 22%.[84] The major and second sites are nearly identical in conformation and make diagonal hydrogen bonds to the turned urea molecule (O1X to N1N2 and O1Z to N1N2, respectively); a motif seen in all other published diketone/urea structures.[2,1,71,72] These two components adopt planar zig-zag chain conformations in which the guest carbonyl groups are antiparallel, as expected for this even-chain molecule. Interestingly, the minor site adopts a strained conformation in which the end ketones make a torsion angle of 60°, as shown in Figure 3.3.1.3. (D). This allows the guest carbonyl groups to each make a hydrogen bond to the host, O1Y to N1N2 and O2Y to N1PQ. Notice that there are two pairs of turned ureas: N1/N1N2, and N1Q/N1PQ/N1P/N1PP. The disorder of the host was tethered to the guest such that the major guest site and the second guest site were linked to N1N2, which turns into the channel. The minor component of the guest was tethered to N1PQ/N1Q, which also turns into the channel, but by a different amount.

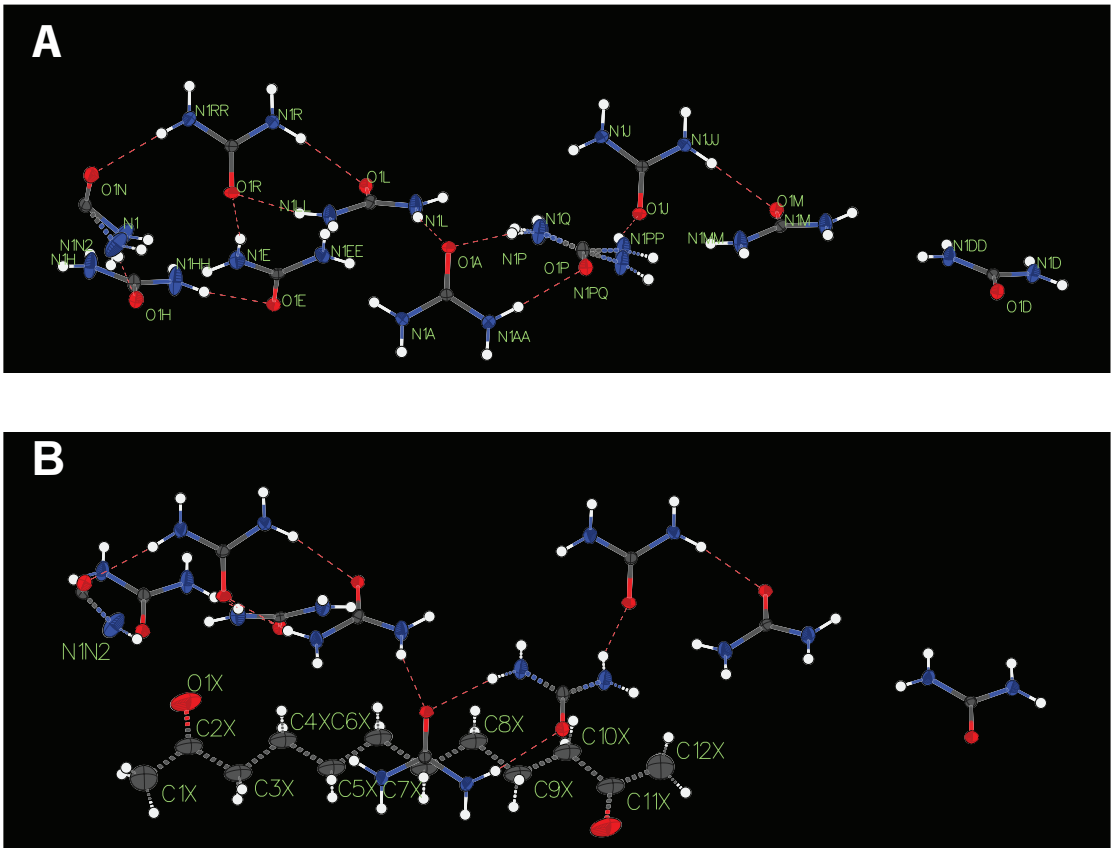

Figure 3.3.1.3. Labeled diagram of one asymmetric unit of the crystal structure of 2,11-dodecanedione/urea from the data acquired on beamline I04 at the DLS. (A) Labeled host molecules. Notice that there are two disordered host molecules, with disordered nitrogen atoms N1N:N1N2 on one, while the other has N1P:N1Q and N1PP:N1PQ. (B) This is the major guest site, whose *s.o.f.* = 54%.

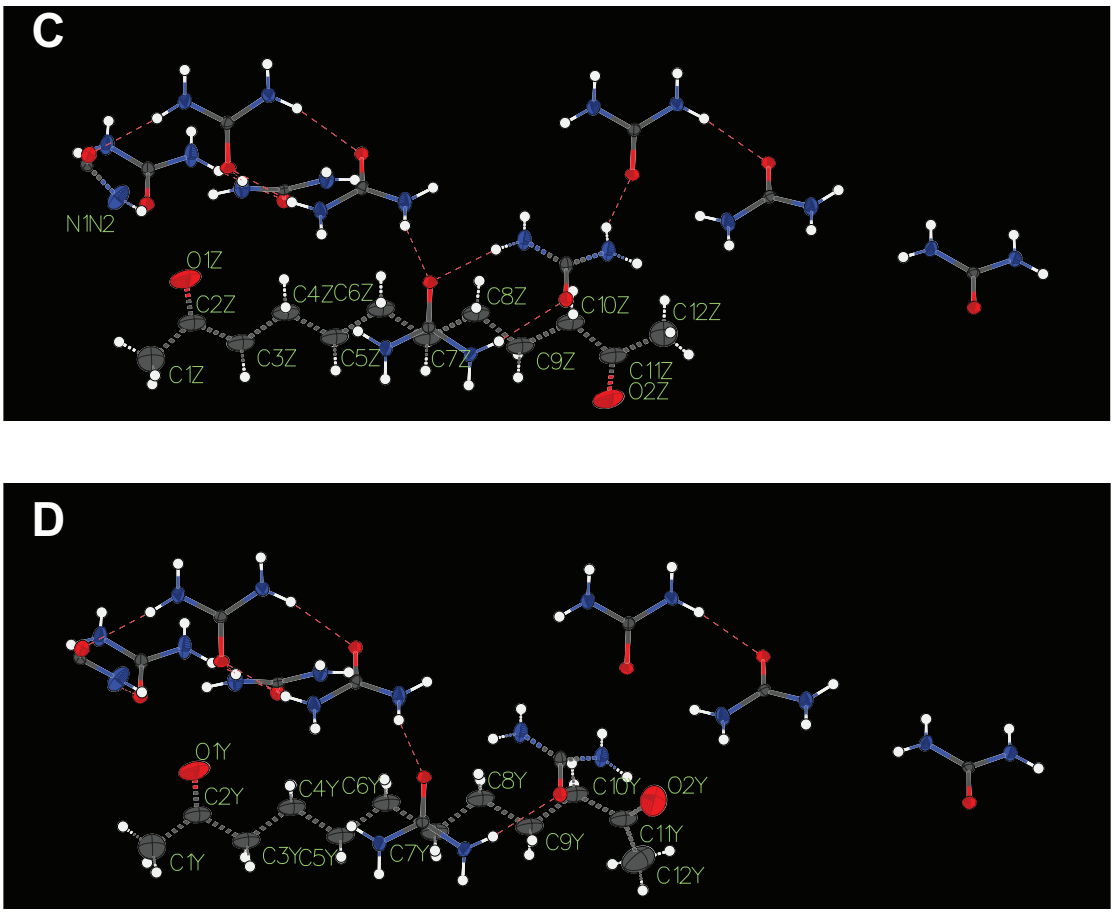

Figure 3.3.1.3. Labeled diagram of one asymmetric unit of the crystal structure of 2,11-dodecanedione/urea from the data acquired on beamline I04 at the DLS. (C) This is the second site, whose *s.o.f.* = 24%. (D) This is the minor site, whose *s.o.f.* = 22%.[84]

In this model, various types of restraints and constraints were applied:

1. The values of U_{iso} of hydrogen atoms were 1.2 or 1.5 times the U_{eq} values for the heavy atom to which the hydrogen is bonded, depending on the position of the heavy atom.

2. The 1,2-distances and 1,3-distances of the disordered guests were restrained.

3. The bond distances in urea molecules were restrained.

4. The urea molecules were restrained to be planar.

5. Rigid bond restraints were applied to the disordered guests.

6. The U_{ij} values of the guests were constrained using EADP.

7. The SUMP command was used to restrain the site occupancy factors (*s.o.f.*s) of the three guest sites to unity and the *s.o.f.* of the minor guest to that of the unturned urea molecule.

8. The hydrogen positions are treated with riding models, depending on the type of heteroatom.

3.3.2. Supplemental data for the crystal structure refinement

Table 3.3.2.1. Crystal data and structure refinement for BW_E_110-16-z24.	
Identification code	BW_E_110-16-z24
Empirical formula	$C_{43}H_{120}N_{38}O_{23}$
Formula weight	1537.75
Temperature/K	170.0
Crystal system	Hexagonal
Space group	$P6_122$
a/Å	8.1855(4)
b/Å	8.1855(4)
c/Å	209.210(10)
α/°	90
β/°	90
γ/°	120
Volume/$Å^3$	12139.6(13)
Z	6
$\rho_{calc}g/cm^3$	1.262
μ/mm^{-1}	0.248
F(000)	4968.0
Crystal size/mm^3	0.40 × 0.25 × 0.25
Radiation	Synchrotron (λ = 0.97949 Å)

2θ range for data collection/°	4.83 to 90.144
Index ranges	-10 ≤ h ≤ 10, -10 ≤ k ≤ 9, -260 ≤ l ≤ 262
Reflections collected	192094
Independent reflections	11439 [R_{int} = 0.0815, R_{sigma} = 0.0327]
Data/restraints/parameters	11439/479/513
Goodness-of-fit on F^2	1.099
Final R indexes [I>=2σ (I)]	R_1 = 0.0889, wR_2 = 0.2040
Final R indexes [all data]	R_1 = 0.0899, wR_2 = 0.2057
Largest diff. peak/hole / e $Å^{-3}$	0.43/-1.41
Flack parameter	0.33(5)

Table 3.3.2.2. Fractional Atomic Coordinates (×10^4) and Equivalent Isotropic Displacement Parameters ($Å^2$×10^3) for BW_E_110-16-z24. U_{eq} is defined as 1/3 of of the trace of the orthogonalized U_{ij} tensor.

Atom	x	y	z	U(eq)
O1A	6706.7(16)	3597.2(17)	5395.7(2)	15.1(2)
O1E	-3841.5(17)	3064.4(15)	5570.3(2)	14.2(2)
O1J	3145.0(16)	6328.7(17)	5131.5(2)	16.0(2)
O1L	3058.1(16)	6767.4(16)	5481.3(2)	14.6(2)
O1P	6717.3(16)	3126.0(16)	5220.0(2)	15.6(2)
O1R	2923.2(16)	6155.5(16)	5653.4(2)	16.0(2)
N1A	5030(2)	818(2)	5449.4(2)	22.7(3)
N1AA	5514(2)	831(2)	5340.8(2)	22.1(3)
N1E	-1147(2)	4243(2)	5629.0(2)	20.1(3)
N1EE	-1013(2)	4654(2)	5519.7(2)	19.9(3)

N1J	4823(3)	9096(2)	5185.6(2)	29.3(4)
N1JJ	4320(3)	9101(2)	5077.2(2)	28.4(4)
N1L	4743(2)	5691(2)	5426.8(2)	22.1(3)
N1LL	4240(2)	5171(2)	5535.1(2)	21.1(3)
N1R	4114(3)	9002(2)	5604.1(2)	25.4(3)
N1RR	4451(3)	8826(2)	5712.8(2)	31.9(4)
C1A	5774(2)	1802(2)	5395.3(2)	13.4(3)
C1E	-2049(2)	3954(2)	5573.0(2)	11.9(3)
C1J	4056(2)	8122(2)	5131.4(2)	16.2(3)
C1L	3983(2)	5900(2)	5481.1(2)	13.4(3)
C1P	5822(2)	4020(2)	5219.0(2)	16.3(3)
C1R	3795(2)	7933(2)	5656.6(2)	15.0(3)
O1D	6742.1(16)	3205.5(16)	4693.0(2)	15.0(2)
O1M	3163.3(15)	6842.4(15)	4956.2(2)	14.4(3)
N1D	5176(2)	4420(2)	4639.0(2)	18.2(3)
N1DD	5593(2)	4815(2)	4748.1(2)	20.7(3)
N1M	5031(2)	5967(2)	4902.8(2)	21.3(3)
N1MM	4248(2)	5136(3)	5008.6(2)	24.5(3)
C1D	5857(2)	4116(2)	4693.3(2)	11.5(3)
C1M	4110(2)	5995(2)	4955.8(2)	12.2(3)
O1H	-3720.6(18)	2849.2(17)	5747.4(2)	17.5(2)
O1N	3026(3)	6513.0(13)	5833	19.7(3)
N1H	-4956(3)	4442(3)	5798.4(2)	29.4(4)
N1HH	-5191(3)	4078(3)	5689.1(2)	29.8(4)
C1H	-4596(2)	3756(2)	5745.0(2)	15.9(3)
C1N	1233(3)	5616.6(16)	5833	15.4(4)
N1	240(4)	4637(17)	5782.0(3)	33.4(8)

N1N2	238(3)	4242(4)	5790.8(2)	33.4(8)
N1PQ	4847(12)	3845(14)	5164.9(3)	25.1(4)
N1Q	5470(20)	4780(20)	5270.6(3)	25.1(4)
N1P	5579(6)	4749(7)	5273.6(2)	25.1(4)
N1PP	5133(4)	4322(4)	5164.4(2)	25.1(4)
O1X	-30(12)	1632(7)	5696.0(3)	77.7(13)
O2X	300(9)	-2125(6)	5152.6(2)	77.7(13)
C1X	-380(20)	-1064(12)	5748.2(2)	74.5(14)
C2X	-306(9)	62(6)	5690.8(2)	37.2(4)
C3X	-409(9)	-829(6)	5626.8(2)	37.2(4)
C4X	-400(8)	327(6)	5569.5(2)	37.2(4)
C5X	-193(9)	-510(6)	5507.0(2)	37.2(4)
C6X	-186(8)	555(6)	5447.2(2)	37.2(4)
C7X	93(9)	-346(6)	5387.5(2)	37.2(4)
C8X	13(7)	558(5)	5324.8(2)	37.2(4)
C9X	274(7)	-427(6)	5267.2(2)	37.2(4)
C10X	-64(7)	262(5)	5203.5(2)	37.2(4)
C11X	36(6)	-825(5)	5147.0(2)	37.2(4)
C12X	-284(17)	-229(11)	5082.7(2)	74.5(14)
O1Z	480(30)	1599(13)	5702.8(5)	77.7(13)
O2Z	-1024(18)	-2541(9)	5152.0(4)	77.7(13)
C1Z	-190(40)	-1340(20)	5744.2(5)	74.5(14)
C2Z	-90(20)	-32(11)	5692.4(3)	37.2(4)
C3Z	-839(13)	-896(10)	5627.8(3)	37.2(4)
C4Z	58(15)	446(9)	5571.6(3)	37.2(4)
C5Z	-622(13)	-559(9)	5507.6(2)	37.2(4)
C6Z	230(16)	703(9)	5449.3(2)	37.2(4)

C7Z	-450(13)	-436(9)	5387.6(2)	37.2(4)
C8Z	397(15)	676(9)	5326.4(2)	37.2(4)
C9Z	-298(14)	-605(9)	5267.9(2)	37.2(4)
C10Z	320(14)	429(8)	5204.2(3)	37.2(4)
C11Z	-370(14)	-876(9)	5147.3(3)	37.2(4)
C12Z	180(40)	69(16)	5083.4(3)	74.5(14)
O1Y	430(30)	1685(14)	5682.8(5)	77.7(13)
O2Y	1819(12)	1485(13)	5092.5(3)	74(4)
C1Y	-450(60)	-1180(20)	5734.5(4)	74.5(14)
C2Y	-160(20)	33(13)	5677.2(3)	37.2(4)
C3Y	-560(20)	-930(12)	5613.1(3)	37.2(4)
C4Y	-180(20)	359(13)	5555.7(3)	37.2(4)
C5Y	-280(20)	-607(13)	5492.4(2)	37.2(4)
C6Y	30(20)	633(13)	5434.2(2)	37.2(4)
C7Y	40(20)	-299(12)	5371.3(2)	37.2(4)
C8Y	306(19)	933(11)	5313.2(2)	37.2(4)
C9Y	336(16)	34(11)	5249.8(2)	37.2(4)
C10Y	311(13)	1162(10)	5192.2(2)	37.2(4)
C11Y	613(10)	471(9)	5128.9(3)	37.2(4)
C12Y	-966(18)	-1395(15)	5106.9(6)	87(6)

Table 3.3.2.3. Anisotropic displacement parameters ($Å^2 \times 10^3$) for BW_E_110-16-z24. The anisotropic displacement factor exponent takes the form: $-2\pi^2[h^2a^{*2}U_{11}+2hka^*b^*U_{12}+\ldots]$.

Atom	U_{11}	U_{22}	U_{33}	U_{23}	U_{13}	U_{12}
O1A	15.2(5)	10.9(5)	15.4(5)	-0.5(3)	1.1(4)	3.6(4)
O1E	9.5(5)	16.3(5)	14.5(5)	-0.4(4)	0.2(3)	4.6(4)
O1J	18.4(5)	10.4(5)	15.5(5)	0.4(3)	-0.6(4)	4.4(4)
O1L	16.5(5)	17.2(5)	13.8(5)	-0.4(4)	-0.2(4)	11.2(5)
O1P	15.9(5)	20.1(5)	14.8(5)	0.5(4)	0.7(4)	11.8(5)
O1R	15.3(5)	10.2(5)	18.7(5)	-0.5(3)	0.2(4)	3.6(4)
N1A	27.8(8)	14.5(6)	14.2(6)	0.6(4)	2.7(5)	1.9(6)
N1AA	30.0(8)	14.2(6)	14.7(6)	-2.2(4)	2.0(5)	5.7(6)
N1E	13.4(6)	27.5(7)	18.4(6)	-0.5(5)	-2.4(4)	9.4(6)
N1EE	13.8(6)	22.2(7)	18.1(6)	1.2(5)	4.0(5)	4.8(5)
N1J	40.1(9)	14.5(6)	14.3(6)	-1.5(5)	-2.2(6)	-0.5(6)
N1JJ	47.2(10)	12.8(6)	14.1(6)	1.6(5)	0.1(6)	6.7(7)
N1L	26.0(7)	36.6(9)	14.6(6)	1.5(5)	2.2(5)	23.9(7)
N1LL	29.1(8)	30.2(8)	14.0(6)	2.9(5)	0.9(5)	22.4(7)
N1R	39.5(9)	14.3(6)	14.7(6)	0.9(5)	-0.5(5)	7.6(6)
N1RR	50.6(11)	16.6(7)	13.4(6)	-2.3(5)	-2.6(6)	5.5(7)
C1A	12.2(6)	12.3(7)	12.6(6)	-0.3(4)	-0.2(5)	3.9(5)
C1E	11.3(7)	8.8(6)	16.8(6)	-1.6(5)	-0.2(4)	5.8(5)
C1J	18.8(7)	11.5(7)	12.3(6)	-0.2(5)	0.7(5)	3.1(6)
C1L	13.1(7)	15.7(7)	12.3(6)	-1.5(5)	-0.9(5)	7.9(6)
C1P	16.1(7)	25.1(8)	12.5(6)	0.7(5)	0.9(5)	13.8(7)
C1R	15.5(7)	11.7(7)	14.5(6)	-0.5(4)	1.7(5)	4.4(6)
O1D	19.0(5)	17.4(5)	14.2(5)	-0.4(4)	-0.4(4)	13.4(5)

O1M	16.7(5)	17.2(5)	14.2(5)	0.5(4)	-0.1(4)	12.1(5)
N1D	23.3(7)	24.2(7)	14.8(5)	-0.9(5)	-1.8(5)	17.7(6)
N1DD	31.9(8)	26.6(7)	14.3(5)	-1.7(5)	0.9(5)	22.6(7)
N1M	26.9(7)	31.2(8)	15.7(6)	1.2(5)	3.1(5)	22.0(7)
N1MM	37.2(9)	36.5(9)	15.6(6)	4.8(5)	2.6(5)	30.2(7)
C1D	12.1(6)	11.0(6)	12.0(6)	0.5(4)	1.3(4)	6.2(6)
C1M	12.5(6)	12.5(6)	12.8(6)	-1.8(5)	-1.7(5)	7.1(6)
O1H	22.7(6)	20.6(6)	15.3(5)	0.0(4)	-0.7(4)	15.6(5)
O1N	22.0(9)	20.5(6)	17.0(6)	-1.4(5)	0	11.0(4)
N1H	48.9(11)	46.9(10)	15.4(6)	-1.2(6)	1.5(6)	41.3(9)
N1HH	40.5(9)	57.9(12)	14.7(6)	0.9(6)	-0.5(6)	42.3(9)
C1H	18.6(7)	22.6(7)	12.5(6)	1.1(5)	0.7(5)	14.8(6)
C1N	22.4(10)	14.4(7)	12.2(8)	1.7(5)	0	11.2(5)

N1	26.7(9)	46.9(17)	33.6(9)	-19.3(11)	-15.8(7)	23.6(9)
N1N2	26.7(9)	46.9(17)	33.6(9)	-19.3(11)	-15.8(7)	23.6(9)
N1PQ	35.6(8)	43.3(9)	14.8(5)	-1.7(5)	-2.1(5)	33.4(7)
N1Q	35.6(8)	43.3(9)	14.8(5)	-1.7(5)	-2.1(5)	33.4(7)
N1P	35.6(8)	43.3(9)	14.8(5)	-1.7(5)	-2.1(5)	33.4(7)
N1PP	35.6(8)	43.3(9)	14.8(5)	-1.7(5)	-2.1(5)	33.4(7)
O1X	141(4)	52.9(12)	68.0(14)	-15.3(11)	-11.5(19)	70.2(18)
O2X	141(4)	52.9(12)	68.0(14)	-15.3(11)	-11.5(19)	70.2(18)
C1X	124(4)	64(2)	55.0(15)	1.0(15)	3(2)	62(2)
C2X	36.3(8)	24.5(4)	55.3(7)	-2.4(4)	4.7(6)	18.6(4)
C3X	36.3(8)	24.5(4)	55.3(7)	-2.4(4)	4.7(6)	18.6(4)
C4X	36.3(8)	24.5(4)	55.3(7)	-2.4(4)	4.7(6)	18.6(4)
C5X	36.3(8)	24.5(4)	55.3(7)	-2.4(4)	4.7(6)	18.6(4)
C6X	36.3(8)	24.5(4)	55.3(7)	-2.4(4)	4.7(6)	18.6(4)
C7X	36.3(8)	24.5(4)	55.3(7)	-2.4(4)	4.7(6)	18.6(4)
C8X	36.3(8)	24.5(4)	55.3(7)	-2.4(4)	4.7(6)	18.6(4)
C9X	36.3(8)	24.5(4)	55.3(7)	-2.4(4)	4.7(6)	18.6(4)
C10X	36.3(8)	24.5(4)	55.3(7)	-2.4(4)	4.7(6)	18.6(4)
C11X	36.3(8)	24.5(4)	55.3(7)	-2.4(4)	4.7(6)	18.6(4)
C12X	124(4)	64(2)	55.0(15)	1.0(15)	3(2)	62(2)
O1Z	141(4)	52.9(12)	68.0(14)	-15.3(11)	-11.5(19)	70.2(18)
O2Z	141(4)	52.9(12)	68.0(14)	-15.3(11)	-11.5(19)	70.2(18)
C1Z	124(4)	64(2)	55.0(15)	1.0(15)	3(2)	62(2)
C2Z	36.3(8)	24.5(4)	55.3(7)	-2.4(4)	4.7(6)	18.6(4)
C3Z	36.3(8)	24.5(4)	55.3(7)	-2.4(4)	4.7(6)	18.6(4)
C4Z	36.3(8)	24.5(4)	55.3(7)	-2.4(4)	4.7(6)	18.6(4)
C5Z	36.3(8)	24.5(4)	55.3(7)	-2.4(4)	4.7(6)	18.6(4)

C6Z	36.3(8)	24.5(4)	55.3(7)	-2.4(4)	4.7(6)	18.6(4)
C7Z	36.3(8)	24.5(4)	55.3(7)	-2.4(4)	4.7(6)	18.6(4)
C8Z	36.3(8)	24.5(4)	55.3(7)	-2.4(4)	4.7(6)	18.6(4)
C9Z	36.3(8)	24.5(4)	55.3(7)	-2.4(4)	4.7(6)	18.6(4)
C10Z	36.3(8)	24.5(4)	55.3(7)	-2.4(4)	4.7(6)	18.6(4)
C11Z	36.3(8)	24.5(4)	55.3(7)	-2.4(4)	4.7(6)	18.6(4)
C12Z	124(4)	64(2)	55.0(15)	1.0(15)	3(2)	62(2)
O1Y	141(4)	52.9(12)	68.0(14)	-15.3(11)	-11.5(19)	70.2(18)
O2Y	51(5)	57(6)	60(5)	-3(4)	15(4)	-14(5)
C1Y	124(4)	64(2)	55.0(15)	1.0(15)	3(2)	62(2)
C2Y	36.3(8)	24.5(4)	55.3(7)	-2.4(4)	4.7(6)	18.6(4)
C3Y	36.3(8)	24.5(4)	55.3(7)	-2.4(4)	4.7(6)	18.6(4)
C4Y	36.3(8)	24.5(4)	55.3(7)	-2.4(4)	4.7(6)	18.6(4)
C5Y	36.3(8)	24.5(4)	55.3(7)	-2.4(4)	4.7(6)	18.6(4)
C6Y	36.3(8)	24.5(4)	55.3(7)	-2.4(4)	4.7(6)	18.6(4)
C7Y	36.3(8)	24.5(4)	55.3(7)	-2.4(4)	4.7(6)	18.6(4)
C8Y	36.3(8)	24.5(4)	55.3(7)	-2.4(4)	4.7(6)	18.6(4)
C9Y	36.3(8)	24.5(4)	55.3(7)	-2.4(4)	4.7(6)	18.6(4)
C10Y	36.3(8)	24.5(4)	55.3(7)	-2.4(4)	4.7(6)	18.6(4)
C11Y	36.3(8)	24.5(4)	55.3(7)	-2.4(4)	4.7(6)	18.6(4)
C12Y	75(11)	51(9)	106(12)	-13(9)	42(10)	10(8)

Table 3.3.2.4. Bond lengths for BW_E_110-16-z24.

Atom	Atom	Length/Å		Atom	Atom	Length/Å
O1A	C1A	1.273(2)		C2X	C3X	1.507(3)
O1E	C1E	1.272(2)		C3X	C4X	1.5247(17)
O1J	C1J	1.271(2)		C4X	C5X	1.5238(17)
O1L	C1L	1.2709(19)		C5X	C6X	1.5239(17)
O1P	C1P	1.2687(19)		C6X	C7X	1.5242(17)
O1R	C1R	1.2617(19)		C7X	C8X	1.5233(17)
N1A	C1A	1.3448(19)		C8X	C9X	1.5244(17)
N1AA	C1A	1.3456(18)		C9X	C10X	1.5237(17)
N1E	C1E	1.3409(18)		C10X	C11X	1.507(3)
N1EE	C1E	1.3433(19)		C11X	C12X	1.497(4)
N1J	C1J	1.3478(19)		O1Z	C2Z	1.193(3)
N1JJ	C1J	1.3416(19)		O2Z	C11Z	1.193(3)
N1L	C1L	1.3460(18)		C1Z	C2Z	1.497(4)
N1LL	C1L	1.3426(18)		C2Z	C3Z	1.507(3)
N1R	C1R	1.3457(19)		C3Z	C4Z	1.524(2)
N1RR	C1R	1.3460(19)		C4Z	C5Z	1.5234(19)
C1P	N1PQ	1.3499(17)		C5Z	C6Z	1.524(2)
C1P	N1Q	1.3496(17)		C6Z	C7Z	1.5237(19)
C1P	N1P	1.3492(15)		C7Z	C8Z	1.523(2)
C1P	N1PP	1.3499(15)		C8Z	C9Z	1.524(2)
O1D	C1D	1.2730(18)		C9Z	C10Z	1.523(2)
O1M	C1M	1.2725(19)		C10Z	C11Z	1.507(3)
N1D	C1D	1.3435(17)		C11Z	C12Z	1.497(5)
N1DD	C1D	1.3445(17)		O1Y	C2Y	1.193(3)

N1M	C1M	1.3476(18)		O2Y	C11Y	1.194(3)
N1MM	C1M	1.3447(19)		C1Y	C2Y	1.497(4)
O1H	C1H	1.2644(18)		C2Y	C3Y	1.507(3)
O1N	C1N	1.271(3)		C3Y	C4Y	1.5239(19)
N1H	C1H	1.3477(19)		C4Y	C5Y	1.5238(17)
N1HH	C1H	1.3417(19)		C5Y	C6Y	1.5236(19)
C1N	N1	1.343(2)		C6Y	C7Y	1.5241(17)
C1N	N1[1]	1.343(2)		C7Y	C8Y	1.5237(18)
C1N	N1N2	1.344(2)		C8Y	C9Y	1.5240(17)
C1N	N1N2[1]	1.344(2)		C9Y	C10Y	1.5240(18)
O1X	C2X	1.193(3)		C10Y	C11Y	1.507(3)
O2X	C11X	1.193(3)		C11Y	C12Y	1.497(4)
C1X	C2X	1.497(4)				

[1]+X,1+X-Y,7/6-Z

Table 3.3.2.5. Bond angles for BW_E_110-16-z24.

Atom	Atom	Atom	Angle/°		Atom	Atom	Atom	Angle/°
O1A	C1A	N1A	121.06(13)		C2X	C3X	C4X	114.6(3)
O1A	C1A	N1AA	120.96(13)		C5X	C4X	C3X	111.2(2)
N1A	C1A	N1AA	117.98(15)		C6X	C5X	C4X	114.6(2)
O1E	C1E	N1E	121.00(13)		C5X	C6X	C7X	110.8(2)
O1E	C1E	N1EE	120.61(12)		C8X	C7X	C6X	114.7(2)
N1E	C1E	N1EE	118.38(15)		C9X	C8X	C7X	111.9(2)
O1J	C1J	N1J	120.84(13)		C8X	C9X	C10X	113.4(2)
O1J	C1J	N1JJ	121.15(13)		C11X	C10X	C9X	113.2(2)
N1JJ	C1J	N1J	117.99(16)		O2X	C11X	C10X	122.4(3)
O1L	C1L	N1L	121.08(13)		O2X	C11X	C12X	121.3(4)
O1L	C1L	N1LL	120.97(13)		C12X	C11X	C10X	116.3(3)
N1LL	C1L	N1L	117.96(15)		O1Z	C2Z	C1Z	121.4(4)
O1P	C1P	N1PQ	115.7(5)		O1Z	C2Z	C3Z	121.9(4)
O1P	C1P	N1Q	125.0(5)		C1Z	C2Z	C3Z	116.7(4)
O1P	C1P	N1P	119.79(16)		C2Z	C3Z	C4Z	114.7(4)
O1P	C1P	N1PP	122.28(15)		C5Z	C4Z	C3Z	112.0(3)

N1Q	C1P	N1PQ	117.9(2)		C6Z	C5Z	C4Z	114.7(4)
N1P	C1P	N1PP	117.91(16)		C5Z	C6Z	C7Z	111.1(3)
O1R	C1R	N1R	121.31(13)		C8Z	C7Z	C6Z	115.4(3)
O1R	C1R	N1RR	121.03(13)		C7Z	C8Z	C9Z	111.3(3)
N1R	C1R	N1RR	117.65(15)		C10Z	C9Z	C8Z	114.4(3)
O1D	C1D	N1D	120.91(12)		C11Z	C10Z	C9Z	113.2(4)
O1D	C1D	N1DD	120.88(12)		O2Z	C11Z	C10Z	122.7(4)
N1D	C1D	N1DD	118.21(14)		O2Z	C11Z	C12Z	120.7(4)
O1M	C1M	N1M	120.92(13)		C12Z	C11Z	C10Z	115.4(5)
O1M	C1M	N1MM	120.84(12)		O1Y	C2Y	C1Y	121.0(4)
N1MM	C1M	N1M	118.23(15)		O1Y	C2Y	C3Y	122.5(4)
O1H	C1H	N1H	121.16(13)		C1Y	C2Y	C3Y	116.4(4)
O1H	C1H	N1HH	121.22(14)		C2Y	C3Y	C4Y	115.1(3)
N1HH	C1H	N1H	117.61(14)		C3Y	C4Y	C5Y	112.7(3)
O1N	C1N	N1	121.60(15)		C6Y	C5Y	C4Y	113.6(3)
O1N	C1N	N1[1]	121.60(17)		C5Y	C6Y	C7Y	113.3(3)
O1N	C1N	N1N2	121.66(12)		C6Y	C7Y	C8Y	113.0(3)
O1N	C1N	N1N2[1]	121.66(13)		C9Y	C8Y	C7Y	114.0(3)
N1	C1N	N1[1]	116.8(3)		C8Y	C9Y	C10Y	112.8(3)
N1N2	C1N	N1N2[1]	116.7(3)		C11Y	C10Y	C9Y	114.4(4)
O1X	C2X	C1X	121.3(3)		O2Y	C11Y	C10Y	122.3(5)
O1X	C2X	C3X	122.4(3)		O2Y	C11Y	C12Y	120.3(5)
C1X	C2X	C3X	116.0(3)		C12Y	C11Y	C10Y	115.6(4)

[1]+X,1+X-Y,7/6-Z

Table 3.3.2.6. Torsion angles for BW_E_110-16-z24.

A	B	C	D	Angle/°		A	B	C	D	Angle/°
O1X	C2X	C3X	C4X	-7.9(10)		C6Z	C7Z	C8Z	C9Z	177.2(8)
C1X	C2X	C3X	C4X	178.1(8)		C7Z	C8Z	C9Z	C10Z	173.8(8)
C2X	C3X	C4X	C5X	171.0(5)		C8Z	C9Z	C10Z	C11Z	179.4(8)
C3X	C4X	C5X	C6X	179.6(5)		C9Z	C10Z	C11Z	O2Z	-13.0(17)
C4X	C5X	C6X	C7X	178.1(5)		C9Z	C10Z	C11Z	C12Z	179.2(14)
C5X	C6X	C7X	C8X	176.8(5)		O1Y	C2Y	C3Y	C4Y	0(3)
C6X	C7X	C8X	C9X	-179.2(5)		C1Y	C2Y	C3Y	C4Y	-178(2)
C7X	C8X	C9X	C10X	172.1(4)		C2Y	C3Y	C4Y	C5Y	169.8(12)
C8X	C9X	C10X	C11X	-175.2(4)		C3Y	C4Y	C5Y	C6Y	177.8(12)
C9X	C10X	C11X	O2X	2.0(8)		C4Y	C5Y	C6Y	C7Y	176.8(12)
C9X	C10X	C11X	C12X	179.9(6)		C5Y	C6Y	C7Y	C8Y	178.7(11)
O1Z	C2Z	C3Z	C4Z	31(2)		C6Y	C7Y	C8Y	C9Y	179.6(11)
C1Z	C2Z	C3Z	C4Z	-152.8(16)		C7Y	C8Y	C9Y	C10Y	171.6(10)
C2Z	C3Z	C4Z	C5Z	174.4(8)		C8Y	C9Y	C10Y	C11Y	171.9(8)
C3Z	C4Z	C5Z	C6Z	-179.7(8)		C9Y	C10Y	C11Y	O2Y	-125.6(11)
C4Z	C5Z	C6Z	C7Z	177.1(8)		C9Y	C10Y	C11Y	C12Y	69.6(13)
C5Z	C6Z	C7Z	C8Z	-177.0(8)						

Table 3.3.2.7. Hydrogen atom coordinates (Å×10^4) and isotropic displacement parameters (Å^2×10^3) for BW_E_110-16-z24.

Atom	x	y	z	U(eq)

H1AA	5184	1416	5486	27
H1AB	4389	-422	5448	27
H1AC	5991	1436	5305	26
H1AD	4866	-410	5341	26
H1EA	-1796	3815	5665	24
H1EB	94	4862	5630	24
H1EC	-1574	4499	5483	24
H1ED	227	5268	5522	24
H1JA	4695	8490	5222	35
H1JB	5450	10337	5185	35
H1JC	3859	8502	5041	34
H1JD	4955	10342	5078	34
H1LA	4603	6159	5391	27
H1LB	5380	5087	5427	27
H1LC	3764	5291	5571	25
H1LD	4883	4574	5534	25
H1RA	3712	8463	5567	30
H1RB	4725	10239	5607	30
H1RC	4273	8170	5748	38
H1RD	5056	10067	5714	38
H1DA	5339	3986	4602	22
H1DB	4567	5051	4640	22
H1DC	6034	4644	4784	25
H1DD	4979	5442	4748	25
H1MA	4983	6539	4868	26

H1MB	5681	5376	4903	26
H1MC	3679	5154	5044	29
H1MD	4907	4555	5008	29
H1HA	-4580	4262	5836	35
H1HB	-5566	5071	5796	35
H1HC	-4974	3655	5653	36
H1HD	-5798	4712	5688	36
H1A	858	4404	5752	40
H1B	-1001	4018	5782	40
H1NA	824	3970	5761	40
H1NB	-1003	3642	5792	40
H1PA	4879	3222	5131	30
H1PB	4218	4457	5163	30
H1QA	5999	4729	5307	30
H1QB	4840	5396	5269	30
H1PC	5948	4531	5310	30
H1PD	4955	5367	5272	30
H1PE	5415	4019	5127	30
H1PF	4512	4941	5166	30
H1XA	594	-241	5779	112
H1XB	-144	-2080	5735	112
H1XC	-1622	-1608	5768	112
H3XA	-1575	-2077	5625	45
H3XB	675	-1042	5623	45
H4XA	-1591	362	5569	45
H4XB	657	1638	5574	45

H5XA	998	-544	5508	45
H5XB	-1243	-1828	5504	45
H6XA	843	1884	5450	45
H6XB	-1396	548	5444	45
H7XA	1332	-279	5390	45
H7XB	-891	-1696	5387	45
H8XA	-1220	503	5321	45
H8XB	1012	1902	5325	45
H9XA	-607	-1801	5271	45
H9XB	1574	-219	5268	45
H10A	-1322	156	5204	45
H10B	890	1611	5198	45
H12A	-225	-1047	5050	112
H12B	691	1081	5075	112
H12C	-1529	-330	5082	112
H1ZA	880	-1557	5740	112
H1ZB	-1373	-2548	5740	112
H1ZC	-153	-783	5786	112
H3ZA	-2216	-1384	5627	45
H3ZB	-639	-1985	5622	45
H4ZA	-253	1467	5574	45
H4ZB	1446	1029	5574	45
H5ZA	-323	-1590	5506	45
H5ZB	-2012	-1142	5506	45
H6ZA	1623	1334	5452	45

H6ZB	-130	1692	5449	45
H7ZA	-159	-1472	5390	45
H7ZB	-1839	-1018	5385	45
H8ZA	1789	1303	5329	45
H8ZB	47	1667	5322	45
H9ZA	167	-1511	5271	45
H9ZB	-1693	-1341	5269	45
H10C	-160	1322	5201	45
H10D	1715	1173	5203	45
H12D	1487	430	5074	112
H12E	51	1199	5084	112
H12F	-652	-802	5050	112
H1YA	-1215	-2513	5722	112

H1YB	-1106	-889	5768	112
H1YC	774	-938	5751	112
H3YA	-1906	-1936	5612	45
H3YB	209	-1544	5609	45
H4YA	1087	1487	5560	45
H4YB	-1116	788	5555	45
H5YA	693	-993	5492	45
H5YB	-1525	-1764	5489	45
H6YA	1246	1823	5439	45
H6YB	-984	959	5433	45
H7YA	-1162	-1502	5367	45
H7YB	1075	-597	5372	45
H8YA	-730	1225	5312	45
H8YB	1506	2140	5318	45
H9YA	-772	-1253	5248	45
H9YB	1484	-80	5248	45
H10E	-918	1121	5191	45
H10F	1306	2495	5198	45
H12G	-1436	-1239	5066	130
H12H	-1990	-1878	5138	130
H12I	-507	-2288	5102	130

Table 3.3.2.8. Atomic occupancy for BW_E_110-16-z24.

Atom	Occupancy		Atom	Occupancy		Atom	Occupancy
N1	0.219(2)		H1A	0.219(2)		H1B	0.219(2)
N1N2	0.781(2)		H1NA	0.781(2)		H1NB	0.781(2)
N1PQ	0.219(2)		H1PA	0.219(2)		H1PB	0.219(2)
N1Q	0.219(2)		H1QA	0.219(2)		H1QB	0.219(2)
N1P	0.781(2)		H1PC	0.781(2)		H1PD	0.781(2)
N1PP	0.781(2)		H1PE	0.781(2)		H1PF	0.781(2)
O1X	0.539(3)		O2X	0.539(3)		C1X	0.539(3)
H1XA	0.539(3)		H1XB	0.539(3)		H1XC	0.539(3)
C2X	0.539(3)		C3X	0.539(3)		H3XA	0.539(3)
H3XB	0.539(3)		C4X	0.539(3)		H4XA	0.539(3)
H4XB	0.539(3)		C5X	0.539(3)		H5XA	0.539(3)
H5XB	0.539(3)		C6X	0.539(3)		H6XA	0.539(3)
H6XB	0.539(3)		C7X	0.539(3)		H7XA	0.539(3)
H7XB	0.539(3)		C8X	0.539(3)		H8XA	0.539(3)
H8XB	0.539(3)		C9X	0.539(3)		H9XA	0.539(3)
H9XB	0.539(3)		C10X	0.539(3)		H10A	0.539(3)
H10B	0.539(3)		C11X	0.539(3)		C12X	0.539(3)
H12A	0.539(3)		H12B	0.539(3)		H12C	0.539(3)
O1Z	0.242(3)		O2Z	0.242(3)		C1Z	0.242(3)
H1ZA	0.242(3)		H1ZB	0.242(3)		H1ZC	0.242(3)
C2Z	0.242(3)		C3Z	0.242(3)		H3ZA	0.242(3)
H3ZB	0.242(3)		C4Z	0.242(3)		H4ZA	0.242(3)
H4ZB	0.242(3)		C5Z	0.242(3)		H5ZA	0.242(3)

H5ZB	0.242(3)		C6Z	0.242(3)		H6ZA	0.242(3)
H6ZB	0.242(3)		C7Z	0.242(3)		H7ZA	0.242(3)
H7ZB	0.242(3)		C8Z	0.242(3)		H8ZA	0.242(3)
H8ZB	0.242(3)		C9Z	0.242(3)		H9ZA	0.242(3)
H9ZB	0.242(3)		C10Z	0.242(3)		H10C	0.242(3)
H10D	0.242(3)		C11Z	0.242(3)		C12Z	0.242(3)
H12D	0.242(3)		H12E	0.242(3)		H12F	0.242(3)
O1Y	0.219(2)		O2Y	0.219(2)		C1Y	0.219(2)
H1YA	0.219(2)		H1YB	0.219(2)		H1YC	0.219(2)
C2Y	0.219(2)		C3Y	0.219(2)		H3YA	0.219(2)
H3YB	0.219(2)		C4Y	0.219(2)		H4YA	0.219(2)
H4YB	0.219(2)		C5Y	0.219(2)		H5YA	0.219(2)
H5YB	0.219(2)		C6Y	0.219(2)		H6YA	0.219(2)
H6YB	0.219(2)		C7Y	0.219(2)		H7YA	0.219(2)
H7YB	0.219(2)		C8Y	0.219(2)		H8YA	0.219(2)
H8YB	0.219(2)		C9Y	0.219(2)		H9YA	0.219(2)
H9YB	0.219(2)		C10Y	0.219(2)		H10E	0.219(2)
H10F	0.219(2)		C11Y	0.219(2)		C12Y	0.219(2)
H12G	0.219(2)		H12H	0.219(2)		H12I	0.219(2)

3.4. Conclusions

In this chapter, synchrotron studies of samples of 2,11-dodecanedione/urea grown under different conditions have been described. It is shown that when the starting guest repeat length is shorter than or up to 0.014(11) Å longer than that required for the commensurate phase with $12c_g' = 19c_h'$, a 4D-to-3D lock-in phase transition occurs upon cooling below ca. 260 K. If the guest molecules elongate to lock into the commensurate

structure, the incommensurate-to-commensurate phase transition exhibits self-compression, much like that observed in 2,8-nonanedione/urea. Given the present data, it appears that greater elongation of the host molecules in the lock-in transition also resulted in larger proportions of the crystal being compressed into a phase with $2c_g' = 3c_h'$. In cases when the starting value of c_g is 0.0419(13) Å longer than the c_g' of the commensurate phase with $12c_g' = 19c_h'$, no lock-in phase transition occurs. In one such case, the crystal apparently underwent a 4D-to-5D phase transition, with the formation of a supplementary long-range modulation along the channel. The crystal structure of the commensurate phase with $12c_g' = 19c_h'$ was solved with high-resolution synchrotron data and was found to have three distinct guest conformations at 170 K. One of these conformations had a strained gauche relationship between its carbonyl groups, such that both could form hydrogen bonds to the host.

This study shows that with slight differences in guest length due to growth conditions, the phase transitions exhibited by the supramolecular crystals change dramatically.

3.5. References

1. Hollingsworth, M. D.; Brown, M. E.; Hillier, A. C.; Santarsiero, B. D.; Chaney, J. D., Superstructure control in the crystal growth and ordering of urea inclusion compounds. *Science* **1996,** *273*, 1355-1359.
2. Brown, M. E.; Chaney, J. D.; Santarsiero, B. D.; Hollingsworth, M. D., Superstructure topologies and host-guest interactions in commensurate inclusion compounds of urea with bis(methyl ketone)s. *Chem. Mater.* **1996,** *8*, 1588-1591.
3. Data collection at DLS, Oxford; notebook DLS_A_070_07 and _08.
4. Notebook ALS_A_128_05series.
5. Notebook APS_B_088.
6. Notebook APS_B_055_03_006 to _035.
7. Notebook BW_E_135_01.
8. Mannsfeld, S. C. B.; Tang, M. L.; Bao, Z. A., Thin film structure of triisopropylsilylethynyl-functionalized pentacene and tetraceno[2,3-b]thiophene from grazing incidence X-ray diffraction. *Adv. Mater.* **2011,** *23*, 127-131.
9. FibonacciBuild s3 Ver. 5.11, a Matlab program which was originally written by Laurent Guérin and modified by Philippe Rabiller and Ilya Frantsuzov.
10. Notebook BW_E_139_14_20K.
11. Notebook ALS_A_128_05_002.
12. Notebook ALS_A_128_05_072.
13. Brown, M. E.; Hollingsworth, M. D., Stress-induced domain reorientation in urea inclusion-compounds. *Nature* **1995,** *376*, 323-327.

14. Notebook BW_D_107_9 for crystallization; notebook ISF_A_033 for mounting.
15. Notebook DLS_A_070_7_0014.cbf (near pixel 1663, 1346).
16. Notebook ALS_A_128_05_0_083.
17. Notebook ALS_A_128_05_072 to _097.
18. Notebook ALS_A_128_05_098.
19. Notebook BW_E_123_06.
20. Notebook BW_E_133_06.
21. Notebook APS_B_226, temperature calibrations of APS using E type thermocouple.
22. The phase transition occurred between APS_B_213_05_007 and APS_B_213_05_008.
23. Notebook APS_B_213_05_003.
24. Notebook APS_B_213_05_009.
25. Notebook APS_B_213_05_003 to _019.
26. Notebook APS_B_213_05_022.
27. Notebook APS_B_213_05_022 to _046.
28. Notebook APS_B_213_05_046.
29. Notebook ALS_A_118_03series.
30. Notebook BW_E_121_011.
31. Notebook BW_E_139_11_20K.
32. Notebook BW_F_043.
33. The phase transition occurred between ALS_A_110_03_012 and ALS_A_110_03_013.
34. Notebook ALS_A_110_03_002.
35. Notebook ALS_A_110_03_020.
36. Notebook ALS_A_110_03_096.
37. Notebook ALS_A_110_03_112.
38. Notebook BW_E_128_05.
39. Notebook ALS_A_102_04_003.
40. Notebook ALS_A_102_05_123.
41. Notebook BW_E_122_06.
42. Notebook BW_E_134_08_20K.
43. Notebook ALS_A_123_03_002.
44. Notebook ALS_A_123_03_033.
45. Notebook BW_E_124_12.
46. Notebook BW_E_134_07_20.
47. Notebook ALS_A_132_03_001.
48. Notebook ALS_A_132_03_030.
49. Notebook ALS_A_132_03_048.
50. Notebook BW_F_91_02.
51. Notebook ALS_B_014
52. Notebook ALS_B_53_03_012.
53. Notebook ALS_B_053_03_027.
54. Notebook BW_E_126_07.
55. Notebook BW_E_133_04.
56. PeakFit 4.12, SeaSolve Software, Inc., Framingham, MA.
57. Notebook ALS_A_135_03_006.
58. Notebook ALS_A_135_03_046.
59. Notebook BW_F_092_02.
60. Notebook ALS_B_025_03_021 and _022.
61. Notebook ALS_B_025_03_010.

62. ALS_B_025_03_033.
63. Notebook BW_D_107_08.
64. Notebook BW_E_139_07.
65. Notebook APS_B_55_02_004.
66. Notebook APS_B_055_03_014.
67. (a) Guerin, L.; Mariette, C.; Rabiller, P.; Huard, M.; Ravy, S.; Fertey, P.; Nichols, S. M.; Wang, B.; Mannsfeld, S. C. B.; Weber, T.; Hollingsworth, M. D.; Toudic, B., Long-range modulation of a composite crystal in a five-dimensional superspace. *Phys. Rev. B* **2015,** *91*, 184101; (b) Huard, M.; Toudic, B.; Rabiller, P.; Ecolivet, C.; Guerin, L.; Bourges, P.; Breczewski, T.; Hollingsworth, M. D., Confined linear molecules inside an aperiodic supramolecular crystal: The sequence of superspace phases in n-hexadecane/urea. *J. Chem. Phys.* **2011,** *135*, 204505; (c) Mariette, C.; Frantsuzov, I.; Wang, B.; Guerin, L.; Rabiller, P.; Hollingsworth, M. D.; Toudic, B., Frustrated pretransitional phenomena in aperiodic composites. *Phys. Rev. B* **2016,** *94*, 184105.
68. Notebook APS_B_55_02_024.
69. Notebook APS_B_055_03_014 to _035.
70. Harris, K. D. M., Meldola lecture: understanding the properties of urea and thiourea inclusion compounds. *Chem. Soc. Rev.* **1997,** *26*, 279-289.
71. Brown, M. E.; Hollingsworth, M. D., Stress-Induced Domain Reorientation in Urea Inclusion-Compounds. *Nature* **1995,** *376*, 323-327.
72. Hollingsworth, M. D.; Brown, M. E.; Dudley, M.; Chung, H.; Peterson, M. L.; Hillier, A. C., Template effects, asymmetry, and twinning in helical inclusion compounds. *Angew. Chem. Int. Ed.* **2002,** *41*, 965–969.
73. Notebook SMN_B_116. The crystal was grown by Shane M. Nichols by cooling a solution of urea, guest, and methanol from above room temperature to approximately 4 ºC in a small Dewar flask.
74. Notebook APS_A_036.
75. Sheldrick, G. M., A short history of SHELX. *Acta Crystallogr. Sect. A* **2008,** *64*, 112-122.
76. Mariette, C.; Huard, M.; Rabiller, P.; Nichols, S. M.; Ecolivet, C.; Janssen, T.; Alquist, K. E.; Hollingsworth, M. D.; Toudic, B., A molecular "phase ordering" phase transition leading to a modulated aperiodic composite in *n*-heptane/urea. *J. Chem. Phys* **2012,** *136*, 104507.
77. Bruker (2012). APEX2. Bruker AXS Inc., Madison, Wisconsin, USA.
78. Notebook BW_E_100, a converion method from miniKappa to Bruker geoniometer geometry.
79. Bruker (2001). SADABS. Bruker AXS Inc., Madison, Wisconsin, USA.
80. Dolomanov, O. V., Bourhis, L. J., Gildea, R. J., Howard, J. A. K. & Puschmann, H., OLEX2: a complete structure solution, refinement and analysis program. *J. Appl. Cryst.* **2009,** *42*, 339–341.
81. Least-Squares function minimized: $\Sigma w (|Fo| - |Fc|)^2$, where: $w = 1/\sigma^2(Fo)$.
82. Standard deviation as observation of weight.
83. Cromer, D. T.; Waber, J. T., International Tables for Crystallography, Vol. C; Table 4.2.4.2. The Kynoch Press: Birmingham, U.K., 1991.
84. Notebook BW_E_110_016_z23.

Chapter 4. Conclusions

In conclusion, phase transitions of 2,8-nonanedione/urea and 2,11-dodecanedione/urea have been extensively studied with synchrotron X-ray methods. To rationalize the unique observation of the mixture of phases, a “self-compression” mechanism is proposed.

The helical 1-D channel structure of UICs makes them perfect models to study how pressure affects the structure. In 2,8-nonanedione/urea, the formation of extended commensurate phases results in a compression of the guest repeat length by 0.761(2) Å. In 2,11-dodecanedione/urea, for batches that have a guest repeat length smaller than that for a commensurate phase with $12c_g' = 19c_h'$, the “self-compression” mechanism is operative. For example, in the batch grown at -20.0 ºC, the compression of the guest repeat length is determined to be 0.8670(14). The astonishing similarities of the phase transition behavior in both 2,8-nonanedione/urea and 2,11-dodecanedione/urea show a generalized potential of this “self-compression” mechanism. Although these “self-compression” phase transitions are first reported here, lock-in phase transitions in other composite systems, including channel systems, should be checked and examined carefully.

The mechanism was supported by a series of studies. In chapter two, there are four types of supporting experiments. First, in 2,8-nonanedione/urea-d_4, deuteration of the host slightly modified the host:guest interaction and affected the phase transition temperatures and sequence of phases. But this UIC still exhibited “self-compression” behavior. Furthermore, the crystal size was large for this sample; thus high-quality data were obtained to better elucidate the “self-compression” mechanisms. Second, a systematic study demonstrated that increased inclusion of 2-nonanone in crystals of 2,8-nonanedione/urea resulted in smaller degrees of compression. In the mixed crystals,

different sequences of phases were observed. These studies on mixed crystal indicate the necessity of the formation of the extended commensurate phase as the driving force for self-compression. Third, studies of 4,4'-oxybis(2-butanone)/urea show the stability of the commensurate structure with $9c_g' = 11c_h'$. Fourth, the crystal structure of 2,8-nonanedione/urea demonstrates that host-guest hydrogen bonding provides the driving force for the lock-in phase transition at 265 K, as expected from earlier crystal structures in this homologous series.

In chapter three, different growth conditions yielded 2,11-dodecanedione/urea with a range of guest repeat lengths. Luckily, different samples exhibited guest repeats that were slightly shorter, slightly longer, and very close to the commensurate phase with $12c_g' = 19c_h'$. Surprisingly, depending on the guest repeat length, two types of phase transitions were observed. This strongly indicates that in UICs, the lock-in phase transition only occurs when the guest is extended while cooling through the phase transition. On the other hand, it is reasoned that if guest contracts during a lock-in transition, unfavorable voids might be generated.

In addition, the crystal structure of 2,11-dodecanedione/urea, in which $12c_g' = 19c_h'$, is reported here. Due to its long axis of 209.210(10) Å, and the complicated host:guest nature of this UIC, the structure was a great challenge. With much effort, and data from a state of the art detector, a structure with three disordered sites has been determined. This research on 2,11-dodecaneione/urea provides a second independent example of "self-compression" and sheds light on what controls lock-in phase transitions.

In summary, a "self-compression" mechanism is proposed and supported here with extensive synchrotron studies on 2,8-nonanedione/urea and 2,11-dodecanedione/urea.

Appendix 5. Supplemental information

5.1.1. Space group determination of the host structure of 2,8-nonanedione/urea

To determine the space group of the host structure, a single crystal of 2,8-nonanedione/urea was selected for a variable temperate synchrotron oscillation study.[1] After the temperature scans, the crystal was misoriented, and a dataset was collected on beamline 14-BM-C at APS, using an ADSC Quantum 315 r detector. In the data collection, the following parameters were used: temperature = 290.0 K, distance = 200.00 mm, λ = 0.97870, ϕ = 0-360°, frame width = 1°. Using Olex2,[2] the structure was solved with the XS structure solution program using Direct Methods and refined with the XL refinement package using full matrix least squares minimization.[3]

The host structure was refined isotropically,[4] and the following parameters were determined for CH_4N_2O (*M* = 60.06 g/mol): hexagonal space group $P6_122$ (no. 178), ***a*** = 8.2316(17) Å, ***c*** = 11.0219(19) Å, *V* = 646.8(3) Å^3, *Z* = 6, μ = 0.178 mm^{-1}, *Dcalc* = 0.925 g/cm^3. A total of 1704 reflections were measured (7.872° ≤ 2θ ≤ 47.234°); after merging, there were 107 unique reflections (R_{int} = 0.0284, R_{sigma} = 0.0153), which were used in all calculations. The final R_1 was 0.1989 (for I > 2σ(I)), and wR_2 was 0.4421 (all data). Attempts to treat the model anisotropically were not successful. The largest Q peak is in the center of the channel, but because this UIC is incommensurate at 290 K, the guest structure cannot be solved in this 3-D treatment of the data.

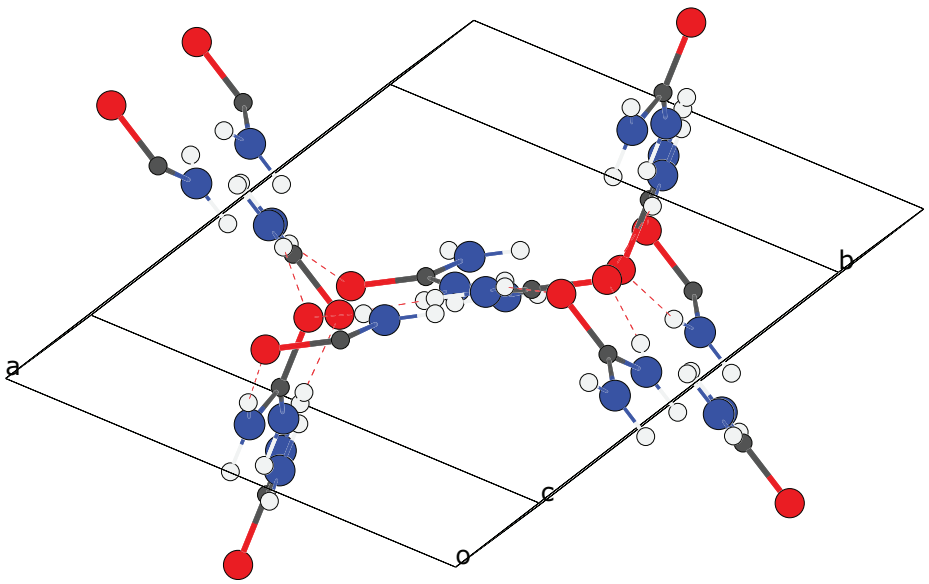

Figure 5.1.1. Diagram of the unit cell of the host structure of 2,8-nonanedione/urea at 290.0 K. The figure was made with Olex2.[2]

Table 5.1.1. Crystal data and structure refinement for APS_B_208_0m_c.	
Identification code	APS_B_208_0m_c
Empirical formula	$C_1H_4N_2O$
Formula weight	60.06
Temperature/K	290.0
Crystal system	Hexagonal
Space group	$P6_122$
a/Å	8.2316(17)
b/Å	8.2316(17)
c/Å	11.0219(19)
α/°	90
β/°	90
γ/°	120

Volume/Å^3	646.8(3)
Z	6
ρ_{calc}g/cm^3	0.925
μ/mm^{-1}	0.178
F(000)	192.0
Crystal size/mm^3	15 × 5 ×5
Radiation	Synchrotron (λ = 0.97870)
2θ range for data collection/°	7.872 to 47.234
Index ranges	-5 ≤ h ≤ 5, -6 ≤ k ≤ 6, -7 ≤ l ≤ 7
Reflections collected	1704
Independent reflections	107 [R_{int} = 0.0284, R_{sigma} = 0.0153]
Data/restraints/parameters	107/0/10
Goodness-of-fit on F^2	2.419
Final R indexes [I>=2σ (I)]	R_1 = 0.1989, wR_2 = 0.4423
Final R indexes [all data]	R_1 = 0.1988, wR_2 = 0.4421
Largest diff. peak/hole / eÅ^{-3}	0.71/-0.64
Flack parameter	0.0(8)

Table 5.1.2. Fractional atomic coordinates (×10^4) and equivalent isotropic displacement parameters (Å^2×10^3) for APS_B_208_0m_c. U_{eq} is defined as 1/3 of of the trace of the orthogonalized U_{ij} tensor.

Atom	*x*	*y*	*z*	U(eq)
O1	3590(30)	6793(13)	833	25(11)

N1	910(20)	5640(20)	1854(11)	28(12)
C1	1790(50)	5890(20)	833	10(12)

Table 5.1.3. Bond lengths for APS_B_208_0m_c.

Atom	Atom	Length/Å
O1	C1	1.28(3)
N1	C1	1.296(18)
N1	H1A	0.86
N1	H1B	0.86

Table 5.1.4. Bond angles for APS_B_208_0m_c.

Atom	Atom	Atom	Angle/°
O1	C1	N1	118.9(16)
N1	C1	N1	122(3)

Table 5.1.5. Hydrogen atom coordinates (Å×10^4) and isotropic displacement parameters (Å^2×10^3) for APS_B_208_0m_c.

Atom	*x*	*y*	*z*	U(eq)
H1A	1530	6065	2516	34
H1B	-299	5035	1868	34

5.1.2. Measurement of ferroelastic distortion and indexation of layer line in oscillation images of 2,8-nonanedione/urea

The indexation of layer lines and measurement of the ferroelastic distortion observed in the synchrotron oscillation image of APS_A_098_029 at 169.1 K is shown here. Using Wxdiff,[5] the $(h\ k\ 1)_g$ peaks of the commensurate phase with $4c_g' = 5c_h'$ were extracted from the original oscillation image, as shown in Figure 5.1.2. On each layer line, the vertical positions (y-values) of the $(h\ k\ 1)_g$ peaks were within one pixel of the central (h k 0) peak, which was not used because of its breadth along ***a*b****. Thus this measurement is a good approximation without applying unwarping and proper geometry conversion of the original data. The peak positions of the $(h\ k\ 1)_g$ peaks are used to calculate $\sin\theta$. Using Bragg's law, the d-spacings corresponding to the cell parameters ***a*** and ***b*** are measured using the (2 0 l) and (0 4 l) peaks (Table 5.1.6). The calculated d-spacings for higher indices agree well with those expected from the cell constants determined from this measurement, as shown in Table 5.1.7. With this procedure, the ferroelastic distortion shown in Figure 2.2.1.6 was obtained.

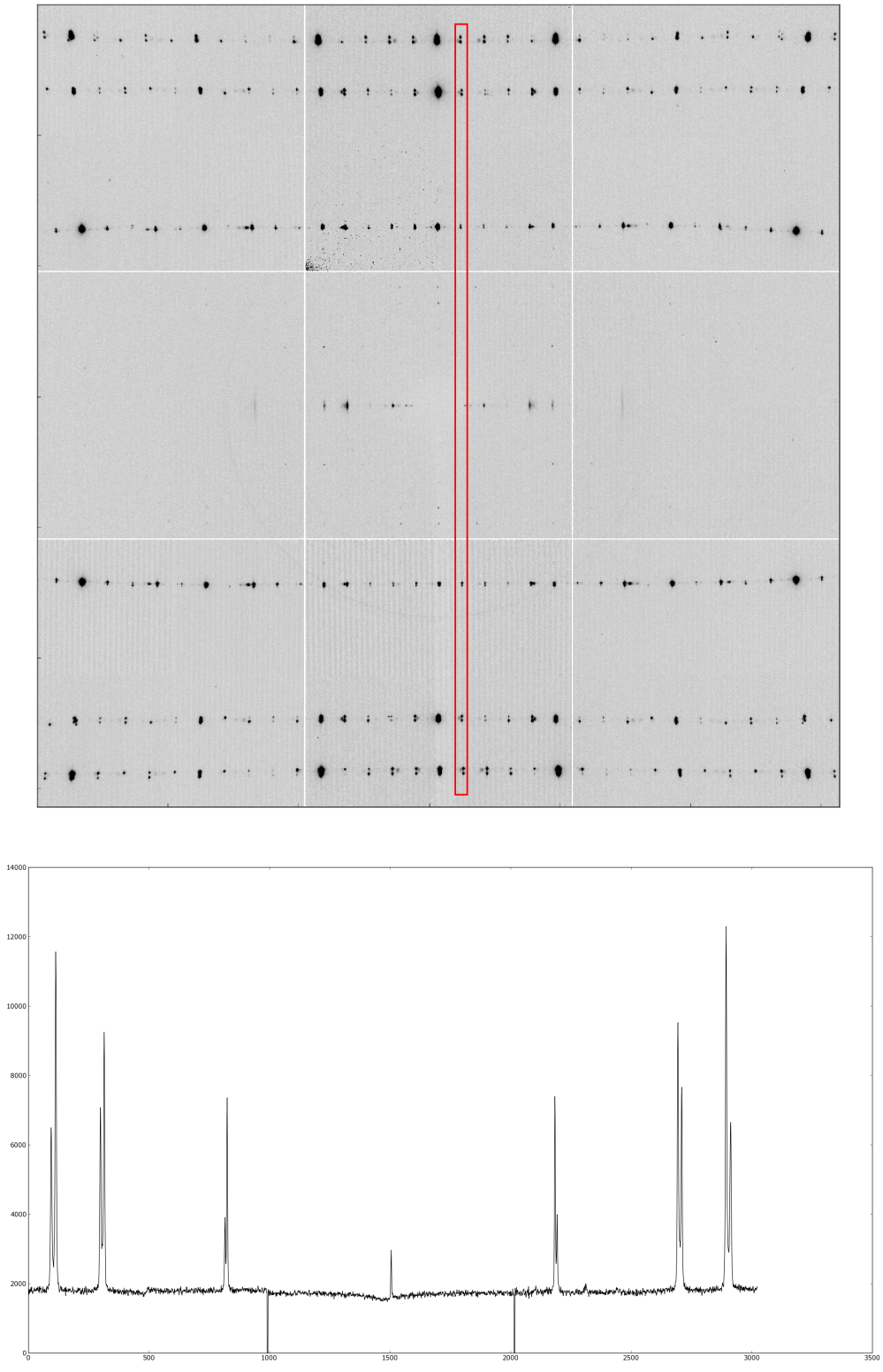

Figure 5.1.2. Top: Synchrotron oscillation image of 2,8-nonanedione/urea taken at 169.1 K.[6] Bottom: Column sum of peak intensities of the $(h\ k\ 1)_g$ layer line using Wxdiff.

	Pixels from center	Distance from center (mm)	tan2θ	θ	sinθ	d_{hk}	Index
2215	680.5	69.68	0.1394	0.0692	0.0692	7.0737	1 1
2225	689.9	70.64	0.1413	0.0702	0.0701	6.9787	0 2
2725	1190	121.9	0.2438	0.1196	0.1193	4.1026	2 0
2740	1206	123.4	0.2469	0.1210	0.1207	4.0534	1 3
2925	1390	142.3	0.2847	0.1388	0.1382	3.5401	2 2
2944	1409	144.2	0.2885	0.1404	0.1400	3.4963	0 4

Table 5.1.6. Peak positions and d-spacing measurements from the synchrotron oscillation image.

Calculated *d*-spacing	h	k	l	Measured d_{hk}	Difference in d_{hk}
13.985	0	1	0	N/A	N/A
8.2053	1	0	0	N/A	N/A
7.0771	1	1	0	7.0737	0.0034
6.9925	0	2	0	6.9787	0.0138
4.1026	2	0	0	4.1026	N/A
4.0532	1	3	0	4.0534	0.0002
3.5385	2	2	0	3.5401	0.0016
3.4963	0	4	0	3.4963	N/A

Table 5.1.7. Calculations of *d*-spacing using the values of ***a*** and ***b*** estimated in Table 5.1.2.1.

5.1.3. Synthesis of 2,8-nonanedione and its analog

5.1.3.1. Synthesis of 2,8-nonanedione[7,8]

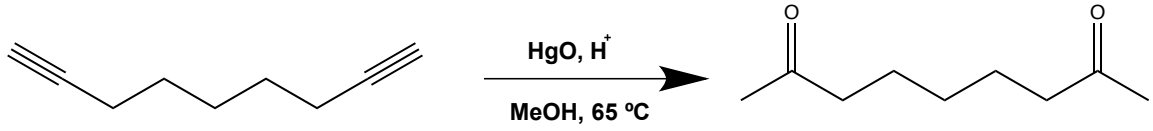

Figure 5.1.3.1. Synthesis of 2,8-nonanedione.

To a 500 ml round bottom flask containing water (70 mL, distilled) was added sulfuric acid (15 mL) and mercuric oxide (1.06 g, 4.89 mmol, 99.7%, Baker). While stirring at 65 ºC, a solution of 1,8-nonadiyne (10.0 g, 83.3 mmol, 98%, Aldrich) in methanol (350 mL, ACS grade, Fisher) was added to the mixture in the flask. After two and half hours, the reaction mixture was extracted with diethyl ether (3 x 100 mL). The organic layer was dried over $MgSO_4$, filtered, and concentrated on a rotary evaporator, yielding 6.1 g of crude product, which was recrystallized twice with 50 mL hexane. Recyrstallization yielded 3.15 g of pure product. The mother liquor in the recrystallization process was purified with flash column chromatography to give a pure product (1.61 g). The two white solids were combined to give a total of 4.76 g of pure product (28.8% yield).

Physical data: R_f = 0.19 (4:1 hexanes/EtOAc v/v, PMA stain as indicator). ^1H NMR (400 MHz, $CDCl_3$, BW_E_030_07): δ1.26 (2H, m, -C**H**$_2$-), δ1.55 (4H, p, -C**H**$_2$-), δ2.11 (6H, s, -C**H**$_3$), δ2.41 (4H, t, -C**H**$_2$-$COCH_3$).

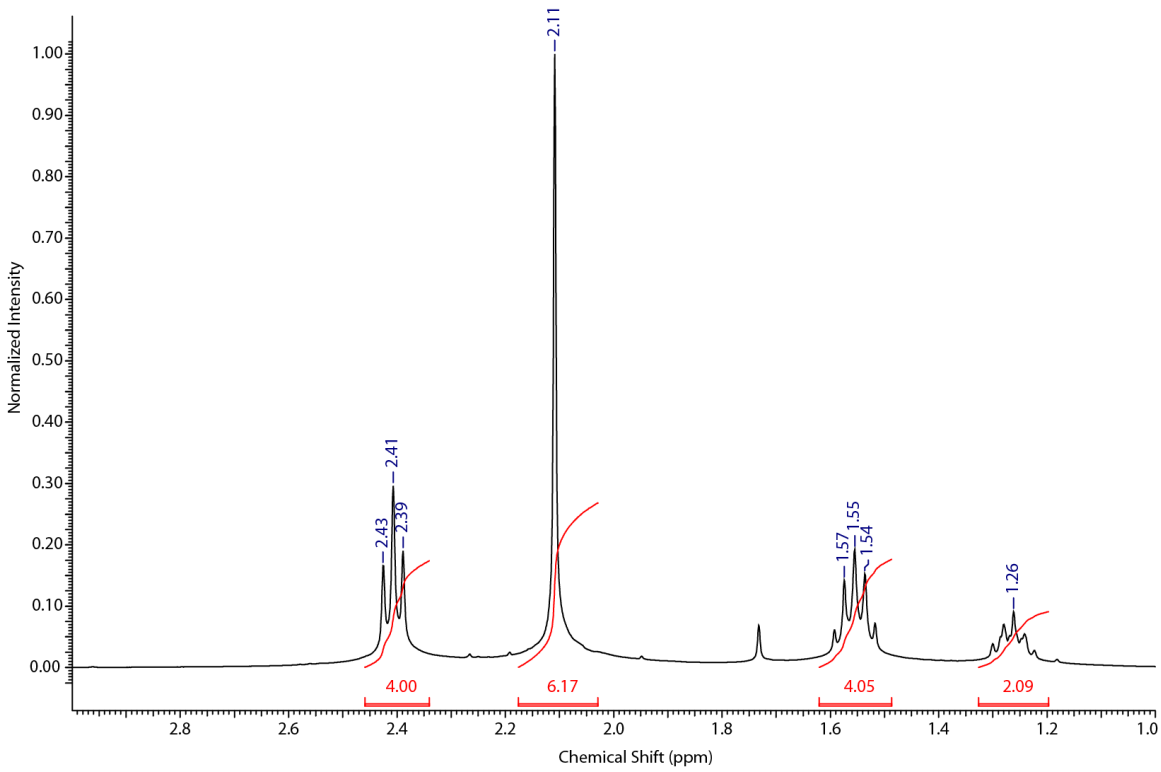

Figure 5.1.3.2. ^{1}H NMR (Varian Mercury VX at 400 MHz) spectrum of 2,8-nonanedione in $CDCl_3$.[9]

5.1.3.2. Synthesis of 4,4'-oxybis(butan-2-one)

Attempts to synthesize 4,4'-oxybis(butan-2-one) (**4**) by reacting methyl magnesium bromide and a dinitrile, or with methyl lithium and a carboxylic acid were unsuccessful.[10] As shown in Figure 5.1.3.3, formation of the ether via an S_N2 type reaction in the final step was successful. The protected alcohol (2-(2-methyl-1,3-dioxolan-2-yl)ethanol, (**1**)) was obtained following the procedure described in the master's thesis of Angela Adams.[11] The alcohol was tosylated and then reacted with the alkoxide formed from the same protected alcohol to give ether (**3**). Following deprotection of the ketones, 4,4'-oxybis(butan-2-one) was obtained.

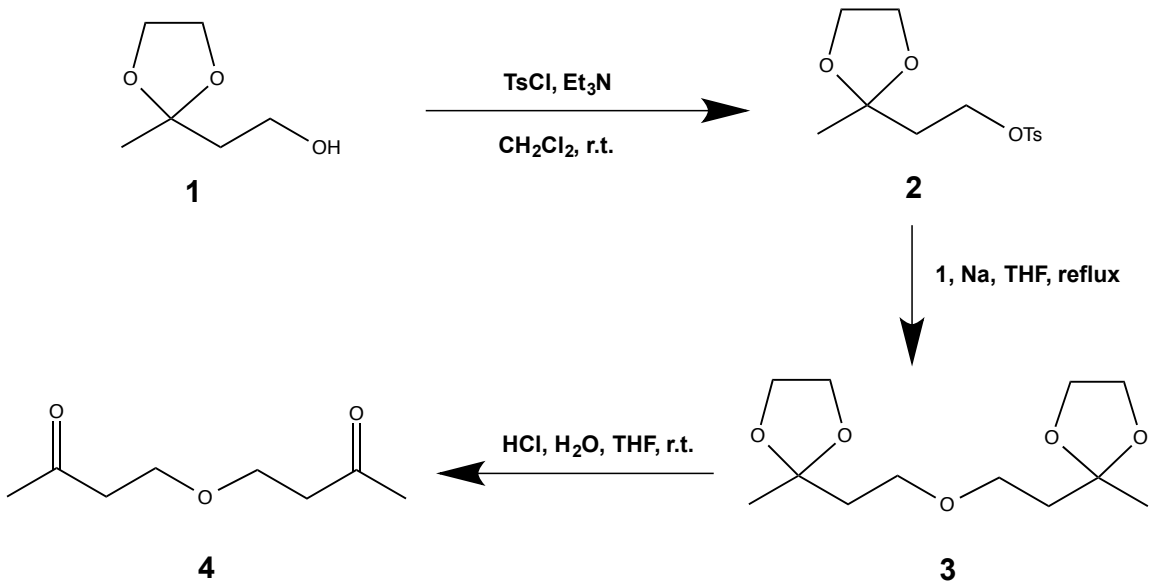

Figure 5.1.3.3. Synthetic route for 4,4'-oxybis(butan-2-one).

Synthesis of **2:**[12]

In a round bottomed flask, 2-(2-methyl-1,3-dioxolan-2-yl)ethanol (**1**) (2.004 g, 15.16 mmol) was added and then dried under vacuum before purging the flask with argon. The alcohol was then dissolved in CH_2Cl_2 (20 mL, distilled), before triethylamine (4.478 g, 99%, Aldrich) was added and the solution cooled to 0 ºC. *p*-Toluenesulphonyl chloride (4.574 g, 23.99 mmol, 99+%, Acros) dissolved in dichloromethane (20 mL, distilled) and chloroform (5 mL) was added to the reaction mixture via a dropping funnel at 0 ºC. After stirring at 0 ºC for 3 hours, the mixture was stirred for 18 hours at room temperature. The reaction was quenched with 10 mL satd. aq. $NaHCO_3$. The mixture was extracted from water with dichloromethane. After flash column chromatography, the purified product **2** (3.698 g, 12.91 mmol, 85.2% yield) was obtained as an oil.

Physical data: R_f = 0.74 (1:1 hexanes/EtOAc v/v, PMA stain as indicator). ^{1}H NMR (400 MHz, $CDCl_3$, BW_E_154_16): δ1.29 (3H, s, R-C**H**$_3$), δ2.06 (2H, t, R-C**H**$_2$-CH_2-OTs), δ2.46 (3H, s, ROTs-C**H**$_3$), δ3.89 (4H, m, RO-C**H**$_2$-C**H**$_2$-OR), δ4.16 (2H, m, -C**H**$_2$-OTs), δ7.37 (2H, m, α-Ar**H**-CH_3), δ7.81 (2H, m, β-Ar**H**-CH_3).

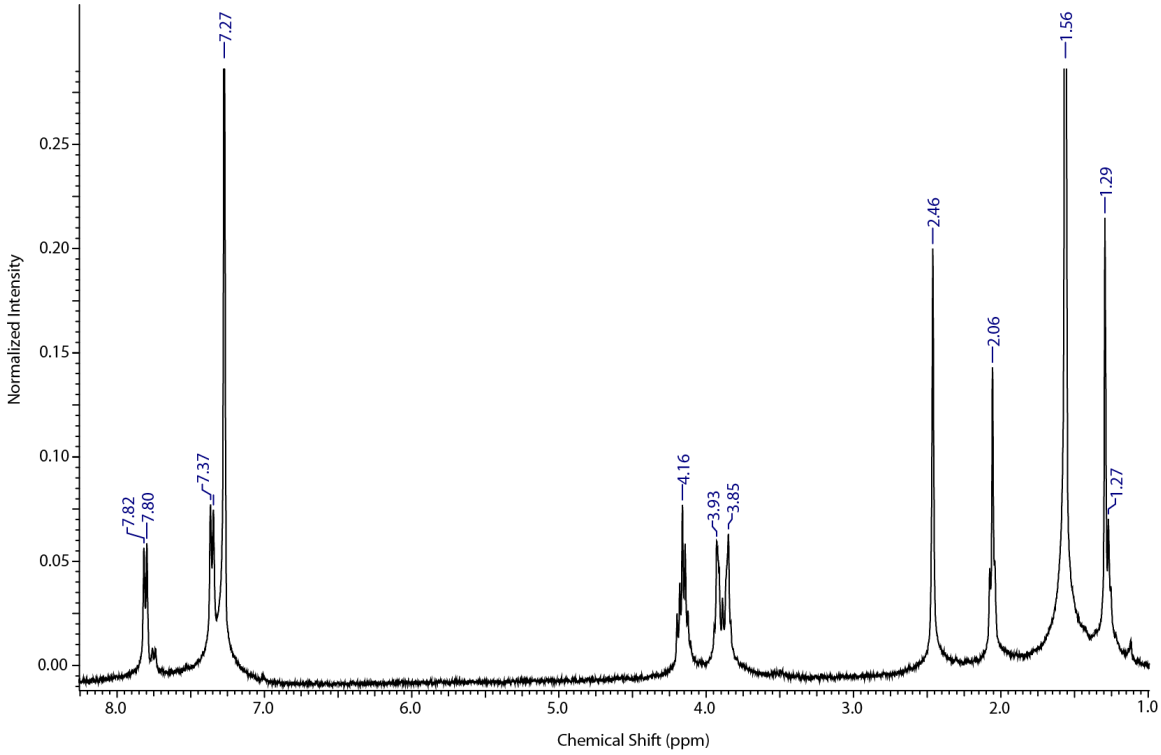

Figure 5.1.3.4. ^{1}H NMR (using Mercury VX 400 MHz) spectrum of **2** in $CDCl_3$.[13]

Synthesis of **3:**[14]

In a flame-dried round flask, **1** (0.743 g, 5.62 mmol) was added and vacuum dried over two hours before purging with argon. The alcohol was then dissolved in THF (20 mL, distilled from sodium benzophenone ketyl). Freshly-cut sodium metal pieces (0.124 g, 5.39 mmol, 99.95%, Aldrich) were added to the mixture at room temperature under an argon atmosphere. After refluxing overnight, the leftover sodium was removed. Compound **2** (1.405 g, 4.91 mmol) was added to the mixture via a dropping funnel over a period of 15 minutes. After refluxing for 13 hours, the reaction was quenched with satd. aq. $NaHCO_3$ and washed with satd. aq. $NaHCO_3$ (3 x 15 mL). After flash column chromatography, the purified product **3** (0.705 g, 2.86 mmol, 52% yield) was obtained as an oil.

Physical data: R_f = 0.47 (1:1 hexanes/EtOAc v/v, PMA stain as indicator). ^{1}H NMR (400 MHz, $CDCl_3$): δ1.35 (6H, s, R-C**H**$_3$), δ1.96 (4H, t, R-C**H**$_2$-CH_2-OR'), δ3.53 (4H, t, R-CH_2-C**H**$_2$-OR'), δ3.92 (8H, m, RO-C**H**$_2$-C**H**$_2$-OR).

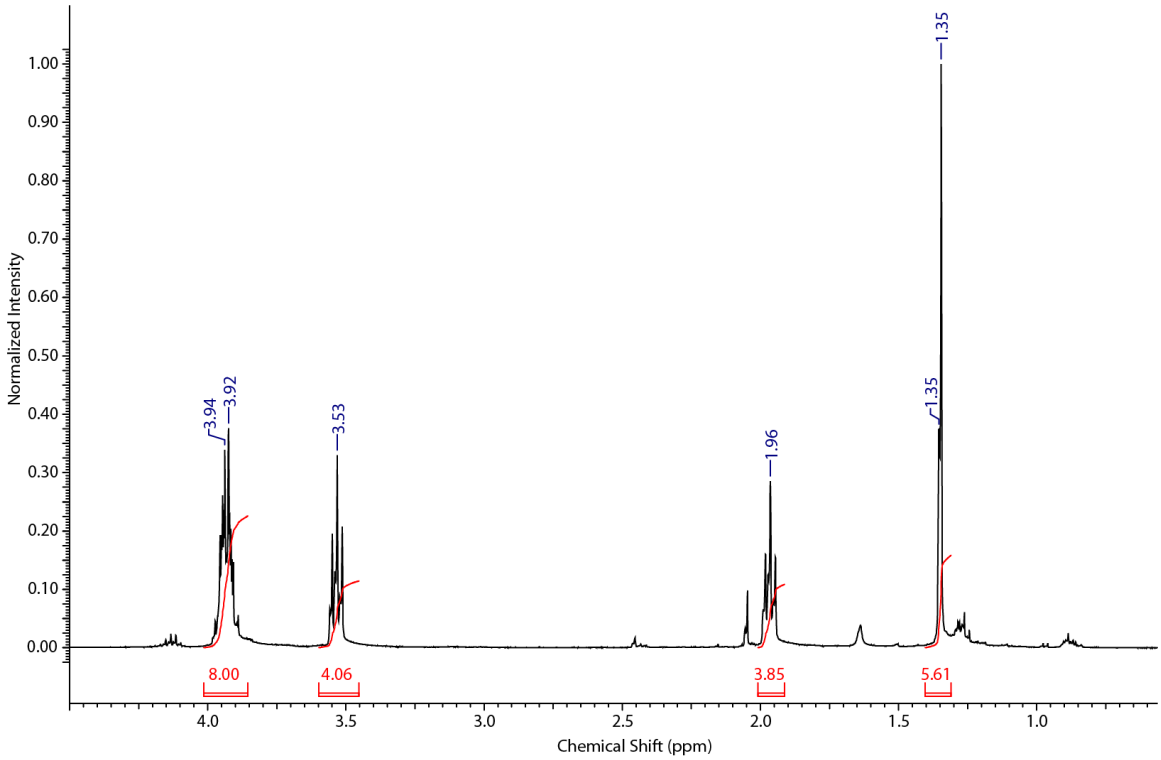

Figure 5.1.3.5. ^{1}H NMR (using Mercury VX 400 MHz) spectrum of **3** in $CDCl_3$.[15]

Synthesis of 4:[16]

In a round bottomed flask, **3** (0.705 g, 2.86 mmol), 2.5 M HCl/H_2O (1.5 mL), H_2O (1.0 mL), and THF (10 mL) were added. The mixture was stirred at room temperature for 9 hours. The mixture was added to diethyl ether/H_2O (10 mL/ 10mL), and then extracted with diethyl ether (3 x 15 mL). The organic layer was dried over $MgSO_4$. After flash column chromatography and vacuum drying, the product (0.16 g, 0.96 mmol, 34% yield) was obtained as a clear oil.

Physical data: R_f = 0.32 (1:1 hexanes/EtOAc v/v, PMA stain as indicator). ^{1}H NMR (400 MHz, $CDCl_3$): δ2.17 (6H, s, R-C**H**$_3$), δ2.65 (4H, t, R-C**H**$_2$-CO-CH$_3$), δ3.68 (4H, t, R-C**H**$_2$-OR').

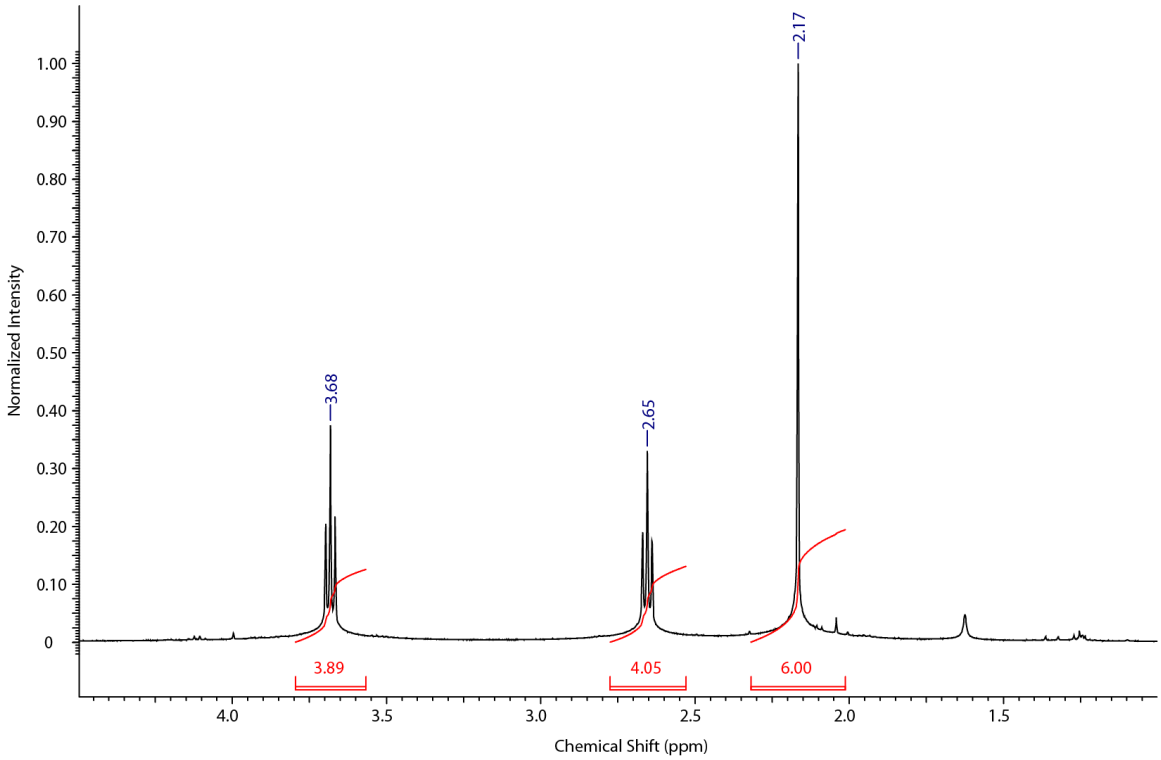

Figure 5.1.3.6. ^{1}H NMR (Varian Mercury VX at 400 MHz) spectrum of **4** in $CDCl_3$.[17]

5.1.4. Crystallization of 2,8-nonanedione/urea and related materials

5.1.4.1. Crystal growth of 2,8-nonanedione/urea-d$_4$

The guest (0.818 g, 5.23 mmol, recrystallized[7]) and urea-d$_4$ (2.846 g, 44.42 mmol, Aldrich 98% D) were dissolved in 14 mL methanol-d (Aldrich 99.5% D).[18] The solution was held at 20.0 °C with a Lakeshore Cryotronics DRC-91C temperature controller and slowly purged with argon. Large needle crystals (0.8-1.2 mm thick, 5-9 mm long) were grown over a one week period. A hexagonal needle was selected, coated with nail polish, and glued onto a glass fiber. Synchrotron oscillation images were obtained at APS beamline 14-BM-C.[19]

5.1.4.2. Crystal growth of UICs from a solution containing a 98.5:1.5 mixture of 2,8-nonanedione and 2-nonanone

A mixture of 2,8-nonanedione (0.16860 g, 1.0792 mmol, recrystallized[20]), 2-nonanone (0.00229 g, 0.0161 mmol, 99+%, Sigma-Aldrich), and urea (0.547 g, 9.12 mmol, 99.5+%, Sigma-Aldrich) was dissolved in methanol (5.1 mL, HPLC grade, Sigma-Aldrich). The growth solution was placed in a HAKKE (C40) temperature controller set to run from 33.0 ºC to -13.0 ºC over 26 hours and then from -8.1 ºC to -17.0 ºC over eight hours. The flask was stirred during the growth. It was noted that crystals were formed above -4.3 ºC. Crystals were harvested at -16.5 ºC.[21]

5.1.4.3. Crystal growth of UICs from a solution containing a 97.0:3.0 mixture of 2,8-nonanedione and 2-nonanone

A mixture of 2,8-nonanedione (0.7740 g, 0.4955 mmol, recrystallized[20]), 2-nonanone (0.00214 g, 0.0150 mmol, 99+%, Sigma-Aldrich), and urea (0.25593 g, 4.2612 mmol, 99.5+%, Sigma-Aldrich) was dissolved in methanol (2.4 mL, HPLC grade, Sigma-Aldrich). The growth solution was put in a HAKKE (C40) temperature controller set to run from 33.0 ºC to -13.0 ºC over 26 hours then from -8.1 ºC to -17.0 ºC over eight hours. The flask was stirred during the growth. It was noted that crystals were formed above -4.3 ºC. Crystals were harvested at -16.5 ºC.[22]

5.1.4.4. Crystal growth of UICs from a solution containing a 94.0:6.0 mixture of 2,8-nonanedione and 2-nonanone

A mixture of 2,8-nonanedione (0.16868 g, 1.0798 mmol, recrystallized[20]), 2-nonanone (0.00986 g, 0.0693 mmol, 99+%, Sigma-Aldrich), and urea (0.58175 g, 9.69 mmol, 99.5+%, Sigma-Aldrich) was dissolved in methanol (6.0 mL, HPLC grade, Sigma-Aldrich). The growth solution was placed in a HAKKE (C40) temperature

controller set to run from 13.0 ºC to -13.0 ºC over 48 hour. The flask was stirred during the growth. It was noted that crystals were formed above -4.3 ºC. Crystals were harvested and mounted.[23]

5.2.1. Determination of the channel axis length (c_h) in 2,11-dodecanedione/urea

In order to establish the unit cell parameters of 2,11-dodecanedione/urea, 9978 reflections from a synchrotron X-ray dataset on DLS beamline I04 were obtained from a 180º ω scan (using 0.25º frames, a detector distance of 170 mm, and λ = 0.97949 Å).[24] The unit cell dimensions of the hexagonal host unit cell were determined to be ***a*** = ***b*** = 8.1855 (4) Å, and ***c*** = 209.210(10) Å at 170.0 K. From the separation between the $(1\ 0\ -2\ 0)_h$ and $(1\ 0\ 2\ 0)_h$ peaks during a temperature scan on ALS beamline 8.2.2 from 160 K to 290 K,[25] the thermal expansion of the channel axis could be measured. The least squares line for this data is as follows:

$$c_h = 10.942(2) + 1.161(10) \times 10^{-4}\,T.$$

The slope of this line and the value of ***c*** from the full dataset at 170.0 K were used to give the following relationship:

$$c_h = 10.991(2) + 1.61(10) \times 10^{-4}\,T.$$

This method has also been applied to the crystals of 2,8-nonanedione/urea and 2,8-nonanedione/urea-d_4.

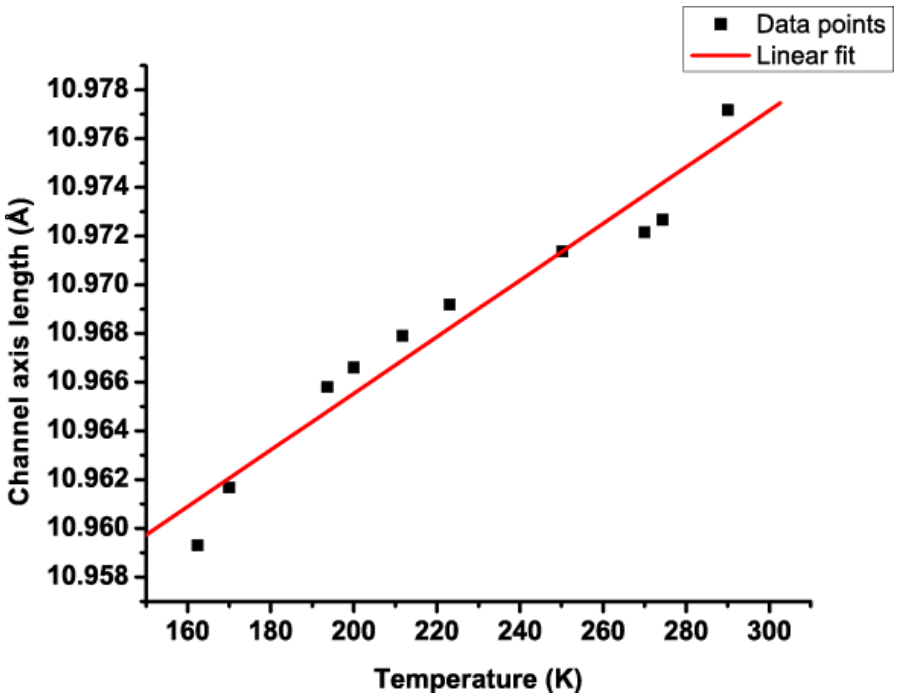

Figure 5.2.1. Linear least squares fit of c_h as a function of temperature using the separations between the $(1\ 0\ -2\ 0)_h$ and $(1\ 0\ 2\ 0)_h$ peaks in unwarped oscillation images of 2,11-dodecanedione/urea.

5.2.2. Estimation of the unit cell parameters for the phase with $2c_g' = 3c_h'$ in 2,11-dodecanedione/urea

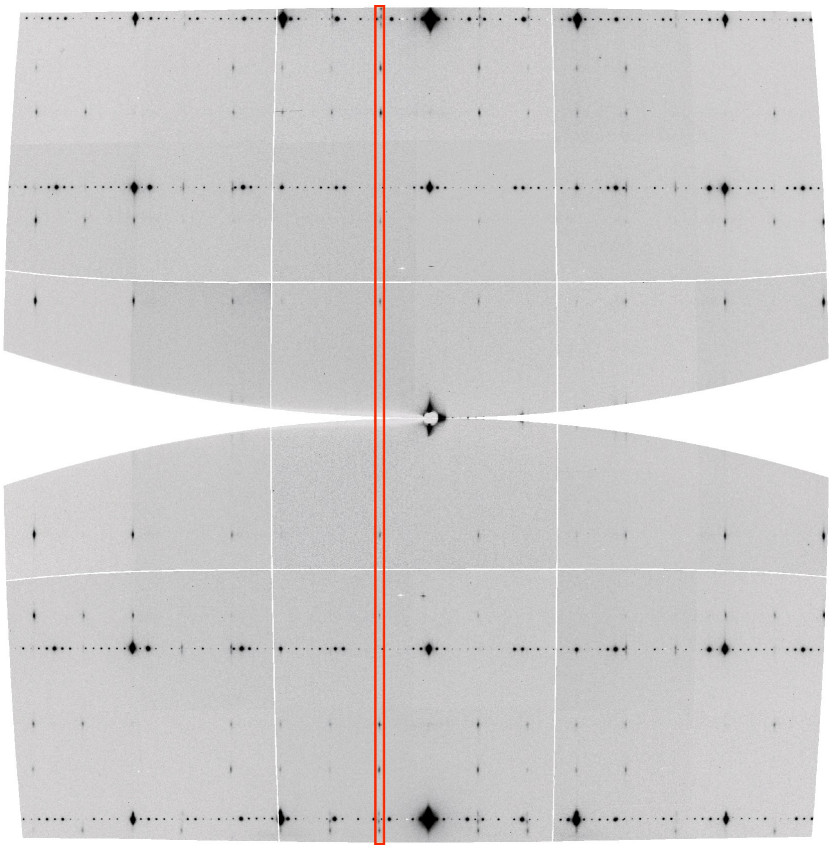

Figure 5.2.2. Unwarped oscillation image at 162.4 K of a crystal of 2,11-dodecanedione/urea grown at -20 °C. The parameters were as follows: distance = 500.02 mm, φ = 60-120°, time = 8 s, λ = 1.18080 Å, beam size (x, y) = (100, 200) μm on ALS beam line 8.2.2.[26] The red rectangle shows the (*h k* -1) peaks of the phase with $2c_g' = 3c_h'$ to be analyzed.

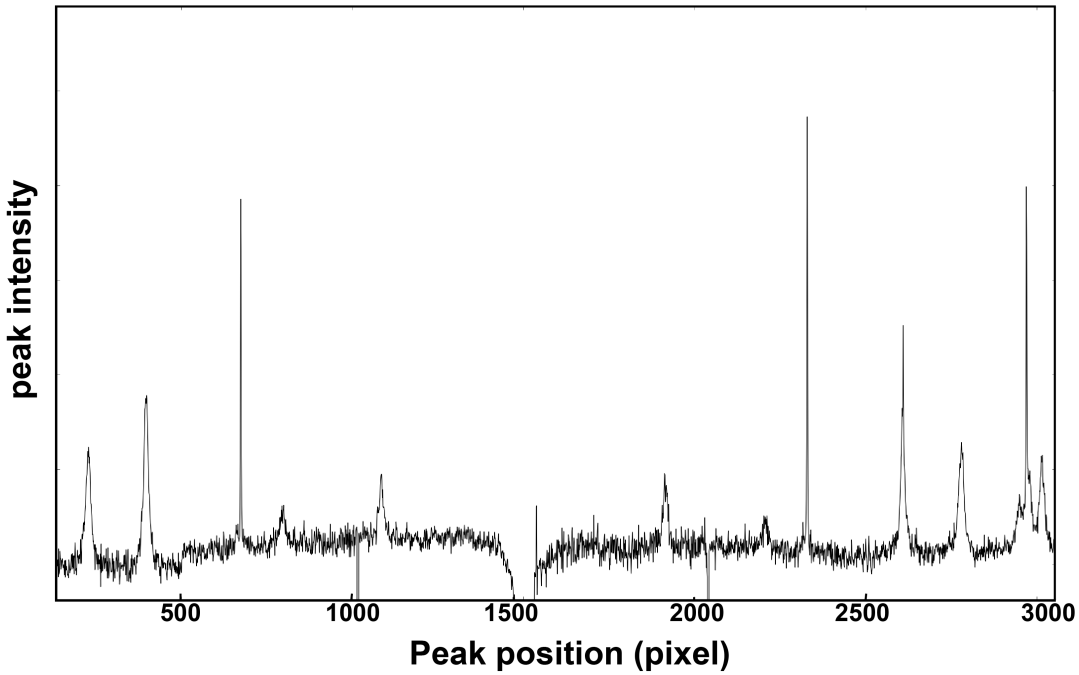

Figure 5.2.3. Peak positions of the commensurate phase with $2c_g' = 3c_h'$ of 2,11-dodecanedione/urea from the oscillation image shown in Figure 5.2.2.

As shown in Table 5.2.1, using the peak positions of the (0 1 *l*) and (1 0 *l*) from the unwarped oscillation image, the cell parameters of the phase with $2c_g' = 3c_h'$ were estimated to be ***a*** = 8.270 Å and ***b*** = 13.957 Å. Although the corrections will be small for such a large detector distance (500 mm), these numbers can be improved by using a geometry conversion to account for the unwarping procedure. With the present procedure, the measured d-spacing at higher indices agree well with calculated values. For ***a*** = 8.270 Å, ***b*** = 13.957 Å, this corresponds to a 2.6% distortion from hexagonal metric symmetry. Using the same procedure, the cell parameters of the phase with $12c_g' = 19c_h'$ that exists at that same temperature can also be determined: $\boldsymbol{a}_h = \boldsymbol{b}_h$ = 8.130 Å.

Peak position (pixel)	Pixels from center (pixel)	d_{hk} (Å)	*h*	*k*	Calculated *d*-spacing (Å)
1923.3196	414.2069	13.9572	0	1	13.9572
2211.6538	702.5411	8.2702	1	0	8.2702
2336.8032	827.6905	7.0404			
2616.7000	1107.5873	5.3047	1	2	5.3335
2786.2449	1277.1322	4.6283	0	3	4.6524
2957.5874	1448.4747	4.1088	2	0	4.1351
2977.3329	1468.2202	4.0570			
2987.0270	1477.9143	4.0320	1	3	4.0548
3021.9027	1512.7900	3.9450	2	1	3.9647

Table 5.2.1. Peak indexing of the Bragg peaks in the layer line shown in Figure 5.2.3. Peak positions were determined with Peakfit v4.12.

5.2.3. Crystallizations of 2,11-dodecanedione/urea

5.2.3.1. 2,11-dodecanedione/urea grown at -20.0 ºC

A mixture of 2,11-dodecanedione (0.30168 g, 1.5213 mmol, recrystallized[27]) and urea (2.82376 g, 47.0157 mmol, 99.5+%, Sigma-Aldrich) was dissolved in methanol (53.0 mL, HPLC grade, Sigma-Aldrich). The flask containing the growth solution was placed in a HAKKE (C40) temperature controller set at -20.0 °C and purged with argon. Crystals were harvested after one day of evaporation.[28]

5.2.3.2. 2,11-dodecanedione/urea grown at -10.0 ºC

A mixture of 2,11-dodecanedione (0.30192 g, 1.5225 mmol, recrystallized[27]) and urea (1.85625 g, 30.9066 mmol, 99.5+%, Sigma-Aldrich) was dissolved in methanol (31.0 mL, HPLC grade, Sigma-Aldrich). The flask containing the growth solution was placed in a HAKKE (C40) temperature controller set at -10.0 °C and purged with argon. Crystals were harvested after two days of evaporation.[29]

5.2.3.3. 2,11-dodecanedione/urea grown at 0.0 ºC

A mixture of 2,11-dodecanedione (0.30121 g, 1.5219 mmol, recrystallized[27]) and urea (1.37433 g, 22.8826 mmol, 99.5+%, Sigma-Aldrich) was dissolved in methanol (25.0 mL, HPLC grade, Sigma-Aldrich). The flask containing the growth solution was placed in a HAKKE (C40) temperature controller set at 0.0 °C and purged with argon. Block-like crystals were harvested after three days of evaporation.[30]

5.2.3.4. 2,11-dodecanedione/urea grown at 10.0 ºC

A mixture of 2,11-dodecanedione (0.30426 g, 1.5343 mmol, recrystallized[27]) and urea (1.39463 g, 23.2206 mmol, 99.5+%, Sigma-Aldrich) was dissolved in methanol (15.0 mL, HPLC grade, Sigma-Aldrich). The flask containing the growth solution was placed in a Neslab (RTE-140) temperature controller at 10.0 °C and purged with argon. Crystals were harvested after three days of evaporation.[31]

5.2.3.5. 2,11-dodecanedione/urea grown at 20.0 ºC

A mixture of 2,11-dodecanedione (0.30900 g, 1.5582 mmol, recrystallized[27]) and urea (1.39363 g, 23.2040 mmol, 99.5+%, Sigma-Aldrich) was dissolved in methanol (12.0 mL, HPLC grade, Sigma-Aldrich). The flask containing the growth solution was

placed in a Neslab (RTE-140) temperature controller at 20.0 °C and purged with argon. Block-like crystals were harvested after three days of evaporation.[32]

5.2.3.6. 2,11-dodecanedione/urea grown at 30.0 ºC

A mixture of 2,11-dodecanedione (0.30130 g, 1.5194 mmol, recrystallized[27]) and urea (1.39680 g, 23.2567 mmol, 99.5+%, Sigma-Aldrich) was dissolved in methanol (10.0 mL, HPLC grade, Sigma-Aldrich). The sample was crystallized by evaporation while immersed in a 4-liter Dewar filled with water. The temperature of the water bath was maintained at 30.0 °C with a Lakeshore DRC 91C temperature controller.[33] Crystals were harvested after five days of evaporation.

5.2.3.7. 2,11-dodecanedione/urea grown at 35.0 ºC

A mixture of 2,11-dodecanedione (0.308 g, 1.55 mmol, recrystallized[27]) and urea (1.407 g, 23.43 mmol, 99.5+%, Sigma-Aldrich) was dissolved in methanol (8.5 mL, HPLC grade, Sigma-Aldrich). The sample was crystallized by evaporation in a 4 liter Dewar filled with water. The sample was crystallized by evaporation over 3 days in an ethylene glycol/water bath maintained at 35.0 °C with a Neslab (RTE-140) temperature controller.[34]

5.2.3.8. 2,11-dodecanedione/urea grown at 40.0 ºC

A mixture of 2,11-dodecanedione (0.30687 g, 1.5475 mmol, recrystallized[27]) and urea (1.40899 g, 23.4597 mmol, 99.5+%, Sigma-Aldrich) was dissolved in methanol (8.0 mL, HPLC grade, Sigma-Aldrich). The flask containing the growth solution was placed in a Neslab (RTE-140) temperature controller at 40.0 °C. Crystals were harvested after two days of evaporation.[35]

5.2.3.9. 2,11-dodecanedione/urea grown at 46 ºC

A mixture of 2,11-dodecanedione (0.301 g, 1.5179 mmol, recrystallized[27]) and urea (1.367 g, 22.76 mmol, 99.5+%, Sigma-Aldrich) was dissolved in methanol (6.0 mL, HPLC grade, Sigma-Aldrich). The sample was crystallized by evaporation in an oil bath held at 46(2) °C over 24 hours.[36]

5.2.3.10. 2,11-dodecanedione/urea grown from 40 °C to room temperature

A mixture of 2,11-dodecanedione (0.05179 g, 0.2439 mmol, recrystallized[37]) and urea (0.62698 g, 10.439 mmol, 99.5+%, Sigma-Aldrich) was dissolved in methanol (12.0 mL, HPLC grade, Sigma-Aldrich). The solution was immersed in a 4-liter Dewar containing water at 40 °C and yielded crystals when it was allowed to cool to room temperature.[38]

5.2.3.11. 2,11-dodecanedione/urea grown from -13.0 °C to -23.0 °C

A mixture of 2,11-Dodecanedione (0.04836 g, 0.2612 mmol, recrystallized[37]) and urea (0.5749 g, 9.572 mmol, 99.5+%, Sigma-Aldrich) was dissolved in methanol (5.0 mL, HPLC grade, Sigma-Aldrich). The growth solution was placed in a HAKKE (C40) temperature controller, which was set to run from -13.0 °C to -23.0 °C over a 24-hour period. Crystals were harvested and then immediately placed in a freezer kept below -13 °C.[39]

5.3. References

1. Notebook BW_F_304 and APS_B_204_08.
2. Dolomanov, O. V., Bourhis, L. J., Gildea, R. J., Howard, J. A. K. & Puschmann, H., OLEX2: a complete structure solution, refinement and analysis program. *J. Appl. Cryst.* **2009,** *42*, 339–341.
3. Sheldrick, G. M., A short history of SHELX. *Acta Crystallogr. Sect. A* **2008,** *64*, 112-122.

4. The host structure of 2,8-nonanedione/urea was documented in BW_F_304. The structure solution file is APS_B_208_0m_c.
5. Mannsfeld, S. C. B.; Tang, M. L.; Bao, Z. A., Thin film structure of triisopropylsilylethynyl-functionalized pentacene and tetraceno[2,3-b]thiophene from grazing incidence X-ray diffraction. *Adv. Mater* **2011,** *23*, 127-131.
6. Notebook APS_A_098_029.
7. Notebook BW_E_021_08.
8. Notebook BW_D_06, BW_D_07.
9. Notebook BW_E_030_07.
10. Notebook BW_E_031, BW_E_034, BW_E_035, BW_E_036, BW_E_043, BW_E_044, BW_E_045, BW_E_050.
11. Adams, A. D., Synthesis of guest molecules for studies of urea inclusion compounds. *M. S. thesis, Kansas State University* **2009**, 73.
12. Notebook BW_E_217.
13. Notebook BW_E_154_016.
14. Notebook BW_E_218.
15. Notebook BW_E_168_09.
16. Notebook BW_E_220.
17. Notebook BW_E_220_07.
18. Notebook BW_E_022_19.
19. Notebook ALS_A_214_03.
20. Notebook BW_D_079_07.
21. Notebook BW_D_213_08.
22. Notebook BW_D_213_11.
23. Crystal harvasting at notebook BW_D_151_11; crystal mounting at notebook BW_D_229_04.
24. Data collection at DLS, Oxford; notebook DLS_A_070_07 and _08.
25. Notebook ALS_A_128_05series.
26. Notebook ALS_A_128_05_072.
27. Notebook BW_E_112_06.
28. Notebook BW_E_135_01.
29. Notebook BW_E_123_06.
30. Notebook BW_E_121_011.
31. Notebook BW_E_128_05.
32. Notebook BW_E_122_06.
33. Notebook BW_E_124_12.
34. Notebook BW_F_91_02.
35. Notebook BW_E_126_07.
36. Notebook BW_F_092_02.
37. Notebook BW_C_219_06.
38. Notebook BW_D_107_08.
39. Notebook BW_D_107_09.